Final Report

UWB-GPS Compatibility Analysis Project

8 MARCH 2001

Prepared by
STRATEGIC SYSTEMS DEPARTMENT
The Johns Hopkins University/Applied Physics Laboratory

FOREWORD

This report documents work conducted by The Johns Hopkins University Applied Physics Laboratory (JHU/APL) to analyze the potential for interference to the Global Positioning System (GPS) from ultra-wideband (UWB) signals. The intent of this report is to provide technical information to the Federal Communications Commission (FCC) to support regulatory decisions with regard to UWB emissions under Part 15 Rules. The results presented are based on the analysis of data collected by the Applied Research Laboratories, University of Texas (ARL:UT). Technical results are presented that quantify the relationship between key GPS performance parameters, and UWB signal parameters. While this work has been conducted under a contract with Time Domain Corporation, a proponent of UWB technology, JHU/APL has conducted an independent evaluation and this technical report does not make advocacy statements or policy recommendations with regard to UWB technology or Time Domain Corporation.

Both the GPS and the emerging UWB technology involve very complex engineering and operational issues, many of which are well beyond the scope of this report. In this report, the principal issues bearing on the potential for UWB interference with GPS are presented to put the results in context. In some cases, more in-depth technical information is included in the appendices.

TABLE OF CONTENTS

TABLE OF CONTENTS (CONT'D)

TABLE OF CONTENTS (CONT'D)

TABLE OF CONTENTS (CONT'D)

LIST OF FIGURES

LIST OF FIGURES (CONT'D)

LIST OF FIGURES (CONT'D)

LIST OF FIGURES (CONT'D)

LIST OF TABLES

PAGE

EXECUTIVE SUMMARY

The Johns Hopkins University Applied Physics Laboratory (JHU/APL) has conducted a focused and independent assessment of the effects of ultra-wide band (UWB) emissions on GPS receiver performance. This assessment is based on a statistical evaluation of data collected by the Applied Research Laboratories University of Texas at Austin (ARL:UT) along with a strictly theoretical analysis. The ARL:UT data were gathered using six specific GPS receivers, two configurable UWB device types and four other devices currently regulated under FCC Part 15 rules.

The objective of this assessment was to quantify the relationship among key GPS performance parameters and UWB emissions parameters such that from this work policy makers can gauge the impact of potential UWB emissions. The results of this work are being provided to the FCC to assist them in making informed regulatory decisions with regard to UWB emissions under Part 15. Based on this assessment, JHU/APL has drawn the following conclusions.

1. UWB time coding or modulation implementation determines the nature of the resulting UWB signal. This nature in turn determines the impact on a particular GPS receiver implementation and its performance. The choices of time coding parameters can produce significant differences in the amount and type of performance effect experienced by GPS receivers.

2. The theoretical analysis and statistical data evaluation show that properly time coded UWB signals can be produced that have characteristics similar to white noise within the GPS frequency spectrum. White noise energy is uniformly distributed in frequency and will not excite any complex interactions in GPS receivers. The properties of white noise allow it to be characterized by average power when taken in the context of overall GPS receiver performance, and this performance is a well studied interaction. The UWB devices tested by ARL:UT produce signals that are white noise-like. The aggregate signal produced by more than one of these devices is also white noise-like.

3. There exist coding schemes that can produce non-white noise-like UWB signals that may have a greater impact on GPS performance than those effects shown herein.

4. For UWB devices with average powers that are compliant with the current FCC Part 15 regulations, the performance of GPS receivers exhibits severe degradation when the separation between the GPS receiver and UWB devices is less than about 3 meters. This distance is based solely on the GPS receivers and UWB devices tested by ARL:UT. As the separation decreases below 3 meters, all users of these GPS receivers will be severely impacted, and in the extreme, lose lock on all satellites. This phenomenon is exhibited across all relevant measures of performance analyzed. The single Part 15 device that was analyzed induced similar behavior in the GPS receivers.

5. For separations greater than 3 meters, GPS receiver performance converges to nominal levels. The minimum separation at which degradations are acceptable depends on individual user scenarios including performance thresholds, GPS receiver and UWB device(s).

6. Variations in the measures of performance due to different GPS receivers are greater than those due to the operating modes of the UWB tested devices. The impact of UWB devices on all GPS receivers cannot be assessed using a single GPS receiver.

The reader is encouraged to use the results presented in the remainder of this report to draw additional appropriate conclusions. Based on this report and the inputs from other organizations, JHU/APL believes that sufficient information is available for the FCC to establish criteria for regulating UWB emissions. Methodologies such as those presented in this report can be used to help the FCC evaluate the application of these criteria.

CHAPTER 1
INTRODUCTION

1.0 Background

A new class of ultra-wideband (UWB) radio systems is emerging that may hold promise for great benefit for public safety, consumers, and businesses. Recent advances in the development of UWB technology led the Federal Communications Commission (FCC), in 1998, to issue a Notice of Inquiry [Reference (1)] to investigate the possibility of permitting UWB radio systems to operate on an unlicensed basis under Part 15 of its rules [Reference (2)]. Part 15 sets out regulations under which an intentional, unintentional, or incidental radiator may be operated without an individual license where the emission may occur in a part of the spectrum assigned for use by particular services (e.g., a radio station). Technical limits are defined for the maximum allowable signal level that may be emitted. Also, operation of a device under these regulations is subject to the condition that no harmful interference is caused and interference from authorized users or other intentional or unintentional radiators must be accepted [Reference (2), Section 15.5 (b)].

In May 2000, the FCC issued a Notice of Proposed Rule Making (NPRM) [Reference (3)] whereby it proposed to amend Part 15 of the rules to pave the way for new types of products incorporating UWB technology. Underlying this proposal was the belief that UWB devices can operate in spectral regions already assigned to existing radio services without causing interference, thereby permitting scarce spectrum resources to be used more efficiently. The NPRM was also designed to ensure that existing and planned radio services, particularly safety-of-life services, are adequately protected.

Of particular concern is the Global Positioning System (GPS) on which many military, commercial and civil systems have come to rely. Because some of the uses of UWB operate most effectively around 2 GHz, their emissions may include the two frequencies, which are used by GPS (L1 centered at 1575.42 MHz and L2 centered at 1227.6 MHz).

1.1 Investigating Potential Interference to GPS

Concern about potential interference with GPS led to the initiation of several test and evaluation efforts. These include work by Stanford University for the Department of Transportation (DOT) and work by the National Telecommunications and Information Administration (NTIA). In addition to the work sponsored by the government, Time Domain Corporation, a developer of UWB systems and components, has taken a very active position in addressing potential GPS interference issues. Under Time Domain sponsorship, a comprehensive testing program was conducted by the Applied Research Laboratories, University of Texas (ARL:UT) in which several high-quality GPS receivers were operated in the presence of UWB signals. The ARL:UT Test Plan is Reference (4) and their Test Report is Reference (5).

Well into the ARL:UT test effort, Time Domain Corporation contracted with The Johns Hopkins University Applied Physics Laboratory (JHU/APL) to analyze the data collected by the ARL:UT test program and prepare this report to be submitted in response to the FCC NPRM. The JHU/APL work began in October 2000 and was initially scheduled to produce the final report in January 2001. However, unanticipated delays in the completion of the ARL:UT testing delayed the JHU/APL and completion of the work and this report was rescheduled to coincide with the completion of other related work at NTIA.

It should be emphasized that in this role, JHU/APL is an independent evaluator of the ARL:UT-collected test data and not an advocate for Time Domain Corporation or UWB technology.

1.2 Scope

The ARL:UT database resulting from their testing is the most comprehensive collection of data relating to the potential for UWB interference with GPS that exists today. However, the range of parameters tested was naturally limited by time and the facilities available. Because the JHU/APL analysis was directed only at the ARL:UT data, the scope of our results is similarly limited. Nevertheless, the analysis effort provided a very indepth examination of the data and some analytic extension to produce results that should be very useful in addressing the issues in the NPRM.

1.3 Correlating Analysis Results to the FCC NPRM

The complexity of the GPS system and the UWB technology offered many challenges as well as options for presenting the results of the data analysis. The results only address the differences in performance of the GPS receivers that were attributable to UWB interference. Further, the results are presented in terms that related to the NPRM and the FCC measurement methods.

The NPRM takes the position that "the general emission limits (for intentional radiators) contained in 47 Code of Federal Regulations (C.F.R.) Section 15.209 appear appropriate for UWB devices." These field strength emission limits are 500 microvolts/meter at a distance of 3 meters from the radiator for frequencies above 960 MHz. The NPRM further notes that UWB emissions, because of their high peak-to-average power ratios, extremely narrow pulses and their pulse repetition frequencies are considerably different from those of unintentional radiators and conventional Part 15 transmitters. These differences led to the proposal of several specifications related to measurement of UWB signals. First, the NPRM proposes that the peak signal strength in a 50-MHz bandwidth be no more than 20 dB above the permitted average emission level. Next it proposes that the absolute peak limit for emissions over the UWB's entire bandwidth be variable based on the amount the bandwidth at –10 dB exceeds 50 MHz. In addition, the NPRM proposes an absolute limit of 60 dB on the difference between the peak and average power of UWB transmissions.

The results of this analysis are presented in terms of a "just compliant" UWB device. To show the effects of the UWB signals on the GPS receivers, the highest level results show several measures of performance (MOP) in terms of distance of the UWB devices from the GPS receivers. Because the principal results are based on "Conducted" vice radiated tests, these distances are the result of link calculations and an analysis that adjusted the parameters of the link calculations to best-match the conducted test results to the radiated test observations.

1.4 Organization of the Report

Chapter 2 of the report gives a brief technical review of UWB signals, including their implementation, technical characteristics of UWB emissions, and the parameters of interest in the analysis of the ARL:UT test data.

Chapter 3 gives a brief but comprehensive overview of the GPS and the characteristics of the system that are of interest in this evaluation.

Chapter 4 gives a brief overview of the testing done by ARL:UT, the devices that were tested and the data that were collected. The ARL:UT Test Plan [Reference (4)] describes the tests to be performed; the results of that effort are reported in the Test Report [Reference (5)]. The collected data were posted on an ARL:UT web site and are available for examination and analysis by anyone interested. The URL for the data site is ftp://www.arlut.utexas.edu/pub/uwbdata/UWB_Test_Data/.

Chapter 5 describes the theoretical analysis that addressed two major elements. The first concerns how to treat the results derived from the ARL:UT test data within the limitations and special characteristics of the test configurations. The second concerns the development of a mathematical model that can confirm the results of test data analyses, and provide a tool for estimating performance for conditions beyond those that were tested.

Chapter 6 describes the analysis the ARL:UT-collected data in terms of the objectives and approach, the tools used, the methodology by which the data were analyzed, the measures of performance selected and finally the results of the analysis.

The report includes a list of references, acronyms and abbreviations, and a number of appendices containing more detailed technical material relating to the data analysis.

CHAPTER 2
ULTRA-WIDEBAND (UWB) SIGNALS

2.0 Introduction

The origin of UWB technology (originally called time-domain electromagnetics or baseband signals) was in the 1950s and 1960s at several institutions, such as MIT Lincoln Laboratory, Catholic University of America [Harmuth, Reference (6)], the Sperry Rand Corporation (Ross & Robbins), and USAF's Rome Air Development Center (van Etten). Patents followed in the 1970s and 1980s [Robbins, Reference (7), Robbins & Robbins, Reference (8), Ross, References (9) and (10), Ross & Lamensdorf , Reference (11), and Ross & Robbins, References (12) and (13)]. In 1978, Bennett & Ross published a paper, "Time-Domain Electomagnetics and Its Applications," in the Proceedings of the IEEE, Reference (14). This paper promulgated the concept of UWB and its usefulness throughout the technical community. In the past two decades, several companies (including Time-Domain Corporation, Fantasma, Xtreme, Aetherwire & Location, Inc., and Multispectral Solutions, Inc.) have researched and developed UWB devices for use in communications, radar, and tracking.

2.1 UWB Definition

A UWB electromagnetic signal is loosely defined as any electromagnetic signal for which the bandwidth (at –10 dB) is greater than 25 percent of the "center" frequency. Most UWB implementations have no carrier frequency at all, and thus the determination of peak frequency or median frequency is not necessarily the same as the center frequency, in distinction to the case of a modulated continuous wave carrier. Even for a long sweep chirp waveform, the center frequency is relatively well defined. However, UWB transmissions are not limited to these types, and can be produced with diverse and potentially noise-like signal characteristics.

The class of UWB transmissions examined here consists of impulsive type bursts put together in pulse trains that are then encoded with information. The bursts can be monocycles, doublets, or any type of radiation where the time scale for any significant energy is small compared to any pulse train time parameters, and having enough bandwidth to classify as UWB signals before pulse train encoding. In all that follows, these impulsive signals will be referred to as pulselets. In most cases of UWB transmission, there will be a small number of pulselets to consider. Often, only one or two pulselets comprise the basis for subsequent time encoding. The analysis should not be tied too closely with a specific pulse type. Within certain caveats to be defined, the effects of many burst shapes may be analyzed within the same framework, allowing more general conclusions.

The pulselets are then constructed into pulse trains. Information coding can be added in the form of a time variation between pulselets, switching between the small number of pulselet types, or both. For example, information can be coded as a small time offset from an expected pulselet time locus within the pulse train. The expected time locus needs not follow a regular pattern. In fact, systems are operating in which the expected time locus is drawn from a pseudo-random time offset sequence. This has the benefit of decreasing any spectral content induced by the pulse train coding. Information coding may then be an additional offset from this sequence, or in the choice of pulselet.

One example of a pulselet of a monocycle type is a differential Gaussian, which is defined as:

$$f(t) = -Ate^{-\left(\frac{t}{\tau}\right)^2} \qquad F(\omega) = i\frac{\sqrt{\pi}}{2} A\omega\tau^3 e^{-\left(\frac{\omega\tau}{2}\right)^2}$$

Figure 2-1 shows the electric field intensity as a function of time, as well as power as a function of frequency, showing this monocycle to be a pulselet of small time duration and large bandwidth. This type of pulselet is similar to that in a proposed UWB communication system, where the information is to be completely in the pulse train coding. A pulselet of this type will be used in the Theoretical Analyses section of this report (Chapter 5).

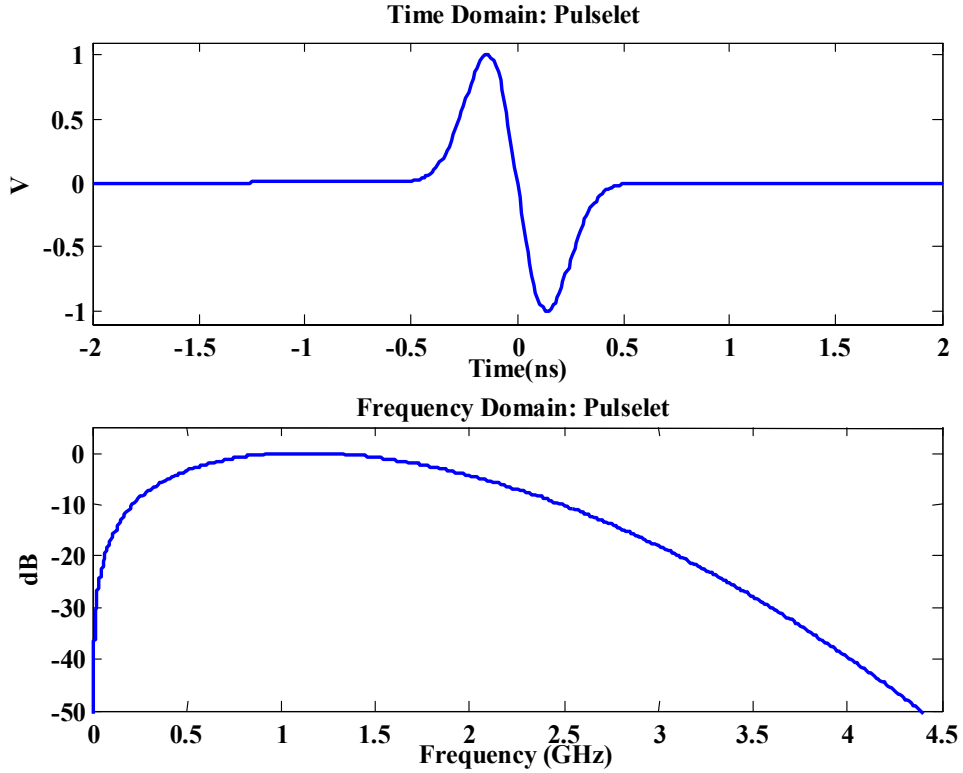

Figure 2-1 Time and Frequency Plots for Monocycle Pulselet

Another example of a set of pulselets, each constructed of two distinct Gaussian monocycles may be defined as:

$$g(t) = \pm\frac{A}{2}\tau^2\left(e^{-\left(\frac{t+\frac{t_0}{2}}{\tau}\right)^2} - e^{-\left(\frac{t-\frac{t_0}{2}}{\tau}\right)^2}\right)$$

$$G(\omega) = \pm\frac{\sqrt{\pi}}{2}A\tau^2 e^{-\left(\frac{\omega\tau}{2}\right)^2}\left(e^{\left(\frac{l\omega t_0}{2}\right)} + e^{-\left(\frac{l\omega t_0}{2}\right)}\right)$$

Figure 2-2 shows the time and frequency plots for this set of pulselets. Here, the two pulselets represent distinct digital values, and the pulse train sequence is not used to carry the data, but rather to separate the bits and possibly decrease the potential for large spectral lines. This type of pulselet scheme is similar to that in another proposal for UWB use [see Reference (15)].

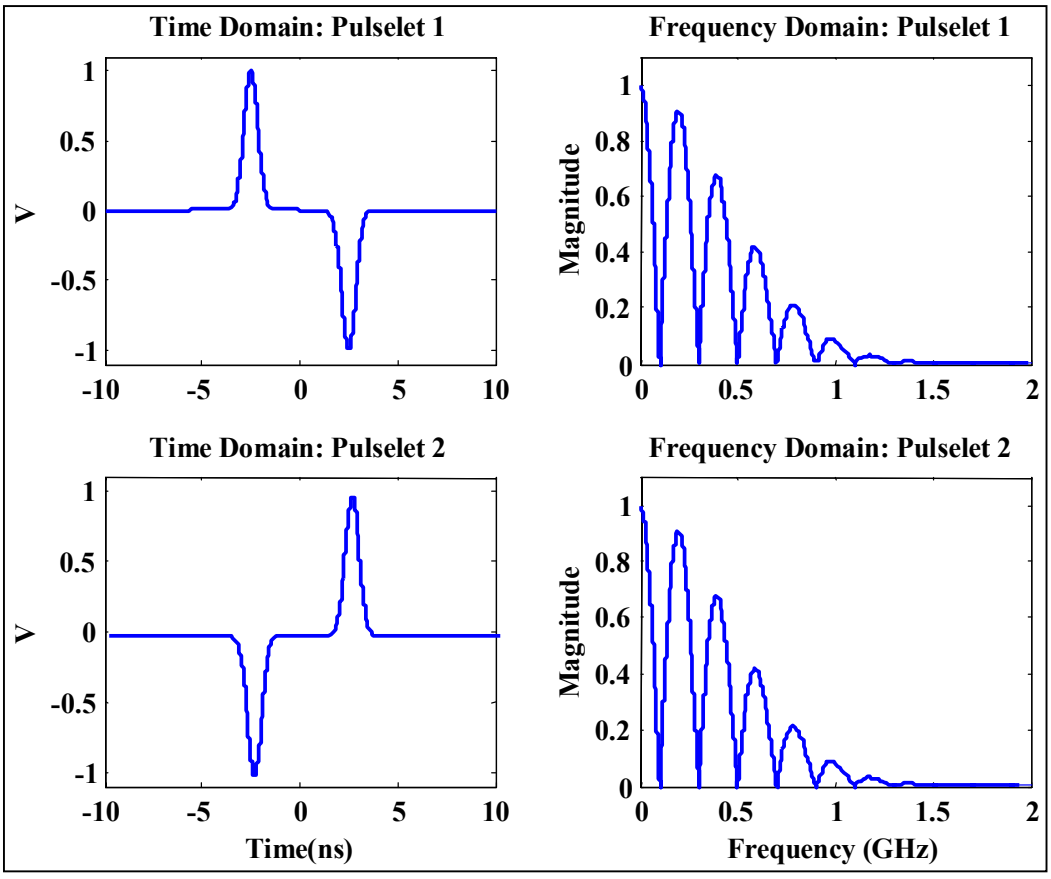

Figure 2-2 Time and Frequency Plots for Two Sets of Gaussian Pairs

CHAPTER 3
GLOBAL POSITIONING SYSTEM (GPS)

3.0 Introduction

The GPS is a satellite-based positioning system originally developed to meet Department of Defense (DOD) weapon system requirements. Since the mid-1980s it has become an increasingly important positioning resource for the civil community, and its use is expanding into many safety-of-life civil applications. GPS satellites transmit specially modulated radio signals that when received by a GPS receiver system will produce an estimate of the user position. Positioning is based on the receiver measuring the signal propagation delay of epochs transmitted from each satellite. The satellite clocks are synchronized by the GPS control system. Therefore, the measurement of four synchronized epoch-delays from four satellites at defined locations will define the position of the user and the offset of his clock relative to GPS time. The satellites are orbiting the earth in approximate 12-hour orbits and their time-varying positions (ephemerides) are defined by message data sent on the same transmissions that supply the epoch measurements. There are many subtle details associated with the ephemeris, clock, and signal propagation that influence the user's position accuracy. However, typical user equipment is designed to make all the necessary corrections, and the user simply sees the results of the navigation computation. There are numerous references for those interested in a more complete understanding of GPS; this report is concerned primarily with the nature of GPS signal reception.

3.1 GPS Signals

The objective of this study is to examine the potential that proposed ultra-wideband (UWB) transmissions would interfere with the safe use of GPS. The important aspects of GPS to this study are the nature of the GPS signals and the receiver techniques used to recover those signals. GPS satellites transmit two navigation signals:[1] the primary signal (referred to as L1) is centered at 1575.42 MHz, the secondary signal (referred to as L2) is centered at 1227.6 MHz. Two signals are used to correct for signal refraction caused by propagation through the ionosphere. The signal epoch is identified as a specific phase transition of a biphase code modulation on each signal. There are two codes modulating the L1 signal: a clear/acquisition (C/A) code with a clock rate of 1.023 MHz, and a protected (P/Y) code with a clock rate of 10.23 MHz. The two biphase code modulations are orthogonal to each other (i.e., one shifts the carrier phase between 0 and π and the other between $\pm\pi/2$). The length of the C/A code is 1023 bits long; therefore, the C/A code epoch phase transition provides a GPS "clock-tick" for each millisecond of the satellite clock (i.e., 1023 bits clocked at 1.023 MHz complete one cycle in 1 millisecond). The P/Y code length is very long; it is actually reset at the beginning of each week, and it never completes a full code cycle. The other aspect of the P/Y code is that it can only be

[1] *Other signals are being proposed for the future, but this study is limited to the currently available signals.*

fully recovered by authorized users who can properly decrypt the code signal. The L1 transmission is filtered to limit its spectrum to approximately 20 MHz. The L2 signal is only biphase modulated by the P/Y code, and its spectrum is also filtered to about 20 MHz. Both signals carry identical message modulations at 50 Hz. Both carriers and all clocks (code and data) are derived from the satellite reference oscillator. Nominally, the reference oscillator frequency is 10.23 MHz. The L1 frequency is 154 times the reference and the L2 signal is 120 times the reference. The P/Y clock frequency is at the reference frequency, and the C/A clock is at one-tenth the reference. As you might guess, the data rate is set such that each data bit is equal in length to 20 ticks of the C/A code epoch (i.e., the data rate is equal to the C/A clock rate ÷20460).

The transmitted code signal spectrums are illustrated in Figure 3-1. The envelope for the code modulation is defined, as a function of code clock frequency f_c, as $\left(\frac{\sin(\pi f_c t)}{\pi f_c t}\right)^2$ with the first nulls appearing at ± the code clock frequency relative to the carrier frequency. For the P/Y code the main spectral lobe (i.e., region between the first nulls) fills the bandwidth allowed by the transmit filter, but the C/A code also passes several side lobes. The C/A code spectrum is comprised of lines separated by 1 KHz within the indicated envelope. The lines are set by the repeat cycle of the code sequence. The P/Y code spectrum does not consist of specific lines because of the nature of the code sequence; it depends on the code segment captured in the spectrum. Message data add small details around the 1-KHz C/A code lines.

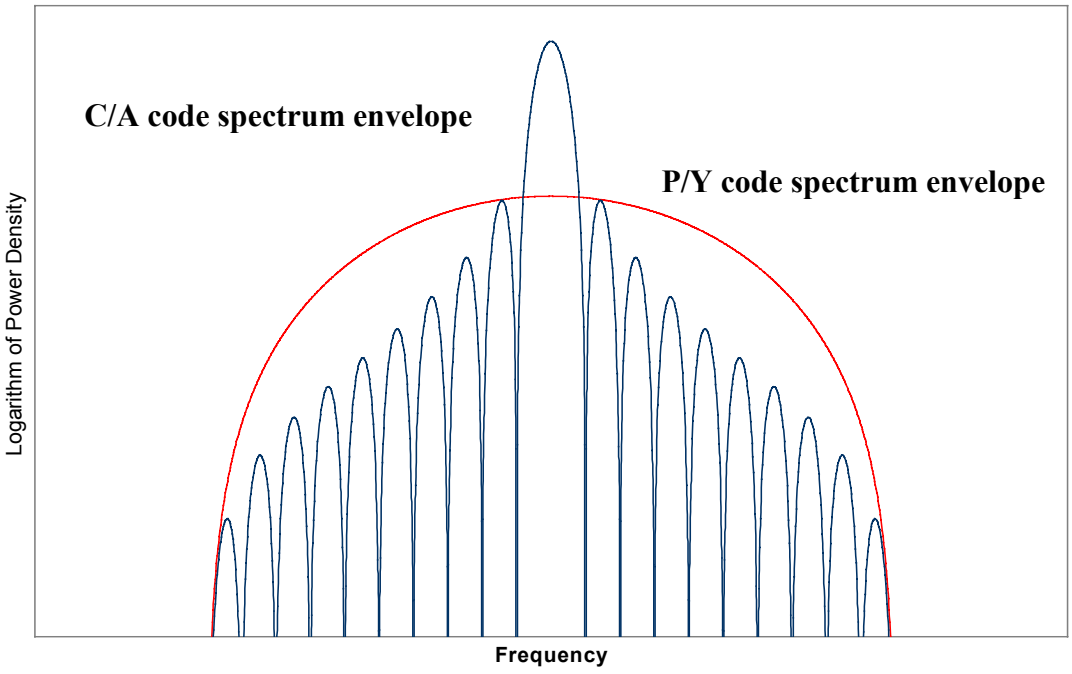

Figure 3-1 P/Y and C/A Spectral Envelopes

Each of the three signals (L1-C/A, L1-P/Y, and L2-P/Y) are transmitted at different power levels. Each satellite provides signal coverage over the its visible region of the earth (on the order of 10^{14} square meters). The limitations on available satellite power and the large service area restrict the power density available to a user. Furthermore, the user requires an antenna with a clear view of the full sky without the complexity of multiple tracking antenna beams. Taken together these constraints limit the power available to a user's GPS receiver. The satellite signals are all transmitted with right-hand circular polarization. The GPS system specification is based on providing a minimum signal power level at the output of a 0 dBi right-hand circularly polarized antenna. The specified values are shown in Table 3-1.

Table 3-1
Specified Minimum GPS Signal Levels
(at the output of a 0 dBi right-hand circularly polarized user antenna)

Signal	Minimum Power (dBm)
L1 – C/A	-130
L1 – P/Y	-133
L2 – P/Y	-136

3.2 GPS Receivers

GPS receivers come in many flavors, and they exhibit a wide range of imaginative designs. This is possible because they are required to be integrated with computers that provide the navigation computations, and most take advantage of their computational capabilities for signal processing and error correction functions. Most receivers digitize the GPS signals and use digital hardware and software to accomplish signal tracking and message recovery. The details of specific receiver designs are not usually available because of the competitive nature of the GPS receiver market place.

The fundamental receiver functions are signal epoch recovery, signal carrier phase tracking, and message recovery. Epoch recovery is accomplished with some variation of a classic Delay Lock Loop (DLL). The DLL is based on correlating the received signal with a locally generated replica signal. The code signal has properties similar to a radar pulse with a pulse width equal to one cycle of the code clock frequency (i.e., a C/A equivalent pulse is about 1 μsec). Classically, two correlation products are formed, one for an "early gate" (local code set ½ "pulse" early) and a "late gate" (½ "pulse" late) and these are swept through the received signal space until the received "pulse" falls between the two gates. At that point, the DLL feedback is activated to attempt to maintain the received signal midway between the two gates. In modern digital implementations, many more correlation products are formed and used creatively to first speed up the acquisition process and secondly to provide a more accurate measurement of the

received epoch. Carrier phase is tracked with a Phase Locked Loop (PLL). The PLL develops a local carrier signal that is compared with the received signal in a phase comparison that produces an output proportional to the phase difference between the two signals. The phase "error" signal is used to control the local signal generation to minimize the phase difference. The local carrier signal also needs to be swept during the acquisition process. Recovery of the GPS signal requires a two-dimensional acquisition search of both modulated signal code and carrier phase. Finally, message recovery is accomplished by developing another tracking loop that develops the data rate clock used to read the digitally encoded message.

3.2.1 GPS Receiver Processing

GPS receiver is an overly simplistic name that tends to be misleading. The basic function of the GPS receiver is to provide its user with an estimate of current position. To accomplish that function, the receiver may be receiving signals simultaneously from up to 12 satellites. It will be measuring an epoch receipt time from each satellite and the phase change along each satellite signal path. These measurements are converted to an estimate of distance to each satellite (*range*) and velocity along each line of site (*range rate*). That is, the receiver is like a radar receiver measuring range and velocity to as many as 12 targets. The difference between radar and GPS is that the transmit and receive clock is not developed from the same oscillator. Therefore, the GPS receiver's range measurement has an error due to the offset between its clock and GPS time, and its range rate measurement has an error due to the offset between its reference oscillator frequency and the GPS reference oscillator frequency. The GPS satellites use atomic standards that allow all satellite clocks to be adequately synchronized. The user is not required to have such a high-quality frequency standard because GPS is designed to provide sufficient measurements to allow the user to estimate the errors in their clock. The user's measured quantities are often referred to as *pseudorange* and *pseudo-range-rate*, recognizing these measurements need to be corrected for clock errors.

To make use of the pseudorange and range-rate along the lines of sight to each satellite in view, the user must know the location of each satellite. Actually, since the satellites are not stationary, the user needs to know something of the dynamics of each satellite. The physics of satellite motion are sufficiently well known that their motion details can be defined with relatively few parameters. Each satellite broadcasts a message that defines its motion with high accuracy (i.e., it provides its ephemeris). The GPS receiver recovers the message data and computes the satellite position, and because of the character of the ephemeris data, it can also compute future positions with very little loss of accuracy. Given a highly accurate knowledge of each satellite's position and velocity, and a measurement of pseudorange and range-rate to each satellite, users can compute their position, velocity, and clock errors. It is important to note that once users have sufficient information to first determine position, they also have information to estimate a future position. Therefore, the receiver can estimate the next pseudorange and range-rate measurements to each satellite before the signal is received. It can even continue to successfully navigate, for some period, with degrading accuracy after losing GPS signals.

Satellite message data include additional information. The message from one satellite includes information about the locations of all other satellites and their status (e.g., are any

currently out of service). Therefore, the GPS receiver provides in the initial navigation operation, sufficient information to describe the full satellite constellation geometry. The message also includes a high degree of redundancy and predictability (including redundancy across satellites and on the two navigation signals). Therefore, not only can users estimate their next pseudorange and range-rate measurements, they can also make a reasonably good estimate of the data bits in the next message cycle. This is not typical of a communications receiver; the information bandwidth of GPS message data are very small after the initial navigation and with the inclusion of all the redundancies.

Pseudorange measurements from four satellites are required to determine a three-dimensional position; the three components of position, and the user epoch error. Similarly, pseudorange-rate measurements from four satellites are required for a three-dimensional velocity determination; the three components of velocity and the user frequency error. Position accuracy depends on the accuracy of each range measurement and on the geometry of the lines-of-sight.

Four measurements with small angular separations will produce a less accurate position measurement than one with larger angular separations. This geometric effect is called Dilution of Precision (DOP). Receivers typically provide several DOP parameters, one for three-dimensional position (PDOP), one for horizontal position (HDOP), and one for vertical position (VDOP). These parameters multiplying the range uncertainty of the satellite measurements provide an estimate of the position uncertainty. A similar process can be defined for velocity uncertainty, but it is not normally provided. The separate horizontal and vertical parameters are used in conditions where the navigator has a different sensitivity to errors in each direction. GPS typically has weaker geometry in the vertical direction. A user less sensitive to vertical error may wish to understand the position uncertainty of the separate components. In a circumstance where users have accurate knowledge of vertical position, they could decide to use GPS to measure only horizontal position and then only HDOP is important to that user.

GPS coverage today typically provides 7 to 8 satellites in-view, and it may provide up to 12. As more satellites are made available to the computation, the DOP parameters and the navigation uncertainty get smaller (i.e., the navigation is more accurate). Receivers with limited tracking capability can use the DOP calculations to select the best group of satellites to track and can decide the best time to shift from a satellite going out of view to one coming into view. At lower elevation angles satellite propagation errors increase and receiver antenna gain decreases; these conditions are also considered in making satellite selections. Most modern receivers have an all-in-view satellite tracking capability and use optimal filtering techniques in their navigation computation to account for measurement uncertainties. Properly used, these techniques allow all measurements to be included with a weighting function that accounts for degraded measurements. Some navigators also exploit additional sensors (e.g., inertial instruments) that provide additional accuracy and robustness in the navigation solution. Naturally this methodology also allows the user to optimally continue navigating as the number of satellites decrease.

In some critical applications, the receiver system may use the measurement redundancy provided by extra satellites to assess the reliability of each measurement. Although the GPS

monitor system will normally provide notification of satellites not to be used, there may be times when a satellite error occurs that has not yet been detected by the monitor system. To guard against this possibility, a receiver can compute its position for the N possible (N-1) groupings of satellites-in-view. Each position measurement can then be used to examine the range measurement from the unused satellite. If any of these range measurements fall outside the expected uncertainty, that satellite can be omitted from the solution and the process can be repeated again beginning with the remaining (N-1) satellites. This type of processing is an example of Receiver Autonomous Integrity Monitoring (RAIM). These techniques are also made more robust when combined with additional sensing information.

The above discussion is only intended to indicate some of the many variations in processes used by GPS receivers. Not all receivers utilize the same strategies with regard to signal recovery and navigation. The degree of complexity is adjusted to minimize cost-to-performance ratio for specific applications with some extras added for anticipated market advantage. It should be clear that characterizing interference of these receivers is a tedious task.

3.2.2 Receiver Outputs

It should be no surprise that all receivers do not output the same information. For our purposes we will classify the receiver outputs into three categories: top level information, message data, and raw measurement data. The following paragraphs provide a brief description of receiver outputs; a more detailed discussion of these outputs and the analysis methods used to identify interference is provided in Chapter 6 of this report.

3.2.2.1 Top Level Information

Top level information consists of the navigation data (position and velocity) and clock data. It can include data related to the nature of the navigation solution, such as the receiver's estimate of position uncertainty, the number of satellites used in the solution, and the PDOP. It is difficult to evaluate interference impact by observing degradation in these factors. As noted before, the navigation solution might continue to look reasonably good for some time after the interference is initiated. This could be a particularly important issue in testing designed to evaluate receiver reacquisition performance (there is an indication of this difficulty within the data evaluated in this study, which is discussed in the data analysis section). The number of satellites being used is not necessarily a good indicator because it may reduce because of natural changes in satellite coverage or because some satellite has been temporarily removed from service. Top-level information includes an indication of the signal-to-noise ratio (SNR) for the signal received from each satellite. This can be a good indicator of the impact of interference (to the extent that the interference acts like additive noise), but it too will vary due to natural variations in parameters like antenna gain. While it is important to characterize how signal interference impacts these outputs, it requires careful analysis to separate the naturally occurring changes from those created by interference, and the description of the impact can be complex.

3.2.2.2 Message Data

At first thought the message data might be a very good thing to evaluate. The basic message bandwidth is actually wider than that used by either range or phase tracking functions. If receivers provided the direct message bit stream as an output, it might be a useful for measuring interference effects. However, GPS receivers only provide interpreted message data, and given the extensive opportunities for message correction, these data are a poor indicator of interference.

3.2.2.3 Measurement Data

The raw measurement data are the pseudorange and range-rate data provided from the receivers tracking functions. These tracking functions provide a direct measure of the noise-in-signal that can be used to assess the impact of interference. Again, as with bit-error-rate and signal-to-noise, these data will provide a direct measure of interference effect, but the causes of performance degradation must be sorted out between natural signal reduction and interference.

3.2.3 Receiver Interference Suppression

The antenna and preselect filtering provide out-of-band interference suppression. The pre-select filter shape factor (i.e., sharpness of the band edges) is normally limited to minimize insertion loss between the antenna and low-noise preamplifier. However, this filtering is important for keeping strong near-band interference from producing nonlinear intermodulation products within the preamplifier. Beyond the preamplifier, after the receiver noise performance is established, sharper filter shapes are used to further reduce out-of-band signal energy into the receiver tracking functions.

The signal tracking functions provide the basic measurements needed for navigation. The DLL is based on recovery of the code modulation that spreads the received satellite signal power over the full transmission bandwidth. The most important aspect of the GPS receiver's ability to suppress interference is the code correlation function. The correlation process compares the phase of each received code bit with that of the local code and integrates the product over the longest allowable interval. If the code is sufficiently unique, other incidental signals will be randomly correlated with the local code and their product is greatly reduced. The bandwidth reduction accomplished by the correlation process (code signal bandwidth-to-1/integration time) can provide a gain equal to this ratio with regard to reducing the impact of an interfering signal. For example, an interference tone centered on the received signal spectrum will be spread by the receiver correlation function in the same way that the original signal was spread by the code modulation. That is, its peak level is reduced by the reciprocal of the code-length. Naturally, the impacts of off-center tones or multiple tones are more complex to analyze.

PLL trackers suppress interference in the opposite manner, that is, they use the narrow band character of the desired signal to allow filtering of signals outside the required tracking bandwidth. The code correlation process essentially reconstructs the received spread spectrum signal into a tone that is filtered in the PLL bandwidth.

Combinations of noise-like and tone interference signals and the composite effects of multiple interfering sources make the analysis of receiver interference suppression quite complex. Specific interference conditions can be analyzed, but the more general estimation of receiver suppression capability can only be estimated statistically and different receiver implementations should be expected to provide different capabilities. These issues and the specific receiver characterizations used are discussed in Chapter 5 of this report.

CHAPTER 4
APPLIED RESEARCH LABORATORIES, UNIVERSITY OF TEXAS (ARL:UT) DATA SYNOPSIS

4.0 Introduction

This chapter describes the Global Positioning System (GPS) data gathering effort performed by ARL:UT and the data products generated and distributed to the general public on their ftp site [Reference (16)]. Details from the ARL:UT Test Plan [Reference (4)] and ARL:UT Final Report [Reference (5)] that are key to The Johns Hopkins University Applied Physics Laboratory (JHU/APL's) data analysis are outlined in this chapter, including some information not obtained directly from ARL:UT's ftp site, but instead from question and answer correspondence between JHU/APL and ARL:UT.

4.1 ARL:UT Data Collection Test Plan/Test Report

ARL:UT's data collection effort was performed using three methods: Conducted, Radiated, and Aggregate. Conducted data collection was performed in an laboratory environment using an instrumented radio frequency (RF) network (Figure B-2) containing a GPS simulator, a White Noise generator, an Federal Communications Commission (FCC) Part 15 compliant Time Domain Corporation (TDC) Ultra-Wideband (UWB) PulsON Application Developer (PAD) device (S/N 103), and several selected GPS receivers. Radiated data collection was performed outdoors using the GPS satellite constellation, a different FCC Part 15 compliant TDC UWB PAD (S/N 123), and the same GPS receivers used in the Conducted tests. Aggregate data collection was performed outdoors using 16 TDC UWB Signal Emitter/Noise Generator devices, and a subset of the GPS receivers used in the Conducted tests. All data collection methods used a Desktop PC to record the receivers' output data streams. During the Conducted tests, the Desktop PC also controlled the RF network attenuators and GPS simulator, and recorded spectral sweeps of each UWB mode.

4.1.1 Conducted Testing

The conducted testing data collection effort produced a set of files from the output data streams of the GPS receivers as they were stimulated with a composite of GPS and non-GPS signals. The GPS signals were created by a GPS simulator (see Subsection 4.1.1.3). The non-GPS signals were created from the White Noise and UWB PAD (S/N 103) sources. Each test consisted of one of three configurations - using the GPS simulator by itself, using the GPS simulator in combination with the White Noise source, or using the GPS simulator in combination with the UWB source operated in 1 of its 18 modes. The GPS simulator was initialized to the same start time and almanac for each test, resulting in data file sets highly

correlated in both time and GPS signal content, and differing only in their non-GPS signal content.

Conducted tests were further divided into Ranging and Acquisition tests. Ranging tests operated the GPS receivers in a scenario where the GPS signal was constantly available and the non-GPS signal (if any) was progressively increased over time. Acquisition tests operated the GPS receivers in warm start scenarios where the input signals forced the receivers to transition from locked to loss-of-lock and back to locked conditions.

The conducted tests were intentionally designed through the use of the laboratory amplifier/attenuator network to produce non-GPS signals with sufficient dynamic range to demonstrate when interference with the GPS signals occurs. Appendix B contains an analysis of UWB PAD device used in the conducted tests, its attenuation levels, the GPS simulator levels, and the laboratory amplifier/attenuator network configuration. It derives equivalent ranges for each UWB mode and attenuator setting that are used to covert all the data analysis results from attenuation space to equivalent range space.

4.1.1.1 Ranging Testing

In ranging tests, the composite signal (i.e., GPS simulator output, GPS simulator and White Noise generator output, or GPS simulator and UWB PAD output) was injected into the GPS receivers. Ranging tests nominally ran for 8 hours, and except for the baseline test, the attenuation on the non-GPS source (White Noise or UWB PAD) was changed every 20 minutes to the amounts shown in Table 4-1. A single file was collected for each baseline test for each receiver, and a single receiver file was collected for each value of the attenuation level of each non-GPS source for each receiver.

Table 4-1 Conducted Ranging Attenuation Settings for Non-GPS Sources (dB)

60	43	40	37	34	31	28	25	22	20
18	16	14	12	10	8	6	4	2	0

Two GPS simulator configurations were employed. The first configuration used GPS signal levels representative of actual levels measured at Holloman AFB on July 26, 2000. This iteration is termed the Live-Sky test. Five Conducted, Ranging, Live-Sky tests, were performed: the baseline test, the White Noise test, and three UWB mode tests. For each Conducted, Ranging, Live-Sky test, the GPS simulator was configured to generate outputs representative of the true GPS constellation on July 26, 2000, from 0600 – 1400 Zulu. For the baseline test, each receiver's output is stored in a single file. For nonbaseline tests, each receiver's output for each attenuation level of each non-GPS source is stored in a separate file. There are 81 receiver data files per Conducted, Ranging, Live-Sky test per receiver. A spectrum sweep file of the pre-attenuated non-GPS signal source accompanies each nonbaseline receiver data file.

The second simulator configuration used GPS signal levels equal to the minimum guaranteed GPS received power levels [Reference (17)]. This iteration was termed the Min-Level test. Twenty Min-Level, Conducted, Ranging tests were performed the baseline test, the White Noise test, and 18 UWB mode tests. For each Min-Level, Conducted, Ranging test, the GPS simulator was configured to generate outputs representative of the true GPS constellation on July 26, 2000, from 0600 – 1400 Zulu, but with the minimum guaranteed power levels. For the baseline test, each receiver's output is stored in a single file. For nonbaseline tests, each receiver's output for each attenuation level of each non-GPS source is stored in a separate file. There are 381 receiver data files per Conducted, Ranging, Min-Level test per receiver. A spectrum sweep file of the pre-attenuated non-GPS signal source accompanies each non-baseline receiver data file.

4.1.1.2 Acquisition Testing

In acquisition tests, the components of the composite receiver input signal were time-gated in order to provoke lock, loss-of-lock, lock responses in the GPS receivers. Acquisition tests nominally ran for 2 hours and each test collected data for a single input signal combination, either simulator only, simulator and White Noise of a specific attenuation (see Table 4-2), or simulator and UWB of a specific attenuation and mode. Each test contained 30 trials. Each trial lasted approximately 3 1/2 minutes and contained one lock, loss-of-lock, lock sequence.

Table 4-2 Conducted Acquisition Attenuations (dB)

45	40	35	30	25	20	15	10	5

For the baseline tests, the GPS simulator output was injected into the receivers until the receiver's acquired lock. Then the following actions were repeated for each trial:

- Allow the simulator to run for 10 seconds
- Shunt the simulator output from the GPS receiver
- Wait 30 seconds
- Regate the simulator output to the GPS receiver
- Run for 3 more minutes

For the interacted tests, only GPS simulator output was injected into the receivers until the receiver's acquired. Then the desired attenuation level of White Noise output or the desired

attenuation level and mode of the UWB output was set, and the following actions were repeated for 30 trials:

- Allow the simulator to run for 10 seconds
- Shunt the simulator output from the GPS receiver, so that only non-GPS signals are input to the receivers.
- Wait 30 seconds
- Regate the simulator output to the GPS receiver
- Run for 3 more minutes.

This entire process was repeated for each UWB mode/attenuation and for each White Noise attenuation. Acquisition tests were run for both the Live-Sky and the Min-Level configurations.

There were 39 Conducted, Acquisition, Live-Sky tests performed; three baseline tests, nine White Noise tests, and nine tests for each of three UWB modes (see Table 4-3). Unlike ranging tests, where any nonbaseline file for a specific receiver and sky combination is associated with a single baseline file, acquisition tests from a specific receiver and sky combination have three baseline files, all collected from a single run of the GPS simulator, and all from July 26, 2000, the first running from 0600 – 0800 Zulu, the second from 0800 – 1000 Zulu, and the third from 1000 – 1200 Zulu. Series of three nonbaseline tests were also performed between GPS simulator reinitializations. Table 4-3 shows a representative association of baseline and nonbaseline tests for a Live Sky scenario. There are 1170 receiver data files per Conducted, Acquisition, Live-Sky test per receiver.

Table 4-3 Time Slice Allocations for Conducted, Acquisition, Live-Sky Tests

6:00 – 8:00 AM	8:00 – 10:00 AM	10:00 – 12:00 Noon
White Noise/05 dB	White Noise/10 dB	White Noise/15 dB
White Noise/20 dB	White Noise/25 dB	White Noise/30 dB
White Noise/35 dB	White Noise/40 dB	White Noise/45 dB
M13/05 dB	M13/10 dB	M13/15 dB
M13/20 dB	M13/25 dB	M13/30 dB
M13/35 dB	M13/40 dB	M13/45 dB
M7/05 dB	M7/10 dB	M7/15 dB
M7/20 dB	M7/25 dB	M7/30 dB
M7/35 dB	M7/40 dB	M7/45 dB
M1/05 dB	M1/10 dB	M1/15 dB
M1/20 dB	M1/25 dB	M1/30 dB
M1/35 dB	M1/40 dB	M1/45 dB
B1	B2	B3

There were 93 Conducted, Acquisition, Min-Level tests performed: 3 baseline tests, 9 White Noise tests, and 9 tests for each of 9 UWB modes (see Table 4-4). Again, acquisition tests for a specific receiver and sky combination have three baseline files, all collected from a single run of the GPS simulator, and all from July 26, 2000, the first running from 0600 – 0800 Zulu, the second from 0800 – 1000 Zulu, and the third from 1000 Zulu to 1200 Zulu. Series of three nonbaseline tests were also performed between GPS simulator reinitializations. There are 2790 receiver data files per Conducted, Acquisition, Min-Level test per receiver.

4.1.1.3 Simulator Specifications

ARL:UT used two unique GPS simulators to gather conducted data. A 12-channel GSS 4760 simulator was part of the Holloman AFB configuration, and a 10-channel GSS 2760 simulator was part of the ARL:UT configuration. Conducted data for four of the GPS receivers were collected using the Holloman AFB configuration, and conducted data for the two remaining GPS receivers were collected using the ALR:UT configuration.

The simulators were configured to use “default” parameter settings except as noted in Appendix E. The simulators were initialized to July 26, 2000, 0600 Zulu and to receiver ECEF position [-740463.42, -5457015.27, 3207281.33] in meters. Each simulation run used the same broadcast ephemeris. No external reference oscillators or timing sources were used with the simulators. These simulators have the option to include a variety of error sources to the simulated signals. Error sources include simulated dual/single frequency ionosphere, troposphere, and timing group delays, anti-spoofing, selective availability, relativity and lever-arms. See Appendix E for more information on the setup and use of the simulators for the tests.

4.1.2 Radiated Testing

The radiated testing data collection effort produced a set of files from the output data streams of the GPS receivers as they were operated in an outdoor environment in the presence of the GPS satellite constellation and transmissions from a UWB device positioned at varying standoff ranges and operating in varying modes. The UWB device was the TDC UWB PAD, the same type as was used in the conducted tests, but a different unit (S/N 123), and was transmitted with an omni-directional antenna. Additional radiated tests were also performed using non-UWB sources placed at varying standoff ranges. There were four non-UWB sources. The first two were an unkeyed Radius SP10 Walkie-Talkie and a Gateway Model GP7-450 PC (with and without its cover), both Part 15 compliant devices and termed Digital Devices 1 and 2, respectively. The second two sources were Sensors and Software model Noggin 250 and model Noggin 1000 Ground Penetrating Radars (GPR). Radiated tests made no attempt to account for satellite constellation variations.

All radiated data are from ranging tests. In the radiated tests, unlike the conducted tests where up to four receivers were tested simultaneously, each receiver was tested separately, and where the receiver antenna was surveyed to a NIMA mark. Receiver positions during radiated tests were slightly different from the conducted tests. Table 4-4 shows the standoff distances between receiver and the injected data sources. The elevation angles of the injected data sources to the receiver were held between 10^{o} and 12^{o}. For radiated tests, a single receiver file was collected for each source standoff range for each UWB PAD operating mode. A single baseline receiver file was collected prior to each test.

Table 4-4. Radiated Standoff Ranges (m)

UWB PAD Device (m)									
8.0	5.0	4.0	3.5	3.0	2.5	2.0	1.5	1.0	0.5
Digital Device 1 and GPRs (m)									
8.0	5.0	4.0	3.5	3.0	2.5	2.0	1.5	1.0	0.5
Digital Device 2 (m)									
			4.0	2.0	1.0	0.5			

Only selected combinations of receiver and UWB mode were tested (see Table 4-4). There are nominally 91 files per Radiated, UWB PAD test per receiver (some receivers have more than one baseline file). There are 22 files per Radiated, GPR test per receiver. There are 11 files per Radiated, Digital Device 1 test per receiver. There are 10 files per Radiated, Digital Device 2 test per receiver.

4.1.3 Aggregate Testing

The primary goal of aggregate testing data collection effort was to characterize the additive properties of multiple UWB transmissions incident on a GPS receiver. Here, the GPS

receivers were operated in an outdoor environment in the presence of transmissions from between 1 and 16 UWB devices positioned in varying standoff ranges and operating in two modes (described in Subsection 4.3.2). The UWB devices used in aggregate testing were TDC UWB Signal Emitters/Noise Generators, all transmitted with omni-directional antennas. Aggregate tests also made no attempt to account for satellite constellation variations.

All aggregate tests were ranging type tests. In the aggregate tests, as in the radiated tests, each receiver was tested separately and antenna surveyed to a NIMA mark. Receiver positions during aggregate tests were also slightly different than for the conducted tests. Table 4-5 shows the standoff distances between receiver and the injected data sources. The elevation angles of the UWB sources to the receiver were held between 10^{o} and 12^{o}. The UWB Signal Emitters were arranged in a circle around the GPS receiver. For aggregate tests, a single receiver file was collected for each source standoff range for each aggregation of UWB Signal Emitters (1, 2, 4, 8 and 16). A single baseline receiver file was collected prior to each test.

Table 4-5 Aggregate Standoff Ranges (m)

8.0	5.0	4.0	3.0	2.0	1.0

There are 31 files per Aggregate test per receiver.

4.2 GPS Receivers

The data collection effort used six GPS receivers whose salient features are described below. See Appendix A for more detailed receiver descriptions. A seventh receiver, the Allen Osborne Turborogue SNR-8000, "was acquired for this testing, but was removed from the test program due to the interference it caused with other GPS receivers when used in the conducted test setup."[1]

4.2.1 Receiver Descriptions

4.2.1.1 NovAtel 3151

Receiver 1 is a Model 3151R GPS receiver manufactured by NovAtel Communications Ltd. More specifically, the OEM2 GPS Card version was used during the testing. This receiver is a survey quality receiver with numerous imbedded OEM applications. Twelve channels are used to parallel track coarse/acquisition (C/A) code and C/A carrier. To increase its accuracy performance, this receiver employs a narrow correlator.

[1] ARL:UT Test Report, page 19.

4.2.1.2 Ashtech Z-12

Receiver 2 is a Model Z-12 GPS receiver manufactured by the Ashtech Precision Products division of Magellan Corporation. This receiver is a survey quality receiver with numerous stand-alone and base station differential applications. The Z-12 uses 12 channels to track C/A code and carrier phase, L1 P code and carrier phase, and L2 P code and carrier phase. With Anti-Spoofing activated, this receiver employs the Ashtech Z tracking technology to mitigate the effects of the encryption and successfully track the P/Y code.

4.2.1.3 Garmin 155XL

Receiver 3 is a Model 155XL manufactured by Garmin Corporation. This receiver is an aviation quality receiver with imbedded navigation applications and user interfaces, but no ability to output raw measurement data. The Garmin 155XL uses 12 channels to track C/A code only.

4.2.1.4 Ashtech Z-Sensor

Receiver 4 is a Model Z-Sensor GPS receiver manufactured by the Ashtech Precision Products division of Magellan Corporation. This receiver is a survey quality receiver with numerous stand-alone and rover differential applications. The Z-Sensor is essentially the Z-12 technology adapted to a single circuit board with limited user interfaces. The Z-Sensor tracks C/A code and carrier phase, L1 P code and carrier phase, and L2 P code and carrier phase, but with 36 channels instead of the 12 channels used with the Z-12. With Anti-Spoofing activated, this receiver employs the Ashtech Z tracking technology to mitigate the effects of the encryption and successfully track the P/Y code.

4.2.1.5 NovAtel MiLLenium

Receiver 6 is a MiLLenium GPS receiver manufactured by NovAtel Communications Ltd. More specifically, the standard OEM3 GPS Card version enclosed in a ProPak II housing was used during the testing. This receiver is an aviation quality receiver that allows numerous autonomous and differential applications. Twelve channels are used to track L1 C/A code, L1 and L2 carrier phase, and L2 P code (or encrypted Y code). To increase its accuracy performance, this receiver employs both a narrow correlator.

4.2.1.6 Trimble 4700

Receiver 7 is a Model 4700 GPS receiver manufactured by Trimble. This receiver is a survey quality receiver that allows numerous autonomous applications. Nine channels are used to track L1 C/A code, L1 and L2 carrier phase, and L2 P code (or encrypted Y code).

4.2.2 Receiver Data Formats

Each receiver outputs its data streams in manufacturer unique formats. Table 4-6 shows the common GPS parameters, whether or not they are supported by the receivers' unique formats, and the applicable portion of the output stream. The data stream formats for the Novatel, Ashtech and Garmin receivers are described below. Efforts to obtain the Trimble receiver's data stream format were unsuccessful.

4.2.2.1 Novatel Receiver Output Stream Formats

The Novatel 3151 and MiLLenium receiver outputs are binary data streams containing four unique message types. Two types contain measurement records, are termed RGEB (3151) and RGEC (MiLLenium) records, and contain the same information, coded differently. One type contains satellite records, SATB, and one type contains Ephemeris records, REPB. The record formats are described in References (18) and (19).

4.2.2.2 Ashtech Receiver Output Stream Formats

The Ashtech Z-12 and Z-Sensor receiver outputs are binary data streams with ASCII headers containing six unique message types. The PBN records contain solution data. The MPC records contain measurement data. The SNV records contain ephemeris data. The ALM records contain almanac data and are only in the Ashtech Z-12 data streams. Two other record types, RPC and BPS, are also only in the Ashtech Z-12 data streams records. The format of these two messages Ashtech proprietary. The PBN, MPC, and SNV record formats are described in Reference (20).

4.2.2.3 Garmin Receiver Output Stream Formats

The Garmin 155XL receiver outputs are ASCII data streams containing eight unique message types. The GPGGA records contain solution data. The GPGSA records contain dilution of precision (DOP) and active satellite data. The GPGSV records contain data on satellites in view. The GPBOD, GPRMB, and GPWPL records contain waypoint data. The GPRMC records contain navigation data. The PGRME records contain estimated error data. These records are standard NMEA-0183 formats and are described in Reference (21).

Table 4-6 Receiver File Output Parameters

Outputs	NovAtel 3151, NovAtel Millenium	Ashtech Z-12, Ashtech Z-Sensor	Garmin 155XL
Ephemeris	Raw (REPB)	Parameters (SNV)	Not Available
Almanac	Not Available	Parameters (ALM)	Not Available
Time	GPS (RGEC/SATB)	GPS (PBN)	UTC (GGA/GSA)
Satellites in View	Not Available	Not Available	(GSV)
Satellites Tracked	(RGEC/SATB)	(MPC)	(GSV)
Satellites in Solution	(SATB)	(MPC)	(GSA)
Satellite IDs	(RGEC/SATB)	(MPC)	(GSV)
Satellite AZ/EL	(SATB)	(MPC)	(GSV)
Range	Range+Std (RGEC)	Code Xmit (MPC)	Not Available
Carrier Phase	(RGEC)	(MPC)	Not Available
S/N or C/No	C/No (RGEC)	S/N (MPC)	S/N (GSV)
Tracking Status	Locktime (RGEC)	Loss of Lock (PBN)	Not Available
Range Smoothing	Not Available	Corr/Quality (MPC)	Not Available
Position Solution	Not Available	XYZ (PBN)	LLH (GGA)
Velocity Solution	Not Available	dXdYdZ (PBN)	Not Available
Clock Offset	Not Available	(PBN)	Not Available
Clock Drift	Not Available	(PBN)	Not Available
DOP	Not Available	P (PBN)	P, H, V (GGA/GSA)
Sol'n Status/Mode	Status (SATB)	Not Available	Mode (GSA)
GPS Quality	Not Available	Not Available	(GGA)

4.3 UWB Devices

The UWB Devices used in the data collection effort were manufactured by TDC. Two different types of devices were used, the PAD and the Signal Emitter/Noise Generator.

4.3.1 PAD

The TDC PAD is a programmable UWB transmitter. The programmable parameters are: nominal Pulse Repetition Frequency (PRF), duty cycle, and data encoding. Each pulse from a specific PAD device is of fixed amplitude. Nominal PRF can vary from 1 MHz to 10 MHz. The spacing between the times at which each pulse fires is the inverse of the nominal PRF plus-or-minus a known, pseudorandom dither ranging from zero to 12.5 ns. Duty cycle can vary from 25 percent to 100 percent and cycle duration can vary from 1 msec to 10 msec. Data encoding can add a second dither to the pulse fire time equal in magnitude to 25 percent of the nominal pulse width modulated by a binary data stream. All ARL:UT data gathering was performed with no data encoding. For example, a PAD operating at a 10-MHz PRF with a 100 percent duty cycle

and no data encoding will fire a pulse once in every 100 nsec window. The time the pulse is fired is defined by the following equation:

$$tfire_n = t_0 + 100 * (n - 1) + d_{prn}$$

where

$tfire_n$ is the time pulse n is fired in nsec

t_0 is the time the first pulse is fired in nsec

n is the pulse number

d_{PRN} is the pseudorandom dither scale factor (0 to 12.5 nsec)

The pseudorandom dither scale factor is based on a fixed 1000 length pseudorandom code. Two different PADS were used; one for conducted (S/N 103) and one radiated testing (S/N 123). They are functionally equivalent.

UWB PADs were coupled to different RF networks for the conducted and radiated tests. In both tests, the UWB PAD output is piped through a 3-dB attenuator, then a high-pass differential-type filter. The net effect is to reduce the energy in the 0-2 GHz range. In the conducted tests, the filter output is piped through another 3 dB attenuator. In the radiated test, the UWB PAD output is piped through the UWB antenna.

Each configuration of the UWB is called a mode. The data collection effort used 18 unique modes, which are summarized in Table 4-7.

Table 4-7 UWB PAD Operating Modes

UWB Mode #	Nominal PRF (MHz)	On Time (msec)	Off Time (msec)	Duty Cycle (%)
1*,+,▷	1	Continuous	0	100
2+	1	1	1	50
3+	1	4	4	50
4+,▷	1	10	10	50
5+	1	2	6	25
6+	1	8	4	66
7*,+,▷	5	Continuous	0	100
8+	5	1	1	50
9+	5	4	4	50
10+,▷	5	10	10	50
11+	5	2	6	25
12+,▷	5	8	4	66
13*,+,▷	10	Continuous	0	100
14+	10	1	1	50
15+,▷	10	4	4	50
16+,▷	10	1	10	50
17+	10	2	6	25
18+,▷	10	8	4	66

* Used in Conducted, Ranging, Live_Sky & Conducted, Acquisition, Live_Sky tests.
\+ Used in Conducted, Ranging, Min_Level tests
▷ Used in Conducted, Acquisition, Min_Level and Radiated tests

4.3.2 Signal Emitter/Noise Generator

The TDC Signal Emitter/Noise Generator is a semi-programmable device, which operates at a nominal 5-MHz PRF, at a 50-percent (4 msec on, 4 msec off) or 100-percent duty cycle, and no data encoding. Each duty cycle configuration of the UWB Signal Emitter is known as a mode. The pulse duration is the same as for the UWB PAD devices. The dither scale factor varies from -5 to +5 ns, and the dither scale factor is based on a fixed, 2^{23} length pseudorandom code. Sixteen UWB Signal Emitter/Noise Generators were used for the aggregate tests. Specific information on the output power levels of these devices is not available. It is assumed that all the UWB Noise Generators radiate at the same level.

UWB Signal Emitters were coupled to RF networks for the aggregate tests. A UWB Signal Emitter output was piped through a 3-dB attenuator, then a high-pass differential-type filter and then through the UWB antenna.

4.4 Data Hierarchy

Figure 4-1 depicts the entire ARL:UT receiver data files hierarchy with annotations describing the specific configurations for which each set of conducted, radiated and aggregate data files was obtained.

4.4.1 Conducted Data Hierarchy

The conducted testbenches were used repeatedly to acquire data from the GPS receivers as they were subject to 1) simulated GPS input only (baselines), 2) simulated GPS input plus White Noise of varying levels, and 3) simulated GPS input plus UWB energy of varying levels and from up to 18 operating modes. Each ranging tests was performed with the GPS simulator continually operating over the same 8-hour period while adjusting the injected source attenuation every 20 minutes. Every three acquisition tests were performed with the GPS simulator continually operating over the same 6-hour period while adjusting the injected source attenuation every 2 hours and performing an acquire lock, lose lock, reacquire lock cycle every 20 minutes.

The conducted, ranging folder hierarchies are shown in Figure 4-2. The lowest level baseline folders contain data files for all receivers. The remaining lowest level folders contain a single receiver data file and a spectrum analyzer sweep file for the specific injected source, sky, mode (if UWB), and receiver. The conducted, acquisition folder hierarchies are shown in Figure 4-3. The lowest level folders contain a single data file for the specific injected source (UWB, White Noise, or none/baseline), sky, mode (if UWB), receiver, attenuation level and trial.

There are 486 total Conducted, Ranging, Live-Sky receiver data files; 81 files per receiver, comprised of 1 baseline file, 20 White Noise files, 20 UWB Mode 1 files, 20 UWB Mode 7 files, and 20 UWB Mode 13 files.

There are 2,667 total Conducted, Ranging, Min-Level receiver data files; 381 files per receiver, comprised of 1 baseline file, 20 White Noise files, and 20 files for each of all the 18 UWB modes.

There are 7,020 total Conducted, Acquisition, Live-Sky receiver data files; 1,170 files per receiver, comprised of 30 files for each of 3 baselines, 30 files for each of 9 White Noise attenuations, and 30 files for each of the 9 attenuations of UWB Modes 1, 7, and 13.

ARL:UT UWB Data FTP Site Contents

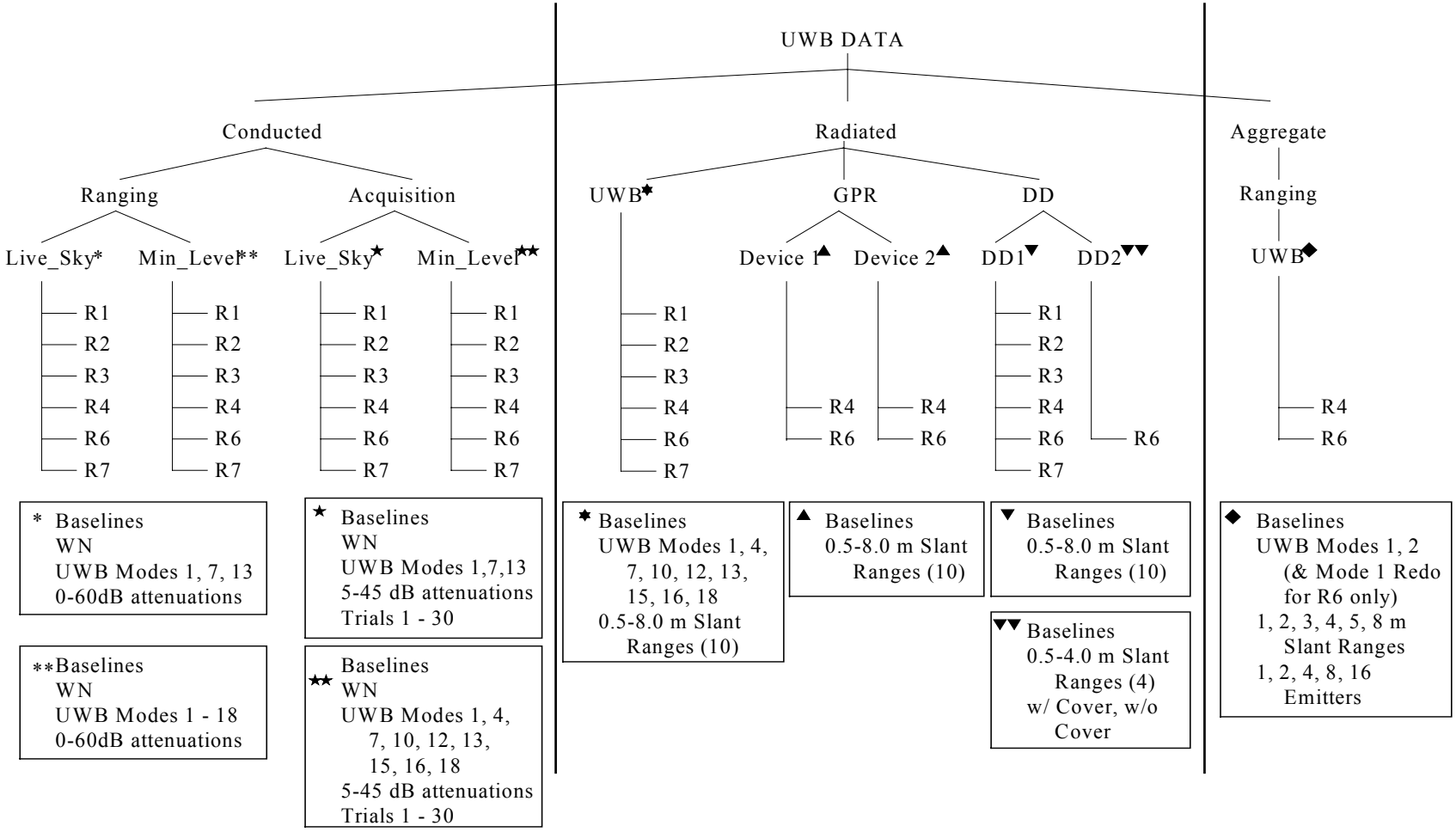

Figure 4-1 ARL:UT CURE Folder Data File Hierarchy

There are 16,740 total Conducted, Acquisition, Min-Level receiver data files; 2,790 files per receiver, comprised of 30 files for each of three baselines, 30 files for each of nine White Noise attenuations, and 30 files for each of the nine attenuations of UWB Modes 1, 4, 7, 10, 12, 13, 15, 16 and 18 attenuations.

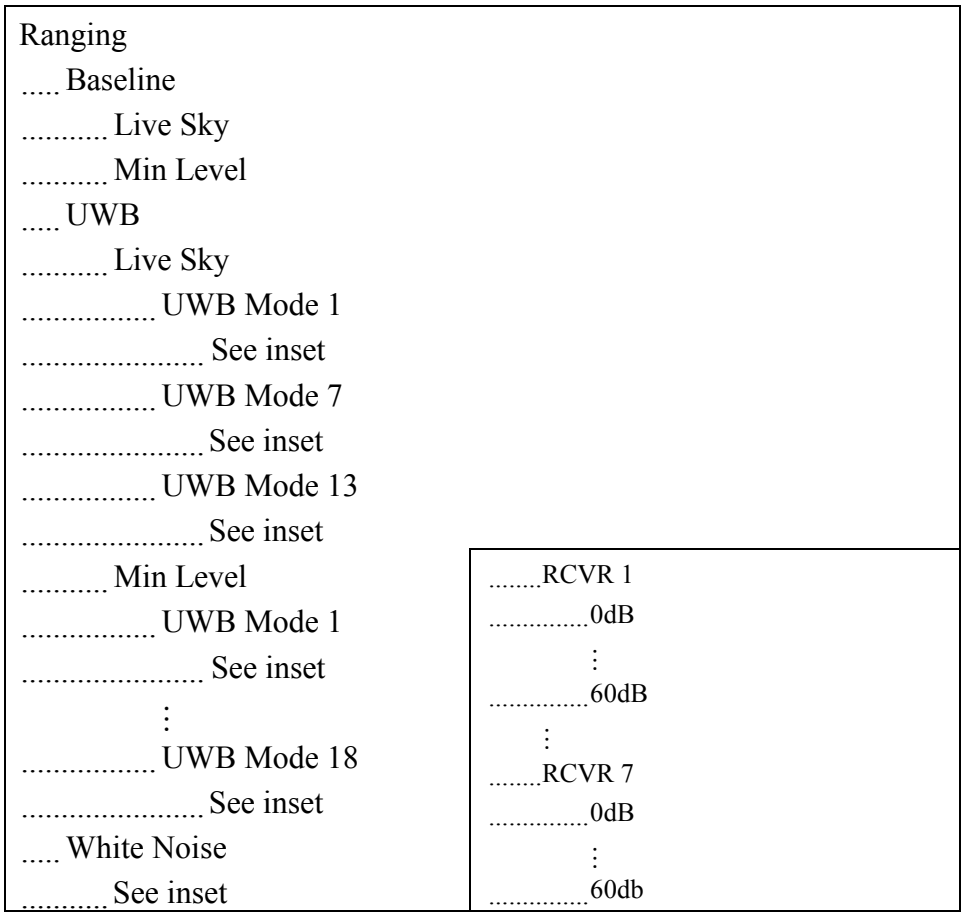

Figure 4-2 Conducted Ranging Data File Folder Hierarchy

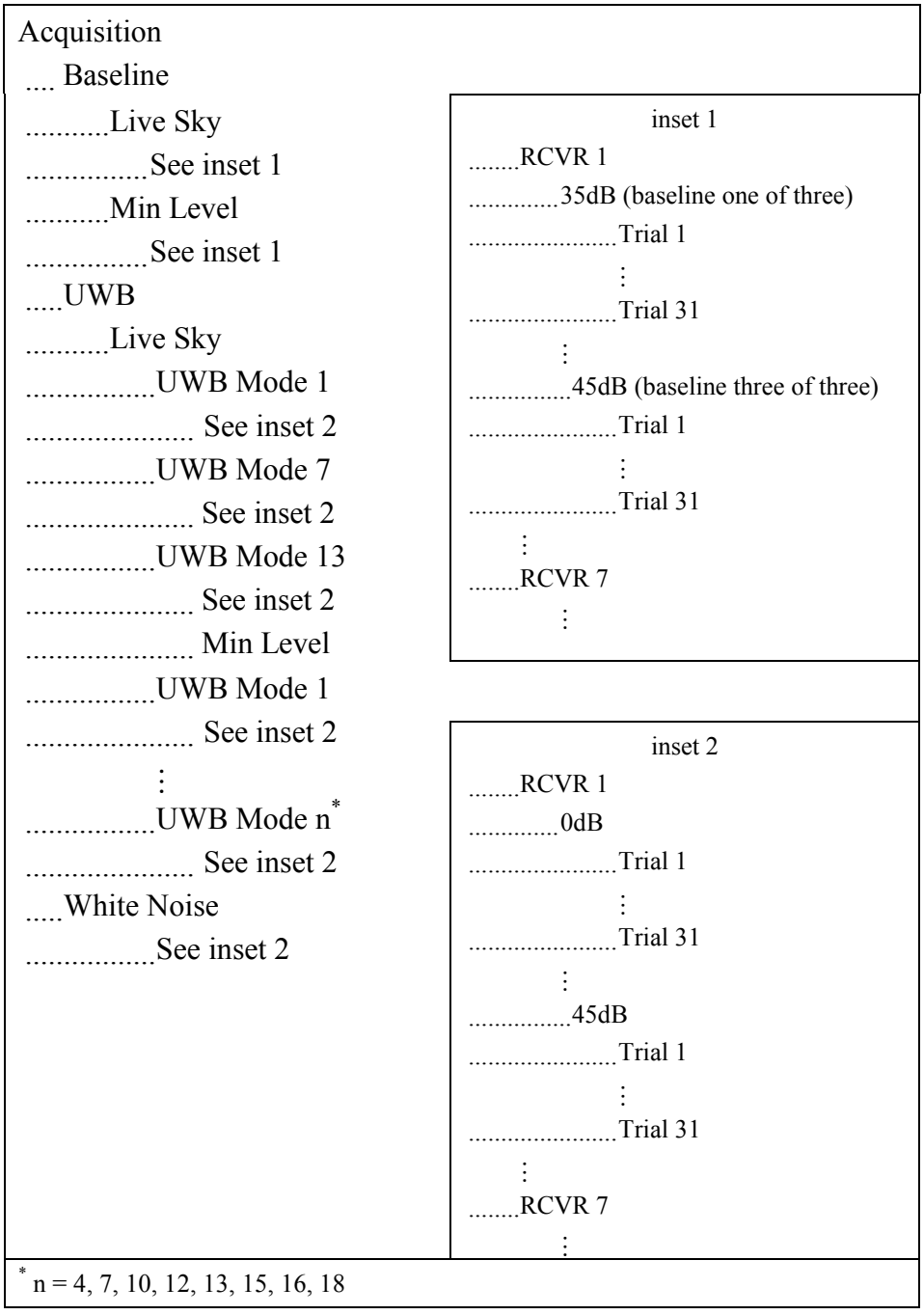

Figure 4-3 Conducted Acquisition Data File Folder Hierarchy

4.4.2 Radiated Data Hierarchy

Radiated ranging tests were conducted with the UWB PAD (S/N 123), with Ground Penetrating Radars, and with Digital Devices. The tests with the UWB PAD were performed for the permutations of receiver, UWB mode, and standoff range shown in Figure 4-4. The lowest level folders contain a single receiver data file and a spectrum analyzer sweep file for the specific receiver, UWB mode and 10 standoff ranges. Receivers one and three have no Baseline_20_Minute folders, and receiver two has Baseline_20_Minute folders in two of its UWN subfolders. Instead, these three receivers have an 8-hour baseline file in their RCVR folder. There are 572 total Radiated, Ranging, UWB receiver data files; 1 baseline and 90 UWB files for receivers 1 and 3, 3 baselines and 90 UWB files for receiver 3, and 9 baselines and 90 UWB files for receivers 4, 5, and 6.

Those tests with each of the Ground Penetrating Radars were performed for permutations of certain receivers and 10 standoff ranges as shown in Figure 4-5. The lowest level folders contain a single receiver data file and a spectrum analyzer sweep file for the specific receiver, Ground Penetrating Radar device and standoff range. There are 44 total Radiated, Ranging, Ground Penetrating Radar receiver data files; 1 baseline and composite 10 files for each of 2 devices and each of 2 receivers.

Those tests with each of the Digital Devices were performed for permutations of certain receivers and four standoff ranges as shown in Figure 4-6. The lowest level folders contain a single receiver data file and a spectrum analyzer sweep file for the specific receiver, Digital Device and standoff range. There are 76 total Radiated, Ranging, Digital Device receiver data files; 1 baseline and 10 composite files for Digital Device 1 on each of 6 receivers, and 1 baseline and 4 composite files for each of the 2 configurations of Digital Device 2 on receiver 6.

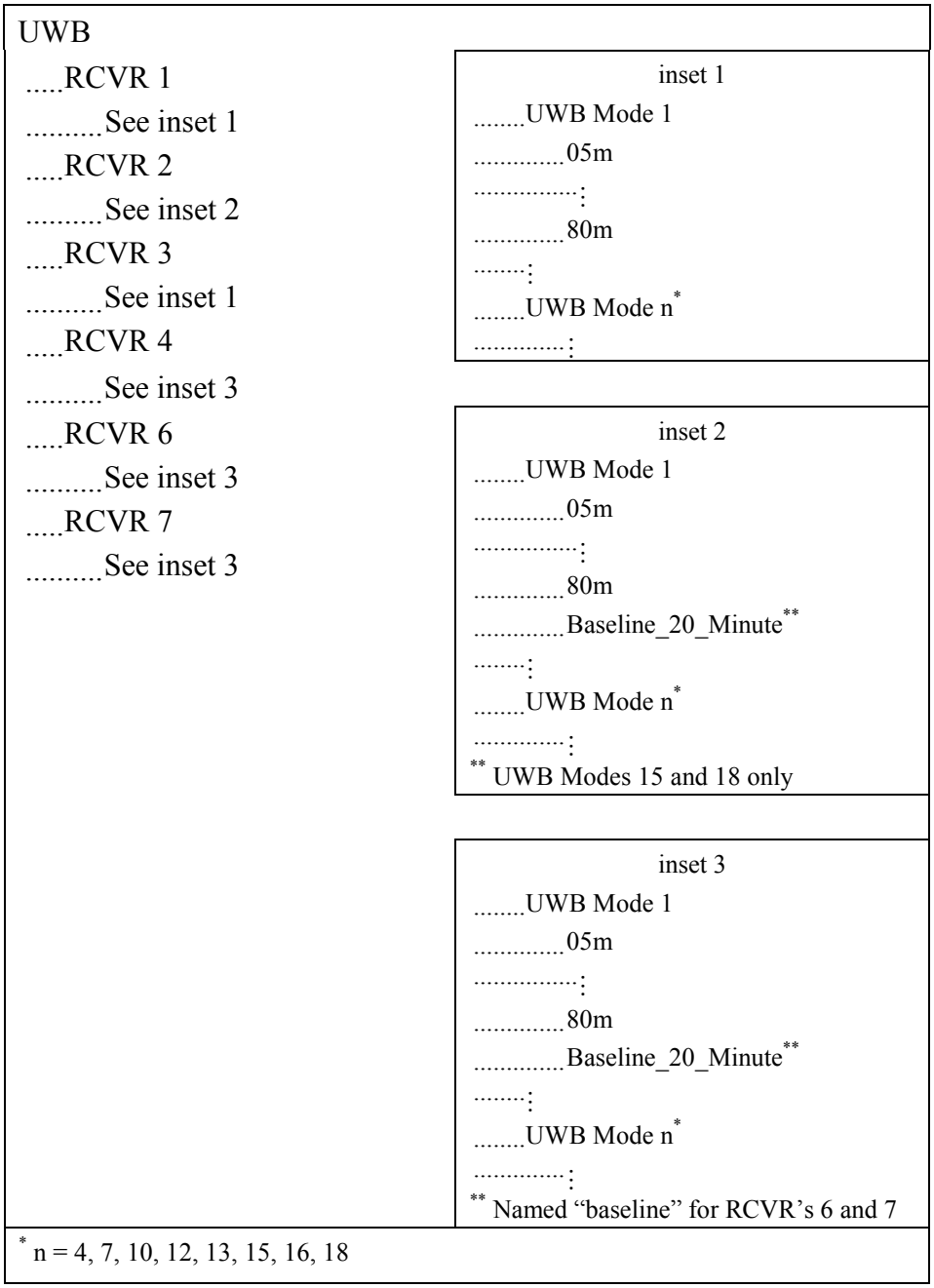

Figure 4-4 Radiated Ranging UWB Data File Folder Hierarchy

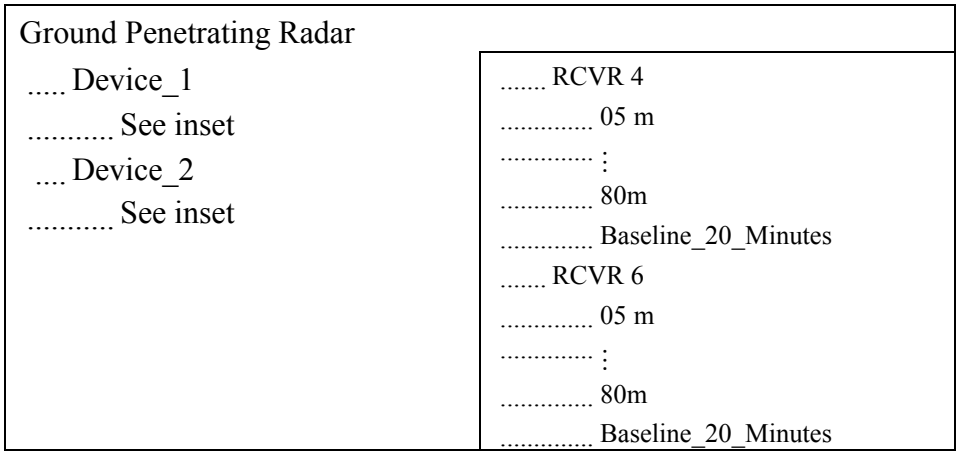

Figure 4-5 Radiated Ranging Ground Penetrating Radar Data File Folder Hierarchy

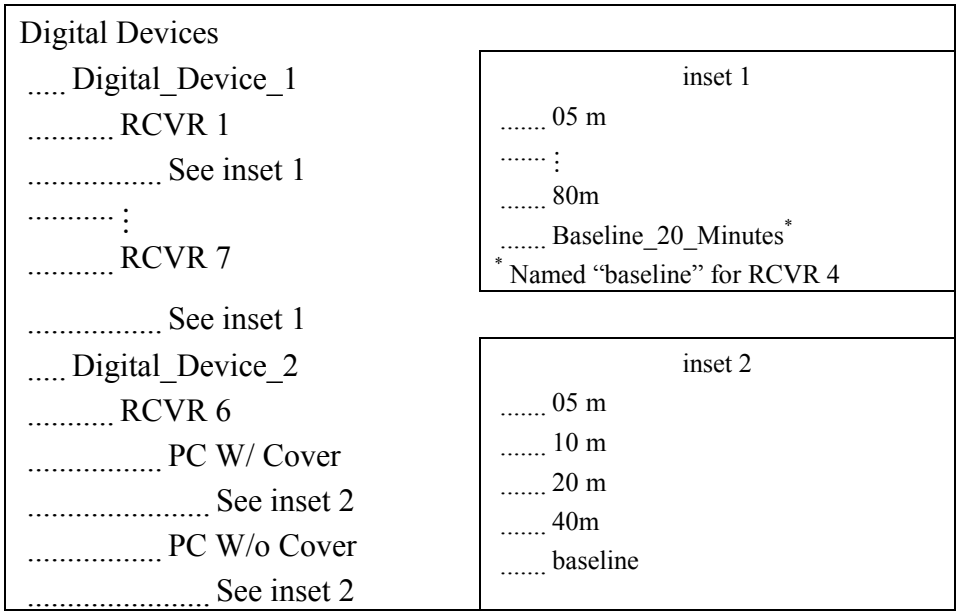

Figure 4-6 Radiated Ranging Digital Devices Data File Folder Hierarchy

4.4.3 Aggregate Data Hierarchy

Aggregate ranging tests were conducted with the UWB Signal Emitters/Noise Generators and two receivers. These test hierarchies are as shown in Figure 4-7. The lowest baseline level folders contain a single receiver data file for the specific receiver and UWB mode. The remaining lowest level folders contain five receiver data files, one each for the different aggregate numbers of UWB Signal Emitter/Noise Generators used (1, 2, 4, 8, 16), and one spectrum sweep file.

There are 155 total Aggregate, Ranging, UWB receiver data files; 1 baseline and 30 UWB files for each of 2 modes and each of 2 receivers plus the redo test for UWB Mode 1 of receiver 6.

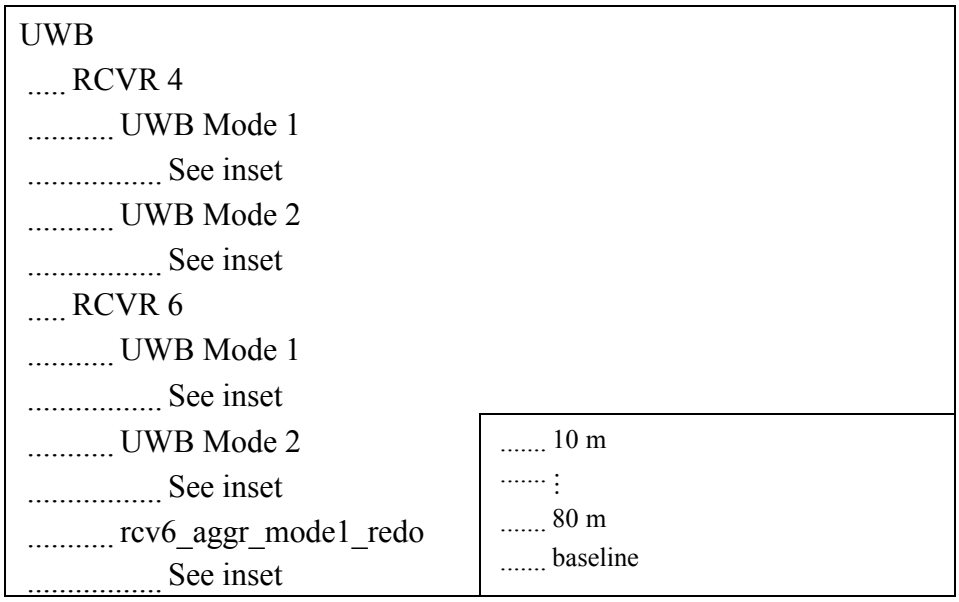

Figure 4-7 Aggregate Ranging Digital Devices Data File Folder Hierarchy

CHAPTER 5
THEORETICAL ANALYSIS

5.0 Introduction

The theoretical analysis consists of two major elements. The first is concerned with how to draw and generalize conclusions from the recorded data of the Applied Research Laboratories, University of Texas (ARL:UT) tests, and will focus on the limitations and special characteristics of the test configurations. The second analysis will provide a simulation model that can be compared to actual test results and will then be extended to analyze expected performance for some untested conditions. The objective of the analysis is to help define the conditions wherein ultra-wideband (UWB) devices can operate effectively without deleterious effect on Global Positioning System (GPS) receivers in the same environment, and to support development of a regulatory basis for assuring the beneficial use of both technologies.

5.1 Test Configuration Analysis

This section will analyze signal conditions that are inherent in the conducted and radiated test configurations. The first signal condition to be evaluated is the apparent UWB device standoff range represented by the conducted tests and its relationship to the conditions in the radiated tests. The second signal condition to assess is the impact of UWB multipath geometry in the radiated tests.

5.1.1 Equivalent Range Analysis

In order to draw comparisons between conducted tests and radiated tests, we must be able to estimate the *equivalent range* represented by the attenuation settings used to vary the level of UWB signals appearing at each GPS receiver. The test configuration is shown in Figure 5-1. This was the test configuration using the Holloman AFB simulation capability where four receivers were tested in parallel. A similar setup with two receivers and a slightly different simulator were used in tests at ARL:UT. There are several things to note about this test configuration. First, the GPS signals are directly cabled to the GPS receiver connectors, bypassing their antennas and preamplifiers. The GPS signal levels were set to produce the same receiver-indicated carrier to noise ratio (C/N_0) that was observed in the previously conducted "live-sky" tests with the simulator set for the same day and time of those tests. Naturally, the UWB signals are also directly cabled to the receivers and at the point where the two signals are combined, the GPS signal power is considerably higher than the nominal received levels. Secondly, the attenuation representing path loss for the UWB signal is not explicitly available. That is, the apparent location of antenna and preamplifier for each receiver is not separately identifiable. The apparent UWB range is represented by the attenuation in the UWB path (including its variable attenuation) and some portion of the attenuation beyond the point where the GPS and UWB signals are

combined. This configuration used for the first four receiver tests and the second configuration used for receivers 6 and 7 are analyzed in Appendix B. The best estimation of equivalent slant range is represented as:

$$R = (0.49\,\mathrm{m})\sqrt{\text{UWB Attenuator Setting Factor}} \quad \text{(Receiver 1)}$$

$$R = (0.31\,\mathrm{m})\sqrt{\text{UWB Attenuator Setting Factor}} \quad \text{(Receiver 2)}$$

$$R = (0.69\,\mathrm{m})\sqrt{\text{UWB Attenuator Setting Factor}} \quad \text{(Receiver 3)}$$

$$R = (0.49\,\mathrm{m})\sqrt{\text{UWB Attenuator Setting Factor}} \quad \text{(Receiver 4)}$$

$$R = (1.14\,\mathrm{m})\sqrt{\text{UWB Attenuator Setting Factor}} \quad \text{(Receiver 6)}$$

In formulating these equations the conducted configurations were analyzed using a simple signal propagation model with simplifying assumptions regarding the transmission coupling between the UWB and GPS antennas. These computations provided an initial equivalent range value for each test condition in the conducted tests. Comparing equivalent UWB degradations between the radiated and conducted tests provided a basis for calculating an adjustment in the equivalent range to best represent actual radiated emissions.

The fundamental strategy for the ARL:UT test analysis is to qualify the conducted test data with both the theoretical analysis and the radiated test data. The qualified conducted test data will then be the basis for assessing the potential UWB interference with GPS receivers. The conducted test data are more clearly defined with regard to the specific signal interference conditions associated with each test case. These signal conditions can be more accurately analyzed with the theoretical model for comparison of theoretical to conducted test results. The only factor missing at the end of such comparisons is the representative radiated test condition. The final step then is to derive an adjustment factor that converts the conducted data results to representative radiated interference conditions. The above equations are the result of this process.

5.1.2 Multipath Geometry

The second test configuration issue considered was the nature of UWB multipath in the radiated test configuration. Figure 5-2 shows the geometry for the radiated tests. At each slant range, the UWB antenna height was adjusted to keep the direct ray path at an elevation angle relative to the GPS antenna location of greater than 5 degrees. The bounce path for each set range is calculated directly from the geometry.

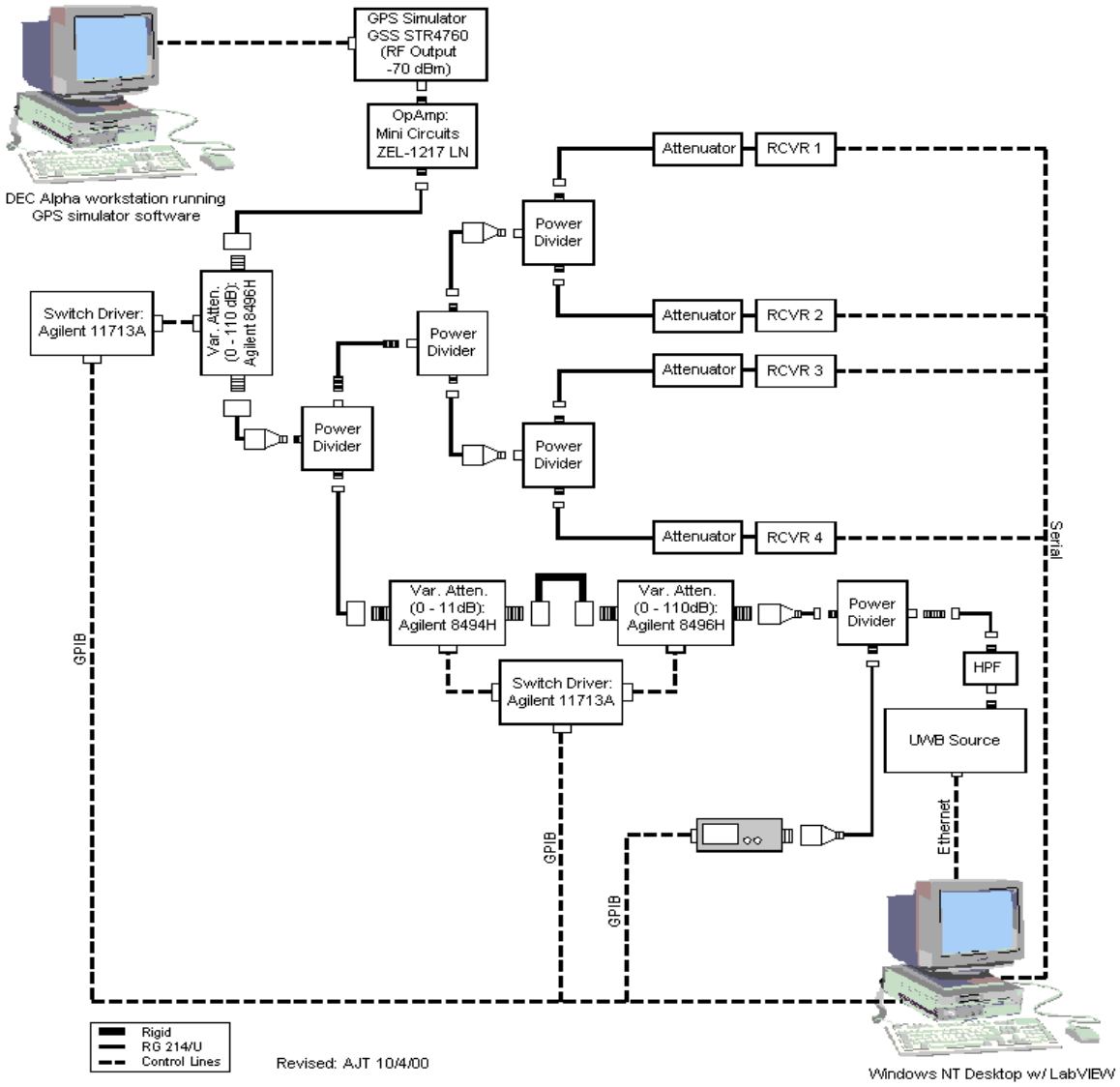

Figure 5-1 Conducted Interference Testing at Holloman AFB

[copied from Reference (5)]

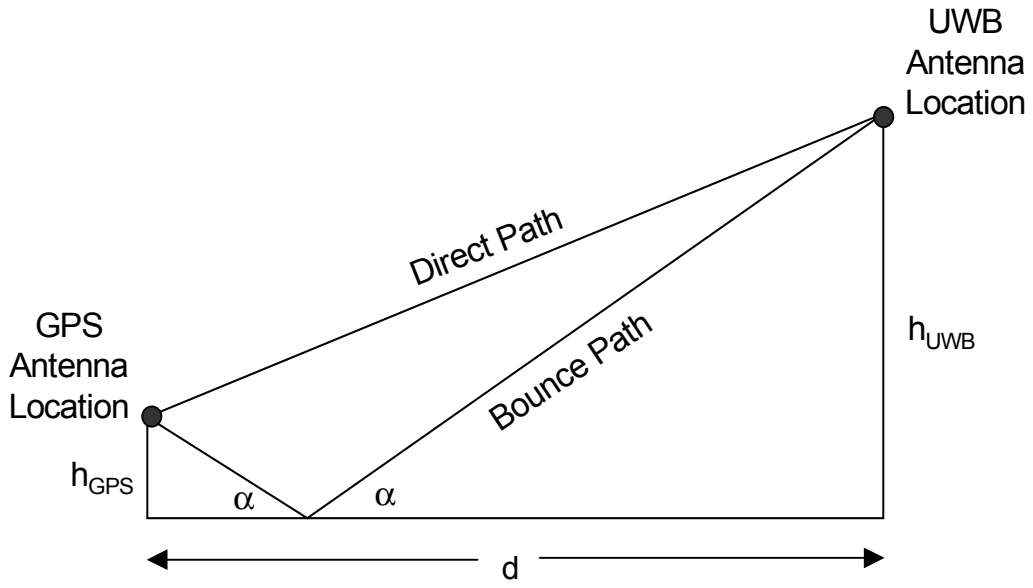

Figure 5-2 Multipath Condition for Radiated Test Configuration

The elevation angle (GPS-to-UWB) is:

$$\theta = \tan^{-1}\left(\frac{h_{UWB} - h_{GPS}}{d}\right)$$

The direct path length is:

$$R = \frac{d}{\cos\theta}$$

The two horizontal segments from each antenna to the reflection point are:

$$d_{GPS} + d_{UWB} = d$$

and :

$$\frac{d_{GPS}}{d_{UWB}} = \frac{h_{GPS}}{h_{UWB}}$$

Therefore:

$$d_{GPS} = \frac{h_{GPS}}{h_{UWB}} d_{UWB} = \frac{h_{GPS}}{h_{UWB}} (d - d_{GPS})$$

$$d_{GPS} \left(1 + \frac{h_{GPS}}{h_{UWB}} \right) = \frac{h_{GPS}}{h_{UWB}} d$$

$$d_{GPS} = \frac{d h_{GPS}}{h_{UWB} + h_{GPS}} \quad or \quad \frac{d_{GPS}}{h_{GPS}} = \frac{d}{h_{UWB} + h_{GPS}}$$

Then the reflection angle α is:

$$\alpha = \tan^{-1} \left(\frac{h_{GPS}}{d_{GPS}} \right) = \tan^{-1} \left(\frac{h_{GPS} + h_{UWB}}{d} \right)$$

And finally, the bounce path length is:

$$d_B = \frac{d_{GPS}}{\cos(\alpha)} + \frac{d_{UWB}}{\cos(\alpha)}$$

Table 5-1 shows the antenna heights derived from the ARL:UT Test Report, the direct ray elevation angle, and the bounce path delay time. Use of the delay time in analysis of the multipath interference is addressed in Subsection 5.2.3.

Table 5-1
Multipath Geometry for ARL:UT Single UWB Radiated Test

d (m)	h_{UWB}(m)	h_{GPS} (m)	θ (degrees)	M-delay (nsec)
0.5	0.597	0.438	17.6	2.16
1.0	0.718	0.438	15.6	1.76
1.5	0.718	0.438	10.6	1.31
2.0	0.718	0.438	8.0	1.03
2.5	1.00	0.438	12.7	1.28
3.0	1.00	0.438	10.7	1.09
3.5	1.00	0.438	9.2	0.95
4.0	1.00	0.438	8.0	0.83
5.0	1.29	0.438	9.7	0.96
8.0	1.29	0.438	6.1	0.61

5.2 Theoretical Modeling

It has been noted[1] that regardless of the lack of spectral features in an individual pulselet power spectrum as defined in Chapter 2 of this report, the choice of time coding can materially affect the spectral content of the entire UWB transmission. This is as expected, and to facilitate the analysis at hand, it is necessary to provide a computational framework for examining differing time coding schemes and the effect this has on the response of the GPS receivers in question to the resultant UWB radiation. Indeed, the ARL:UT test program includes results recorded while operating GPS receivers during UWB functions of devices with different timing code lengths.

5.2.1 UWB Transmissions

The analysis of the signal propagation from the UWB device, through filters, antennas, and the atmosphere and into another, possibly different device must be done with the effects of both pulselet form and pulse train coding in mind. An analysis of the complex effects of this propagation may be computationally intensive, and it is desirable to find a way to minimize recalculation time for varying pulse trains.

5.2.2 Deconvolution of Pulselet and Pulse Train

For an individual pulselet, $w(t)$ describes the radiation as a function of time. If the pulse train time for the k^{th} pulse in the sequence is t_k, the UWB systems are designed so entire transmission signal s is

$$s = \sum_k w(t - t_k) .$$

The Fourier transform of s is the sum of Fourier transforms of the displaced pulselets,

$$S = F\{s\} = \sum_k F\{w(t - t_k)\} = \sum_k e^{-i\omega t_k} F\{w(t)\} = \sum_k e^{-i\omega t_k} W = W \sum_k e^{-i\omega t_k} = WP$$

This can be seen another way as well, since, due to superposition, the sequence is a convolution of the single pulselet $w(t)$ with a pulse train of delta functions

$$p(t) = \sum_k \delta(t - t_k)$$

[1] Interference to GPS from UWB Transmitters, M. Luo et al. Presented at ION GPS 2000, Salt Lake City, Utah, September 2000.

whose Fourier transform is

$$P = \sum_k e^{-i\omega t_k}$$

as above. An example of this convolution ($S = WP \Leftrightarrow s = w \otimes p$) is shown in Figure 5-3.

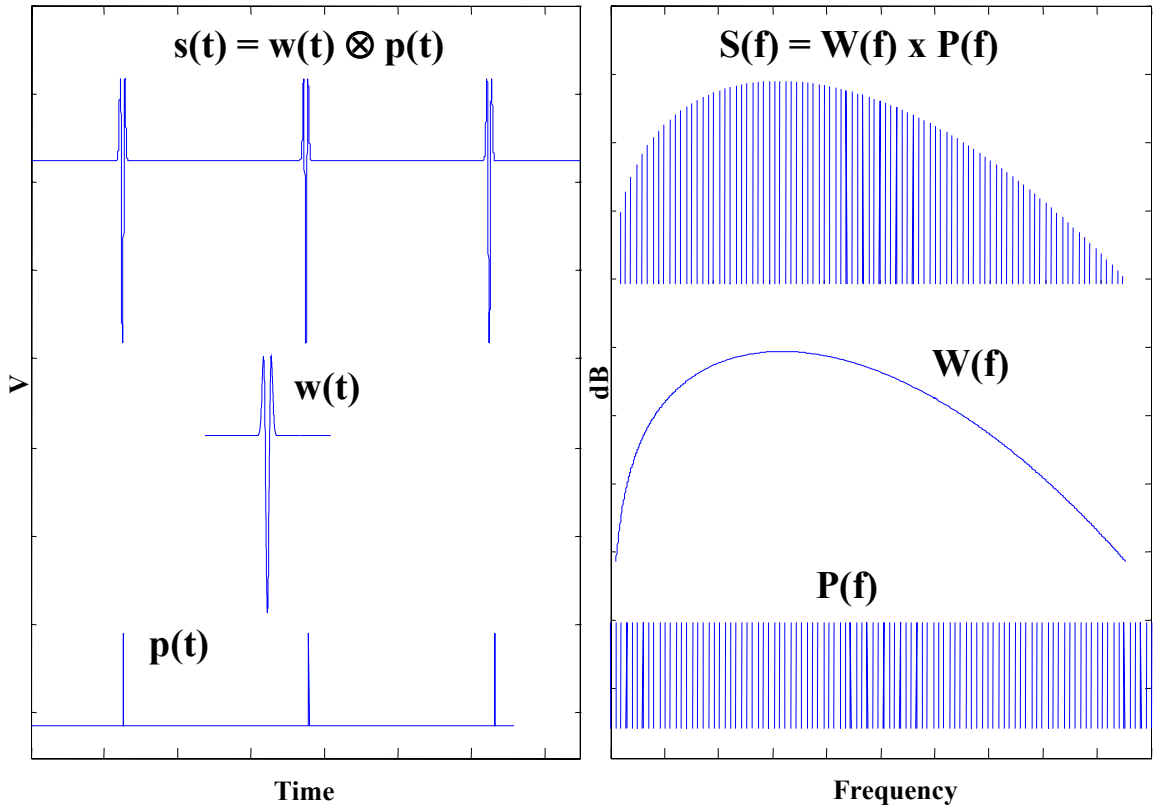

Figure 5-3 Convolution of Pulselet and Pulse Train of Delta Functions

It is desirable to follow in a detailed way the changes in the entire waveform through the UWB device (pulse generation, filter, antenna), transmission (including losses and multipath) and into the GPS receiver (antenna, amplifier, filter, correlation and tracking circuits). All of these effects must be applied to the analysis of the entire transmission signal. However, along much of this propagation, the pulselets will be changed, but separated enough in time that superposition will still hold. For instance, Figure 5-4 shows a nonlinear response to the sequence previously examined in Figure 5-3, and the convolution property still holds. Many UWB transmitter designs have this property, that even in the event of nonlinearity, the interpulse time is large enough compared to the pulselet time span. Therefore, the response can be calculated for a single pulselet, and where appropriate the pulse train effect can be added in later. This will save

computational time, allow quicker evaluations of diverse pulse train coding schemes, and once cast into a band-limited domain in the GPS front end will allow efficient high fidelity digital simulation.

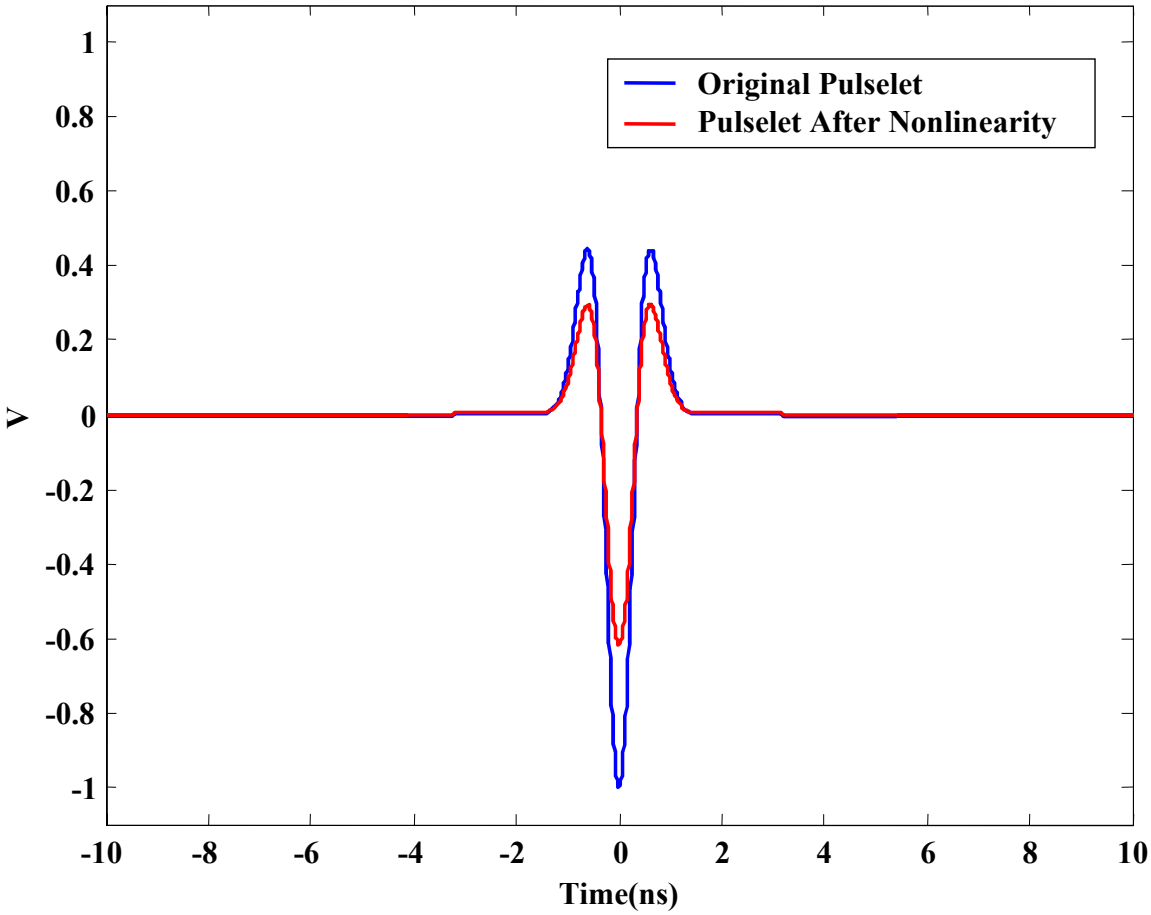

Figure 5-4 Nonlinearity Applied to Pulselet of Figure 5-3

There may arise situations where this type of Fourier analysis breaks down. Before the analysis of the transmission through this situation, the pulselet and pulse train effects can be combined, allowing evaluation in the time domain as well as the frequency domain as needed. At such a point, any type of nonlinear or higher order analysis can also be done. An examination of the potential for such nonlinear responses affecting the output will depend upon the exact amplifier, filter, and correlation system used, but should be a part of determining the validity of the application of the model to the measurements at hand.

5.2.3 Multipath Interference

The problem, of course, with multipath interference is that the multipath is never known until it is measured; it just is what it is. However, worst-case multipath scenarios can be run, and the major contributors can be analyzed.

The multipath signals arising from ground bounce is just such a situation. Supposing that a single pulselet transmission from the direct path arrives at the GPS antenna with shape $w_0(t)$, and the shape of a pulselet bouncing from the ground is $w_1(t)$. This will in general be different from the former due to the dispersion of the ground, so will be a different shape as well as magnitude, but is still referenced to t=0, that is, the multipath time delay t_m has been removed. The signal arriving at the GPS antenna will be:

$$s = w_0 \otimes p(t) + w_1 \otimes p(t + t_m)$$

where the pulse train coding has been shifted by the multipath delay time. In the frequency domain this becomes $S = (W_0 + e^{i\omega t_m} W_1)P$. Once again, the pulse train coding can be separated and added in at the appropriate place in the analysis flow.

In general, the many paths will provide a multitude of pulselets and delay times so that

$$s = w_0 \otimes p(t) + \sum_m w_m \otimes p(t + t_m)$$

describes the signal resulting from all m multipath reflectors considered. Where the dispersive characteristics of the reflectors are the same $(w_i = w_j \equiv w_r)$, the portion of the transform can be cast in another series of delta functions m such that:

$$\sum_m e^{i\omega t_m} W_r = W_r M .$$

5.2.4 GPS Receiver Model

For this to be useful, the waveform needs to be followed into the GPS receiver, and evaluated against receiver performance, such as loss of tracking. At an initial level, simple assumptions about the performance of the antenna and amplifier will allow mixing with the expected GPS tracking loop [at radio frequency (RF)] to view the noise content that can affect the phased locked loop (PLL). However, concerns about linearity, images, and other receiver dependent quantities may benefit from an analysis similar to that in Corbell.[2] The models here,

[2] Design and Validation of an Accurate GPS Signal and Receiver Truth Model - for Comparing Advanced Receiver Processing Techniques, LT P.M. Corbell, Masters Thesis AFIT/GE/ENG/00M-07, Air Force Institute of Technology, March 2000.

however, must be informed by the actual receiver designs corresponding to the data taken. Otherwise, only sensitivity studies will be possible.

5.2.5 Pseudorandom Number (PRN) Pulse Train Coding

Most pulse train coding schemes are cast as time deviations δ_k from an average pulse repetition time T_r such that

$$t_k = k(T_r) + \delta_k .$$

The deviations may encode data, and may also cause deliberate dithering for the purpose of minimizing spectral content and decreasing the probability of detection. In the case of both data and dithering $\delta_k = \delta_k(data) + \delta_k(dithering)$. The dithering may be a pseudorandom choice of time from a given window, so that

$$\langle \delta(dithering) \rangle = 0$$
$$prob(\delta(t, dithering)) = uniform(t < \alpha T_r)$$

In such cases, the pseudorandom code may have a limited number of states before it begins to repeat. In the specific case of UWB radar systems where there are no additional data encoded on the transmitted waveform, the Fourier transform of the pulse train of delta functions becomes:

$$P = \sum_k e^{-i\omega(kT_r + \delta_k)} .$$

With a PRN code of length N, this can be broken into a product of two factors, the first the transform of the finite N PRN sequence, and the second taking into account that this is repeated every NT_r:

$$P = P_{PRN} P_{rep} = \left(\sum_{k=1}^{N} e^{-i\omega(kT_r + \delta_k)} \right) \left(\sum_{j=-\infty}^{\infty} e^{-i\omega(jNT_r)} \right)$$

Where data are present, there will be an additional time displacement $\delta_k(data)$, which may be drawn from $\pm t_{data}$ where the + or – is chosen to transmit the bit of digital data. In all of these cases, a statistical study based on the probability density functions of dithering and data will result in an expectation value for the spectrum itself, as well as variances on the same. The present study will be restricted to the signals used in the test program, except for some special cases.

5.2.6 An Example of a UWB Signal

In this section, the propagation of a simple example UWB device will be followed from pulselet production through the device filter and an ideal antenna. The radiated spectrum will then be examined for any prominent lines or other content. In this example, the recovery diode producing the pulse is assumed to provide a perfect Gaussian. The pulselet in the time domain at this stage is $f_1(t)$, and the Fourier transform is $F_1(\omega)$:

$$f_1(t) = \frac{1}{2} A \tau^2 e^{-\left(\frac{t}{\tau}\right)^2} \qquad F_1(\omega) = \int_{-\infty}^{\infty} f_1(t) e^{-i\omega t} dt = \frac{\sqrt{\pi}}{2} A \tau^3 e^{-\left(\frac{\omega\tau}{2}\right)^2}$$

The next stage is an internal filter in the UWB device. This is modeled here as an ideal *s* filter, a true time derivative. The resultant pulselet is $f_2(t)$.

$$f_2(t) = \frac{\partial f_1}{\partial t} = -Ate^{-\left(\frac{t}{\tau}\right)^2} \qquad F_2(\omega) = i\frac{\sqrt{\pi}}{2} A \omega \tau^3 e^{-\left(\frac{\omega\tau}{2}\right)^2}$$

The antenna of the UWB device is the next stage. A simple model of the antenna is also an ideal *s* filter, so the radiated pulselet $f_3(t)$ becomes:

$$f_3(t) = -Ae^{-\left(\frac{t}{\tau}\right)^2}\left[1 - 2\left(\frac{t}{\tau}\right)^2\right] \qquad F_3(\omega) = -A\frac{\sqrt{\pi}}{2}\tau(\omega\tau)^2 e^{-\left(\frac{\omega\tau}{2}\right)^2}$$

As in the previous section, the whole radiated waveform must include the pulse train coding. The spectrum of this full radiated waveform will be

$$F_r = F_3 P_{PRN} P_{rep}$$

For a 200 ps characteristic time τ, a few 1000 PRN code length pulse train sequence with a code span of 12.5 ns and a pulse repetition frequency (PRF) of 10 MHz, the relative magnitude of the spectrum as a function of frequency is shown in Figure 5-5. This type of coding is similar to the signals used in the test.

5.2.6.1 Interaction with the GPS Receiver

The receiver front-end example described here is equivalent to a double heterodyne design, as in Figure 5-6. To match an actual GPS front end, the model has been patterned after the Mitel GPS RF chipset. This is mainly done due to the availability of performance and design information. Exact results would require the use the designs actually implemented in the receivers under test. However, this is not practical owing to the proprietary nature of most GPS receiver designs.

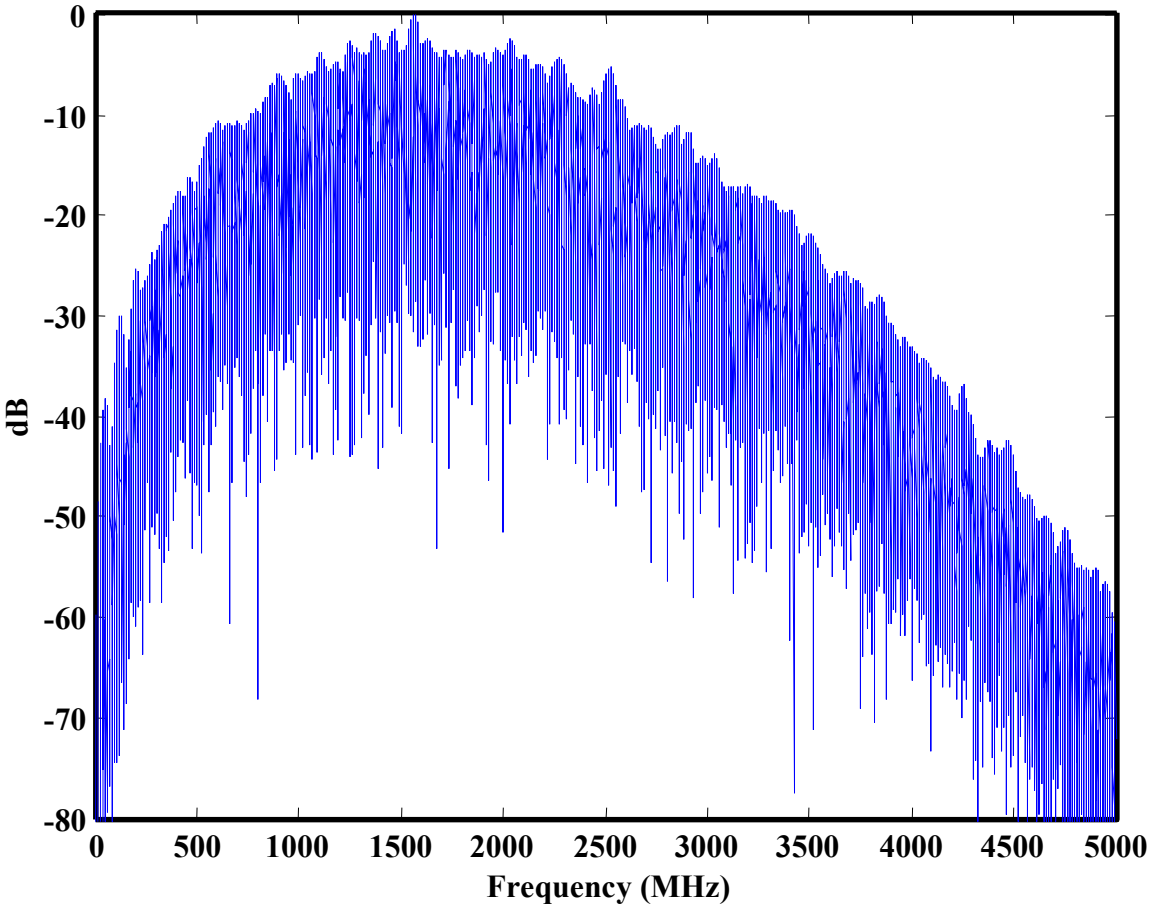

Figure 5-5 Spectrum of Composite Waveform Using Pulselet of Figure 5-3

To follow the example waveform through the GPS receiver, an estimate of propagation and antenna performance is necessary. In this simple example, a resonant filter approximates the antenna response and low-noise amplifier, with a frequency response H_a.

$$F_4 = H_a F_r$$

The receiver design examined here has two Intermediate Frequency (IF) stages, so will consist of a first mixer, first filter, second mixer and second filter. The first mixer will have a mixing frequency ω_5 and phase ϕ_5 so that:

$$f_5 = f_4 \cos(\omega_5 t + \phi_5) = \frac{1}{2} f_4 \left(e^{i\omega_5 t} e^{i\phi_5} + e^{-i\omega_5 t} e^{-i\phi_5} \right)$$

$$F_5(\omega) = \frac{e^{i\phi_5}}{2} F_4(\omega - \omega_5) + \frac{e^{-i\phi_5}}{2} F_4(\omega + \omega_5)$$

The first filter (H_6), second mixer (with mixing frequency ω_7 and phase ϕ_7) and the second filter (H_8) are included in a similar way to follow the signal through the RF portion of the receiver.

$$F_6 = H_6 F_5$$

$$F_7(\omega) = \frac{e^{i\phi_7}}{2} F_6(\omega - \omega_7) + \frac{e^{-i\phi_7}}{2} F_6(\omega + \omega_7)$$

$$F_8 = H_8 F_7$$

In the example, the response of the filter H_6 after the first mixer (IF center 175.42 MHz) is shown in Figure 5-7. The second filter H_8 is shown in Figure 5-8. The final filtered UWB signal through the front end is shown for 1 MHz PRF, 5 MHz PRF, 10 MHz PRF, and 20 MHz PRF in Figures 5-9 through 5-12. These utilized the 1000 PRN code length pulse train sequence actually used in the PAD measurements with a code span of 12.5 ns. For comparison to previous work[3], the frequency for 19.94 MHz undithered is shown in Figure 5-13, while the dithered case for the same PRF is shown in Figure 5-14.

At this point, many receivers perform digitization. Having passed through both IF filter stages, the signal is band limited and therefore the required digitization rate is relatively small. The analysis can be performed in two ways. First, the resultant spectrum can be digitally modeled and put through reasonable digital processing.[4] Alternatively, the correlation can be done analytically at this point with the RF reference correlation corresponding to the correct IF band.

5.2.6.2 Interaction with Correlator

After signals pass through the GPS front end, they are correlated with the expected signal of a GPS satellite. GPS signals are carrier signals phase shifted with codes and data. In the case of Coarse Acquisition (C/A) code, the phase shifts are from a 1023 length PRN code unique to each satellite. The C/A code chip rate is 1.023 MHz, or one complete repetition of the code per millisecond (a 1 kHz repetition frequency). P codes are much longer, with a chip rate of 10.23 MHz the repetition time is about one week. The L1 GPS signals (on a carrier of 1575.42 MHz) contain both C/A and P codes (90° out of phase), while the L2 signals (at 1227.6 MHz) contain only P codes. Only C/A codes will be examined here.

[3] Interference to GPS from UWB Transmitters, M. Luo et al. Presented at ION GPS 2000, Salt Lake City, Utah, September 2000.

[4] See for example, Design and Validation of an Accurate GPS Signal and Receiver Truth Model for Comparing Advanced Receiver Processing Techniques, LT P.M. Corbell, Masters Thesis AFIT/GE/ENG/00M-07, Air Force Institute of Technology, March 2000.

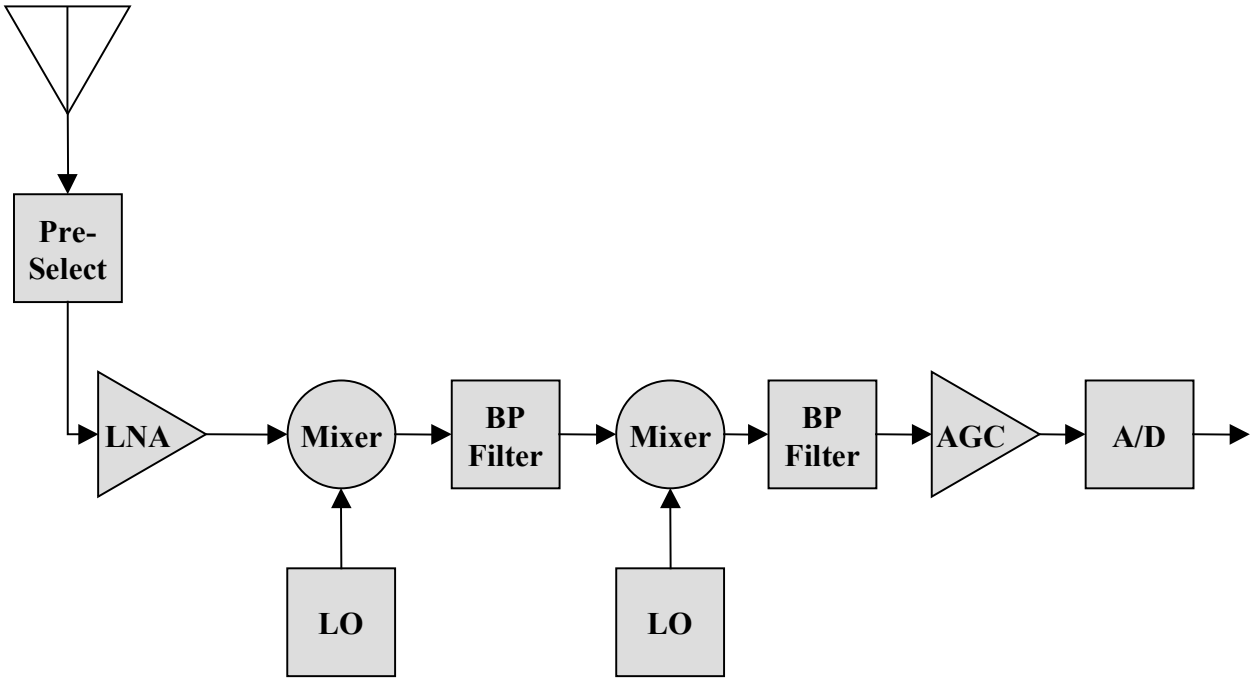

Figure 5-6 Double Heterodyne Front End

The received signal can be correlated with the expected signal by mixing it with an expected phase modulated tone and then integrating the result with a narrow band filter. As mentioned previously, most modern receivers digitize the signals and accomplish correlation and tracking with digital processors. The analysis can be accomplished with equal precision for either analog or digital representations.

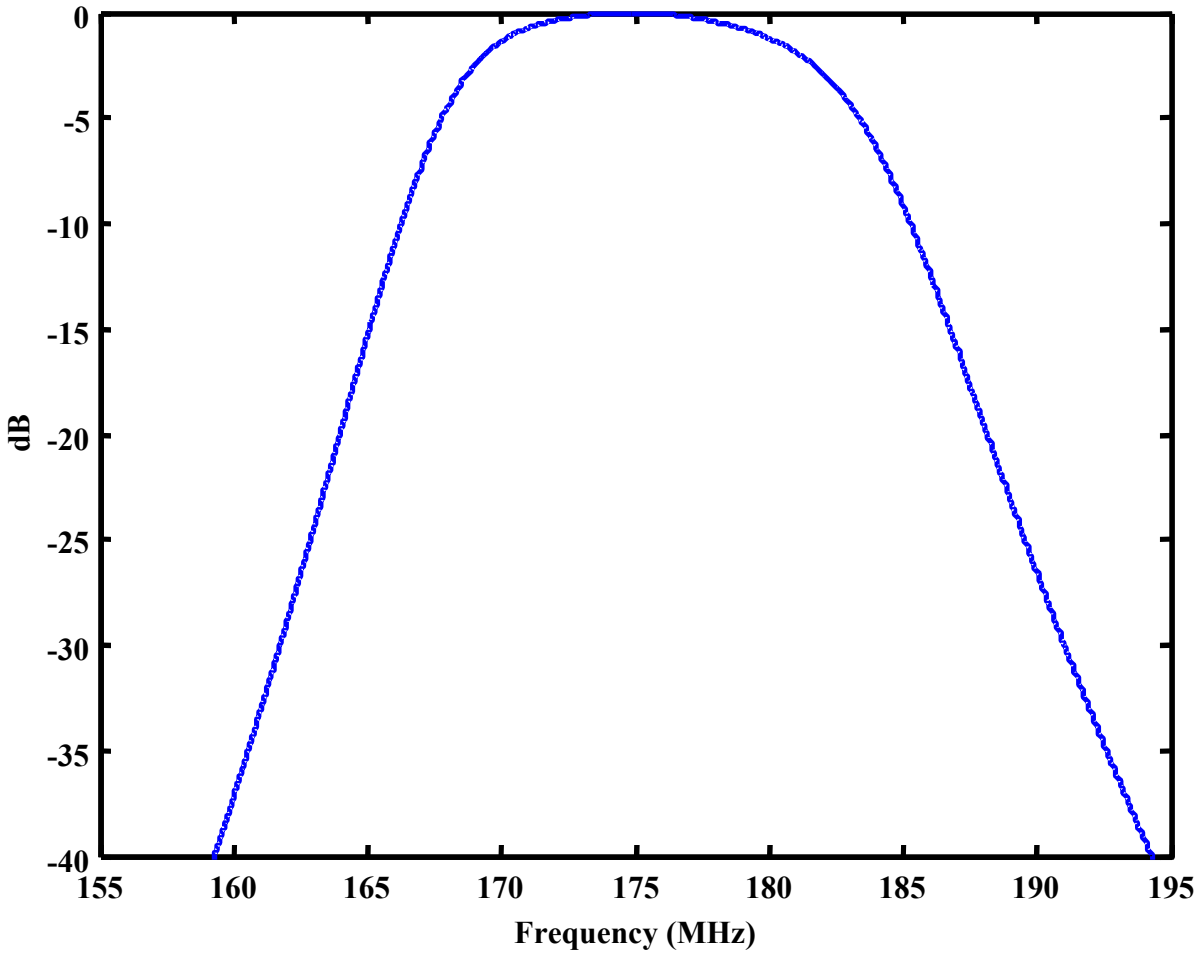

Figure 5-7 First IF Filter (H_6)

In addition to codes, the data rate is 50 Hz, so that 20 C/A code repetitions fit into a data bit. Since the bit clock is recovered for reading message data, it is possible to coherently integrate the correlation over the entire data bit time. When the message bits are known or can be estimated well, the coherent interval can be expanded beyond the 20-millisecond bit time. When the message bit stream is not known or reasonably predicted the signal-to-noise ratio (SNR) is increased further by incoherent integration for intervals longer than a message bit time. These types of choices are made by the receiver designer, are in general proprietary and not in the public domain, and may have a demonstrable effect on tracking performance in the presence of UWB transmissions.

The correlation output depends, of course, on the time offset between the incoming GPS signal and the internally generated signal used to perform the correlation. The tracking is done with a delay lock loop (DLL), with two or three different offset times allowing measurement of the best time offset match. Once the tracking loop has acquired the proper correlation, the signal can be readily tracked to keep the correlation at a maximum.

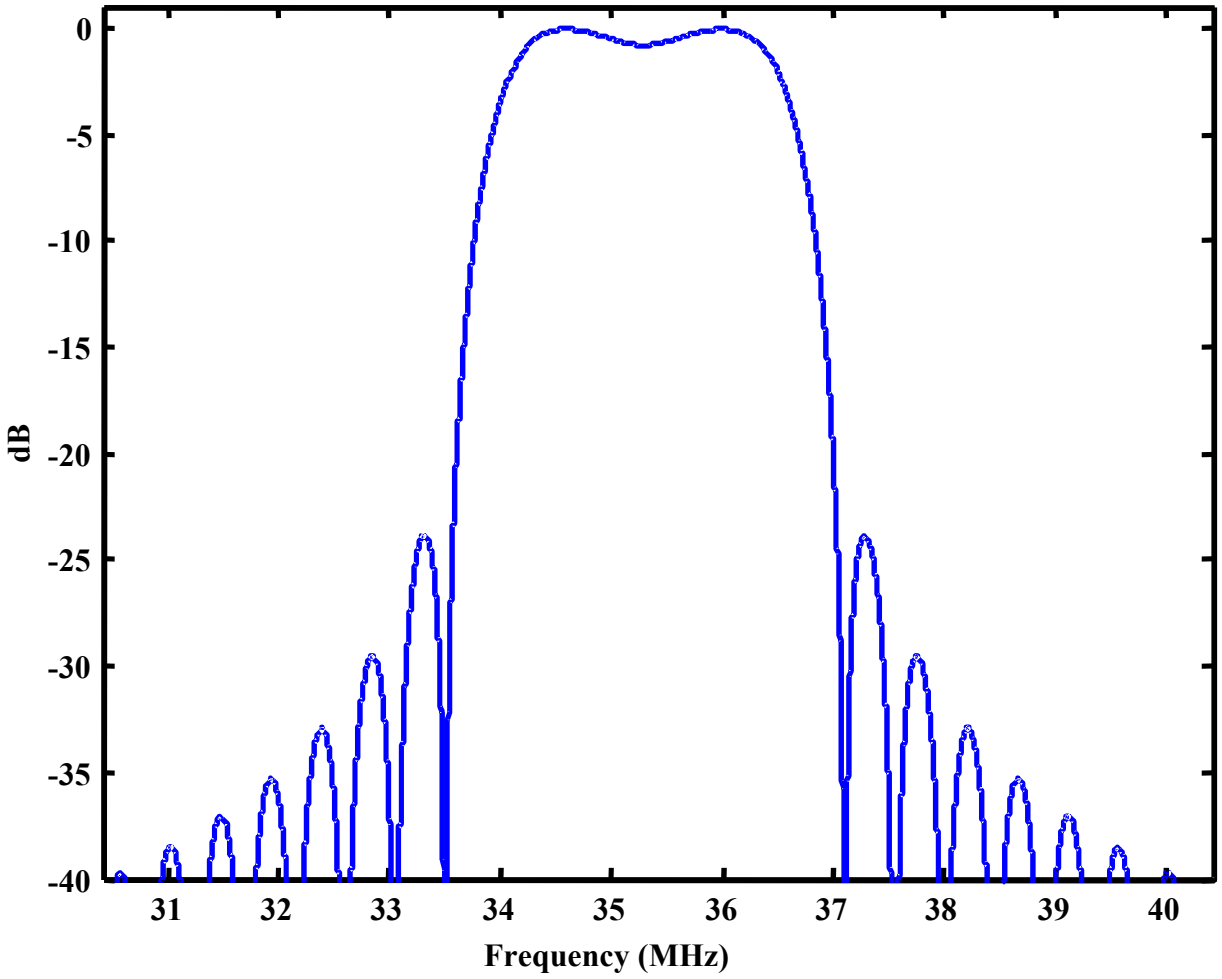

Figure 5-8 Second IF Filter (H_8)

The modeling of the C/A correlation loop begins with the model for the GPS signal. The L1 carrier frequency $\sin(\omega_{L1}t)$ is modulated by a function $y_s(t)$ which is ± 1 depending on the C/A code bit state for satellite s. In addition, the data are coded with a similar function $d_s(t)$, but since we are performing coherent integration over a smaller time window than would allow this value to change, it will not provide useful information at this stage. With a magnitude C_s that contains the power information including that resulting from slant range and propagation effects, the GPS signal g_s becomes

$$g_s = C_s y_s(t) d_s(t) \cos(\omega_{L1} t)$$

$$g_c = y_s d_s$$

with spectra

$$G_c(\omega) = (Y_s(\omega) \otimes D_s(\omega))$$

$$G_s = C_s\left[\frac{1}{2}(G_c(\omega - \omega_{L1})) - \frac{1}{2}(G_c(\omega + \omega_{L1}))\right]$$

Since No Doppler effect was modeled in the current study, this spectrum is filtered by the GPS front end system as above, resulting in an IF signal g_{s1}, and mixed with a reference signal g'_s at a displaced time t' and final IF carrier frequency ω'_{L1}

$$g'_s = y_s(t')\sin(\omega'_{L1}t')$$

In the correlator, the product ($g_{s1}\, g'_s$) is formed, and then integrated over the C/A code span time. These correlations are used for tracking, for instance by using a three-point delay-lock-loop mentioned above. The ability to correctly predict the correct time offset is crucial to tracking performance.

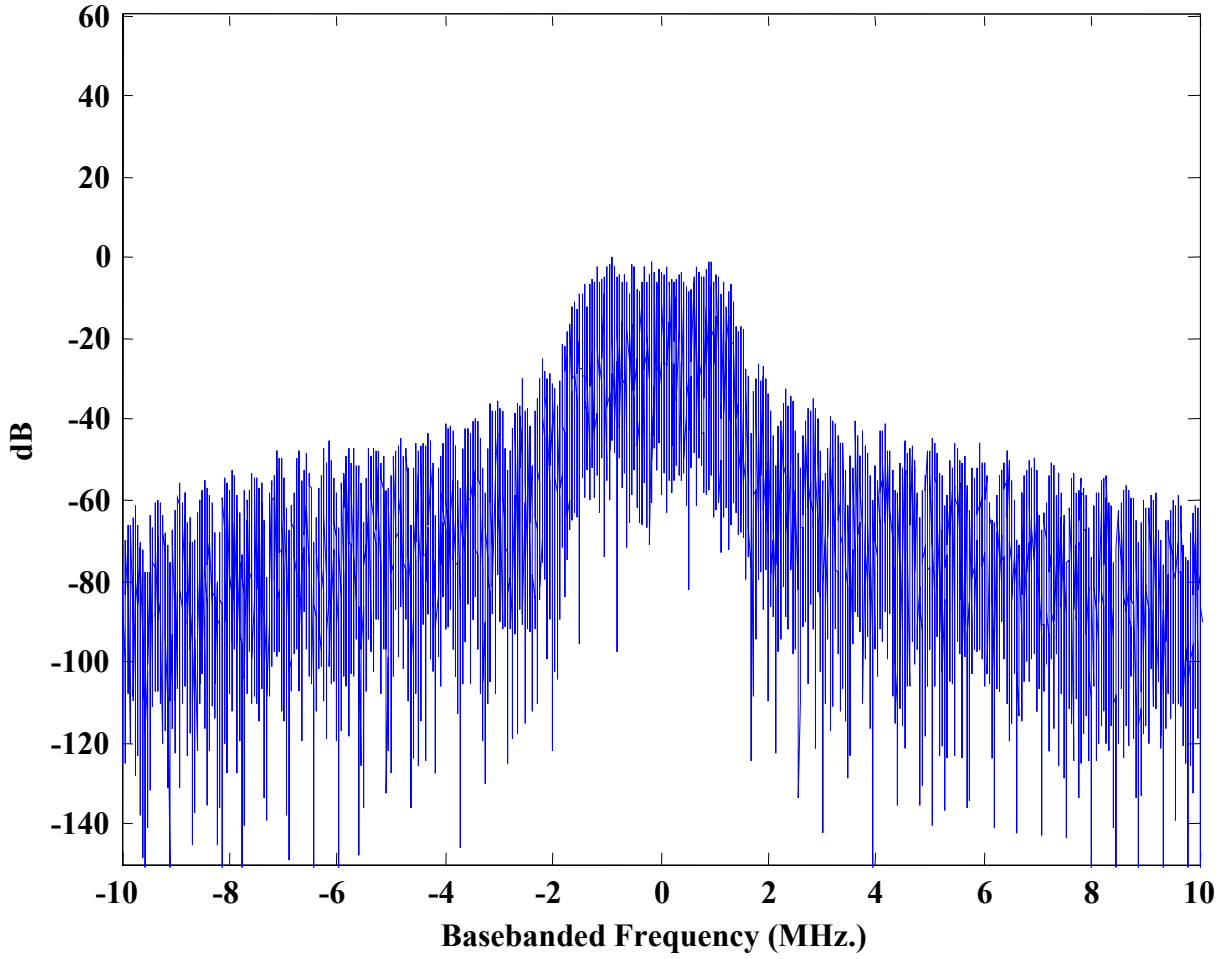

Figure 5-9 UWB Signal Through Front End of Receiver (1 MHz PRF)

The addition of noise allows for the parameterization of this accuracy with the ratio of peak correlation to false correlation levels, a measure of signal to noise. Correlation simulations, which include cross-correlation noise resulting from different satellite codes and an injected noise, were produced for a set of PRFs as above. These were correlated in an integration window of 1 ms for a single realization of injected signals.

Six in view satellites were simulated (PN codes 1 through 6), where the total GPS signal is the sum of all six. To this, the injected signal was added, either white noise or UWB. No additional noise was introduced, to provide a view of the effects of the injected signal alone. Direct comparison to actual receivers, therefore, is not possible before an additional thermal noise term is applied that may be dependent upon the amplifier used in the receiver. The purpose of these simulations is to find the output of the correlator for both a satellite that was simulated, as well as an out of view PN which would result in only false correlation peaks.

In the correlation stage, the incoming signal is multiplied by the expected GPS signal from a given satellite (including a variable time offset) and integrating the result. Correlation power is calculated with an integration time of 1 ms. The images below show that the correlation power for time offsets from ± 20 μs from the correct correlation peak. The actual correlation was calculated for a larger span of time offsets, but the information in this 40 μs window is representative, and provides for a better examination of the correlation peak. An examination of the whole 1 ms span revealed no outstanding false correlations, that is, the type of effect seen from 10 to 20 microsecond offsets is the same all the way across. The dB attenuation values (0 - 60) are tabulated along the vertical axis. The color indicates the correlation power for a given time offset & dB attenuation and is scaled as follows: dark blue is near zero, light blue-green is the level of the correlation peak at 60 dB attenuation (i.e., little to no UWB or WN signal present), red is greater or equal to two times the level of the correlation peak at 60 dB attenuation, and yellow scales linearly between the light blue-green and red. The upper plots depict the results of correlating the input signal (which is comprised of UWB, or WN, and GPS signals from six satellites) and one of the representative satellite chip sequences. The lower plots result for correlating the same input signal with a chip sequence from a satellite not represented in the input signal (i.e. not in view).

Power level ratios were chosen for the 1 MHz PRF versus a single GPS signal as shown in Appendix B. White noise power was set to the 10 MHz PRF power as in the test setup. Correlation with the addition of injected white noise through the GPS front end as a function of time offset and attenuation is shown in Figure 5-15. The inclusion of correlation with a satellite not available shows only noise effects. Results with the UWB signals mentioned above instead of white noise is shown in Figures 5-16 through 5-19 for PRFs of 1 MHz, 5 MHz, 10 MHz, and 20 MHz, respectively. For comparison, the 19.94 undithered case is shown in Figure 5-20.

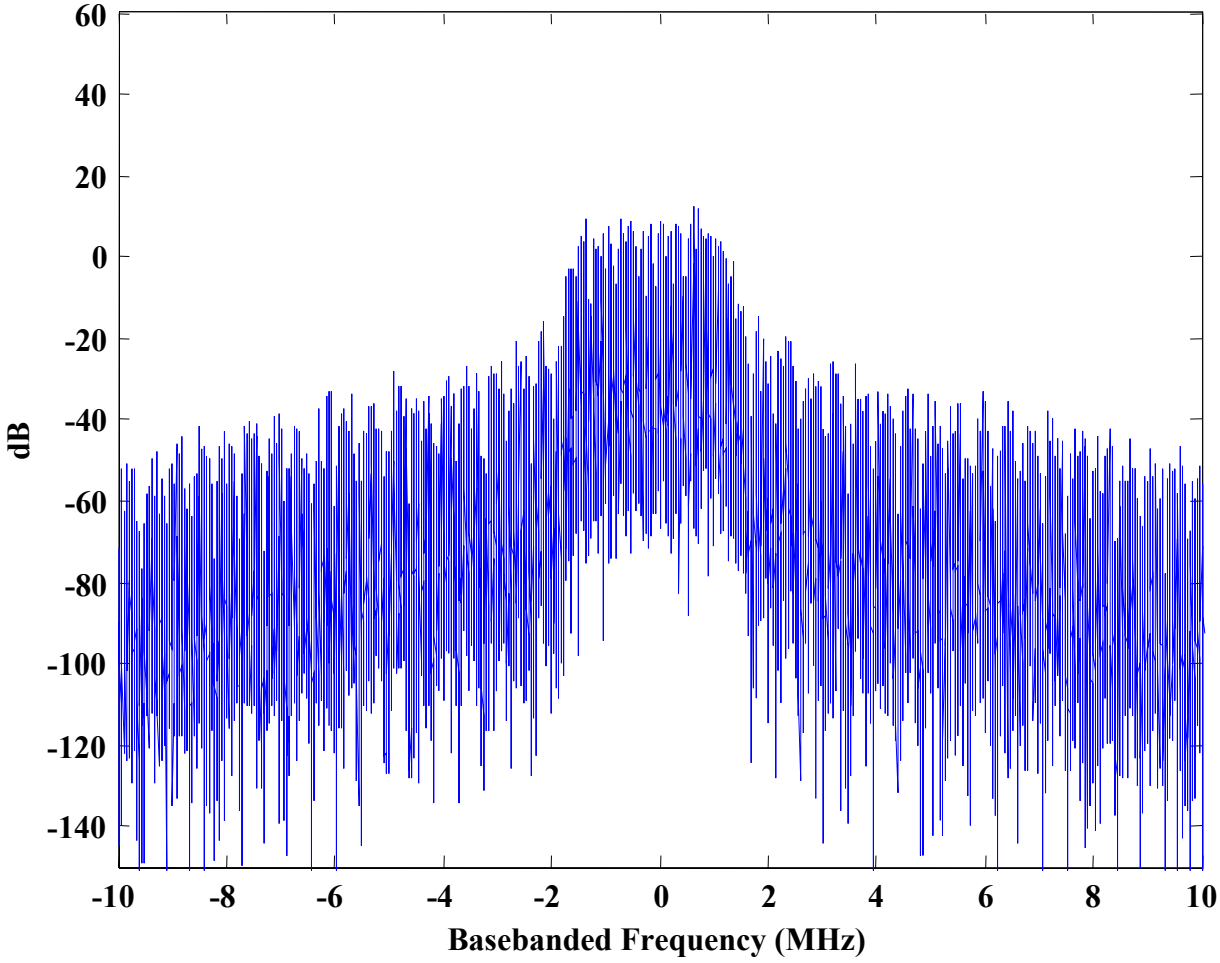

Figure 5-10 UWB Signal Through Front End of Receiver (5 MHz PRF)

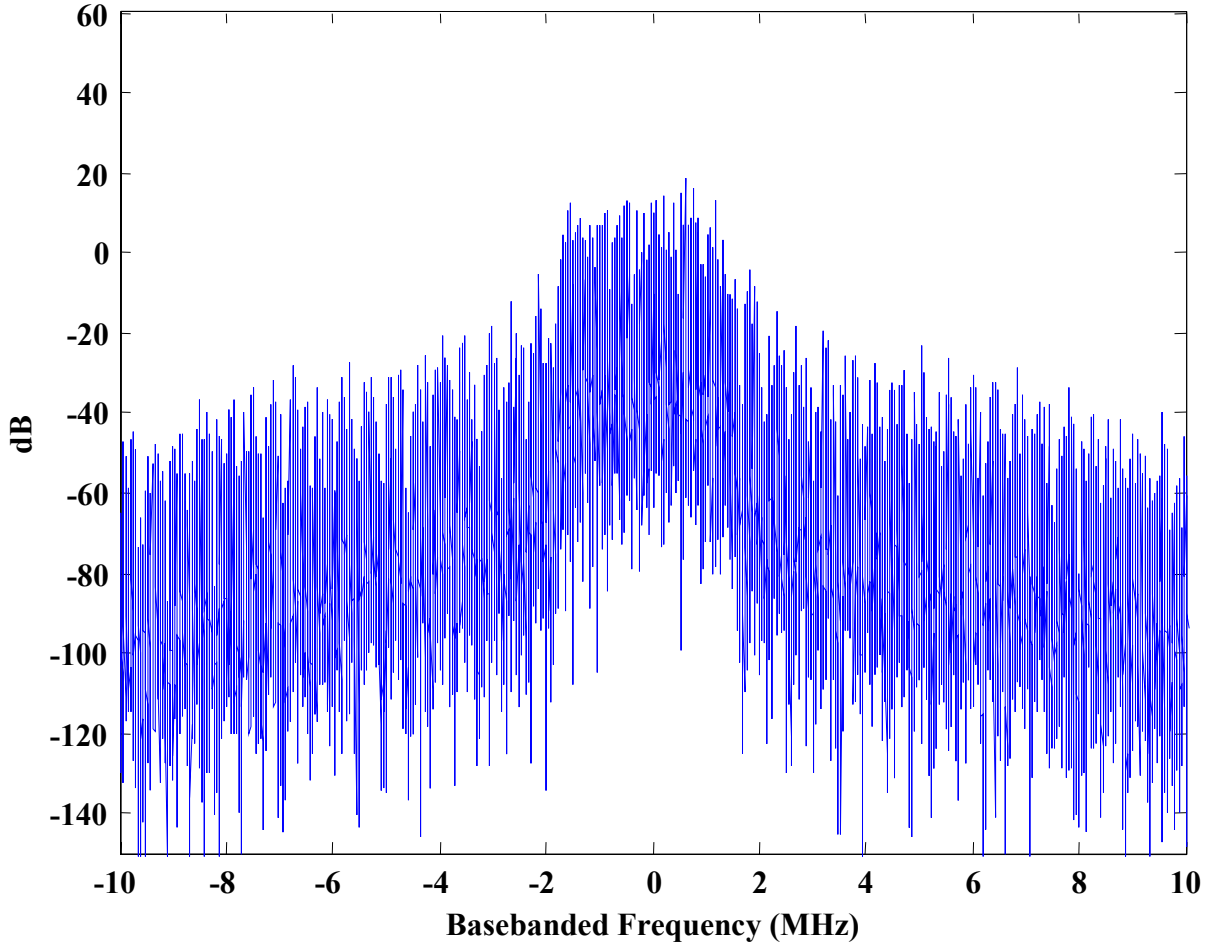

Figure 5-11 UWB Signal Through Front End of Receiver (10 MHz PRF)

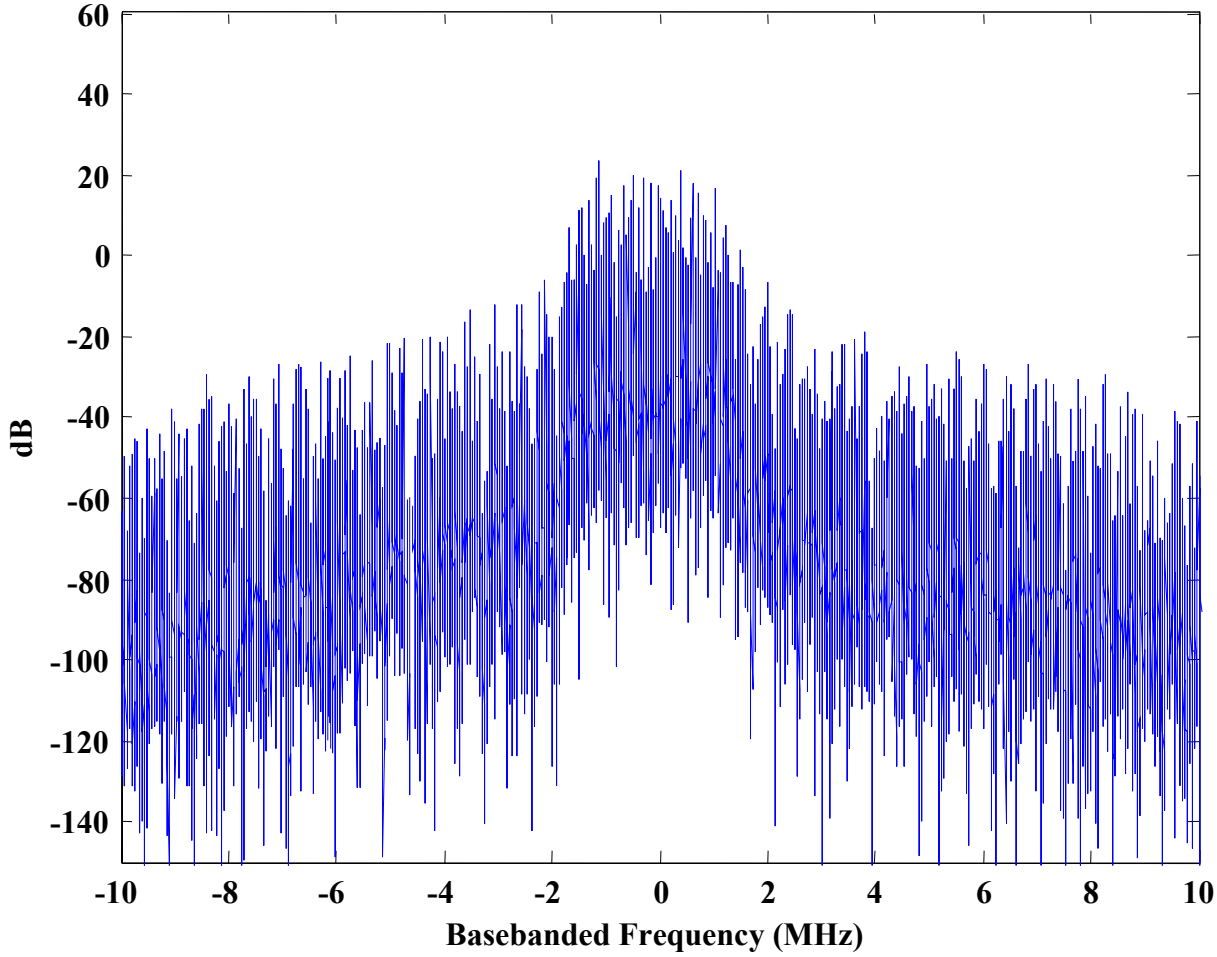

Figure 5-12 UWB Signal Through Front End of Receiver (20 MHz PRF)

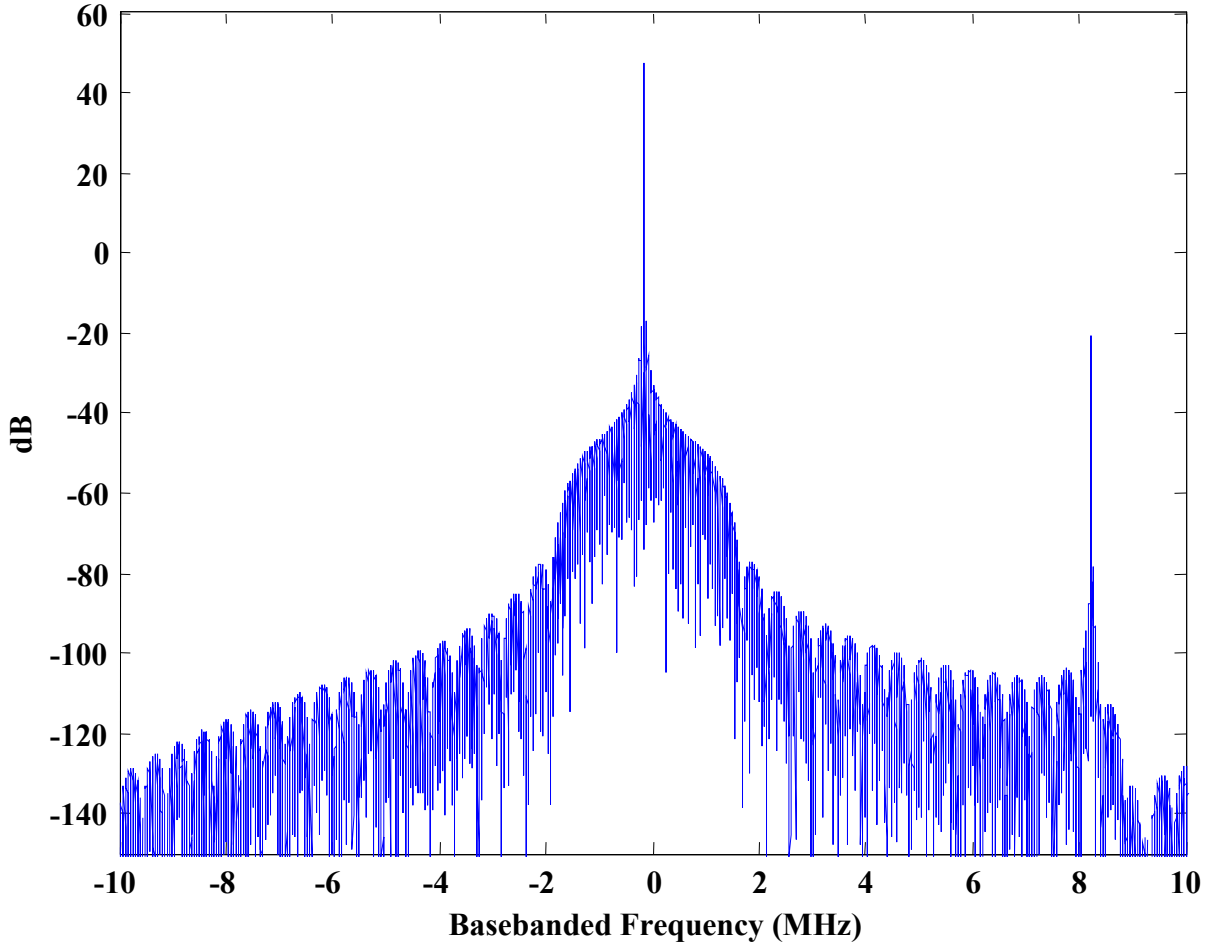

Figure 5-13 UWB Signal Through Front End of Receiver (19.94 MHz PRF; Undithered)

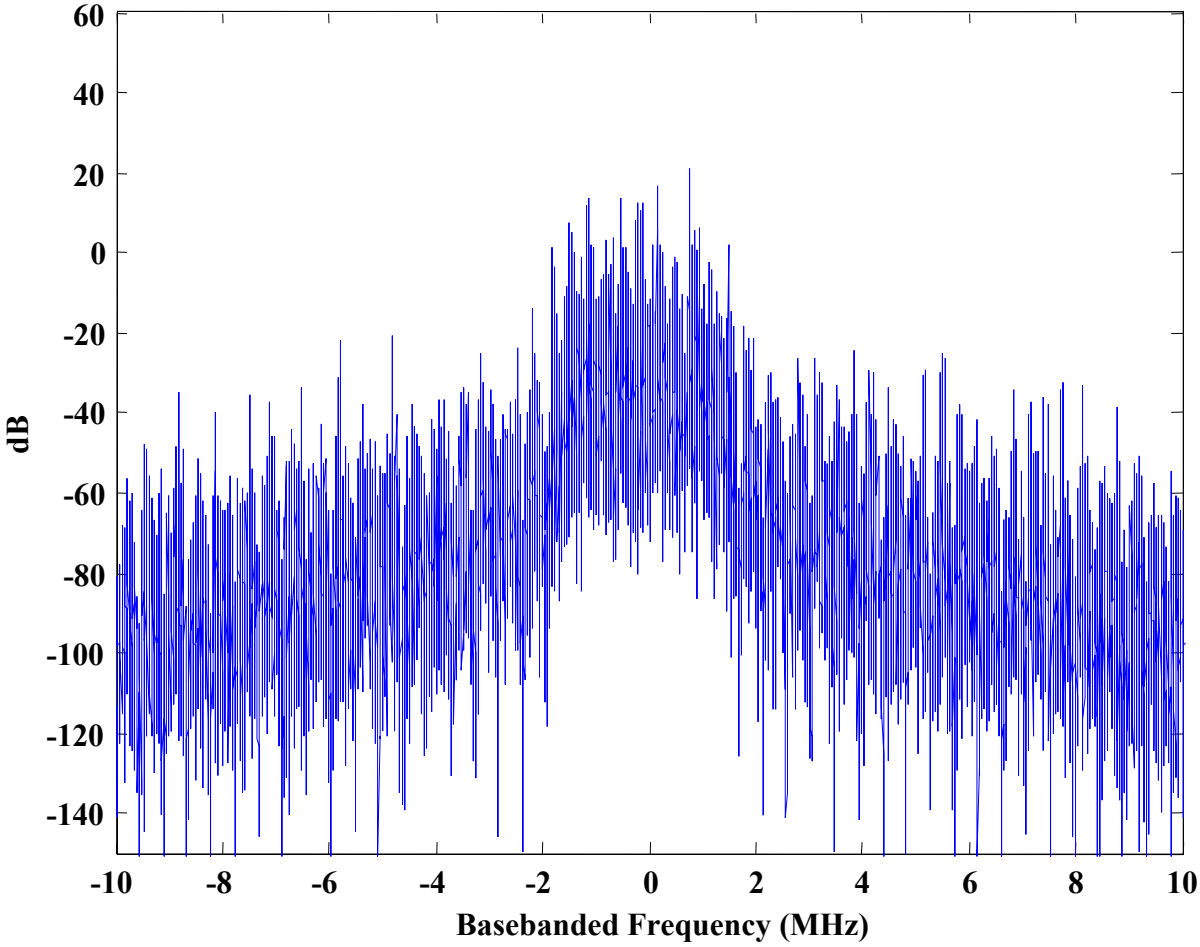

Figure 5-14 UWB Signal Through Front End of Receiver (19.94 MHz PRF Dithered)

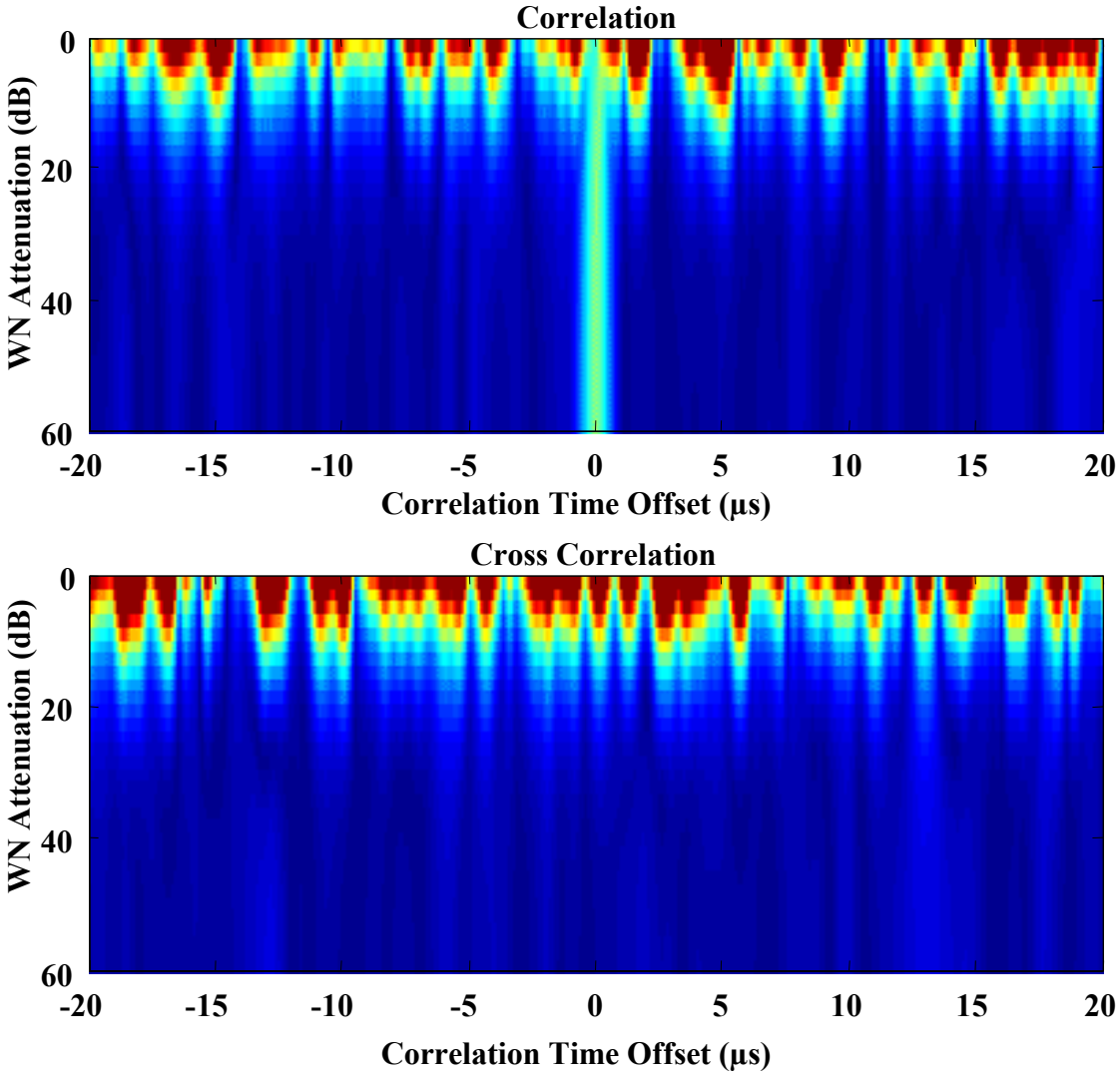

Figure 5-15 GPS Correlation with Injected White Noise

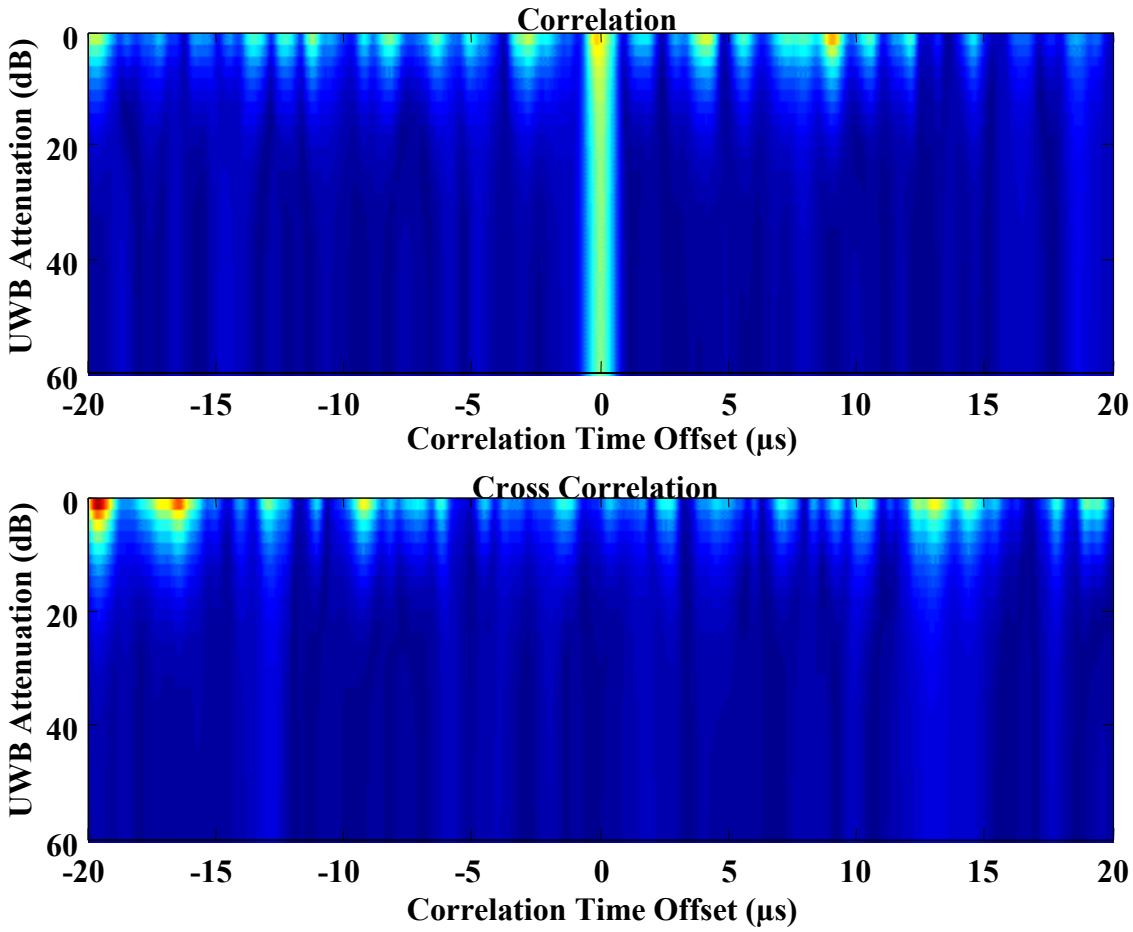

Figure 5-16 GPS Correlation with Injected UWB Signal (PRF=1MHz)

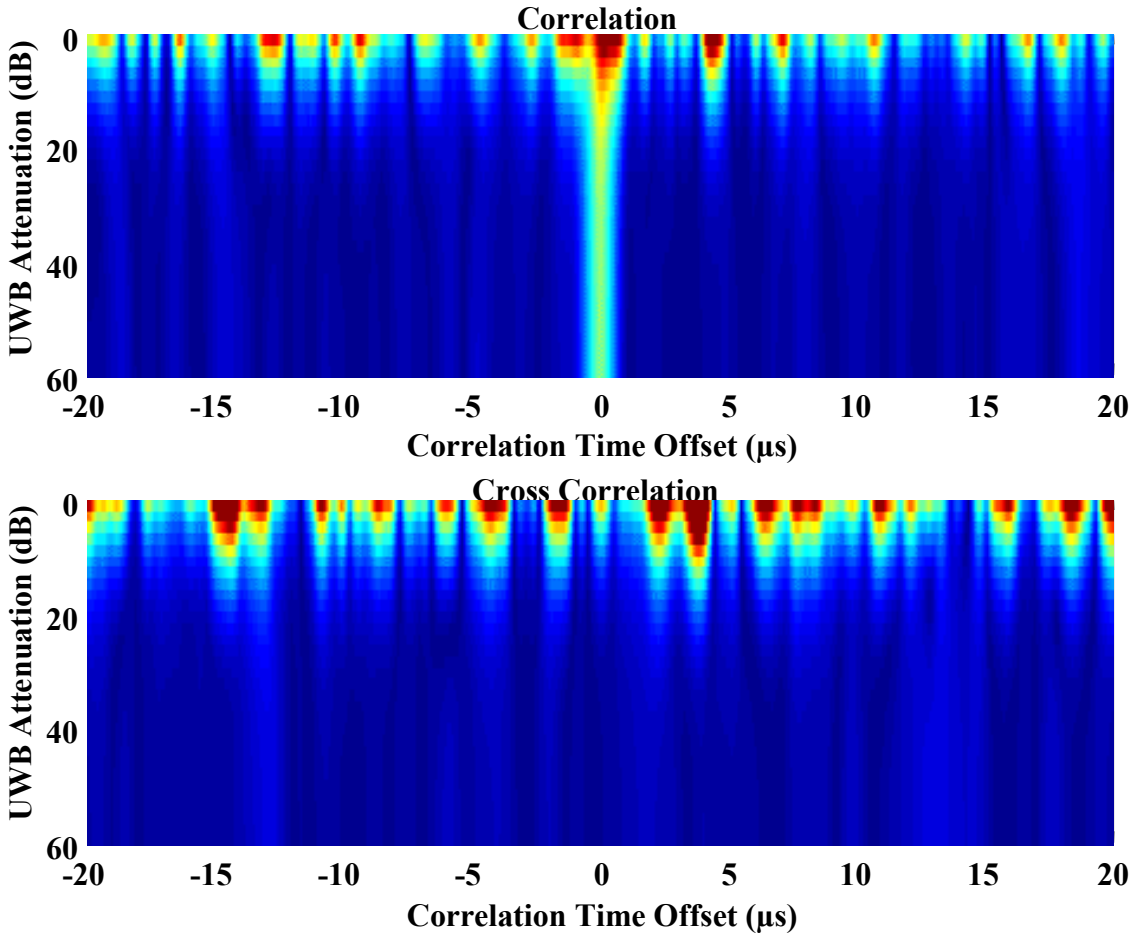

Figure 5-17 GPS Correlation with Injected UWB Signal (PRF=5MHz)

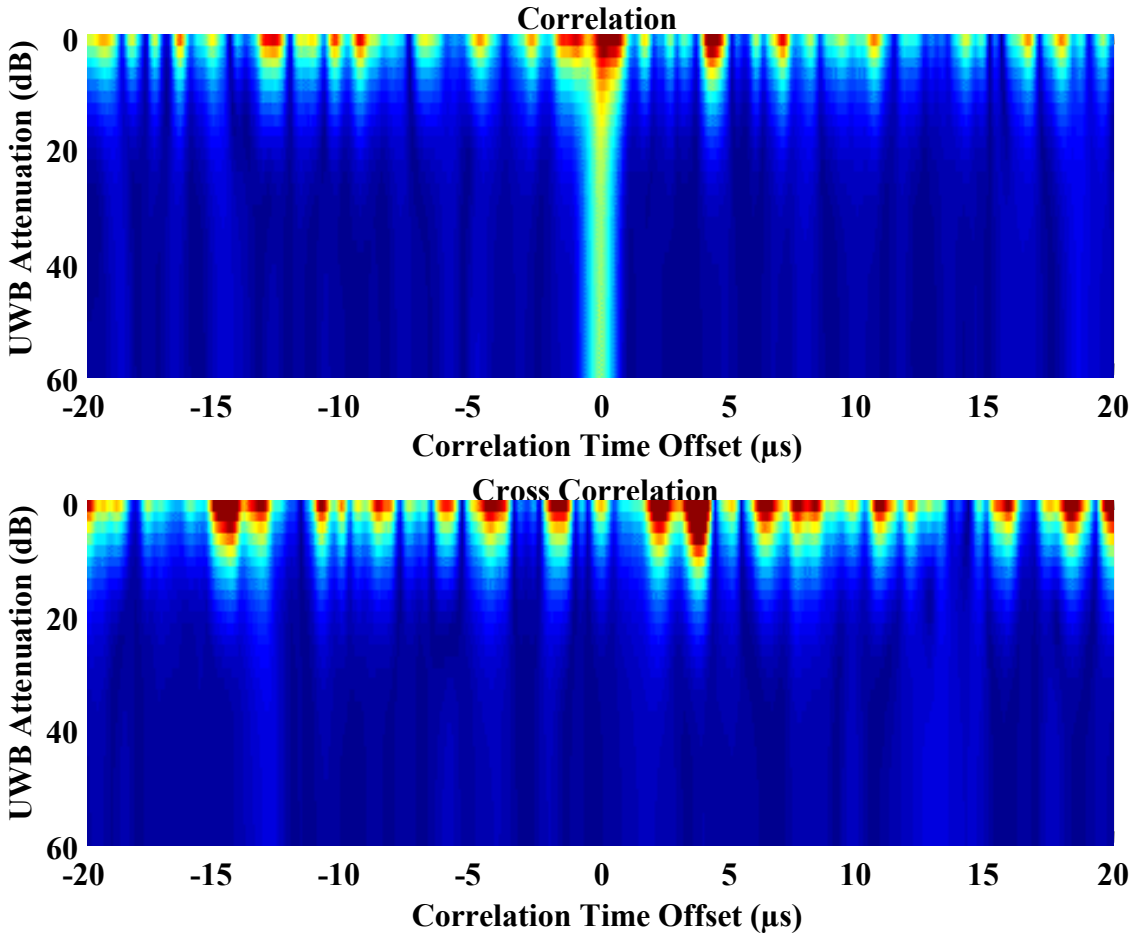

Figure 5-18 GPS Correlation with Injected UWB Signal (PRF=10MHz)

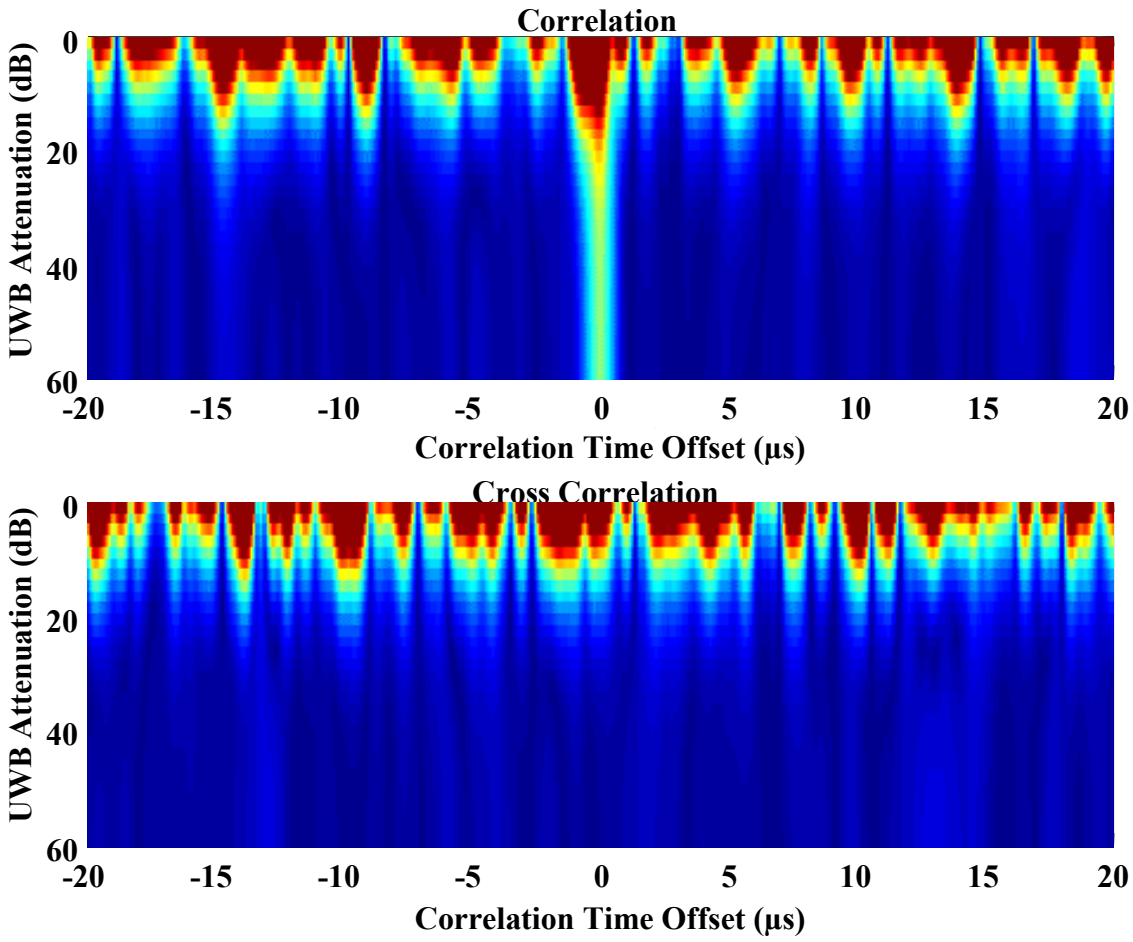

Figure 5-19 GPS Correlation with Injected UWB Signal (PRF=20MHz)

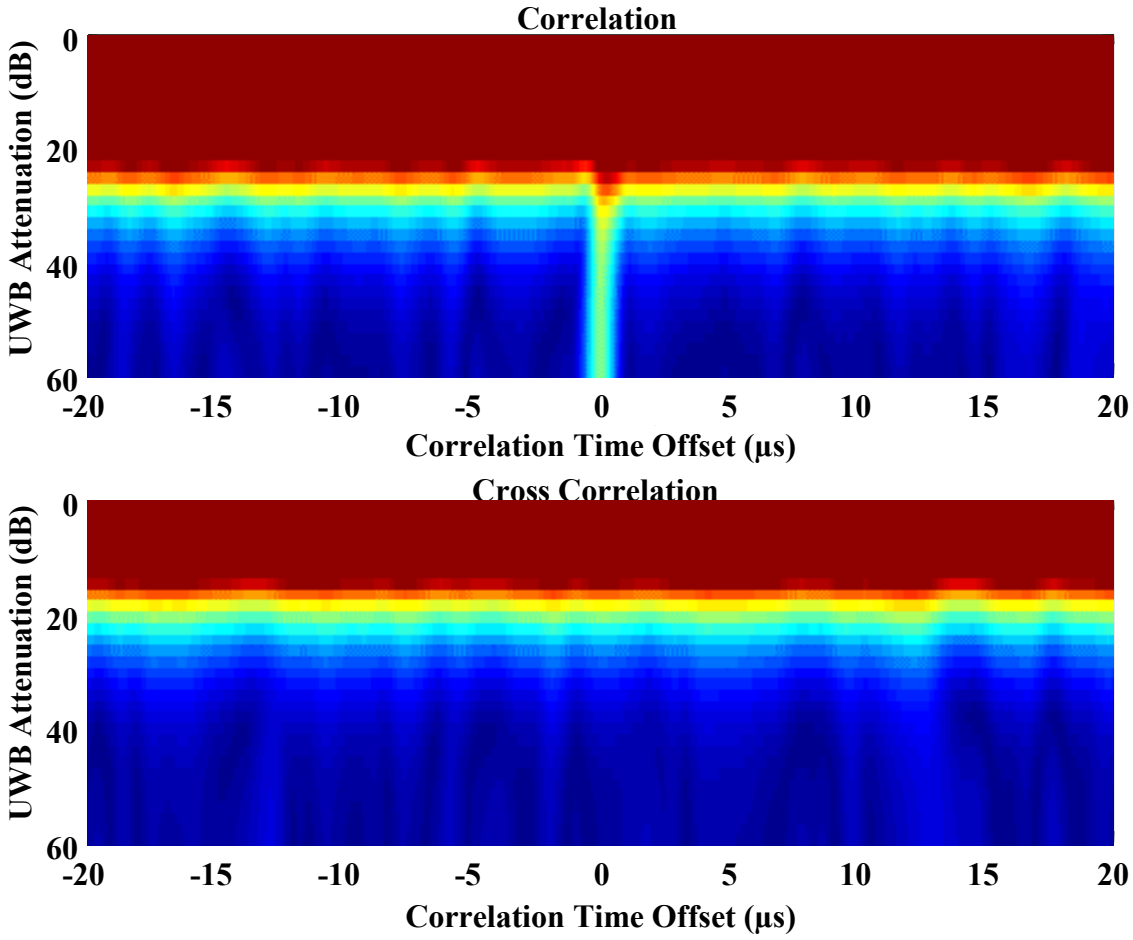

Figure 5-20 GPS Correlation with Injected UWB Signal (PRF=19.94MHz; Undithered)

5.2.7 Evaluation of Interference Potential

The above results are summarized into plots of normalized C/N_0, for each mode, as a function of attenuation of the injected signal. These are shown in Figure 5-21. This interaction occurs in the code tracking before any non-linearity in the front end and AGC. Except for a scale factor dependent upon the specific pulse train coding, the UWB curves have characteristics similar to other types of noise sources.

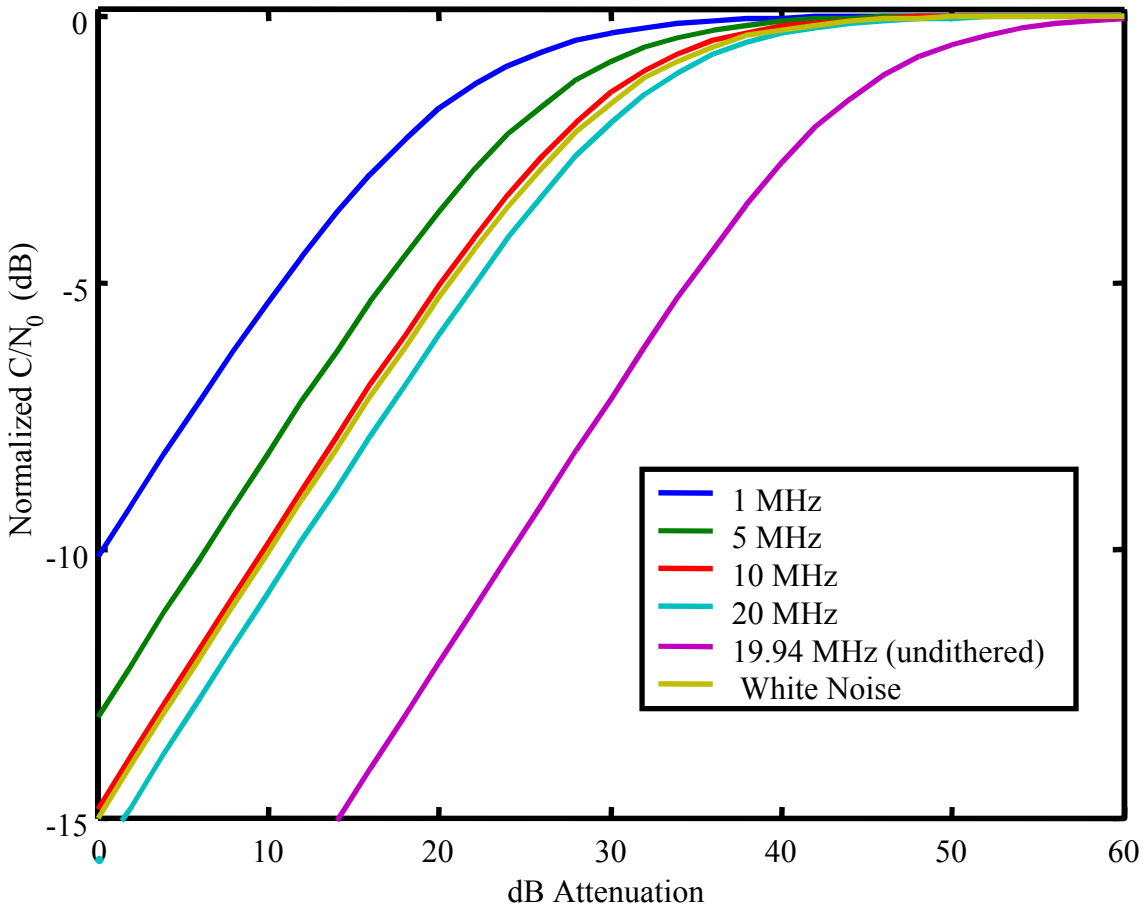

Figure 5-21 Normalized C/N_0

5.2.8 Summary

This theoretical analysis provides an understanding for a means of interference in the GPS C/A code tracking correlation. This allows a prediction for a higher PRF rate, and shows the importance of the details of pulse train coding in how a UWB signal may interact with a GPS receiver. The magnitude of this interaction depends upon details of the pulse train coding beyond average PRF.

CHAPTER 6
DATA ANALYSIS

6.0 Introduction

The primary objective of the The Johns Hopkins University Applied Physics Laboratory (JHU/APL) data analysis has been to produce a specific measures of performance (MOPs) that best represent the Global Positioning System (GPS) performance issues of interest to a large and wide ranging audience. Twelve MOPs are included in this chapter. These MOPs are divided equally into three categories -- receiver navigation outputs, receiver message outputs, and receiver reacquisition. These categories are described in more detail later in this chapter. Each MOP is normalized to represent degradation from nominal or baseline GPS performance and is presented as a hyperbola expressed as a function of the standoff distance or range between a GPS receiver and a UWB device. The normalization permits an informed decision that is based purely on the effects of the UWB device, and not on the natural variations in performance that can be attributed to basic GPS receiver processing or changing satellite geometry. These measures are based solely on the conducted ranging and conducted acquisition portion of the Applied Research Laboratories, University of Texas (ARL:UT) test program. Appendix F contains the results of a favorable comparison or validation between the conducted ranging and radiated ranging tests.

The final results presented in this chapter are based on the data recorded with four GPS receivers (or three when not all data types are available), three ultra-wideband (UWB) device settings, and two simulated GPS power levels. Although more combinations of GPS receivers and UWB device settings were analyzed, only those data that were determined to be correct, representative, and necessary for a complete understanding have been carried completely through the analysis and to the final results. The following GPS receivers were utilized:

- NovAtel 3151
- Ashtech Z-12 and Ashtech Z-Sensor, and
- Garmin 155XL.

The UWB device setting are represented by the following UWB PulsON Application Developer (PAD) modes:

- Mode 1: 1 MHz pulse repetition frequency with a continuous duty cycle
- Mode 7: 5 MHz pulse repetition frequency with a continuous duty cycle, and
- Mode 13: 10-MHz pulse repetition frequency with a continuous duty cycle.

It is noted that the variation across different GPS receivers is greater than the variation between UWB modes, and thus only the highest duty cycles are presented herein. A partial comparison to

other UWB modes (with the 10 MHz pulse repetition frequency and reduced duty cycles) is given in Appendix I. The GPS power levels utilized during the ARL:UT test program are denoted minimum level and live sky. The minimum level represents the GPS signal power received through a GPS antenna from a low elevation satellite near the end of its useful life. The live sky represents the GPS signal power from a high elevation satellite soon after its placement into the constellation. Under actual conditions outside, no receiver actually would receive exclusively minimum level or live sky signal powers. However, since the ARL:UT data collection utilized only a single power level for each test, the results are presented for the homogeneous case only.

Although ARL:UT executed the conducted ranging and conducted acquisition testing as a function of attenuation setting (i.e., a variable attenuator was placed in the UWB signal path and set to values between 0 and 60 dB), the final results are presented as a function of range. The conversion or mapping from test attenuation to equivalent range is described in detail in Appendices A and B. The term "equivalent range" will be used throughout this report to denote results that were subjected to this mapping. Conversely, the term "radiated range" will be used to denote the actual standoff distance used in the radiated portion of the ARL:UT test program. Appendix A also presents the raw MOPs as a function of attenuation setting for each combination of GPS receiver, UWB mode, and GPS power level. This presentation allows the reader to apply alternative mappings from test attenuation to equivalent range that are derived from other scenarios. It is noted that Appendix A also contains raw MOPs when the GPS receiver is injected with white noise instead of the UWB signal.

The following sections in Chapter 6 present the raw MOPs for each of the aforementioned combinations after they have been mapped to equivalent range. This type of presentation allows the reader to gauge the amount of variation that each MOP experiences across the various parameters. Finally, individual raw measures have been collapsed to a condensed MOP. Within the condensed MOPs, two hyperbolas are presented – one for the minimum level and one for the live sky. The coefficients for each hyperbola are computed from a least-squares fit to the appropriate data. Although the coefficients of this fit are not explicitly presented, they are available upon request.

Throughout this chapter, the MOPs are stated for a "compliant UWB device." A compliant device is defined as one that meets the current average or quasi-peak radiated power requirements stated in Section 15.209 of the Federal Communications Commission (FCC) Part 15 regulations. For example, the UWB PAD, while operating in Mode 13, has been measured by an independent FCC compliance laboratory to just meet the current requirements for frequencies above 960 MHz.

6.1 Approach

The approach to the JHU/APL data analysis follows the philosophy – first, thoroughly understand the problem, second, optimize the analysis to yield conclusive results based on a specific yet large database with limited resources, and third, distill the analysis into meaningful terms for the FCC Notice of Proposed Rule Making (NPRM). To understand the entire problem,

one must understand the individual parts of the test program -- the GPS receivers, the UWB devices, the GPS simulator, and the test setups. Beyond that which is documented in the ARL:UT Test Plan and Test Report, we have conducted an extensive analysis of these parts. This understanding is summarized in Chapter 4 and the appendices.

To optimize the database, the analyses have been structured around the following flow-down process. Although, our objective has been to analyze as much data as possible, some data will not be appropriate for any effort while others will demand extensive efforts. In general, the approach has been to prioritize the data according to the following hierarchies (listed from highest to lowest priority). With regard to the test setups, the following hierarchy has been implemented:

- Conducted ranging
  - Conducted acquisition
    - Radiated ranging with UWB Devices
      - Aggregate ranging with UWB noise generators, and finally,
        - Radiated ranging with other FCC compliant devices.

With regard to the GPS receivers, the following hierarchy has been utilized:

- Ashteh Z-12
  - Ashtech Z-Sensor
    - NovAtel 3151
      - NovAtel MiLLenium, and finally,
        - Garmin 155XL.

For the UWB mode, the following hierarchy has been employed:

- UWB modes 1, 7, and 13
  - White Noise, and then,
    - Other UWB modes.

The flow-down approach begins with quality control over nearly all of the data sets based on the basic navigation data output by the GPS receivers. The particular data elements that were examined have varied across test setups as follows:

- Conducted ranging: number of satellites tracked, number of satellites used in the navigation solution, three-dimensional dilution of precision (PDOP), radial position, and satellite ephemeris
- Conducted acquisition: number of satellites tracked and number of satellites used in the navigation solution
- Radiated ranging: number of satellites tracked, number of satellites used in the navigation solution, and satellite ephemeris
- Aggregate ranging: number of satellites tracked and number of satellites used in the navigation solution.

The objectives of the quality control are to: verify the integrity of the individual data sets, verify the hierarchy of the data sets through the test program, ensure a consistency in the performance of the GPS receiver across different baseline data sets, and compute MOPs based on receiver navigation outputs. In addition, this quality control is used to focus the subsequent intermediate quantitative analyses. Both visual and analytical methods have been employed during the quality control process. It is noted that JHU/APL generated MATLAB code has been used to strip and display the raw binary files – rather than manufacturer supplied, public domain, or commercially available software – to ensure a complete and uncorrupted interpretation of the data.

The flow-down approach proceeds with intermediate quantitative analysis on a moderate number of data sets based on the measurement data output by the GPS receivers. The particular data elements that were examined have varied across test setups as follows:

- Conduct range: C/N_0, pseudorange noise, and pseudorange double difference
- Conduct acquisition: time to reacquire and track one satellites, time to reacquire and use four satellites in a navigation solution, and time to reacquire all satellites
- Radiated Range: C/N_0 and pseudorange noise
- Aggregate Range: C/N_0.

The objectives of the intermediate analysis are to: verify any previous conclusions based on analysis of the receiver navigation outputs, verify the conclusions of the theoretical modeling, and compute MOPs based on receiver measurement outputs. Primarily analytical methods using JHU/APL generated MATLAB code have been employed to strip the raw binary files, reformat these data, and then the compute MOPs with inherent error checking and quality control.

The flow-down approach terminates with post-processing renavigation using a very few data sets. This process involves recomputing high precision navigation solutions that incorporate knowledge of the GPS simulator and the errors introduced by the GPS simulator as well as those corrected by the GPS receiver. The primary objective of the renavigation analysis is to understand the test setups. In addition, this process aids in understanding the recorded data elements, real and perceived data anomalies, and the magnitude of the MOPs based on either the receiver navigation or receiver measurement outputs. All analytical methods employed here are based on JHU/APL generated MATLAB code.

6.2 Computing Measures of Performance

Appendix A contains a detailed description of how the per epoch and per satellite data recorded under each test setup configuration and attenuation setting are reduced to the condensed MOPs presented in the next section of this chapter. However, for the casual reader, this section merely contains a flow chart of the process. Figure 6-1 depicts the four nested loops that are executed for each combination of GPS receiver, simulated GPS power level, UWB mode, and attenuation. Once these nested loops are completed, the raw MOPs are condensed to the two hyperbolas. In addition, the results are to be presented as a function of the standoff distance or range between a GPS receiver and a UWB device, where the device is a “compliant device.”

6.3 Raw MOPs

Twelve different MOPs have been chosen to best represent the GPS performance issues of interest to a large and wide ranging audience. They have been divided into the following three broad categories -- receiver navigation outputs, receiver measurement outputs, and receiver reacquisition. Receiver navigation outputs include whole value data items that are typically of value only to an end-user. These data items have nominally undergone some preprocessing, including filtering, smoothing, and editing within the GPS receiver. Therefore, they do not represent the instantaneous or fundamental performance of the GPS receiver. Due to the nature of the preprocessing and the test program chronology, it is noted that the receiver navigation outputs for a particular ranging attenuation setting may be affected or influenced by the previous attenuation setting. The receiver measurement outputs are the per satellite link data that are nominally utilized by higher power users in data quality assessment, differential processing, and post-test renavigation. Although these data may have been subjected to some smoothing within the GPS receiver, they are much more representative of the fundamental performance of the GPS receiver. Finally, the receiver reacquisition category covers the ability of the GPS receiver to acquire satellites that were being tracked just prior to a 30-second loss of satellite signals. This reacquisition differs from the traditional cold start (where the ephemeris, almanac, initial position, and time are unknown) and warm start (all these are known but the ephemeris is not current). In addition, it differs from pure single satellite acquisition, where the GPS receiver has been operating uninterrupted and must begin tracking a new satellite that has come into view. This pure acquisition is reflected in a degradation in number of satellites tracked or number of satellites used in the navigation solution as assessed from the ranging testing.

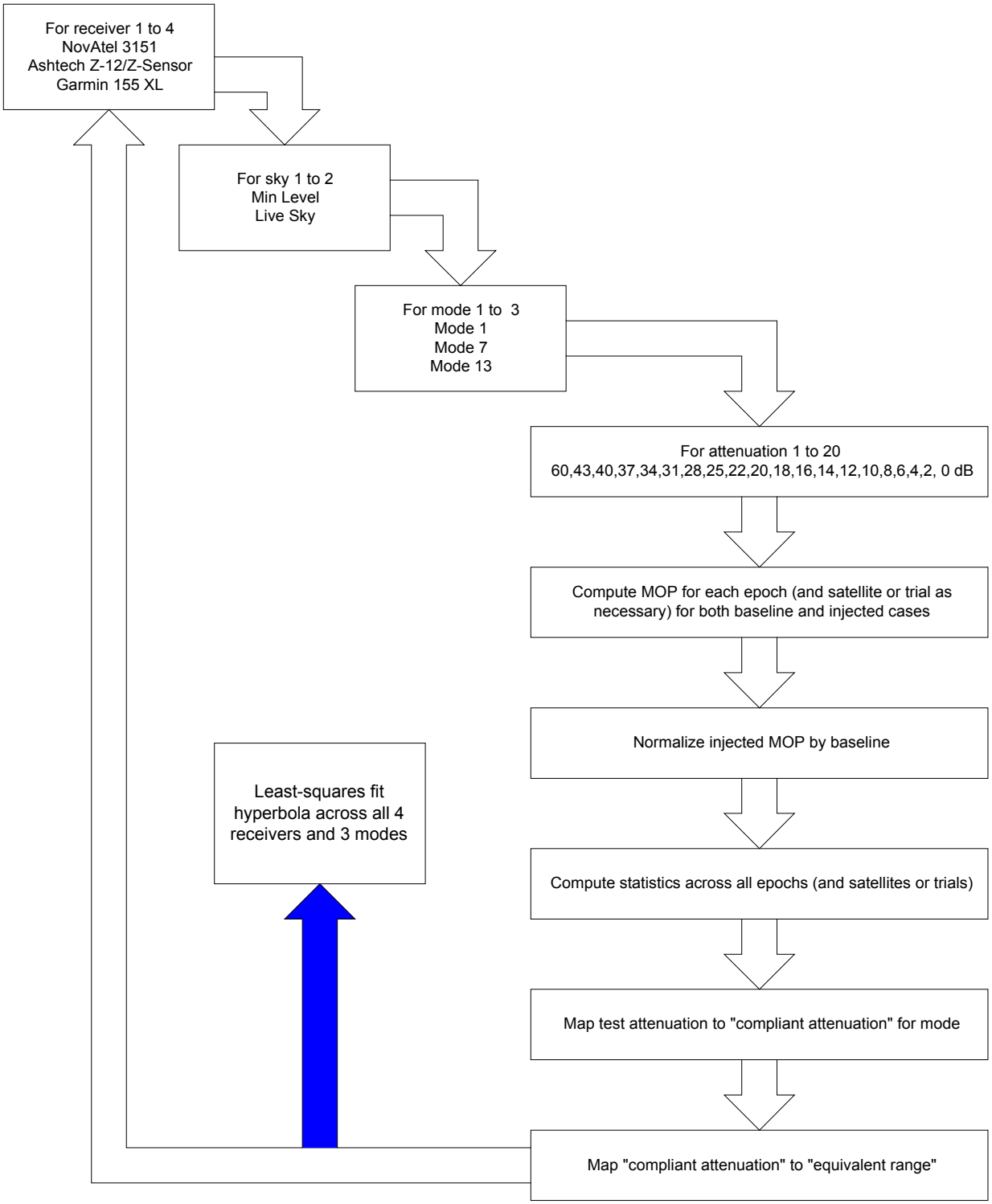

Figure 6-1 Generic Normalization and Condensation Flowchart

For each of these categories, four individual MOPs have been chosen. These individual MOPs are described more thoroughly within the per category presentations in both this chapter and Appendix A. As a part of the presentation in this chapter, a set of four graphs is shown. The upper left-hand graph shows the raw MOP for each GPS receiver and UWB mode combination for a minimum level GPS signal power. The raw MOPs include the effects of normalization; a statistical computation over all epochs, satellites, or trials, as necessary; and mapping to "equivalent range" for a "compliant device." Although no curve fitting has been performed, the data have been edited to remove two types of points. First, points are removed for attenuation settings where too few satellites are being tracked for a valid statistic or actual measure of performance to be computed. Second, points are removed for attenuation settings where anomalies are apparent but are not attributable to the UWB signal. The remaining points have been overlaid for all combinations of receiver and mode. For a particular receiver, a single color has been chosen and the points are connected by a line to allow the reader to more easily trace a particular configuration. This presentation allows the reader to infer the variability in a particular MOP across GPS receivers and UWB modes. Note that only three lines are present for each GPS receiver since only Modes 1, 7, and 13 are carried forward to this point. Appendix A shows similar plots, but before the "equivalent range" and "compliant device" mapping has been applied.

The lower left-hand graph is a similar depiction for the live sky GPS signal power. Finally, the two right-hand graphs are a repeat of the corresponding left-hand ones without the interconnecting lines plus the hyperbola resulting from a least-squares fit to these data are overlaid.

6.3.1 Receiver Navigation Outputs

Receiver navigation data are the whole value items that are output by the GPS receiver for end-users. There are a number of receiver navigation outputs that are natural candidates for evaluation – they include the number of satellites tracked, the number of satellites used in the navigation solution, the position dilution of precision, and the navigated radial position. However, the impact of any type of interference on each of these outputs is not easily defined, and the outputs can vary considerably without interference due to the GPS receivers internal pre-processing. Therefore, taken alone they are difficult to interpret, and thus, it is suggested that the reader interpret them as a collection and not as single observations.

Number of Satellites Tracked

The number of satellites tracked represents those satellites that the GPS receiver has processed through its tracking and correlation steps and output the corresponding measurement data (e.g., pseudorange). The creation of a satellite measurement does not necessarily imply that the data are valid nor that the GPS receiver has sufficient confidence in the measurement to use it in a navigation solution. Under normal conditions, a 12-channel GPS receiver (i.e., all of those in the ARL:UT test program) will track between 8 and 11 satellites. The normalization procedure was to subtract the number of satellites tracked when injected with a UWB signal from the number of satellites tracked under baseline conditions. This difference is computed for each

1-second epoch. Due to its filtered nature, this difference is not adjusted to account for different GPS receiver clock drifts when epoch matching between the baseline and injected cases. The difference data are then averaged over all the valid epochs (with a maximum of 1200 data points from the 20-minute test duration). In the plots, the y-axis represents the decrease in the number of satellites tracked, where a value of 0 represents no degradation and a value of approximately 10 represents loss of the entire satellite constellation. The x-axis is the "equivalent range" in meters. This MOP was available in data from all receivers and is presented in Figure 6-2.

Number of Satellites Used in Navigation Solution

The number of satellites used in the navigation solution represents those satellites for which the GPS receiver acquired valid measurement data and has chosen to use the data in computing the navigation solution. An individual GPS receiver's choice whether to use a particular satellite in the navigation solution is a function of an internal decision tree and is unique to each GPS receiver architecture. Under normal conditions, a 12-channel GPS receiver will use between six and eight satellites in the navigation solution. The normalization procedure was to subtract the number of satellites used when injected with a UWB signal from the number of satellites used under baseline conditions. This difference is computed for each 1 second epoch. Again, exact millisecond level epoch matching is not necessary. The difference data are then averaged over all the valid epochs. In the plots, the y-axis represents the decrease in the number of satellites tracked, where a value of 0 represents no degradation and a value of approximately 4 represents an inability to continue producing a navigation solution. The later value is not the full constellation since at least four satellites are required to compute a three-dimensional position and time. The x-axis is the "equivalent range" in meters. This MOP was available in data from all receivers and is presented in Figure 6-3.

Position Dilution of Precision (PDOP)

The PDOP is a direct measure of the adequacy of the satellite geometry and an indirect measure of the accuracy of the three-dimensional position solution. It is derived from a covariance analysis on the impact of the satellite geometry and the per satellite pseudorange error. In addition to the geometric effects, PDOP will naturally vary as the number of satellites used in the navigation solution changes -- whether due to satellites coming into-view or going out-of-view or due to the aforementioned internal decision tree. Typically acceptable PDOP values are between 1.0 and 2.0. The normalization procedure was to divide the PDOP under the injected scenario by the PDOP under baseline conditions for each one-second epoch. Again, exact millisecond level epoch matching is not necessary. The difference data are then averaged over all the valid epochs. In the plots, the y-axis is the normalized PDOP, where a value of 1 represents no degradation and a value of 2 represents a PDOP that is double the baseline. The x-axis is the "equivalent range" in meters. This MOP was computed for the Ashtech Z-12, Ashtech Z-Sensor, and Garmin 155 XL GPS receivers and is presented in Figure 6-4. The NovAtel 3151 GPS receiver was not used because PDOP was not included in the raw binary data stream.

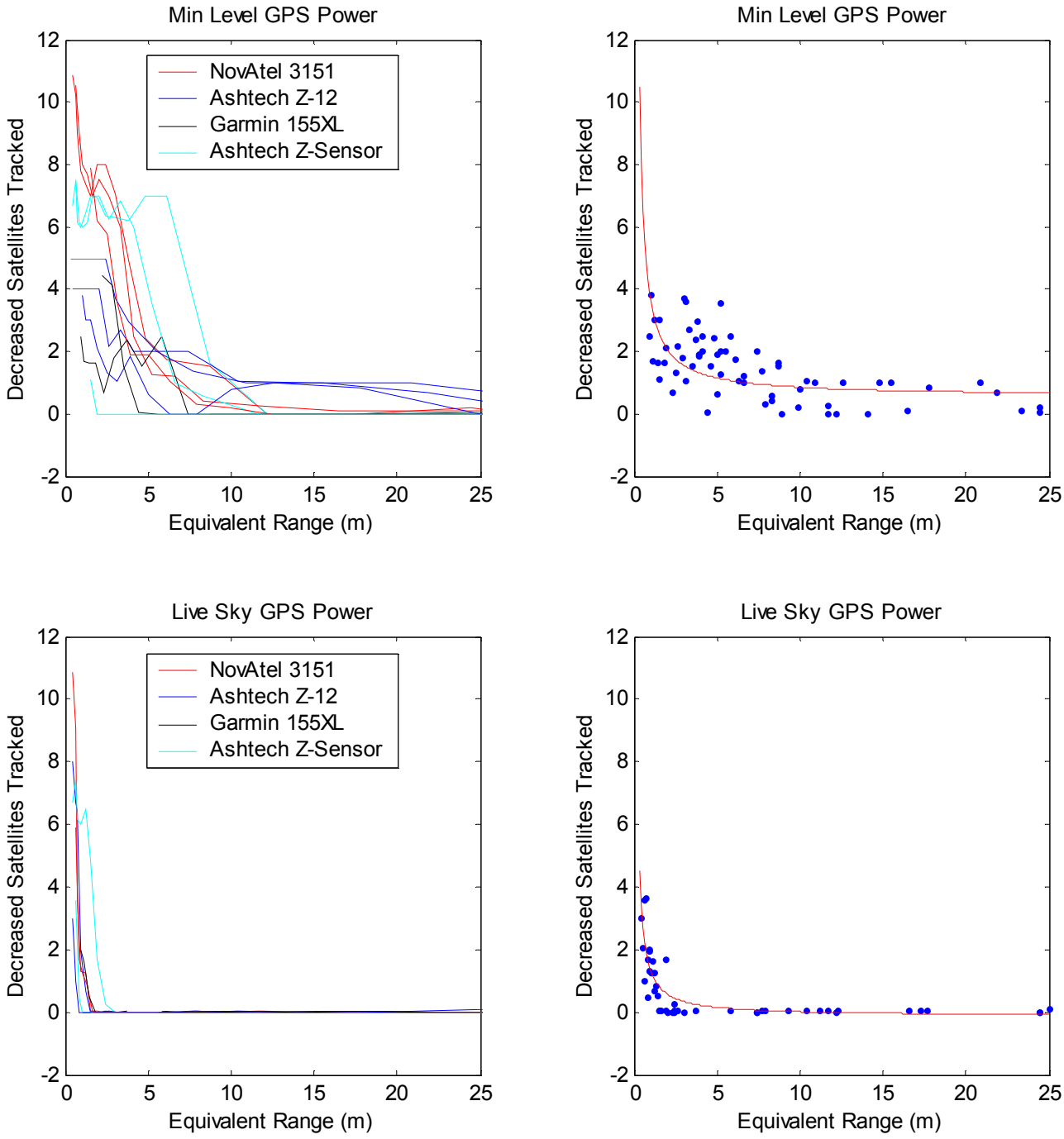

Figure 6-2 Number of Satellites Tracked

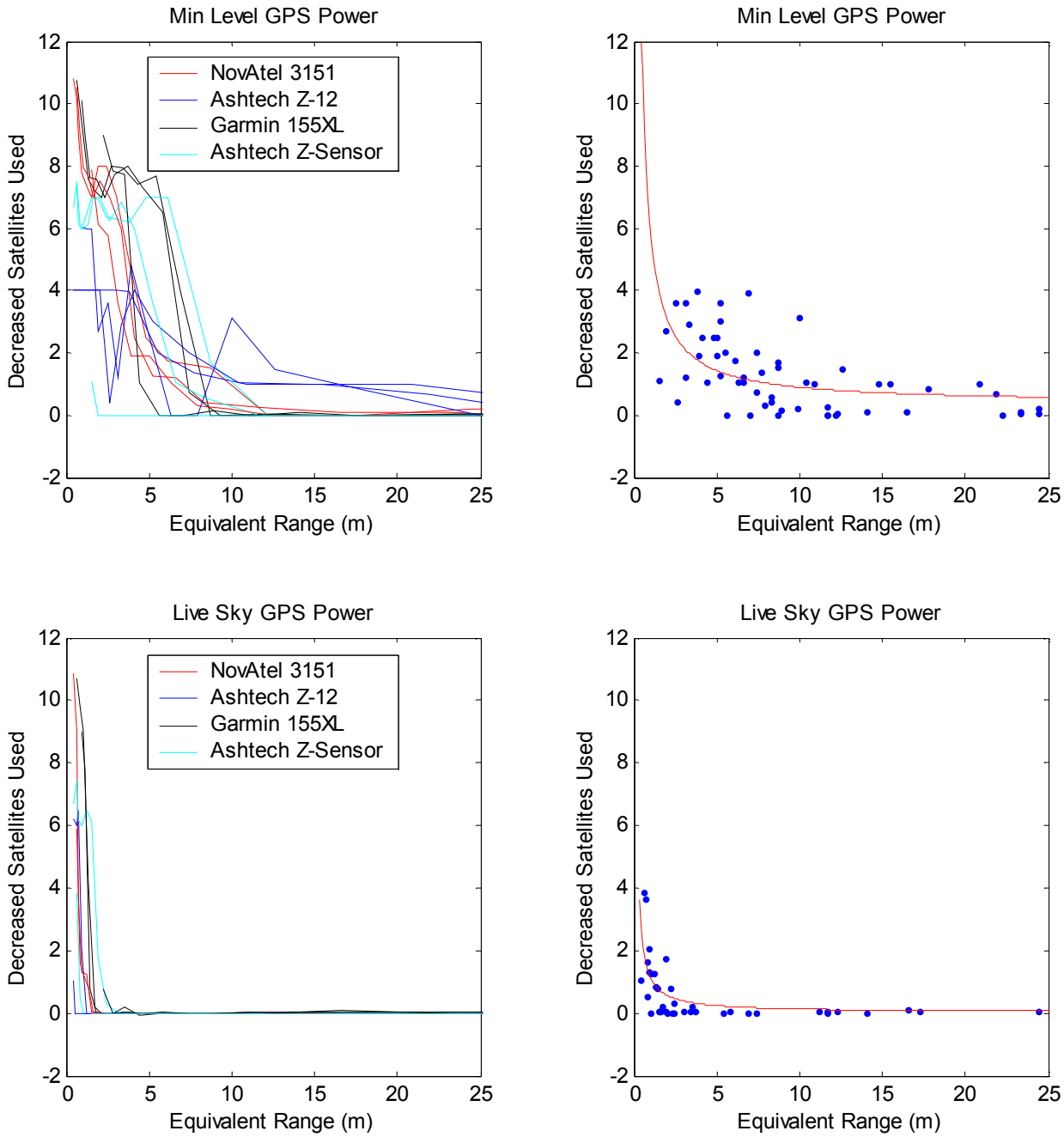

Figure 6-3 Number of Satellites Used in the Navigation Solution

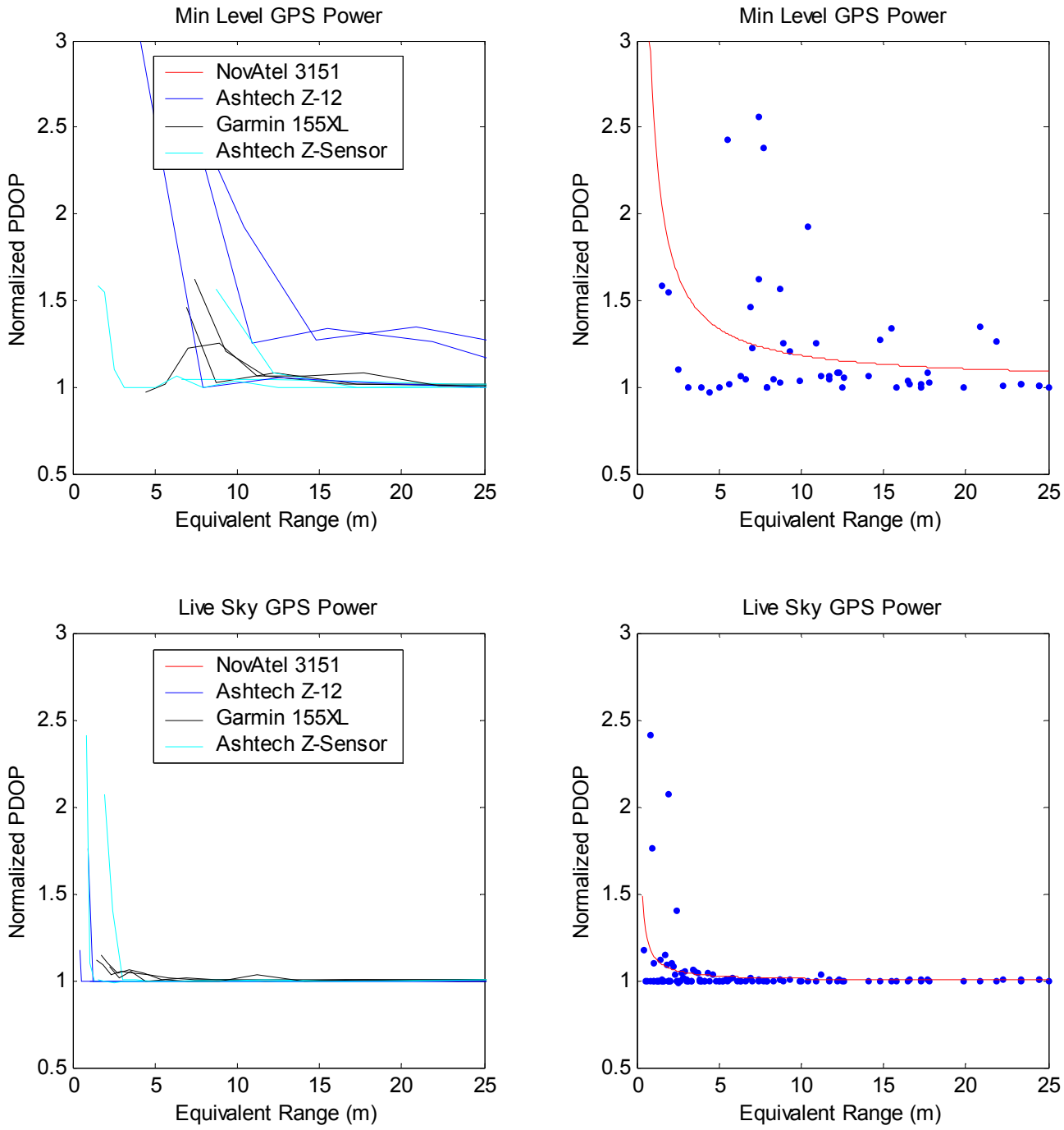

Figure 6-4 Position Dilution of Precision

Receiver Position

The three-dimensional position computed by a GPS receiver naturally oscillates about the true position due to inaccuracies inherent to the satellite ephemeris data, atmospheric effects, and receiver errors. After Selective Availability was disabled in May 2000, the 1-sigma error in three-dimensional position is nominally less than 10 meters but depends on the exact GPS receiver architecture. During the conducted ranging testing, the GPS simulator was setup to create a static GPS receiver position (i.e., x=-740463, y=-5457015, and z=3207281 in the ECEF coordinate frame). The normalization was accomplished by first subtracting the simulated receiver position from both the injected and baseline computed positions for each epoch. The individual components are then root-sum-squared to give the change in radial position error for each one-second epoch. Again, exact millisecond level epoch matching is not necessary. Finally, this change is averaged over all the valid epochs. In the plots, the y-axis is the increase in radial position error, where a value of 0 represents no degradation and all other values represent the magnitude of the error in meters. The x-axis is the "equivalent range" in meters. This MOP was computed for the Ashtech Z-12, Ashtech Z-Sensor, and Garmin 155 XL GPS receivers and is presented in Figure 6-5. The NovAtel 3151 GPS receiver was not used because navigation solutions were not included in the raw binary data stream.

6.3.2 Receiver Measurement Outputs

The receiver measurements are the per satellite link data. Unlike the receiver navigation outputs, they have been subject to only minor preprocessing. Although these data are not typically available to average GPS users, they are of vital importance to high accuracy users and are most representative of the fundamental performance of the GPS receiver. In addition, they provide an excellent crosscheck on the overall quality of the receiver navigation outputs. Except for the first MOP in this section, the per epoch data are not directly available in the raw binary stream, but instead require very meticulous computations based on data that are available in the raw binary stream. In this chapter, these MOPs are only superficially described, and the reader is directed to Appendix C for a more detailed description of their computations. The chosen MOPs are carrier-to-noise ratio (C/N_0), pseudorange noise, and pseudorange accuracy as expressed as a double difference. The analysis herein focuses on the L1 frequency since most commercial users are concerned with the L1 frequency and only have receivers capable of receiving L1 C/A. In addition, the majority of the GPS frequency band concerns voiced in initial replies to the NOI and NPRM were with respect to the L1 frequency band.

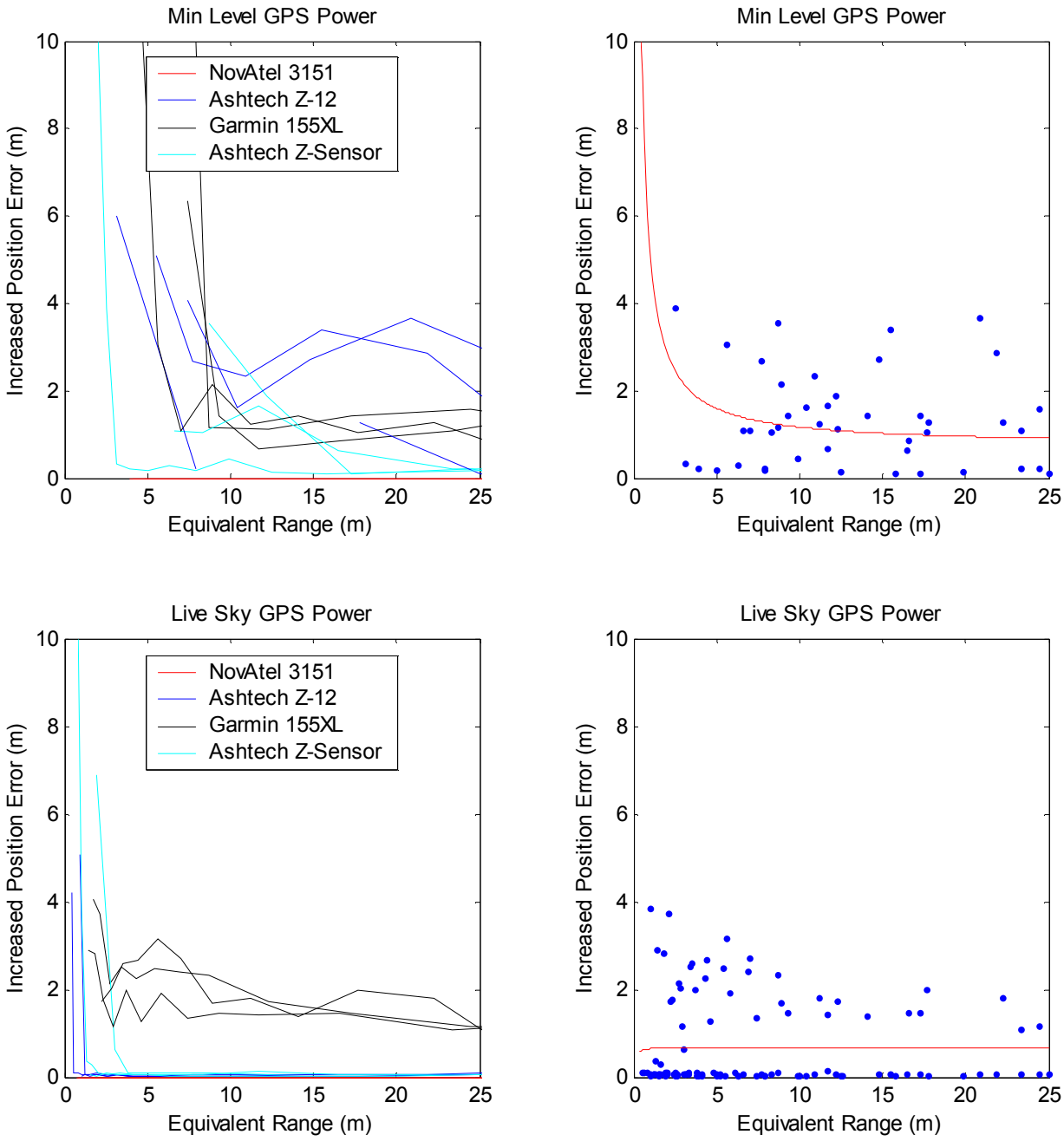

Figure 6-5 Receiver Position

Carrier-to-Noise Ratio

The carrier-to-noise density ratio, typically denoted C/N_0, is a measure of the signal to noise ratio in the GPS receiver. However, there is not a single, common methodology for computing C/N_0 and the values can vary somewhat between GPS receiver architectures and implementations. C/N_0 values of 40 to 50 dB are typically observed under nominal conditions. In general, degradation in C/N_0 does not permit a direct assessment of tracking performance because no thresholds exist; however, it does allow for excellent predictions of degradation in pseudorange noise and pseudorange accuracy. The normalization is accomplished by dividing any non-zero C/N_0 from the injected case by the C/N_0 from the baseline case. No attempt is made to epoch match at the millisecond level. This ratio is then averaged over all epochs and satellites tracked (not just the satellites used in the navigation solutions). The data are considered to be from a single distribution across all satellites, and no ANOVA statistic (nor per satellite link average) is computed. In the plots, the y-axis is normalized C/N_0, where a value of 1 represents no degradation and a value of 0.75 represents an average C/N_0 that is 75 percent of the baseline. The x-axis is the "equivalent range" in meters. This MOP was available in data from all receivers and is presented in Figure 6-6.

Pseudorange Measurement Noise

An excellent method for assessing pseudorange measurement noise that avoids the need for full processing and removal of systematic errors can be accomplished by differencing the code based and carrier inferred pseudoranges. The carrier based value is inherently much less noisy, and the variance of the difference is an excellent quantification of the pseudorange measurement noise. The details of this computation are explained in Appendix C. The normalization is accomplished by computing the code minus carrier pseudorange for each epoch and satellite for both the injected and baseline cases. For the two cases, the variance in this difference is computed across all epochs and satellites tracked. The data are considered to be from a single distribution across all satellites, and no ANOVA statistic is computed. Finally, the ratio of the injected case is divided by the ratio of the baseline case. In the plots, the y-axis is normalized pseudorange measurement noise, where a value of 1 represents no degradation and a value of 2 represents a doubling of the pseudorange measurement noise. The x-axis is the "equivalent range" in meters. This MOP was computed for the Ashtech Z-12, Ashtech Z-Sensor, and NovAtel 3151 GPS receivers and is presented in Figure 6-7. The Garmin 155XL GPS receiver was not used because raw measurement data were not included in the NMEA 0183 data stream.

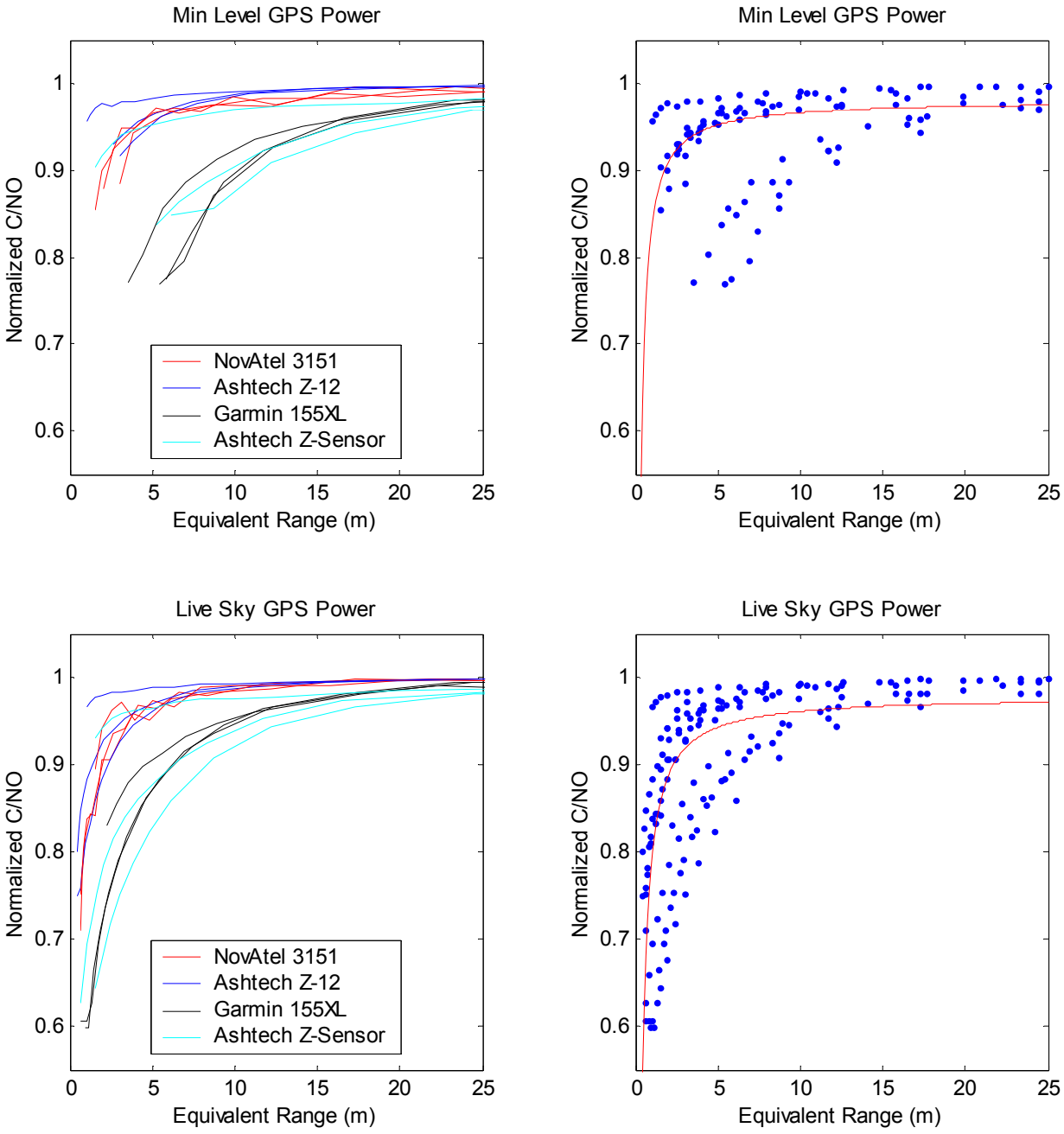

Figure 6-6 Carrier-to-Noise Ratio

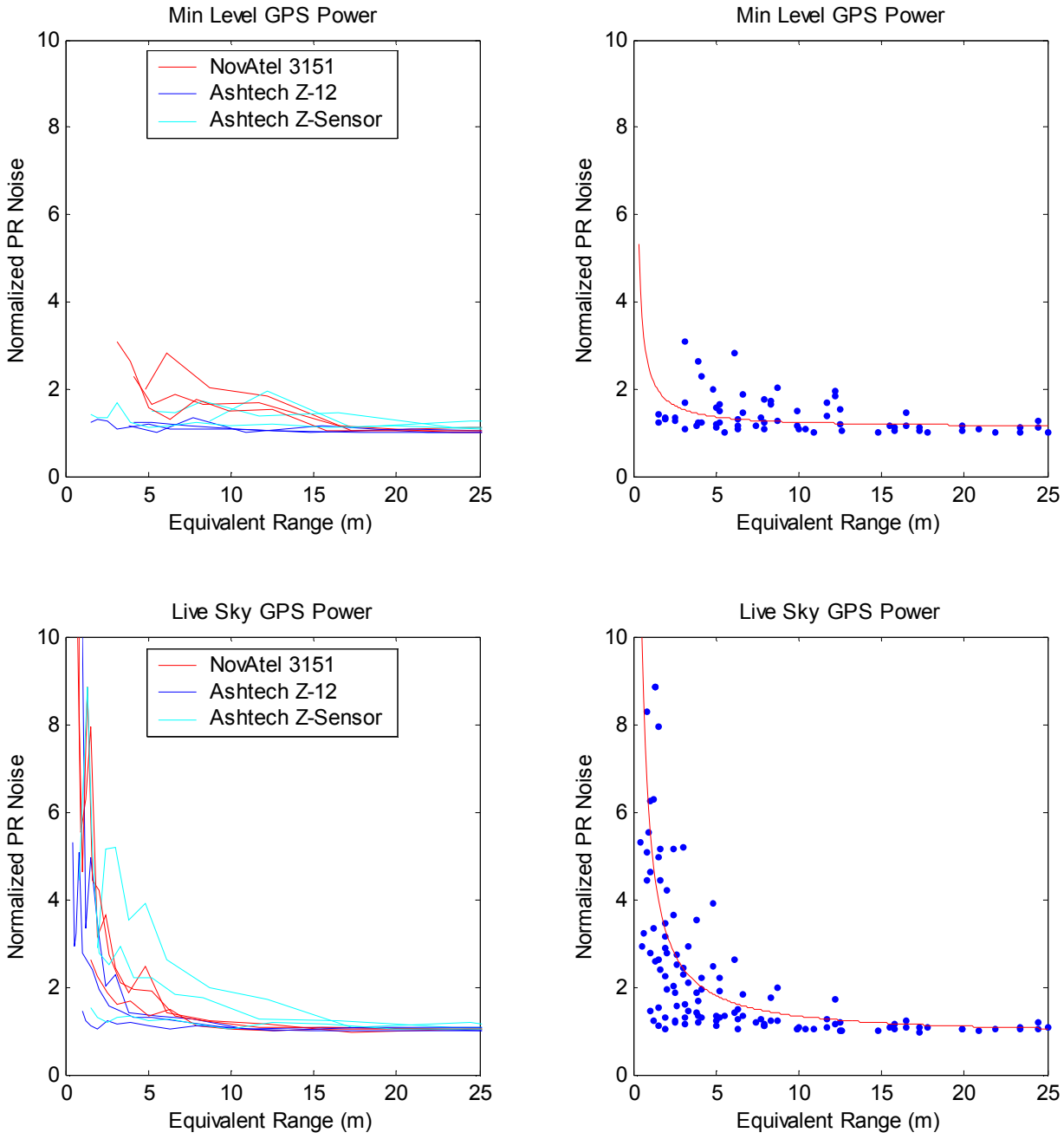

Figure 6-7 Pseudorange Measurement Noise

Pseudorange Measurement Accuracy

Another method for assessing the quality of the pseudorange measurements is to examine the statistics on the pseudorange double differences. This method requires significantly more processing and attention to details, such as epoch matching at the millisecond level. As the name implies, the computation requires two separate difference calculations. The first (or single) difference is the link difference or pseudorange difference between two satellites for the same GPS receiver. This computation results in n-1 (where n is the number of satellites) link differences that are free of the GPS receiver clock error. The second (or double) difference is the difference between the link difference computed for the same satellite pair in the injected case and the baseline case. This computation results in n-1 double differences that should only contain random noise that is two times the actual noise in each measurement. By its nature, the double difference is already normalized. The details of this computation are given in Appendix C.

The mean and variance of the double difference is then computed over all epochs and satellites tracked. The data are again considered to be from a single distribution across all satellites. The bias should be nearly zero and the noise should track with degradation in pseudorange measurement noise and C/N_0. The plots in Figures 6-8 and 6-9 represent the bias (mean) and noise (standard deviation), respectively. The y-axis is the double difference bias or noise in meters. The initial value at an "equivalent range" of 25 meters represents no degradation and subsequent values are the degraded value. When computing absolute degradations, the reader is cautioned to account for the number of pseudorange measurements implicit in the MOP (i.e., 4), the fact that the measurement includes both baseline and injected inaccuracies, and the noise is not simply additive. The x-axis is the "equivalent range" in meters. This MOP was computed for the Ashtech Z-12, Ashtech Z-Sensor, and NovAtel 3151 GPS receivers. The Garmin 155XL GPS receiver was not used because raw measurement data were not included in the NMEA 0183 data stream.

6.3.3 Receiver Reacquisition

Another very important parameter to a GPS user is how quickly the receiver acquires GPS satellite signals that it had previously been tracking. Acquisition testing requires a completely different testing process and is described in Chapter 4. The ability to acquire GPS signals is different depending on the length of time since last signal track. A receiver at first turn-on (i.e., cold start) will take longer to acquire then one that has lost signals for some prolonged length of time (i.e., warm start). The shortest time to acquire is when the receiver has lost signals for a relatively short length of time (i.e., reacquisition). This last case is the one covered in the ARL:UT test program, where the signals were lost for 30 seconds. This time is shorter than the reacquisition criterion used, for example, in the GPS World magazine's receiver survey where signals are assumed to be lost for 1 minute. It is noted that these times differ from the pure acquisition of new (e.g., elevation just increasing over the horizon) satellites with a receiver that has been running all along.

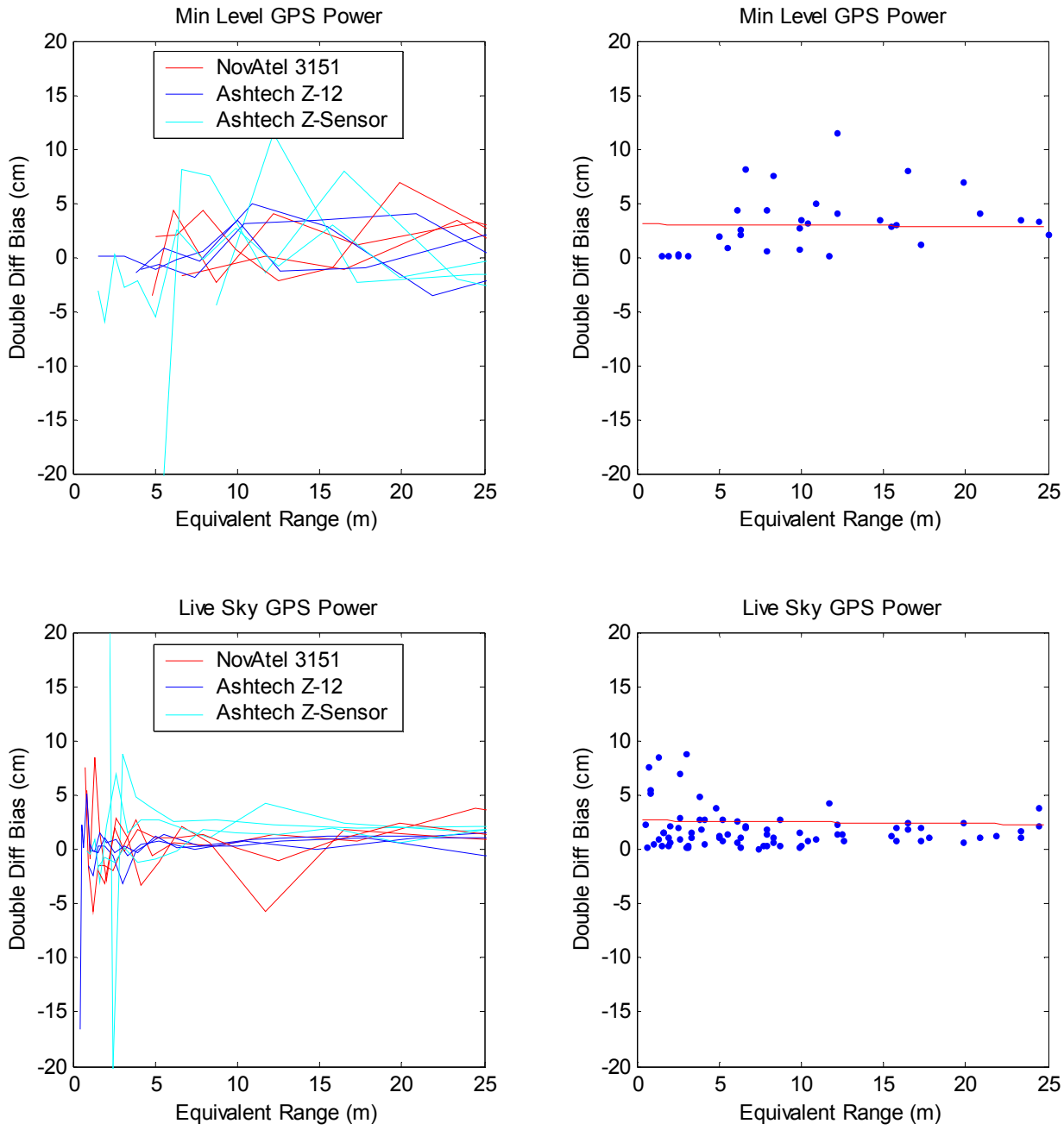

Figure 6-8 Pseudorange Double Difference Bias

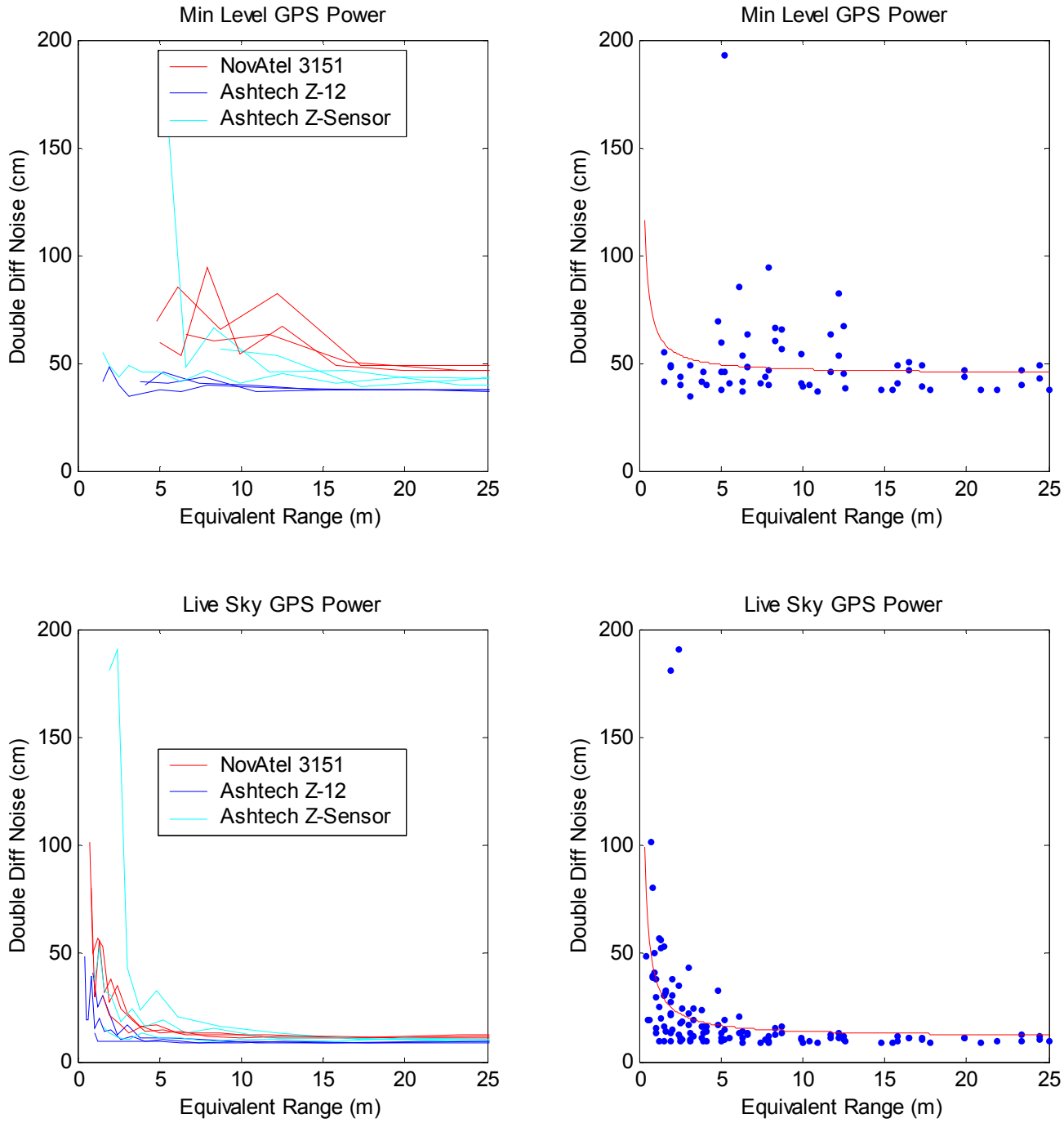

Figure 6-9 Pseudorange Double Difference Noise

Reacquisition is stated in terms of three times: 1) the time between the reintroduction of the GPS signals and when the receiver starts to track its first satellite, 2) the time between the reintroduction of the GPS signals and when the receiver starts to track at least four satellites necessary for a position solution, and 3) the time between the reintroduction of the GPS signals and when the receiver tracks all in-view satellites (i.e., all satellites tracked prior to the loss of GPS signal). Recall that the receiver data navigation outputs were computed from MOPs collected at each time epoch. The reacquisition times were not collected for each time epoch, but rather for each trial (a 3-to-4 minute interval where the receivers were permitted to acquire lock, then forced to drop lock, then allowed to regain lock). Appendix C describes the process of gathering each of the three reacquisition times from a trial's dataset. It also describes the conversion of the times for a specific test (i.e., 30 trials) into an average reacquisition time and a reacquisition probability. What is presented below describes how the reacquisition times for each test are used to produce the data in the condensed MOP plots.

Each UWB reacquisition test was run in one of three (GPS) time intervals. One baseline reacquisition test was also run in each one of these three intervals. After the processing described in Appendix C, each test's data are reduced to an average reacquisition time and a reacquisition probability. Each test's average reacquisition time gets normalized by the average reacquisition time of its associated baseline to produce values that indicate the difference in reacquisition time attributable to UWB. Instances where the normalized value are less than zero are attributed to 1) inaccuracies in the times at which the GPS signals are removed and restored (up to 2 seconds total error), and 2) low reacquisition probabilities. These values are not propagated forward. In the plots, the y-axis represents the increase in reacquisition times in seconds. The x-axis is the "equivalent range" in meters. The reacquisition MOPs were available in data from receivers 1, 2 and 4. Figure 6-10 presents the normalized reacquisition time for one tracked satellite. Figure 6-11 presents the normalized reacquisition time for four navigated satellites. Figure 6-12 presents the normalized reacquisition time for all-in-view tracked satellites. The reacquisition probabilities for four navigated satellites for receivers 1, 2, and 4 are also presented in Figure 6-13.

6.4 Other Data Analyses

Two additional areas of analysis that were applied to the conducted ranging data are navigation message recovery and post-processing renavigation. These analyses do not lend themselves to the computation of specific MOPs that can be plotted as a function of the "equivalent range." Instead, they are quantitative assessments of the basic computations inherent to the GPS receiver and allow one to more thoroughly understand the test setup utilized by ARL:UT. The results of the navigation message recovery analysis are presented in Appendix D, and the results of the post-processing renavigation are presented in AppendixE.

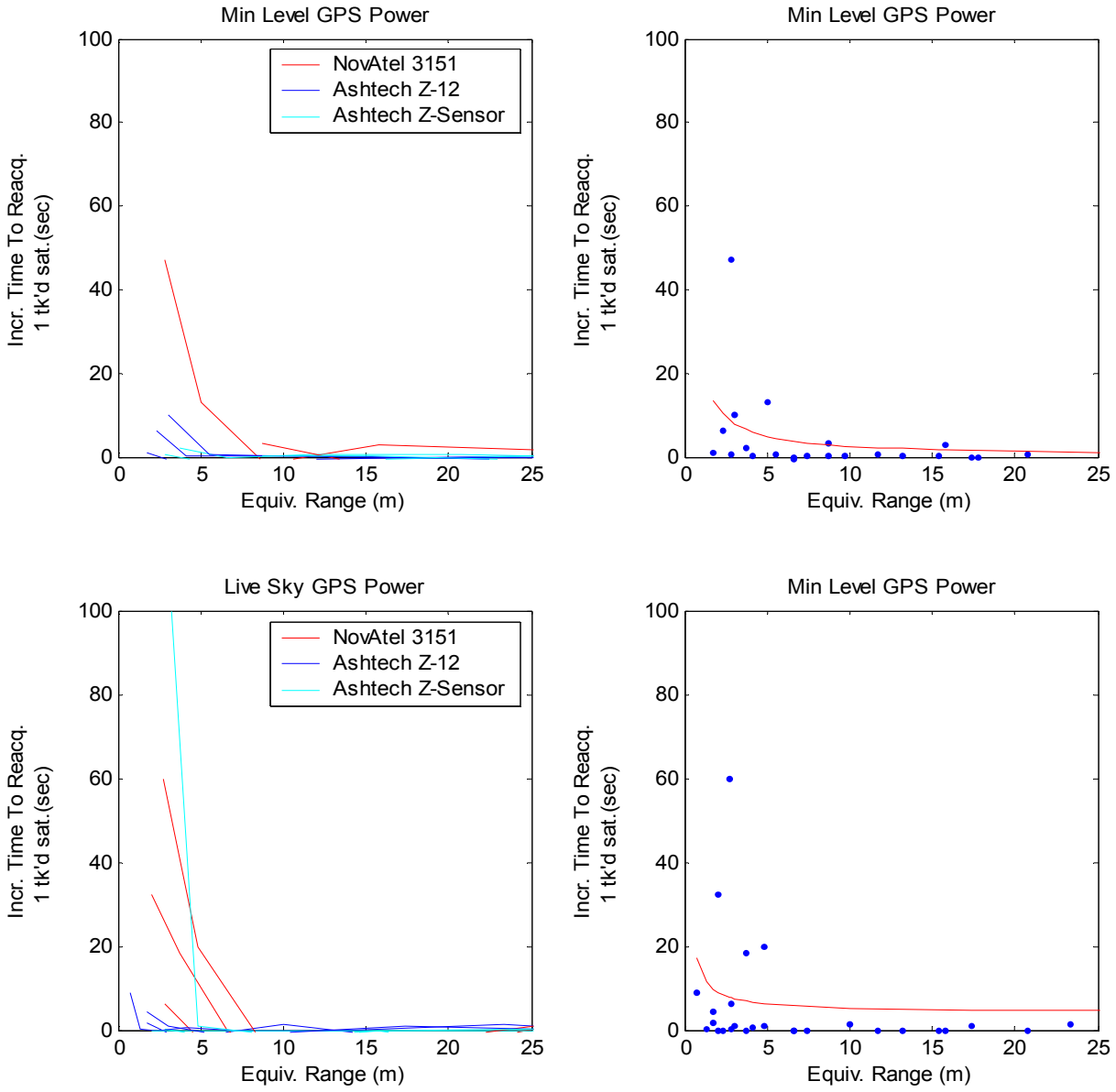

Figure 6-10 Reacquisition of One Tracked Satellite

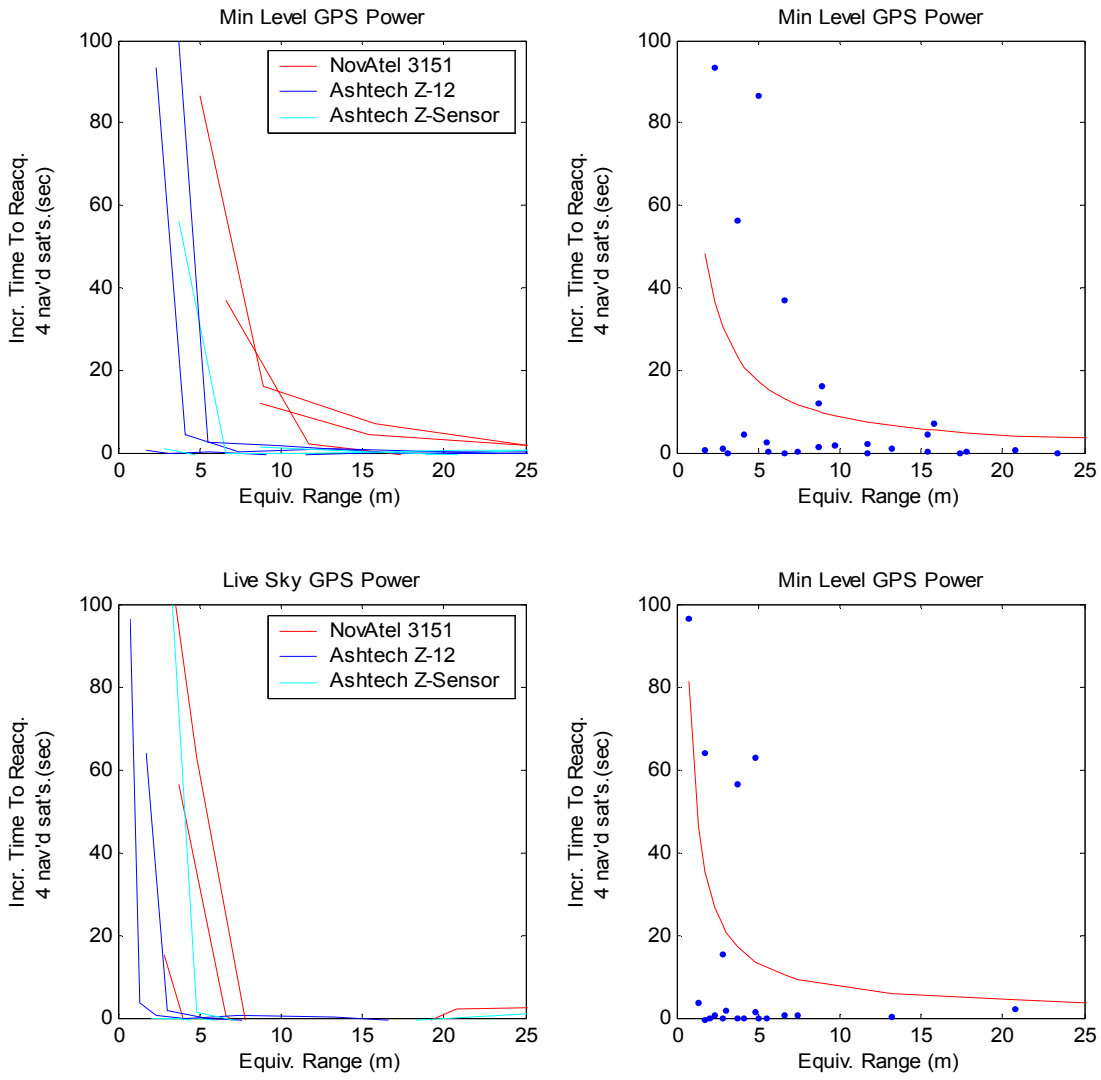

Figure 6-11 Reacquisition of Four Navigated Satellites

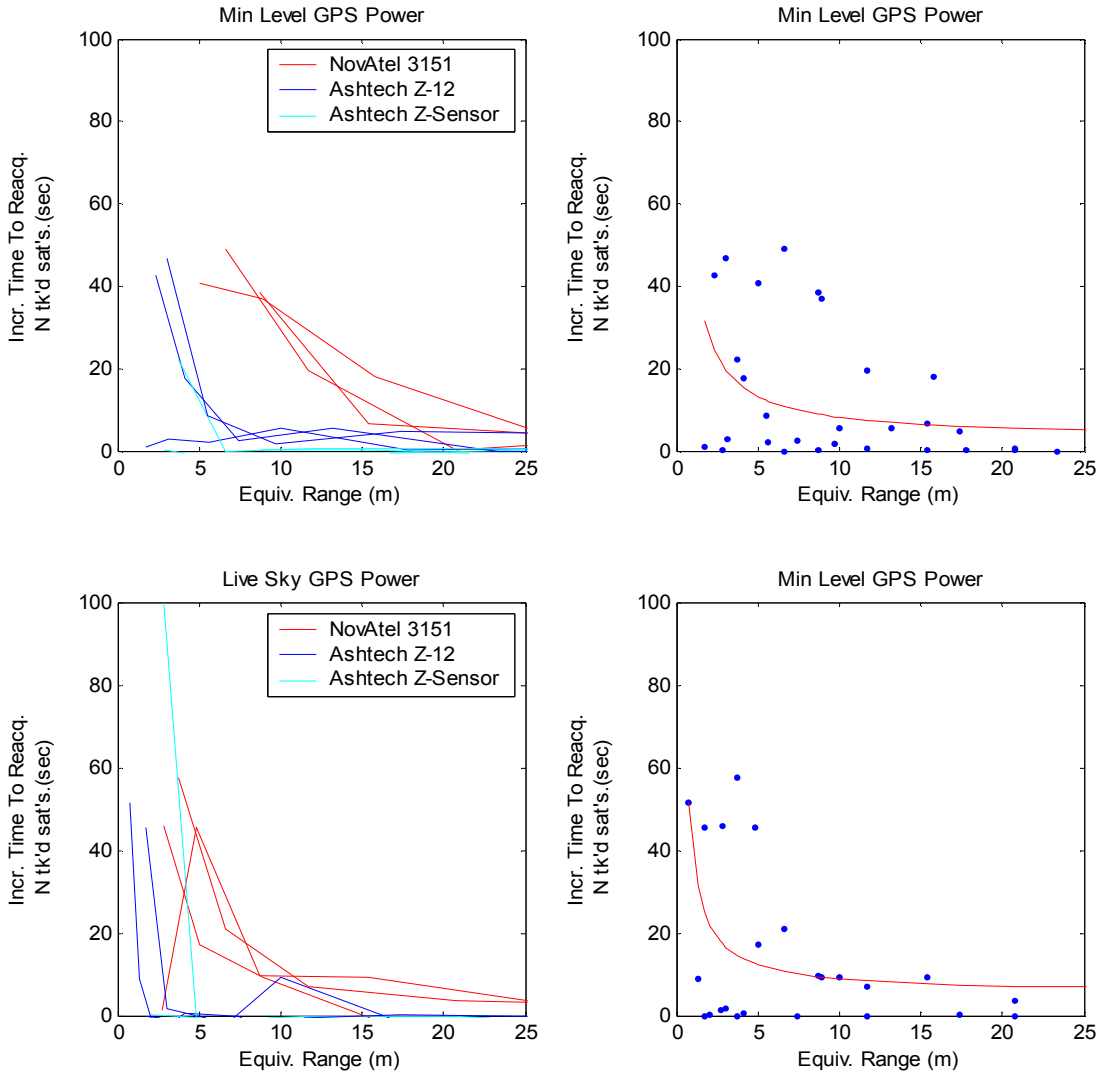

Figure 6-12 Reacquisition of All-In-View Tracked Satellites

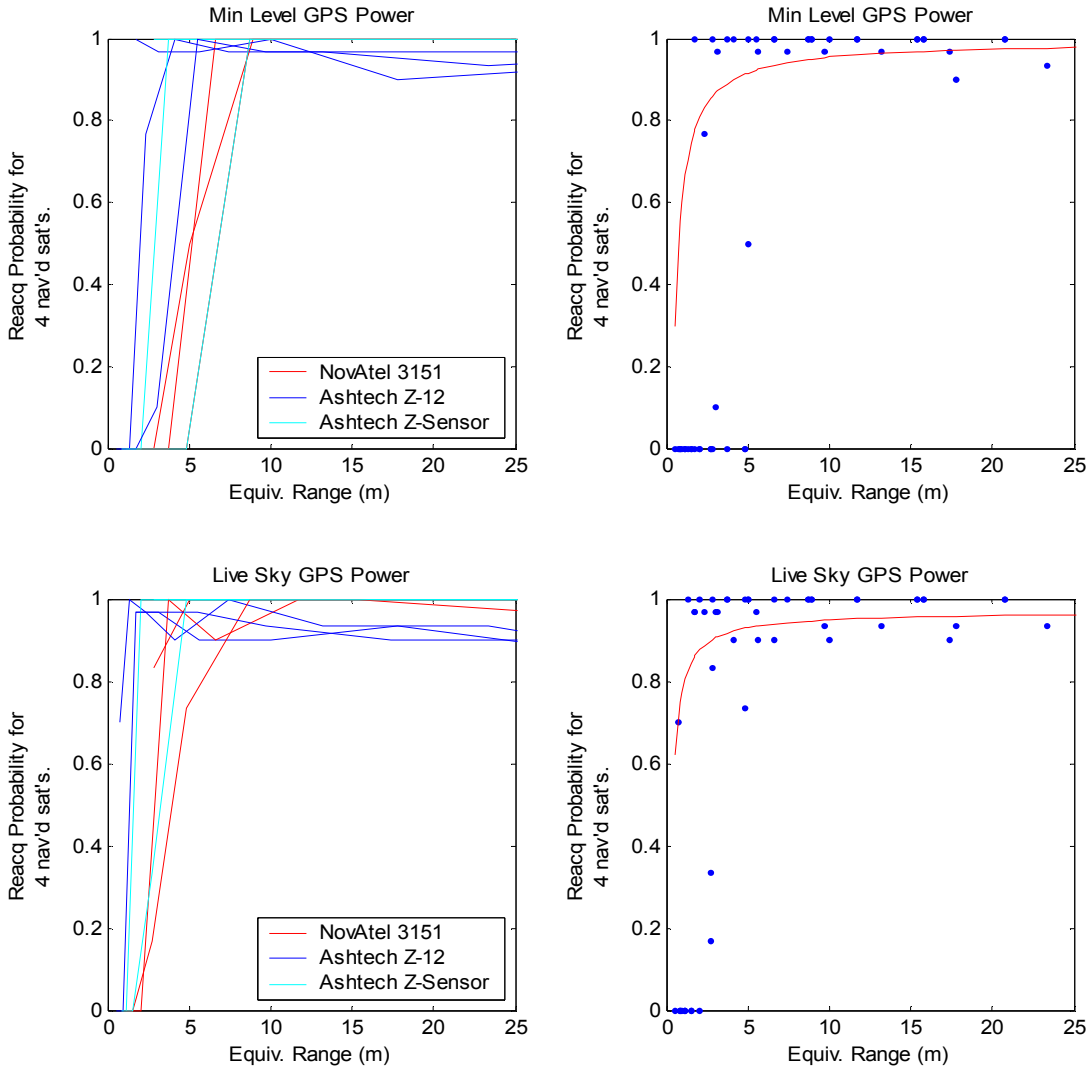

Figure 6-13 Reacquisition Probability of Four Navigated Satellites

6.5 Condensed MOPs

This final section of Chapter 6 presents the 12 MOPs expressed simply as the aforementioned hyperbolic curves that are a function of equivalent range. They are presented in three figures, one for each major category: receiver navigation outputs, receiver message outputs, and receiver reacquisition. Each figure contains a separate graph for each of the corresponding MOPs. Within a single graph, a separate curve is drawn for the two GPS power levels that ARL:UT simulated in the conducted testing. ARL:UT intended the minimum level and live sky GPS power levels to represent the minimum Department of Defense (DoD) threshold and a current satellite constellation, respectively. The levels more realistically represent the GPS signal power received through the beam pattern of a GPS antenna from 1) a low elevation satellite near the end of its useful life and 2) a high elevation satellite soon after its placement into the constellation. Under actual conditions outside, no receiver actually would receive exclusively minimum level or live sky signal powers; therefore, the true MOP for a full constellation lies in between the two curves.

Figures 6-14 through 6-16 contain the 12 plots. Within the confines of the data collection test program, these figures reveal a number of key observations.

- For average powers that are compliant with the current FCC Part 15 regulations, the performance of GPS receivers is observed to degrade most rapidly when the separation between the tested receivers and UWB devices is less than about 3 meters. As the separation decreases below 3 meters, all users of these GPS receivers will be severely impacted, and in the extreme, lose lock on all satellites.

- For separations greater than 3 meters, GPS receiver performance converges asymptotically to nominal levels. The minimum separation at which degradations are acceptable depends on individual user scenarios including performance thresholds, GPS receiver, and UWB device(s).

- The MOPs are observed to vary more widely across the various GPS receivers than across the different modes (i.e., PRF and duty cycle) of the UWB devices used in the test. However, irrespective of the particular GPS receiver manufacturer and model, the degradation in every MOP follows the same trend and has inflection points at nearly the same equivalent range.

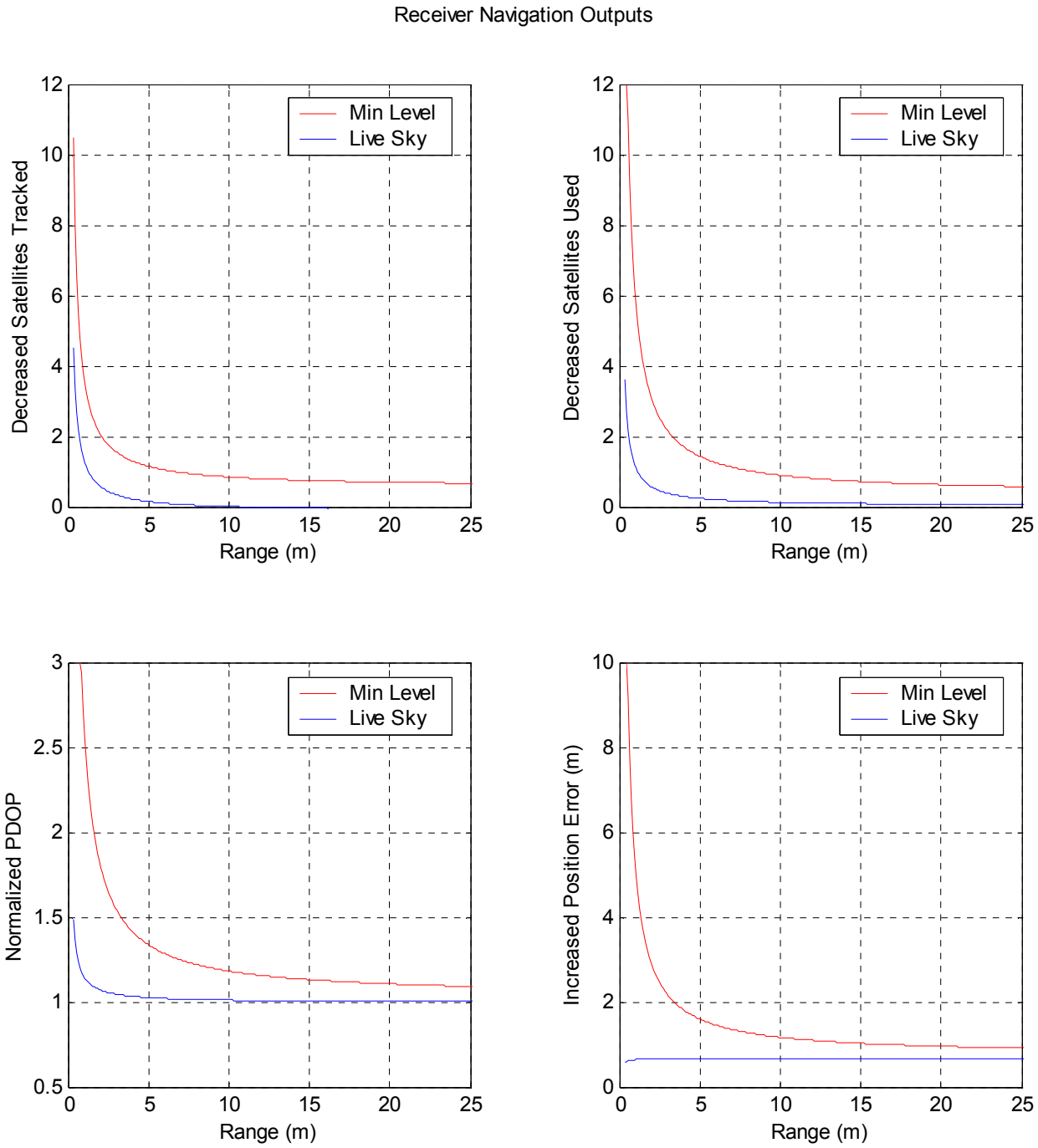

Figure 6-14 Condensed Measures of Performance for Receiver Navigation Outputs

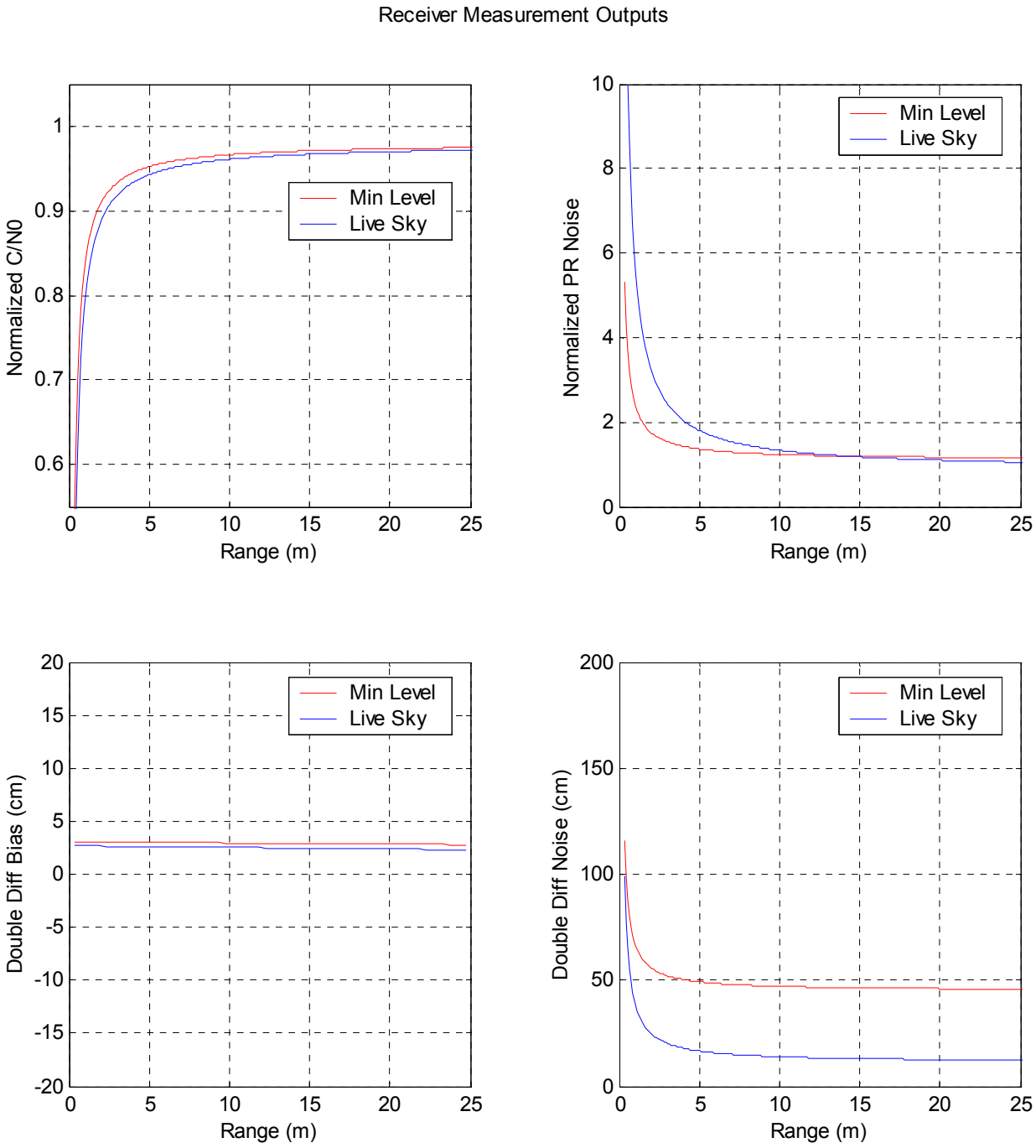

Figure 6-15 Condensed Measures of Performance for Receiver Measurement Outputs

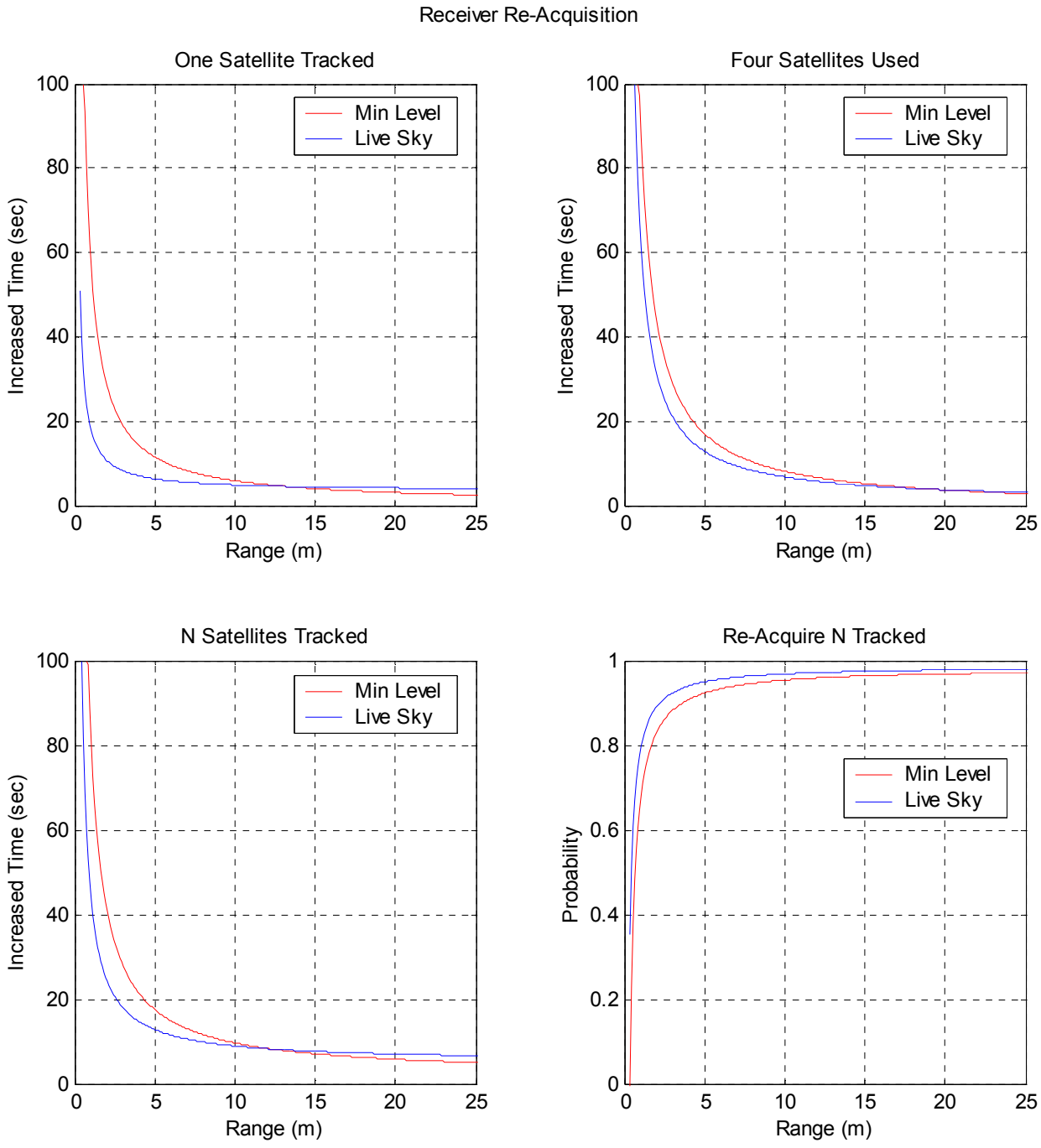

Figure 6-16 Condensed Measures of Performance for Receiver Reacquisition

CHAPTER 7
REFERENCES AND RESOURCES

(1) FCC 98-208, Federal Communications Commission Notice of Inquiry, In the Matter of Revision of Part 15 of the Commission's Rules Regarding Ultra-Wideband Transmission Systems, ET Docket No. 98-153, Released 01 September 1998.

(2) Title 47, Code of Federal Regulations, Chapter I, Part 15.

(3) FCC 00-163, Federal Communications Commission Notice of Proposed Rule Making, In the Matter of Revision of Part 15 of the Commission's Rules Regarding Ultra-Wideband Transmission Systems, ET Docket No. 98-153, Released 11 May 2000.

(4) ASD UWB TP0001, Test Plan for Measuring UWB/GPS Compatibility Effects, Applied Research Laboratories University of Texas at Austin, Draft 3 dated 21 July 2000.

(5) ASD UWB TP0002, Test Report for Measuring UWB/GPS Compatibility Effects, Applied Research Laboratories University of Texas at Austin, Draft dated 16 January 2001.

(6) Harmuth, H.F., Transmission of Information by Orthogonal Functions, First Edition, Springer, New York, 1969.

(7) Robbins, K.W., Short Baseband Pulse Receiver. U.S. Patent 3,662,316, dated May 9, 1972.

(8) Robbins, K.W. & Robbins, G.F., Stable Baseband Superregenerative Selective Receiver. U.S. Patent 3,794,996, dated Feb 26, 1974.

(9) Ross, G.F., Transmission and Reception System for Generating And Receiving Baseband Duration Pulse Signals for Short Baseband Pulse Communication System. U.S. Patent 3,728,632 dated Apr 17, 1973.

(10) Ross, G.F., Energy Amplifying Selector Gate for Baseband Signals. U.S. Patent 3,750,025, dated July 31, 1973.

(11) Ross, G.F. & Lamensdorf, D., Balanced Radiator System, U.S. Patent 3,659,203, dated April, 25, 1972.

(12) Ross, G.F. & Robbins, K.W., Baseband Radiation and Reception System. U.S. Patent 3,739,392, dated June 12, 1973.

(13) Ross, G.F. & Robbins, K.W., Narrow Range-gate Baseband Receiver. U.S. Patent 4,695,752, dated September 22, 1987.

(14) Bennett, C.L. & Ross, G.F., "Time-domain Electromagnetics and Its Application," Proc. IEEE 66, 299-318, 1978.

(15) Fleming, R, and Kushner, C., "Low-Power, Minature, Distributed Position Location and Communication Devices Using Ultra-Wideband, Nonsinusoidial Communication Technology," prepared for Advanced Research Projects Agency/Federal Bureau of Investigation, Aether Wire & Location, Inc., contract # J-FBI-94-058, July 1995.

(16) UWB/GPS Compatibility Effects FTP Site, Applied Research Laboratories University of Texas at Austin, ftp://www.arlut.utexas.edu/pub/uwbdata/UWB_Test_Data.

(17) GPS Standard Positioning Service Signal Specification, 2nd Edition, 06/95.

(18) NovAtel GPSCard Command Descriptions Manual, OM-20000008, Rev. 2.0; NovAtel GPSCard Installation and Operating Manual, OM-20000007, Rev. 2.0.

(19) NovAtel MiLLennium Command Descriptions Manual, OM-20000053, Rev. 1; NovAtel MiLLennium Guide to Installation and Operation, OM-20000016, Rev. 3.

(20) Ashtech Z-12 Receiver Operating Manual, Ashtech Inc., May 1994.

(21) The NMEA 0183 Standard for Interfacing Marine Electronics Devices, Version 3.0, July 2000.

(22) Parkinson, B.W. and Spilker, J.J*, Global Positioning System: Theory and Applications*. Progress in Astronautics and Aeronautics, American Institute of Aeronautics and Astronautics, Inc., 1996.

(23) ICD-GPS-200, Navstar GPS Space Segment/Navigation User Interfaces, Revision C, 25 September 1997.

(24) STR Series Multichannel Satellite Navigation Simulators Reference Manual, Global Simulation Systems, Issue 8.00, May 1999.

(25) Receiver Independent Exchange (RINEX) Format Description, International Coordination of Space Techniques for Geodesy and Geodynamics, August 1989.

(26) "Correcting for the Effects of the Ionosphere on RF Transmissions as Used in the SATRACK System," C. W. Meyrick, M. M. Feen, and R. L. Strauch, Johns Hopkins APL Technical Digest, Volume 9, Number 2, 1988.

(27) "Random Tropospheric Effects in Command Guidance by Multilateration and Interferometry," R. J. Fitzgerald, IEEE Transactions on Aerospace and Electronic Systems, Volume 30, Number 1, Page 249-257, January 1994.

(28) "GPS Theory and Practice," B. Hofmann-Wellenhof, H. Lichtenegger, and J. Collins, Second Edition, Springer-Verlag Wien, New York, 1993.

List of Acronyms and Abbreviations

ANOVA	Analysis of Variances
ARL:UT	Applied Research Laboratories, University of Texas
BC	Broadcast
C/A (Code)	Coarse (Clear)/Acquisition (mode of GPS)
C.F.R.	Code of Federal Regulations
C/I	Carrier to interference ratio
CDDIS	Crustal Dynamic Data Information System
CDRS	Continuously Operating Reference Station
CEP	Circular Error Probable
C/N_0	Carrier to noise ratio
CURE	Center for Ultra-wideband Research at ARL:UT
dB	Decibel
dBm	Decibels referenced to one milliWatt
dBW	Decibels referenced to one Watt
DD	Digital device
DLL	Delay lock loop
DoD	Department of Defense
DOP	Dilution of Precision
DOT	Department of Transportation
ECEF	Earth-Centered Earth-Fixed
ECI	Earth-Centered Inertial
EIRP	Equivalent Isotropic Radiated Power
FAA	Federal Aviation Administration
FCC	Federal Communications Commission
GHz	Gigahertz (10^9 Hertz)
GPR	Ground Penetrating Radar
GPS	Global Positioning System
GSS	Global Simulation Systems
HDOP	Horizontal Position Dilution of Precision
HLC	Horizontal Long Track Crosstrack

IF	Intermediate Frequency
IGS	International GPS Service for Geodynamics Service
JHU/APL	The Johns Hopkins University Applied Physics Laboratory
KHz	Kilohertz (10^3 Hertz)
km	Kilometer
L1, L2, L1/L2	Designations for two GPS operational frequencies
L5	Designation for a proposed GPS operational frequency
LLH	Latitude-Longitude-Height
m	Meter
MHz	Megahertz (10^6 Hertz)
MOP	Measure of performance
NAVSTAR	Navigation, Satellite, Tracking and Ranging
NED	North-East-Down
NIMA	National Imagery and Mapping Agency
NGS	National Geodetic Survey
NOI	Notice of Inquiry
NPRM	Notice of Proposed Rule Making
ns	Nanosecond
NTIA	National Telecommunications and Information Administration
P/Y (Code)	Precise Code, A-S Mode
PAD	PulsON Application Developer (TDC Device)
P-Code	Precise Code
PDOP	Three-dimensional dilution of precision
PDR	Phase-Derived Range
PLL	Phased Locked Loop
PRF	Pulse Repetition Frequency
PRN	Pseudorandom Number; also reference to a GPS Satellite
PSD	Power Spectral Density
RAIM	Receiver Autonomous Integrity Monitoring
RCV	Receiver
RF	Radio Frequency

RINEX	Receiver Independent Exchange (Format)
RMS	Root-mean-square
RSS	Root-sum-square
SNR	Signal to noise ratio
SP3	
TDC	Time Domain Corporation
TEQC	
TGD	Timing Group Delay
TOE	Time of Ephemeris
TOC	Time of Clock
UCAR	University Corporation for Atmospheric Research
UNAVCO	University NAVSTAR Consortium
USCG	U.S. Coast Guard
UWB	Ultra Wideband
VDOP	Vertical Position Dilution of Precision
WGS	World Geodetic Survey
WN	White Noise

APPENDIX A
INDIVIDUAL RECEIVER ANALYSES

A.0 Introduction

This appendix details the performance of the individual Global Positioning System (GPS) receivers during the conducted ranging and conducted acquisition portions of the utilized in the Applied Research Laboratories, University of Texas (ARL:UT) test program. The appendix begins with an outline of the process followed to convert raw measures of performance (MOPs) from a function of test attenuation to a function of "equivalent range" for a "compliant device." The outline is accompanied by an example. The remaining 5 sections are dedicated to a presentation of the 12 (MOPs) for each GPS receiver, each ultra-wideband (UWB) mode (including the white noise source), and each simulated GPS signal power. In contrast to Chapter 6, the MOPs are graphed as a function of test attenuation only. This allows the reader to see the results in the space as originally collected and allows the reader to apply alternative mappings from test attenuation to equivalent range that have been derived from other scenarios.

Within the receiver section, a brief description of the receiver's technology and a summary of the receiver's performance specifications are given. This information is based solely on the *Receiver Survey* in the January 2001 issue of GPS World and documentation available on-line. Both of these sources are based on manufacturer supplied information and no attempt has been made to independently verify the performance. It is further noted that manufacturers do not always interpret specifications in the same manner; therefore, the information is merely supplied as background information.

The ARL:UT test program originally planned to test seven GPS receivers, which are denoted as RCV1 through RCV7 throughout the ARL:UT test plan and the ARL:UT test report. Throughout report, the receivers are denoted by either their simple number or by manufacturer and specific model. This appendix only includes five of these GPS receivers. Receiver 5, an Allen Osborne Turborogue SNR-8000, "was acquired for this testing, but was removed from the test program due to the interference it caused with other GPS receivers when used in the conducted test setup."[1] Similar interference has been noted by other users and is not unique to the test setup employed by ARL:UT. The SNR-8000 is a survey quality GPS receiver, and since several other survey quality receivers were successfully tested, its exclusion is not considered to be detrimental.

Receiver 7, a Trimble 4700 was successfully tested by ARL:UT. Unfortunately, "in numerous correspondences with Trimble, the ARL:UT test team was unable to receive any

[1] *Draft of the ARL:UT Test Report, page 19.*

support in terms of configuring the receiver to output selected messages, nor what information was contained in the binary data streamed through the receiver serial port by default."[2] JHU/APL experienced a similar inability to determine the content of the binary data. The receiver's binary data were converted to the RINEX format using the TEQC software. The TEQC software was downloaded from the University NAVSTAR Consortium (UNAVCO) web site at the University Corporation for Atmospheric Research (UCAR). However, the TEQC software is a black box, and although all the RINEX format data elements were present after the conversion and appeared to have reasonable values, we do not have an independent verification of a correct conversion. With this uncertainty, this GPS receiver has been excluded from the analysis. The Trimble 4700 is a survey quality GPS receiver, and since several other survey quality receivers were successfully tested, its exclusion is also not considered to be detrimental.

A.1 Methodology for Computing Measures of Performance

This section of Appendix A traces the general process used to convert the MOPs from a per epoch, per satellite, or per trial basis to a function of "equivalent range" as stated in Chapter 6. As example, the process is traced with the position dilution of precision (PDOP) for the Ashtech Z-12 GPS receiver using the minimum level GPS signal power and UWB mode 7. The Ashtech Z-12 was chosen simply because its raw binary data stream is the most comprehensive. A similar trace could be generated with each GPS receiver, simulated GPS signal power, and UWB mode.

This process is applicable to every MOP in the three categories. The three categories are receiver navigation outputs, receiver measurement outputs, and receiver reacquisition. The process begins with the assumption that the raw binary data have already been screened and validated and that the specific MOP has been computed for each epoch, each satellite, or each trial. For the receiver navigation outputs -- the number of satellites tracked, the number of satellites used in the navigation solution, position dilution of precision, and receiver position – the injected and baseline data elements, already contained in the raw binary data stream, are simply subtracted or divided. When some interpretation was necessary to determine the applicable data elements, they are noted in the per receiver section. In the case of receiver measurement outputs and receiver reacqusition, more sophisticated processing is required. This processing is detailed in Appendix C.

Figure A-1 contains three graphs for PDOP from the Ashtech Z-12 GPS receiver with the minimum level GPS signal power and UWB mode 7 with a test attenuation setting of 40 dB. The left-hand and center graphs contain the injected and baseline values, respectively, of PDOP as computed for each of the 1200 1-second epochs across the duration of this test configuration. These two graphs contain the whole value data and represent the conclusion of the quality control process. Recall that the quality control is also used to verify data set integrity, verify data set hierarchy, and verify the consistency of baseline data set between different part of the test programs. It is noted that the PDOP is decreasing across this time period as the geometry of the satellite constellation changes.

[2] *Final ARL:UT Test Report, Appendix C, page C-10.*

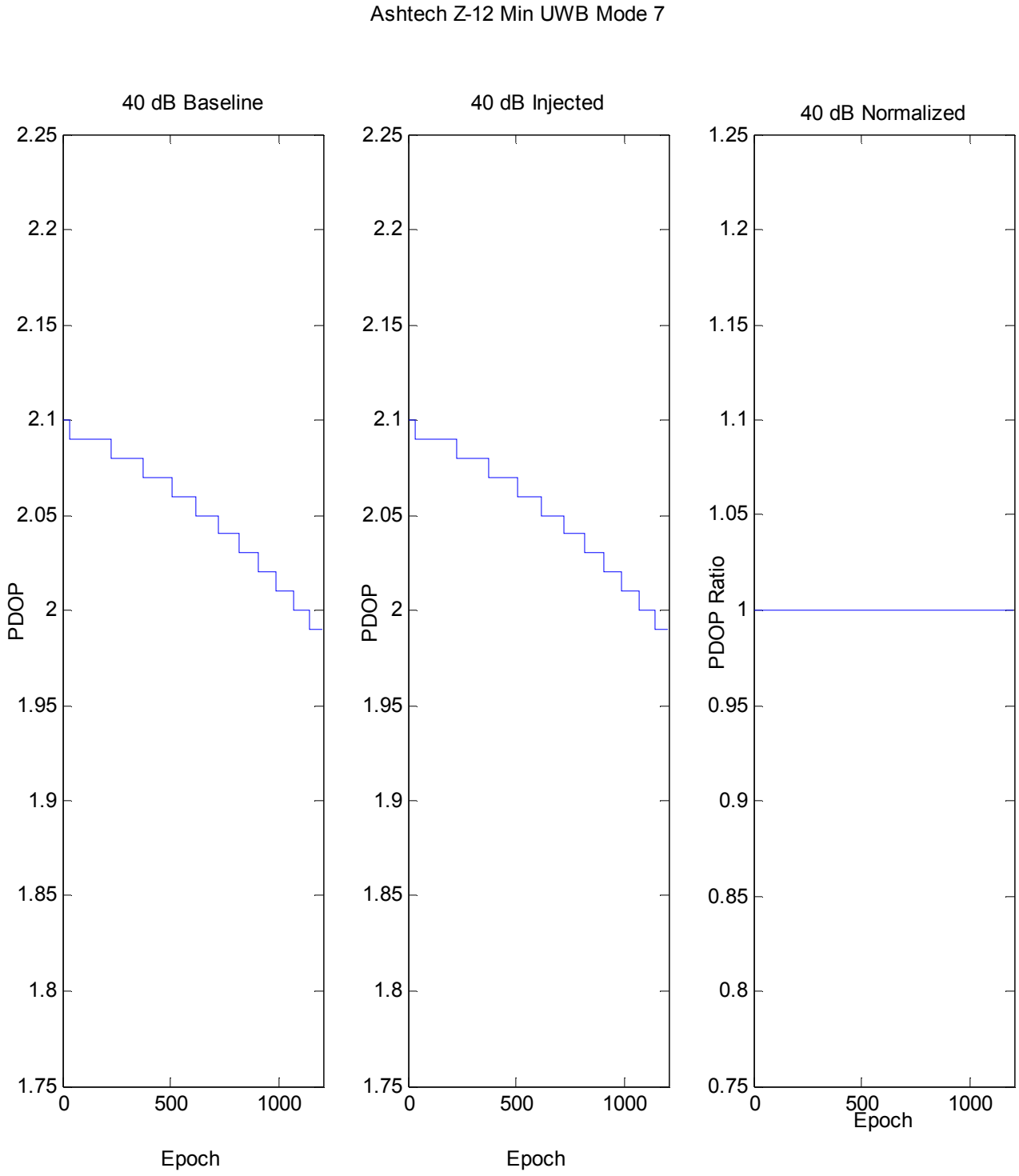

Figure A-1 Whole Value and Normalized PDOP

The right-hand graph in Figure A-1 contains the normalized PDOP where the injected value is divided by the baseline value. Obviously, in this case, no degradation in PDOP has occurred and the normalized PDOP is a constant 1.0 regardless of epoch. To compute a single statistic that best represents the normalized PDOP for this test configuration, the mean of the per epoch values is simply computed. The process of normalization and single statistic computation depends on the particular measure of performance. The following list summarizes this process:

- All receiver navigation outputs: the normalization is the subtraction or division of the per-epoch injected and baseline values. The single statistic is the mean value across all epochs.

- Carrier to Noise Ratio (C/N_0): the normalization is the division of the per epoch and per satellites injected value by the baseline value. The single statistic is the mean value across all epochs and satellites simultaneously — thus treating them as a single population.

- Pseudorange noise: a separate single statistic is first computed for the injected and baseline cases. The statistic is the variance across all epochs and satellites simultaneously – again treating them as a single population. The normalization is then the division of the injected standard deviation by the baseline standard deviation.

- Pseudorange double difference: the methodology inherent to this measure of performance already produces a normalized value for each epoch and satellite. The single statistics are the mean and variance for the bias and noise, respectively. Again, these statistics are computed for a single population across all epochs and satellites simultaneously.

- All receiver reacquisition: the normalization is the subtraction of trial baseline line value from the injected value. The single statistic is the mean value across trials.

The upper graph in Figure A-2 shows the normalized PDOP statistic plotted for each attenuation setting between 0 and 60 dB in the test program. The dotted line is used to show both the individual points and allow for an easy visualization of the general trend. The red line represents valid points, and the black line represents invalid points. In this context, “invalid” denotes points that are nonsensical. For example, when the GPS receiver computes a PDOP or position with less than four satellites in the navigation solution or when the single statistic is based on very few epochs, satellites, or trials, and there is little confidence in the statistic. By this point in the processing, data considered invalid due to test setup or other anomalies have already been screened out in the quality control process. Only valid points are carried forward in the analysis as shown in the lower graph in Figure A-2. Note that the x-axis label has changed from “test attenuation” to “valid attenuation.” All of the results presented in the second part of Appendix A are plotted as a function of this valid attenuation.

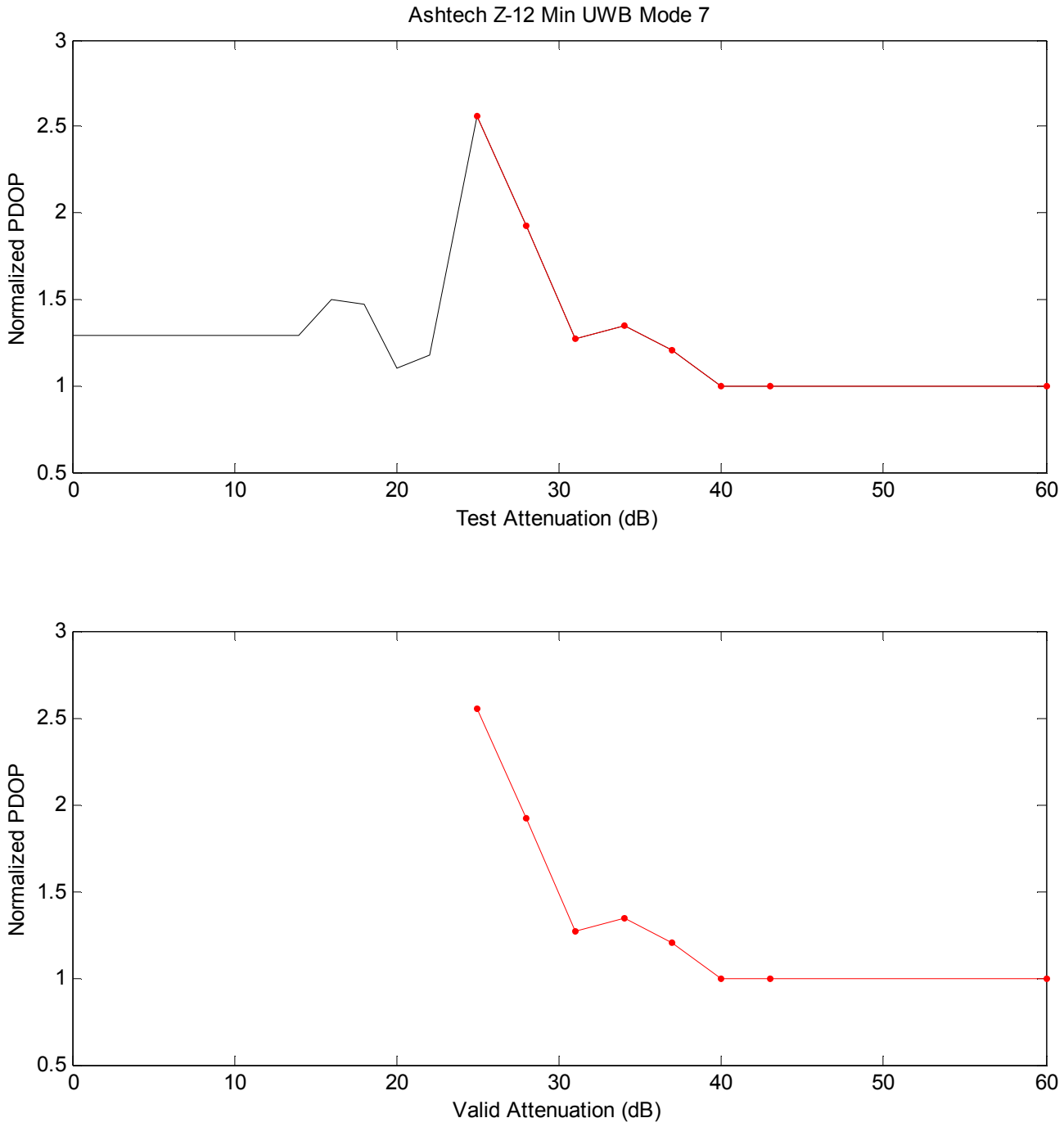

Figure A-2 Normalized Measure of Performance versus Attenuation Setting

In the next step of this process, the remaining "valid attenuation" settings are mapped to an equivalent "compliant attenuation" or "compliant device." This mapping allows the reader to compare results across UWB modes [i.e., different pulse repetition frequency (PRF) and duty cycle] without considering that many of the modes have average powers that are significantly below the current Federal Communications Commission (FCC) Part 15 regulations. As part of the ARL:UT test program, the Time Domain PulsON Application Developer (PAD) was independently tested at an FCC compliance laboratory. According to compliance test report, the PAD when operating in UWB Mode 13 is just compliant under the current average or quasi-peak radiated power criteria above 960 MHz as stated in section 15.209 of the FCC Part 15 regulations. The mapping of other UWB modes to "compliant" is accomplished by increasing the valid attenuation by the average power difference in the L1 band between the mode under investigation and Mode 13. Obviously, in the case of UWB Mode 13, no shift is necessary. However, for UWB modes with lower PRFs or duty cycles, the valid attenuation can be increased by up to 16 dB as shown in Table B-2 of Appendix B. For Mode 7, this shift is approximately 3 dB and is shown in the upper graph of Figure A-3. Note that the x-axis label has changed from valid attenuation to "compliant attenuation."

In the next plot of this series, the "complaint attenuation" is mapped to "conducted range" or distance between the GPS receiver and UWB device. The term "conducted range" implies that the results are presented as if the conducted testing had been executed as a function of physical separation instead of attenuation setting but with ideal antennas that affect no change to the nature UWB or GPS signals. This mapping is described in detail in the first part of Appendix B. Each "complaint attenuation" maps to a single "conducted range" regardless of simulated GPS power level and UWB mode. However, the mapping does vary with GPS receiver since the actual components used in the UWB and GPS signal paths differed between the Holloman Air Force Base and ARL:UT test setups. One mapping applies to the first four receivers, and a second one applied to the final two receivers. The results of this mapping are shown in the lower graph of Figure A-3. As ARL:UT intended, the 60-dB attenuation effectively maps to an infinite range while the remaining attenuations map to ranges less than 50 meters.

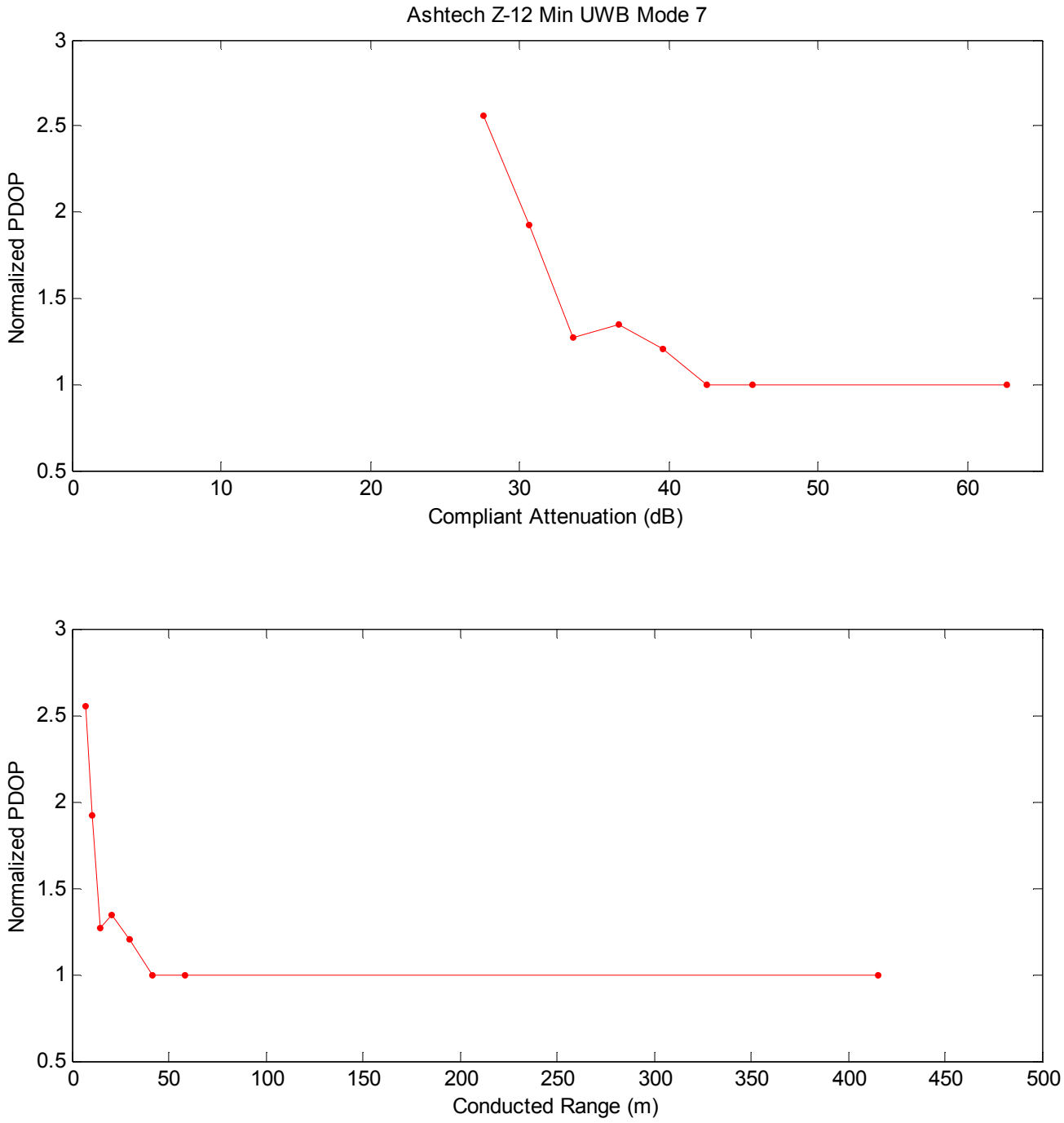

Figure A-3 Mapping to Compliant Attenuation and Conducted Range

In the final plot of this series, the "conducted range" is mapped to an "equivalent range." The term "equivalent range" implies that the results are presented as if the conducted testing had been executed again as a function of physical separation instead of attenuation setting but with actual UWB and GPS antennas. This mapping is based in part on results from the radiated portion of the ARL:UT test program and thus includes the effects of unquantified environmental factors. This mapping is described in detail in the second part of Appendix B. Each "conducted range" value maps to a single "equivalent range" regardless of simulated GPS power level and UWB mode. The mapping does vary with GPS receiver since each corresponding GPS antenna has a different beam pattern and overall gain. This final mapping increases the range by a factor between 1 and 2.2. The results of this final mapping are shown Figure A-4. All of the results presented in Chapter 6 are plotted as a function of this equivalent range.

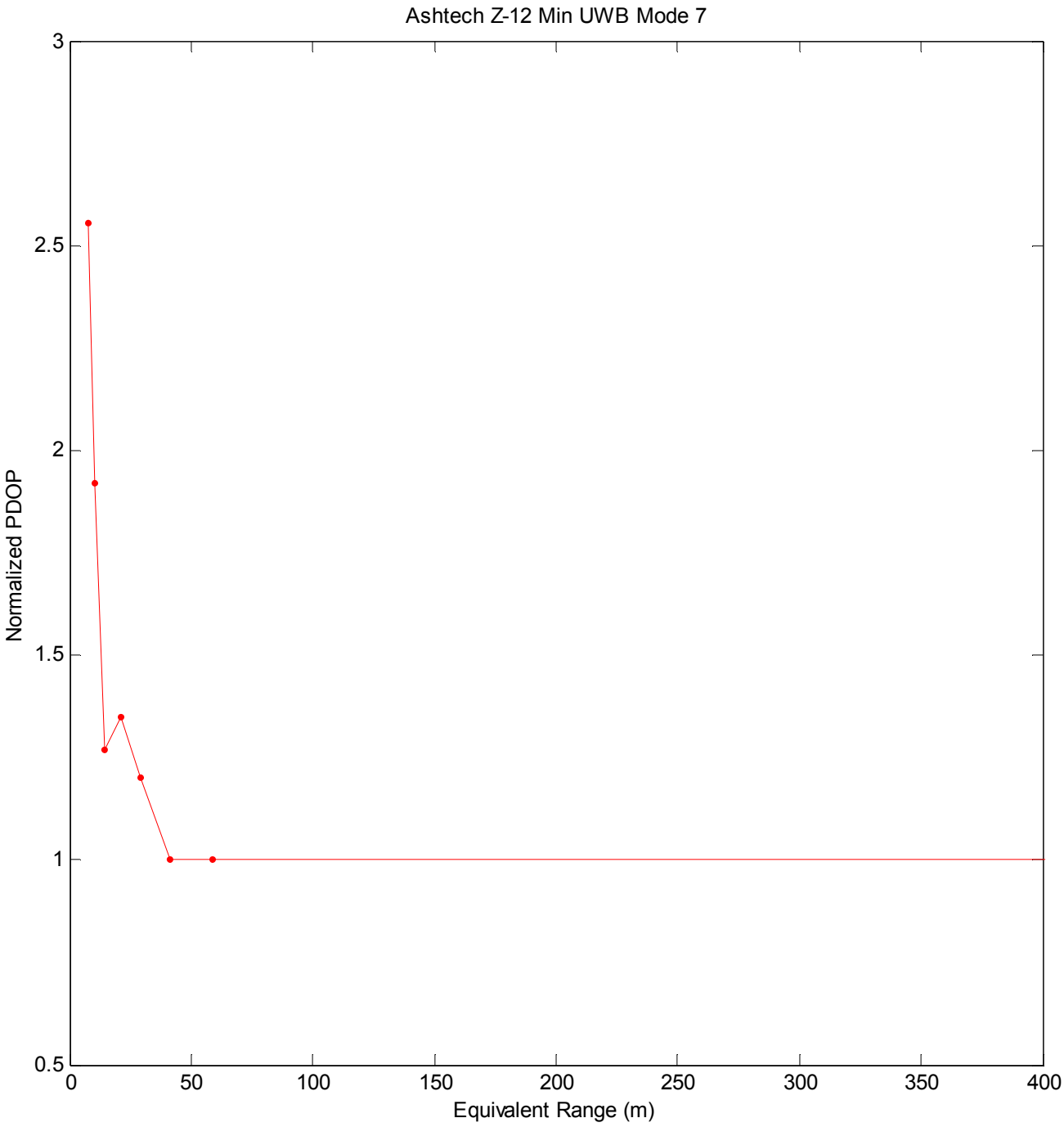

Figure A-4 Final Mapping to Equivalent Range

A.2 NovAtel 3151

Receiver 1 is a Model 3151R GPS receiver manufactured by NovAtel Communications Ltd.. More specifically, the OEM2 GPS Card version was used during the testing. This receiver is a survey quality receiver with numerous imbedded OEM applications. Twelve channels are used to parallel track the L1 C/A code and C/A carrier. To increase its accuracy performance, this receiver employs a narrow correlator. The pertinent performance specifications for this receiver are:

- Autonomous position accuracy = 15 m CEP without Selective Availability
- Pseudorange accuracy = 10 cm RMS over 3 minutes with $C/N_0 > 44$ dBHz
- Cold start acquisition time < 70 sec
- Warm start acquisition time = 60 sec[3]
- Reacquisition time = 3 sec

During the radiated and aggregate testing, a Model 501 GPS antenna manufactured by NovAtel Communications Ltd. was connected to Receiver 1. Only the L1 frequency band is appropriate for this antenna. This antenna incorporates a low noise amplifier with the following specifications:

- ±10 MHz bandwidth
- 23.0 dB gain
- 3.0 dB noise factor

Throughout the conducted, radiated, and aggregate testing, this receiver was configured to output only measurement data in the NovAtel proprietary binary output format described in Reference (18). No receiver generated navigation solutions were output as part of the data stream.

A.2.1 Receiver Specific Measures of Performance

All NovAtel 3151 data collected during the ARL:UT test program were successfully processed as described in Appendix C and at the beginning of this Appendix. It is noted that these data are time tagged with GPS week 48 instead of GPS week 1072 as with the other GPS receivers. This difference is an artifact of the NovAtel interpretation of the GPS week rollover

[3] *"GPS World Receiver Survey," January 2001.*

and does not effect the quality of the data. To support this appendix and, Chapter 6, data were processed for both simulated GPS power levels with UWB modes 1, 7, and 13 and with the white noise source. However, not all MOPs have been computed. Unfortunately, the NovAtel records that contain either PDOP or receiver position were not recorded as a part of the ARL:UT test program. However, the remaining MOPs are adequate for usage in this study.

To compute the number of satellites tracked, a satellite was considered to be tracked by the GPS receiver when an observation existed in the RGEC record for that SV. The number of satellites used in the navigation solution was inferred from the above tracking plus a zero-valued reject code in the SATB record for that SV. Finally, all time tags in seconds of week and measurement data were extracted from the RGEC records.

The following 10 figures depict the available receiver navigation outputs, receiver measurement output, and receiver reacquisition MOPs. Each figure contains an imbedded title that is considered to be sufficient to direct the reader through the data. Therefore, separate figure numbers and captions are not provided. A separate figure is included for each measure of performance. In each figure, four separate graphs are presented. The upper left-hand graph contains the results when the test setup was injected with an UWB Mode 13 signal. The y-axis is the normalized measure of performance, and the x-axis is the actual attenuation setting used during the particular test. Two dotted lines are presented: the red one depicts the minimum level GPS signal power and the blue one depicts the live sky GPS signal power. A dotted line is used to show both the individual points and allow for an easy visualization of the general trend. Where appropriate, a third black line is included to indicate any points considered invalid as defined in the previous section of this appendix.

The upper right-hand graph is a similar depiction of the UWB mode 7 case. The lower two graphs are similar depictions of the UWB Mode 1 and white noise source cases. The white noise source is only presented in this Appendix – these results are not carried forward to Chapter 6. This exact presentation is repeated for every other GPS receiver in this Appendix; therefore, to minimize the monotony, this description is simply referenced in each of the subsequent sections.

NovAtel 3151 Decreased Satellites Tracked

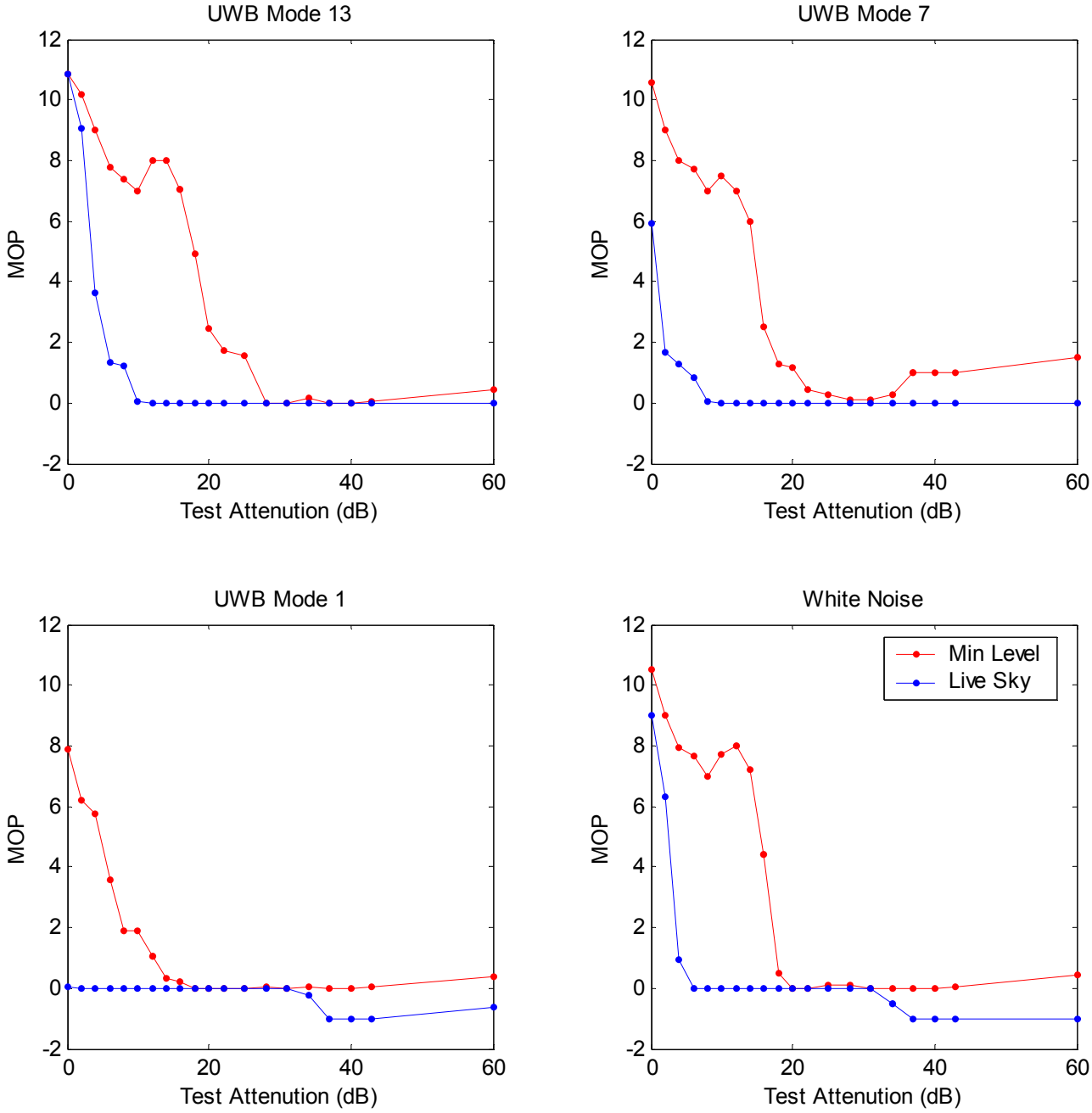

NovAtel 3151 Decreased Satellites Used

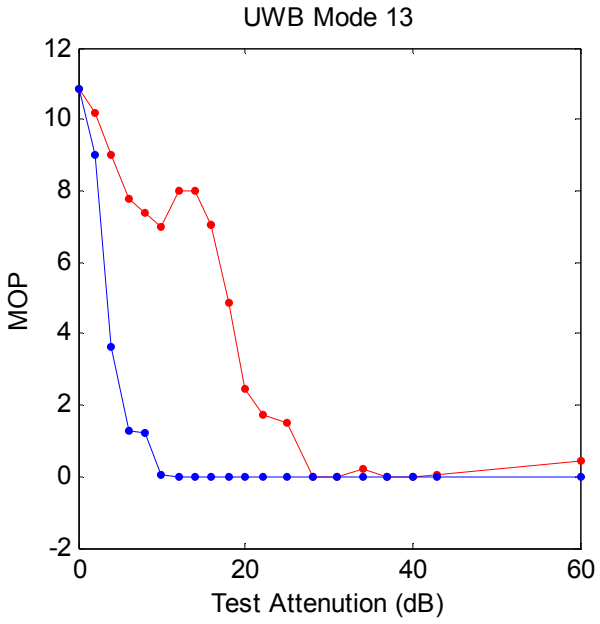

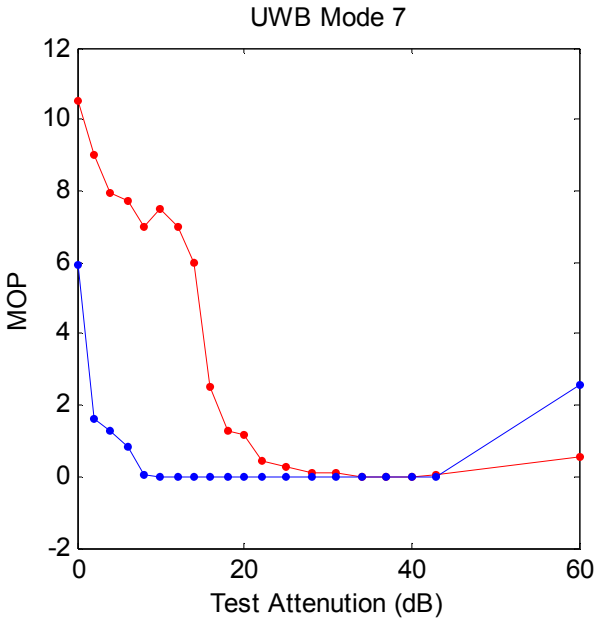

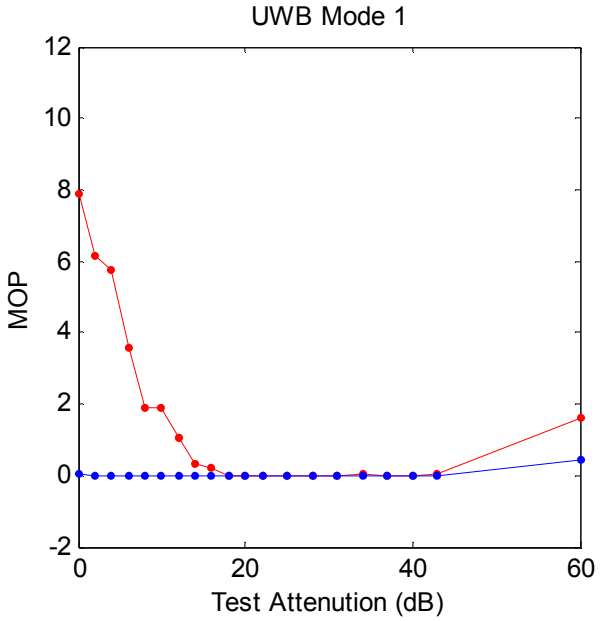

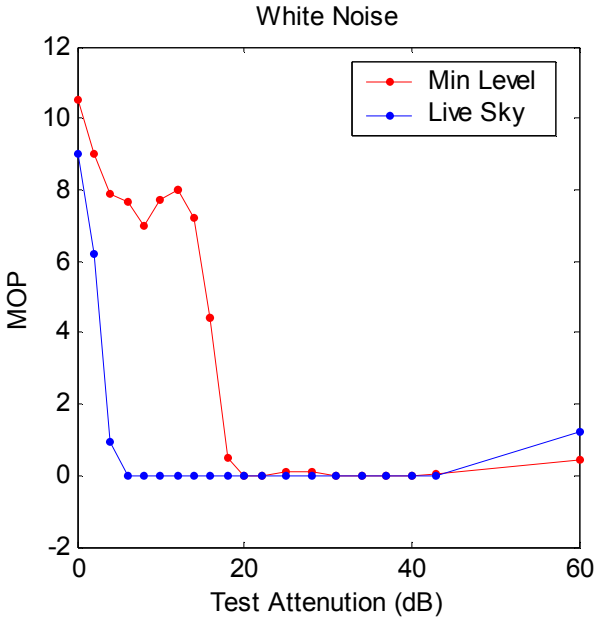

NovAtel 3151 Normalized C/NO

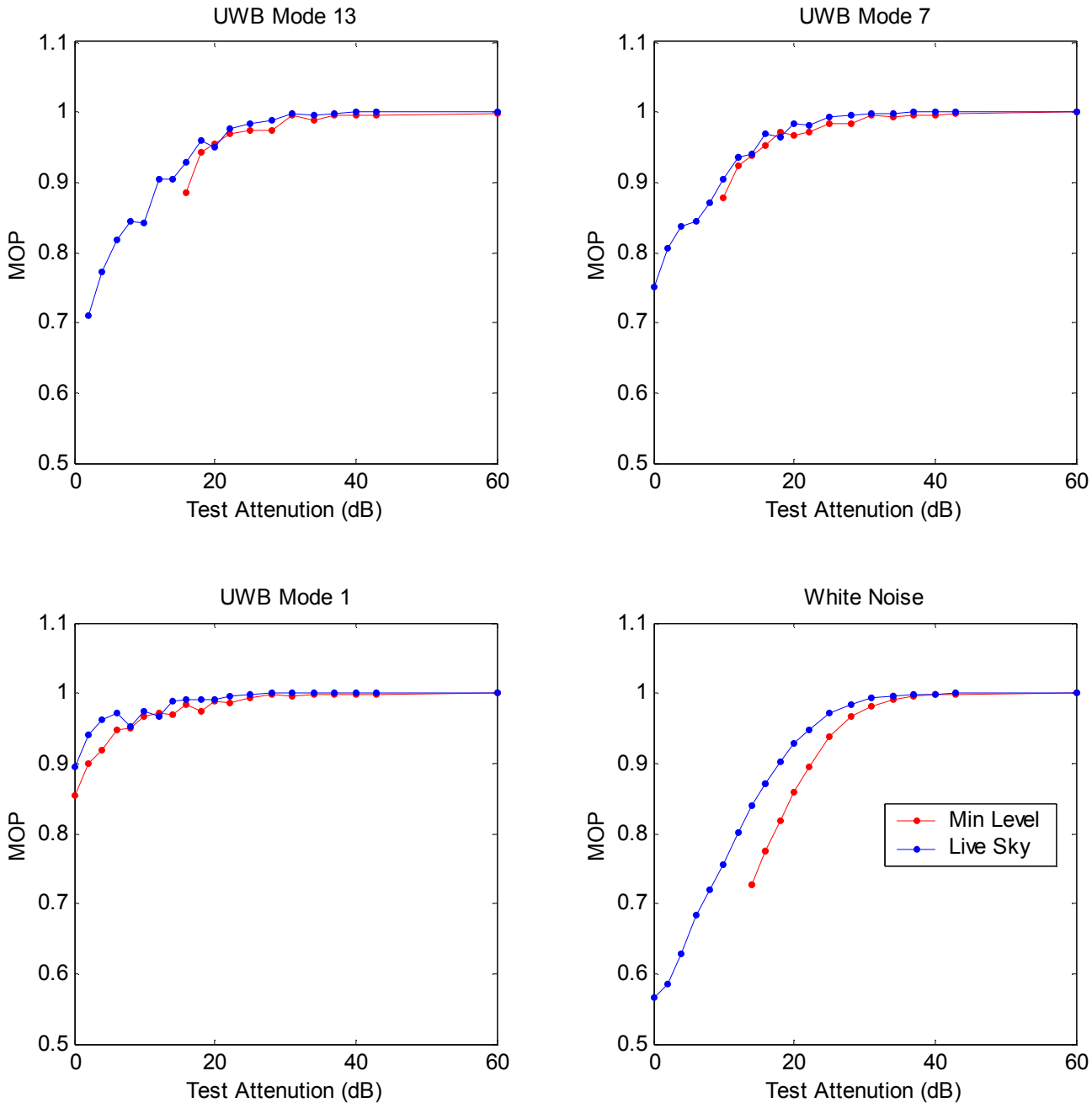

NovAtel 3151 Normalized Pseudorange Noise

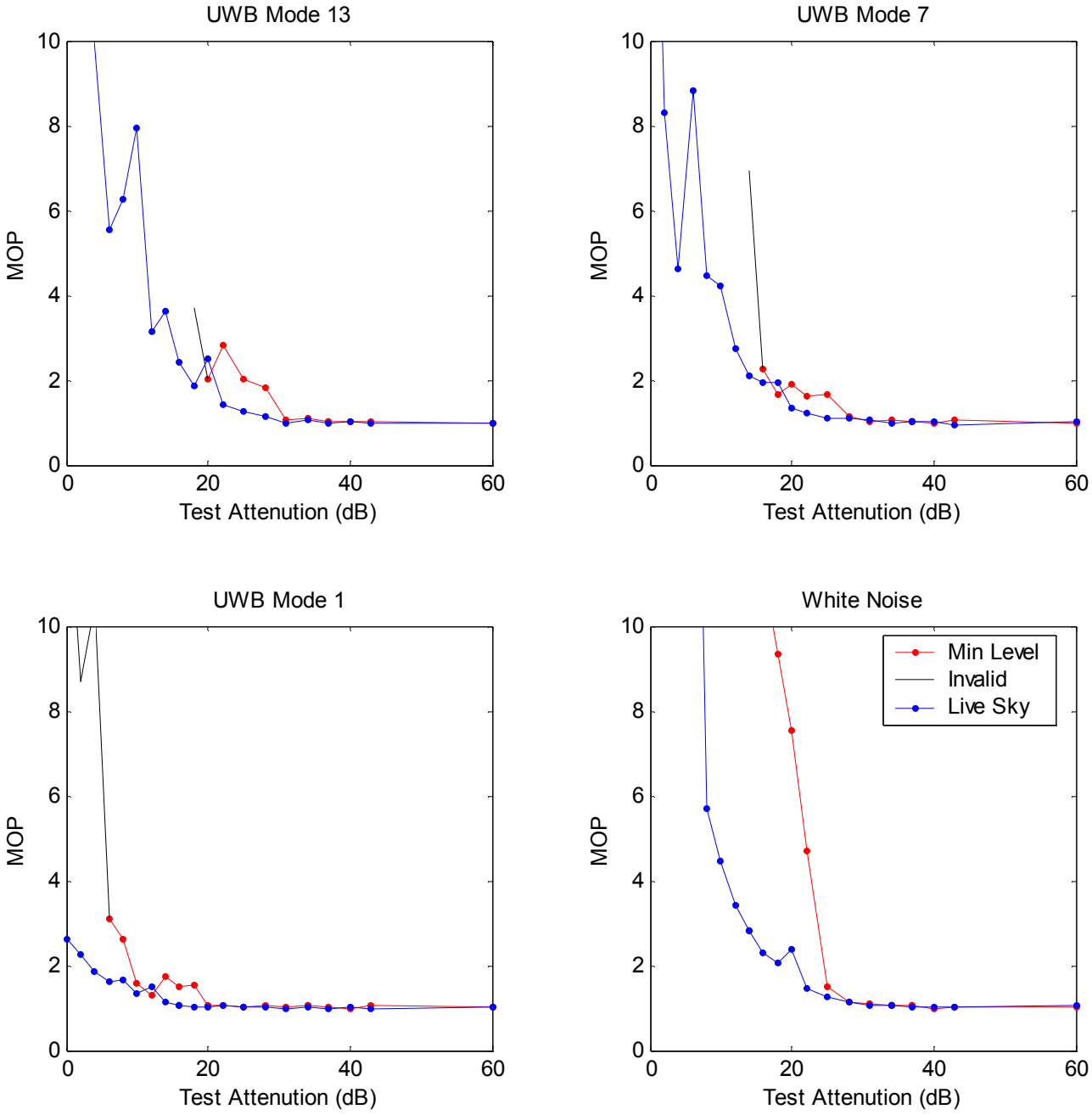

NovAtel 3151 Double Difference Bias (cm)

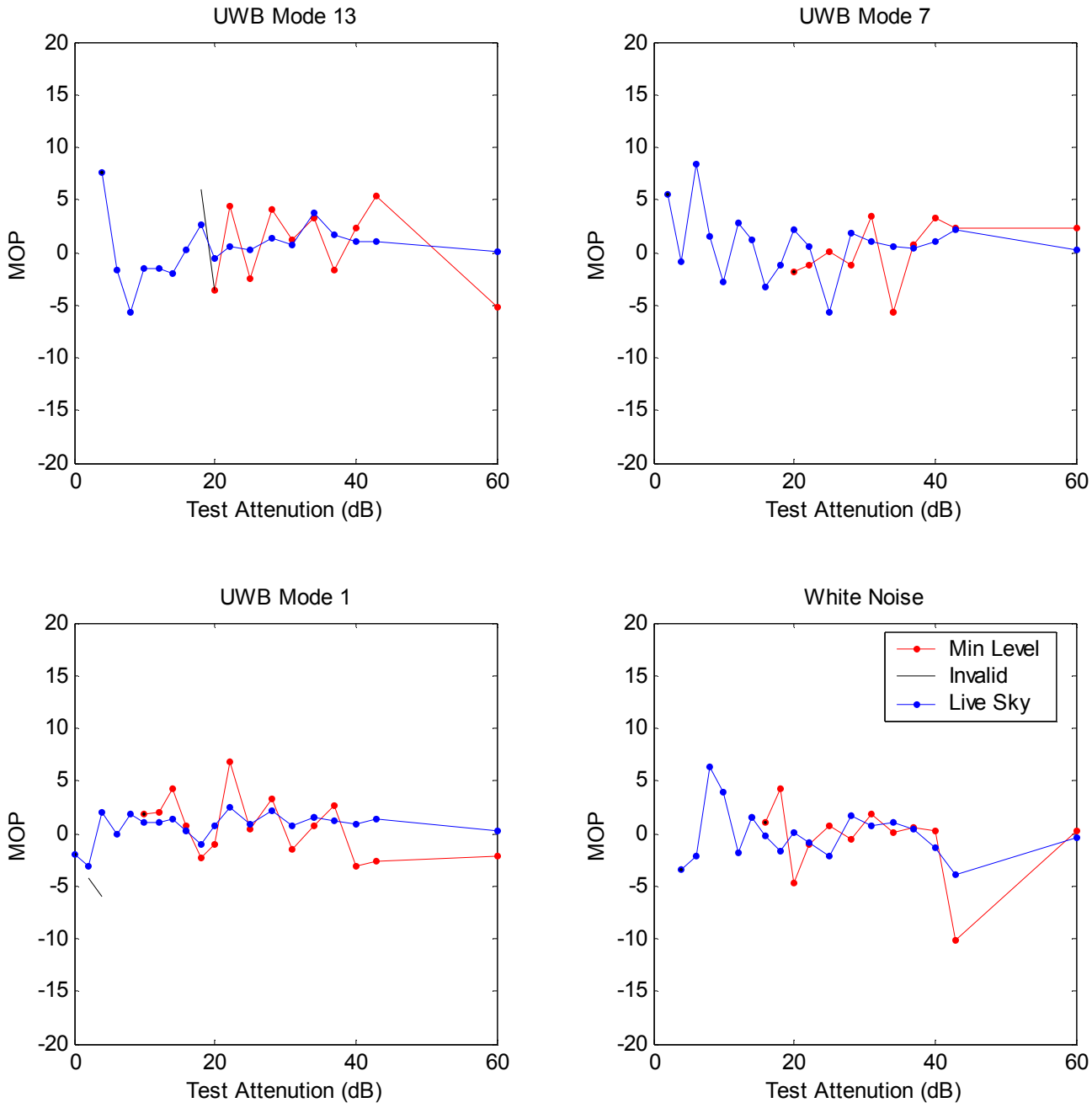

NovAtel 3151 Double Difference Noise (cm)

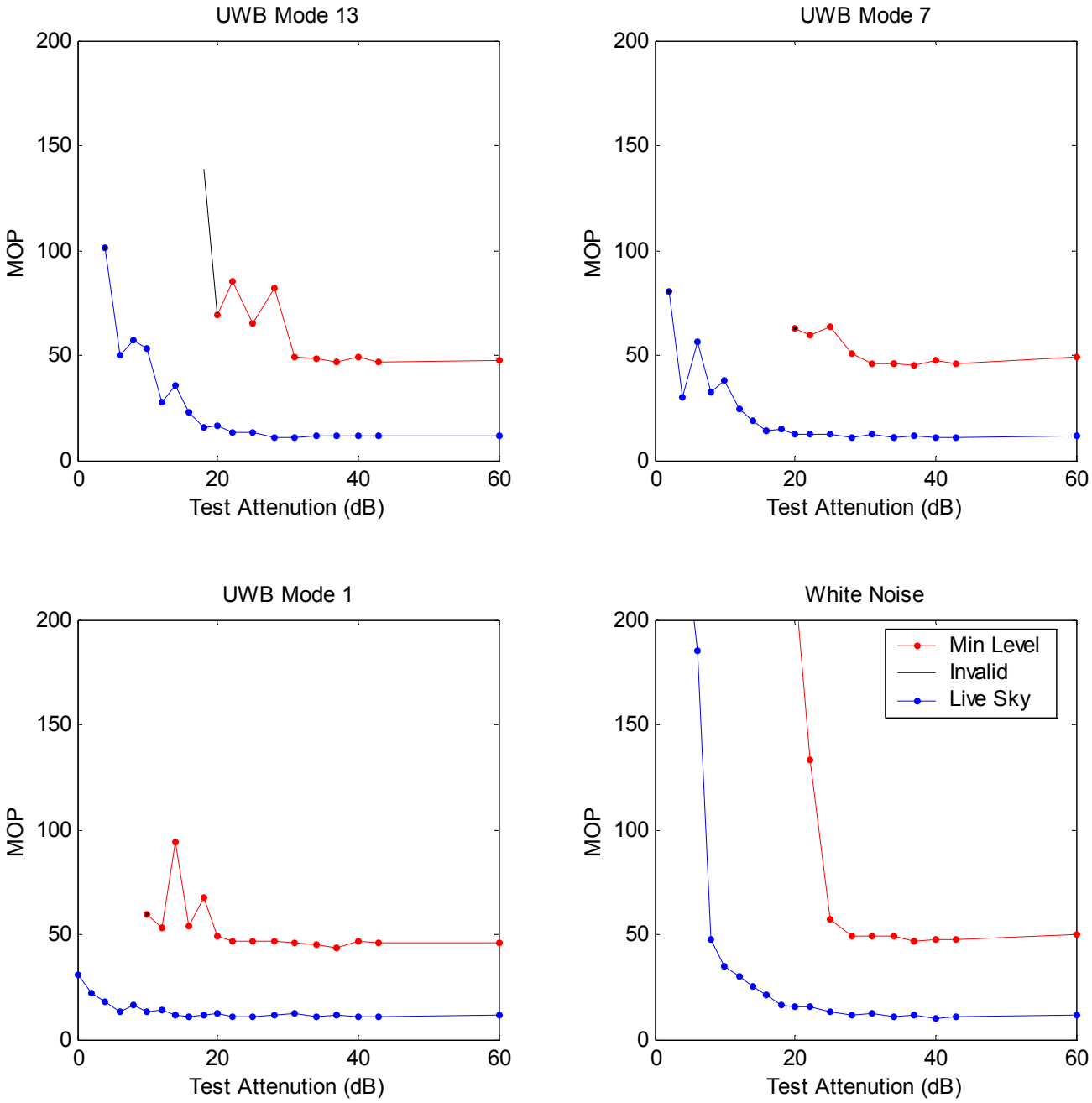

NovAtel 3151 Incr. Time To Reacq. 1 tk'd sat. (sec)

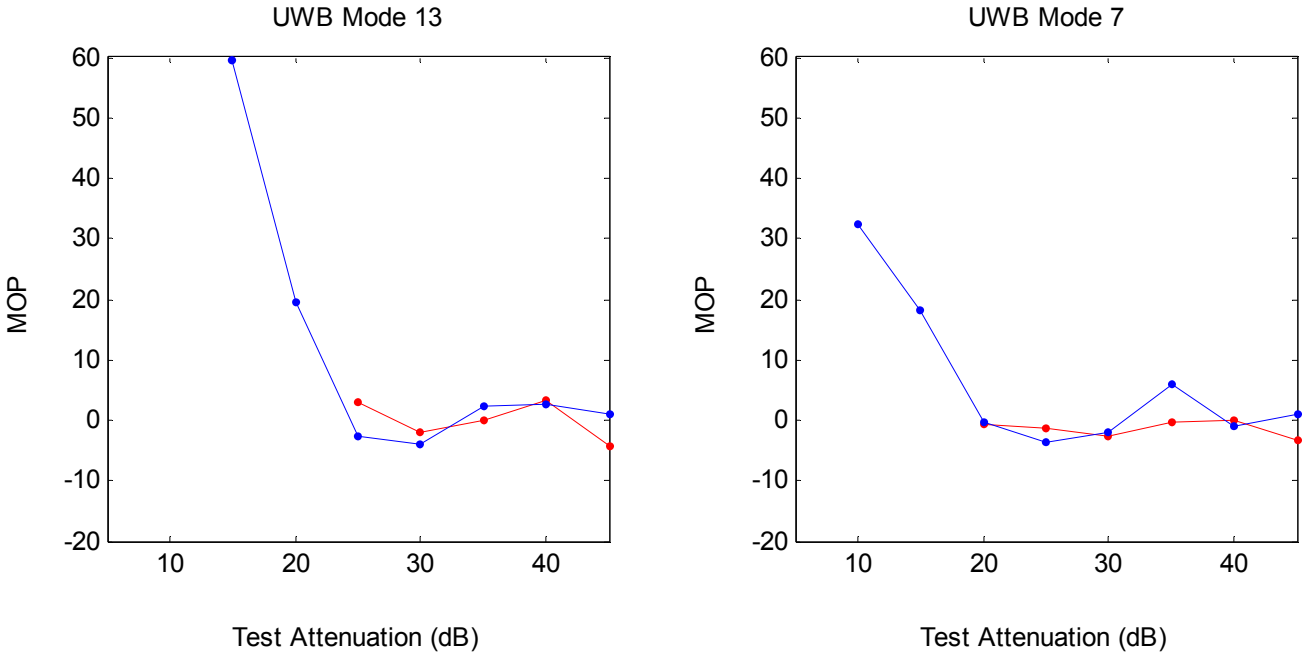

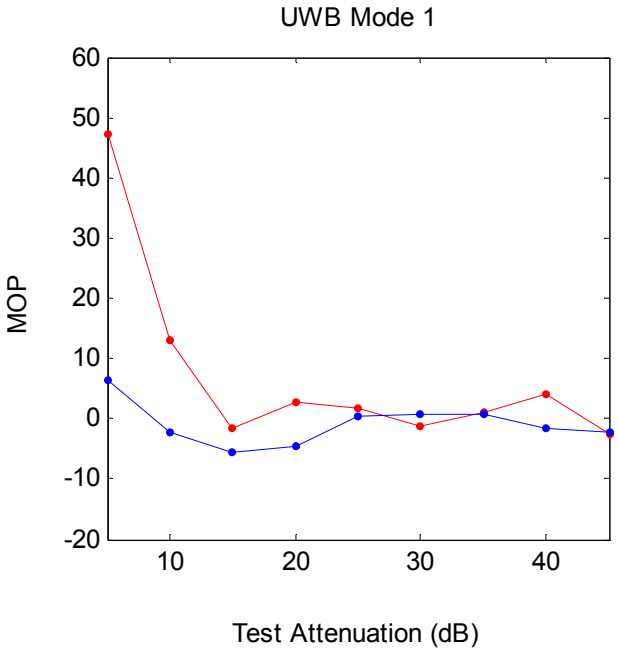

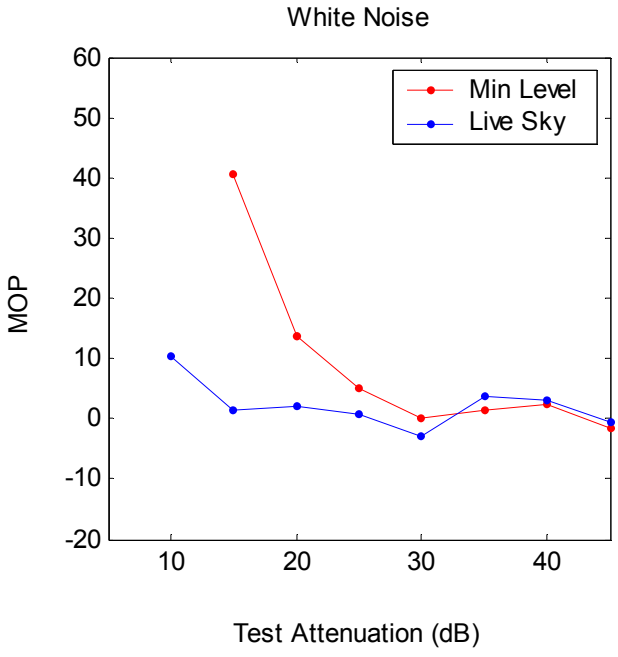

NovAtel 3151 Incr. Time To Reacq. N tk'd sat's. (sec)

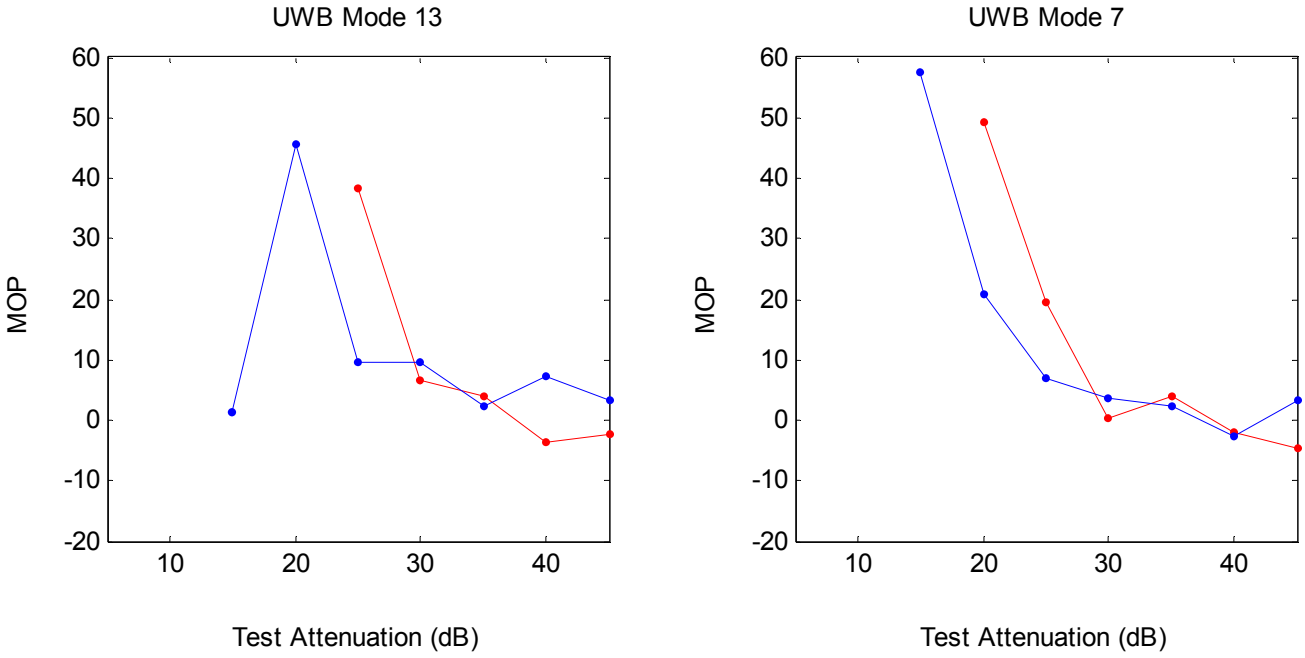

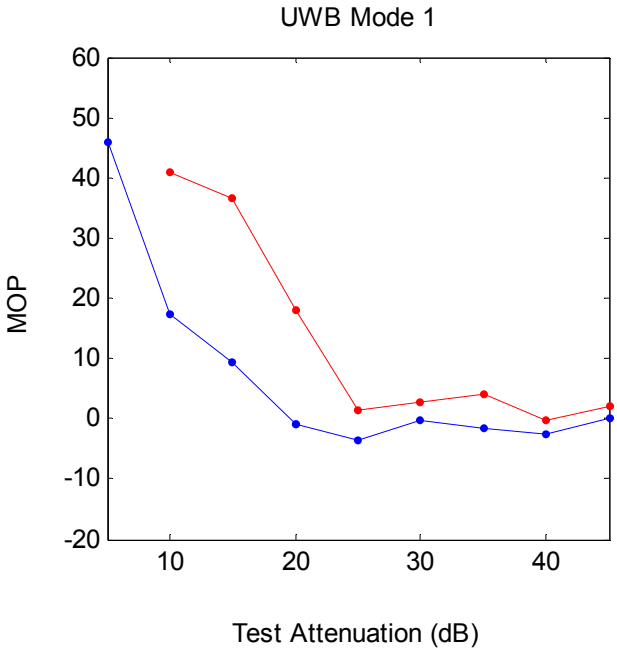

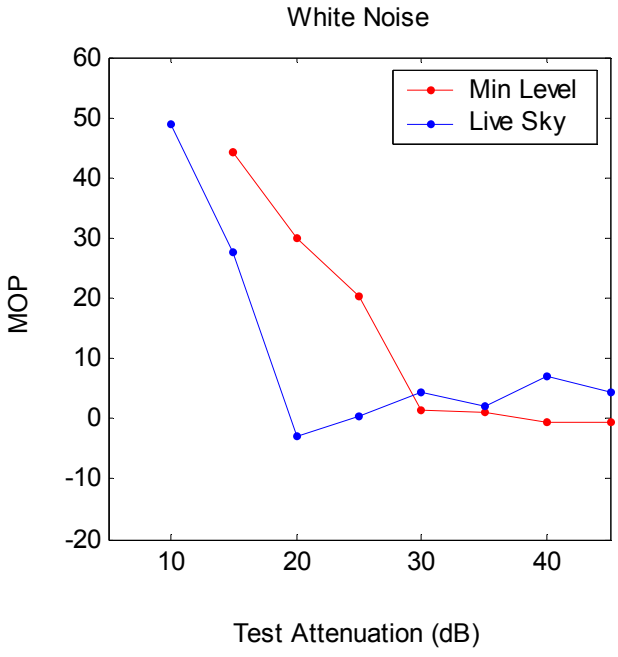

NovAtel 3151 Trials Used to Reacq. 4 navd sat's. (sec)

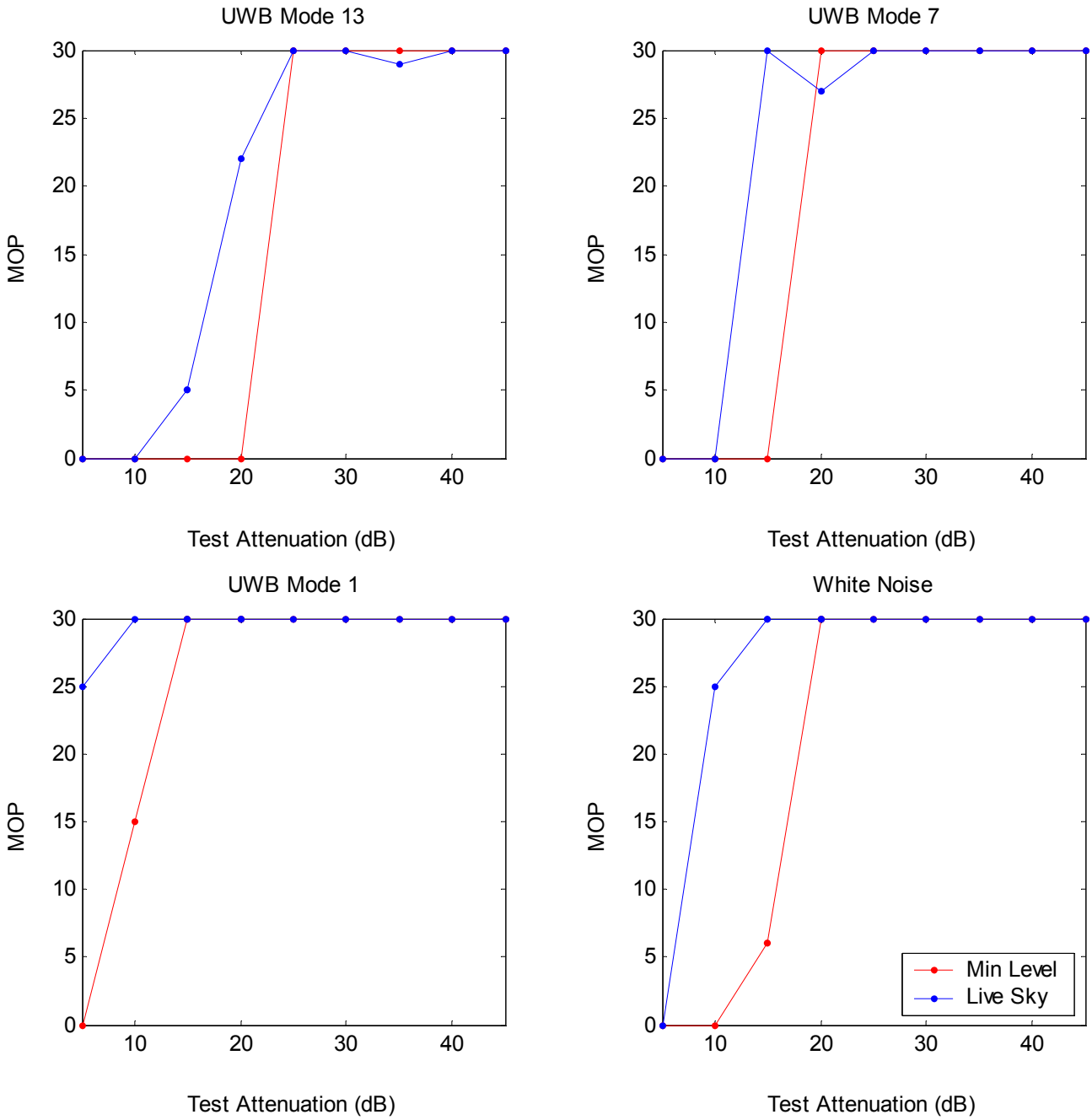

A.3 Ashtech Z-12

Receiver 2 is a Model Z-12 GPS receiver manufactured by the Ashtech Precision Products division of Magellan Corporation. This receiver is a survey quality receiver with numerous stand-alone and base station differential applications. The Z-12 uses 12 channels to track C/A code and carrier phase, L1 P code and carrier phase, and L2 P code and carrier phase. With Anti-Spoofing activated, this receiver employs the Ashtech Z tracking technology to mitigate the effects of the encryption and successfully track the P/Y code. The pertinent performance specifications for this receiver are:

- C/A raw pseudorange accuracy = 25 cm
- Autonomous position accuracy = 1 m CEP without Selective Availability[4]
- Cold start acquisition time = 2 minutes
- Warm start acquisition time < 30 seconds
- Reacquisition time = 5 sec[4]

During the radiated and aggregate testing, a Model 700718 GPS antenna manufactured by Ashtech was connected to Receiver 2. Both the L1 and L2 frequency bands are appropriate for this antenna. This antenna incorporates a low noise amplifier with the following specifications:

- 37.5 dB ± 3.0 dB gain for L1
- 42.0 dB ± 3.0 dB gain for L2
- 2.4 dB noise factor for both L1 and L2

Throughout the conducted, radiated, and aggregate testing, this receiver was configured to output data in the Ashtech proprietary real-time binary output format described in Reference (20). Note that this format is typically used for real-time processing via a computer connected to the receiver's RS-232 serial post, rather than real-time recording and subsequent post test analysis.

A.3.1 Receiver Specific Measures of Performance

All Ashtech Z-12 data collected during the ARL:UT test program were successfully processed as described in Appendix C and the beginning of this appendix. The analysis included both simulated GPS power levels with UWB modes 1, 7, and 13 and with the white noise source. As with the Ashtech Z-Sensor, all MOPs could be computed and are presented in this Appendix and carried forward to Chapter 6. The C/N_0 values are observed to range between 200 to 250 instead of the expected and documented 40 to 50; therefore, the associated units are unknown. Fortunately, due to the normalization process, the unknown units cancel out. The Ashtech Z-12

[4] *"GPS World Receiver Survey," January 2001.*

and Z-Sensor contain the most complete picture of the overall performance.

To compute the number of satellites tracked, a satellite was considered to be tracked by the GPS receiver when a MBEN record existed for that SV. The number of satellites used in the navigation solution was inferred from the above tracking plus a value of 24 for the good-bad indicator included with the measurement data in the MBEN record for that SV. All time tags in seconds of week were extracted from the PBN records. However, the PBN time tags do not include the one millisecond precession with receiver clock drift as expected and typically observed in Ashtech Z-12 data. The pseudorange double difference computations have been adjusted to account for this anomaly.

The MOPs are depicted in the following 12 figures. The reader is directed to the NovAtel 3151 section for a description of the content of these figures.

Ashtech Z-12 Normalized Satellites Tracked

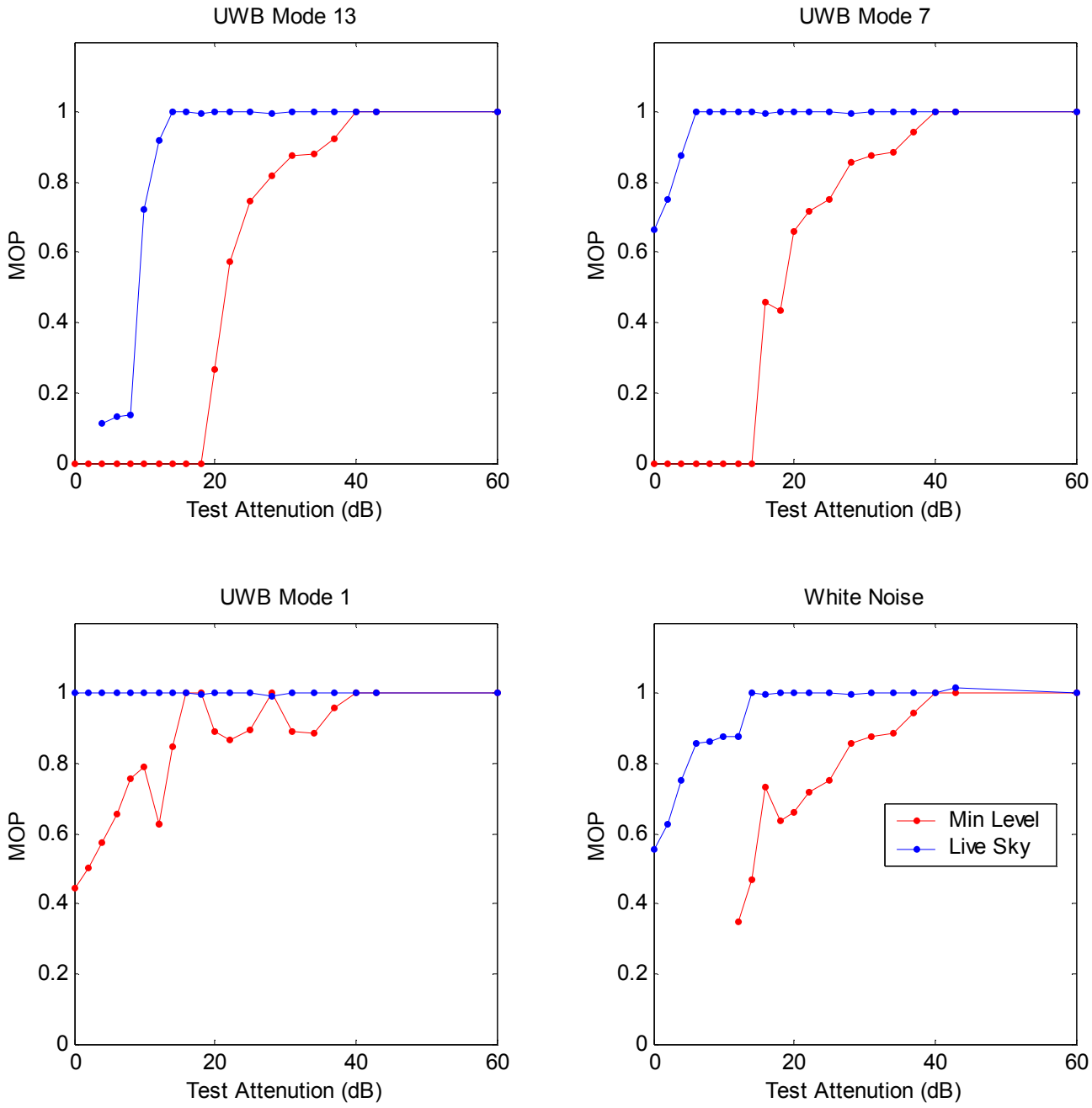

Ashtech Z-12 Normalized Satellites Used

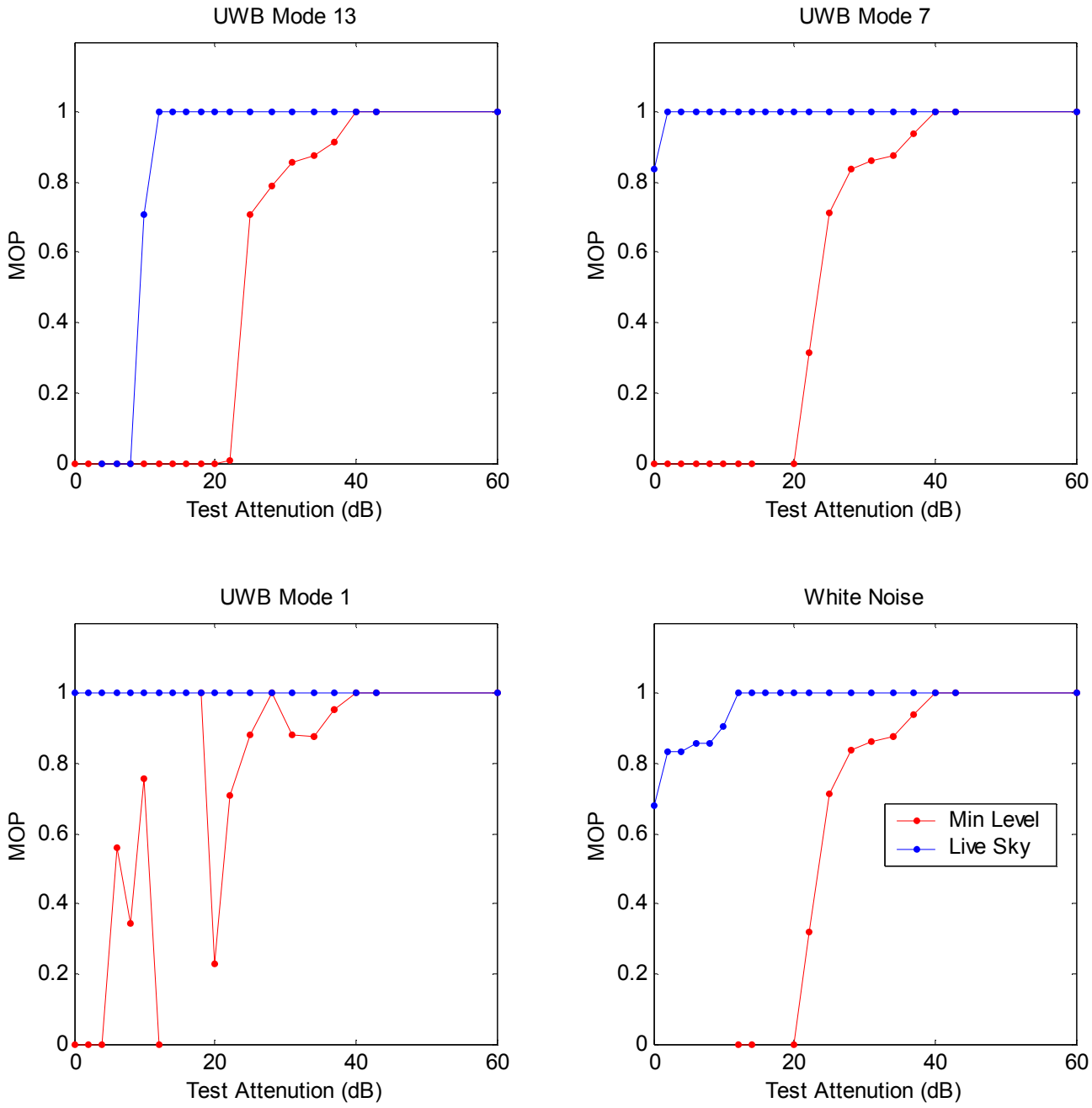

Ashtech Z-12 Normalized PDOP

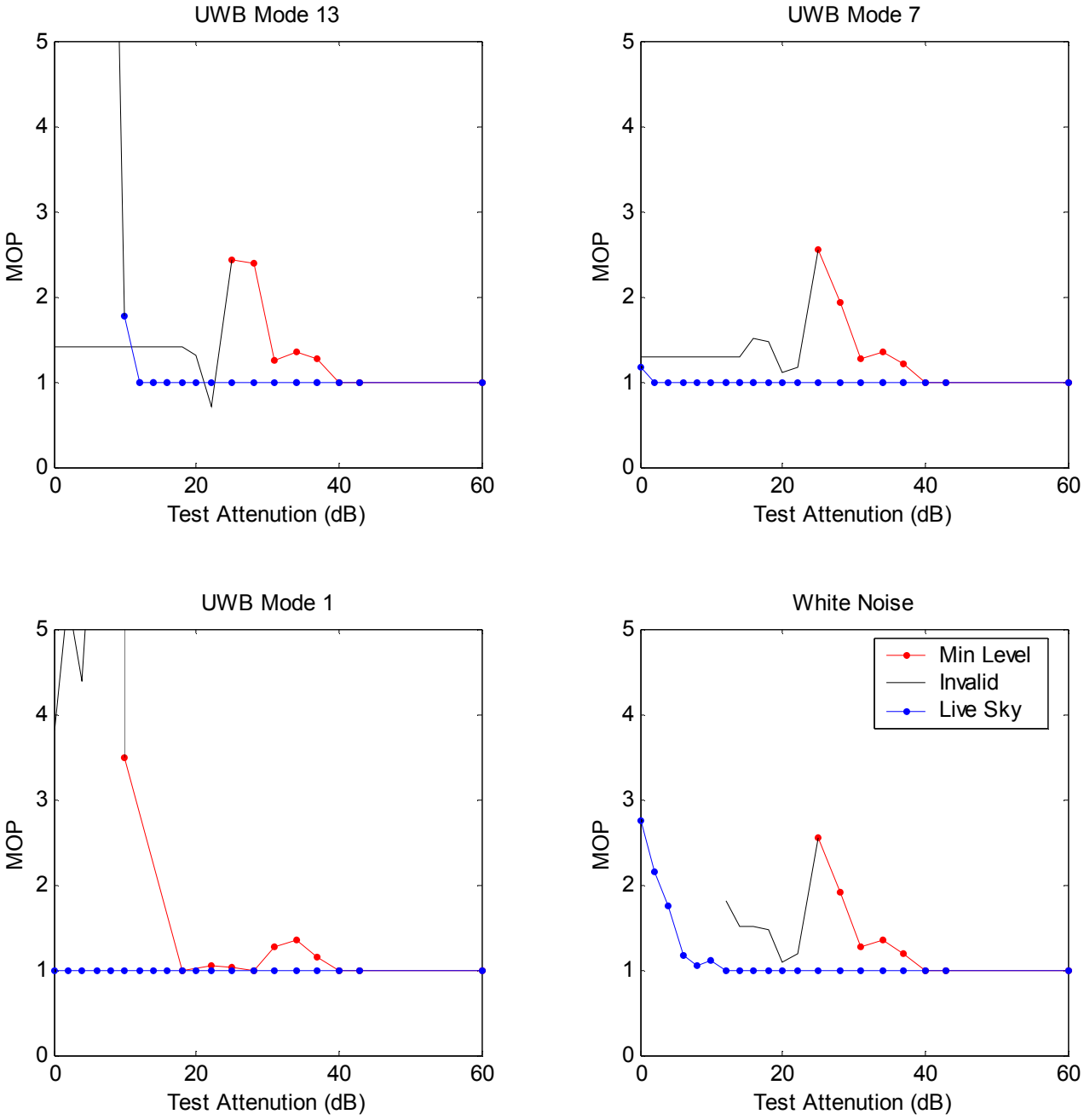

Ashtech Z-12 Increased Position Error (m)

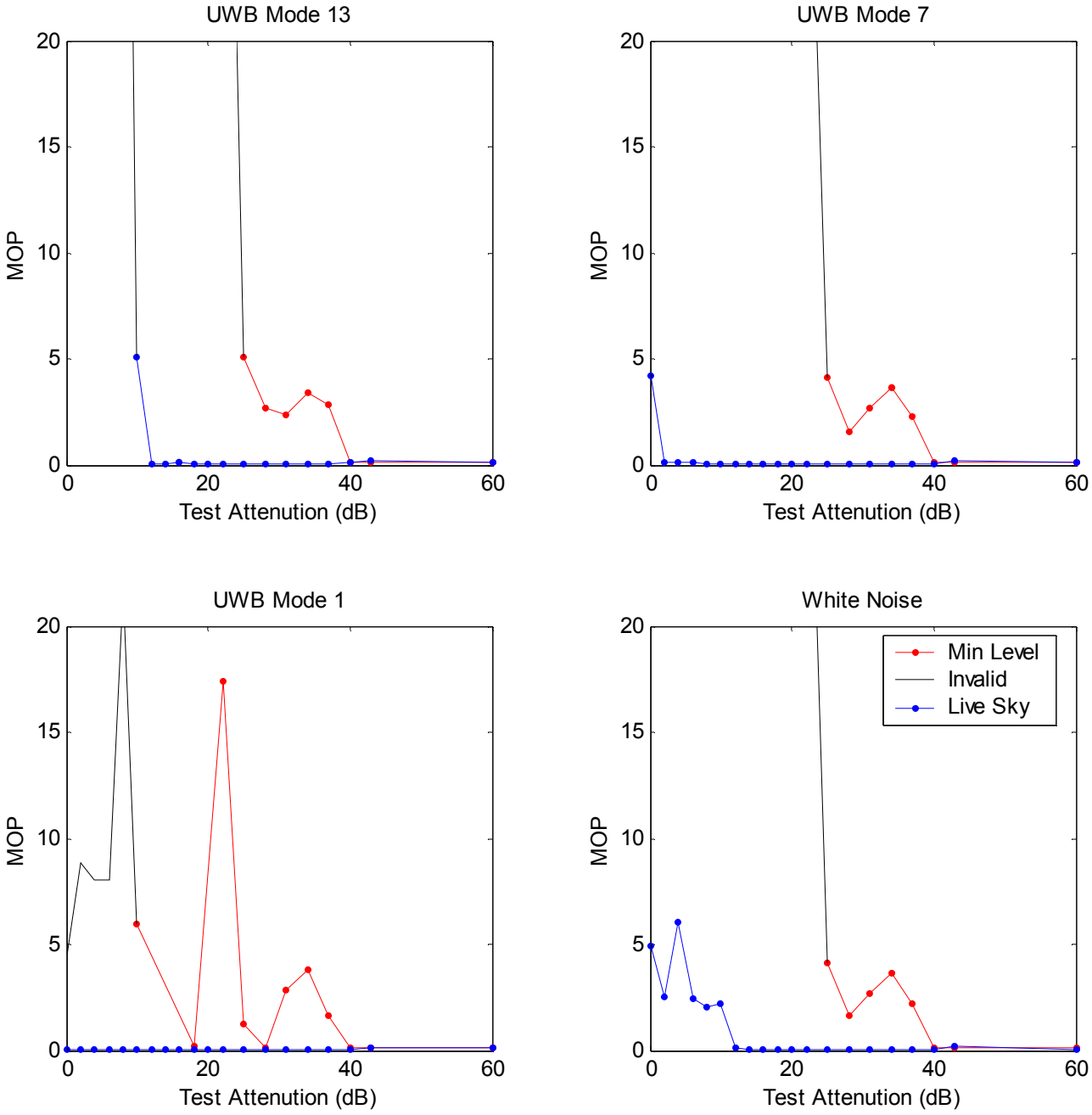

Ashtech Z-12 Normalized C/NO

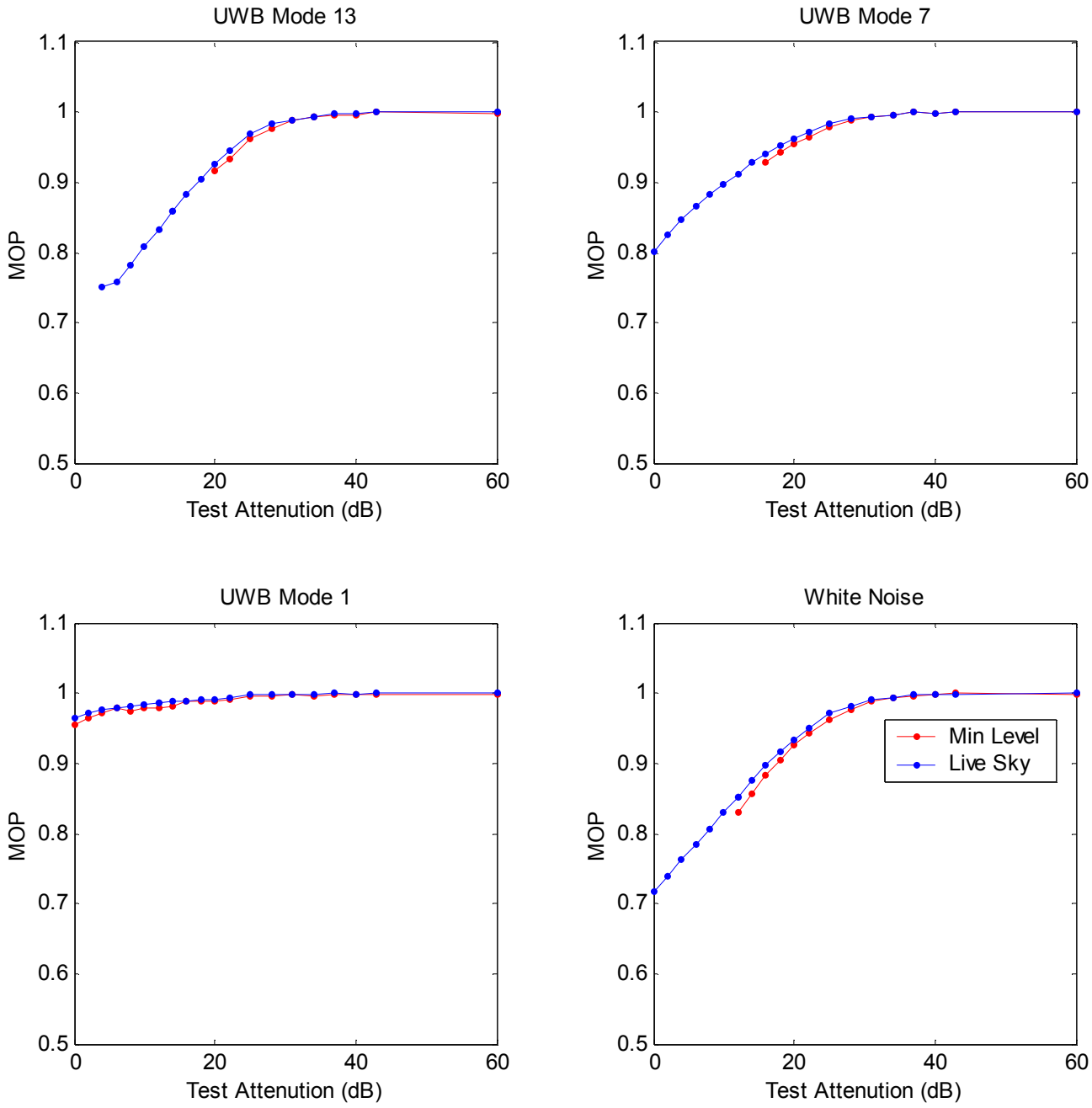

Ashtech Z-12 Normalized Pseudorange Noise

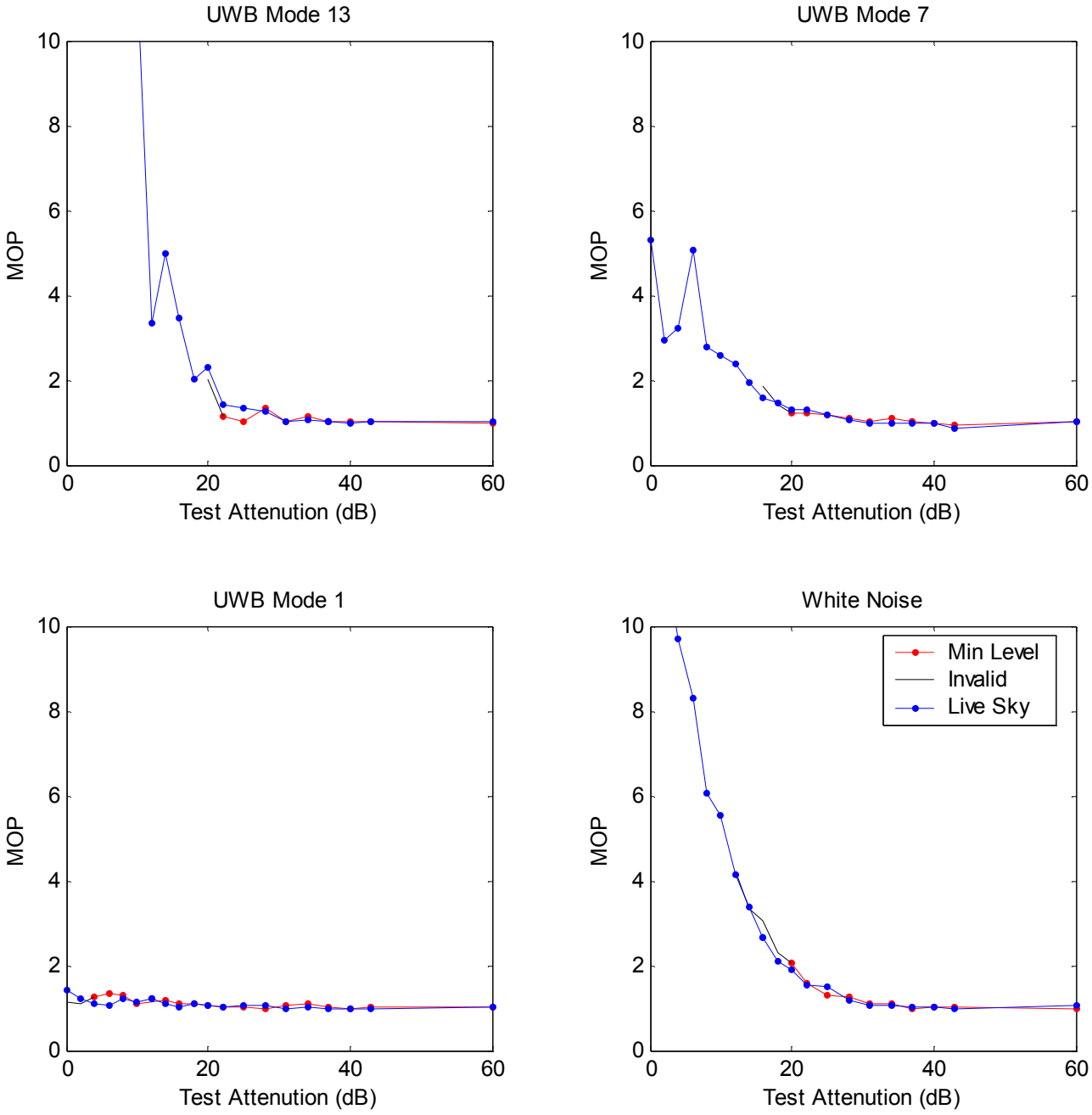

Ashtech Z-12 Double Difference Bias (cm)

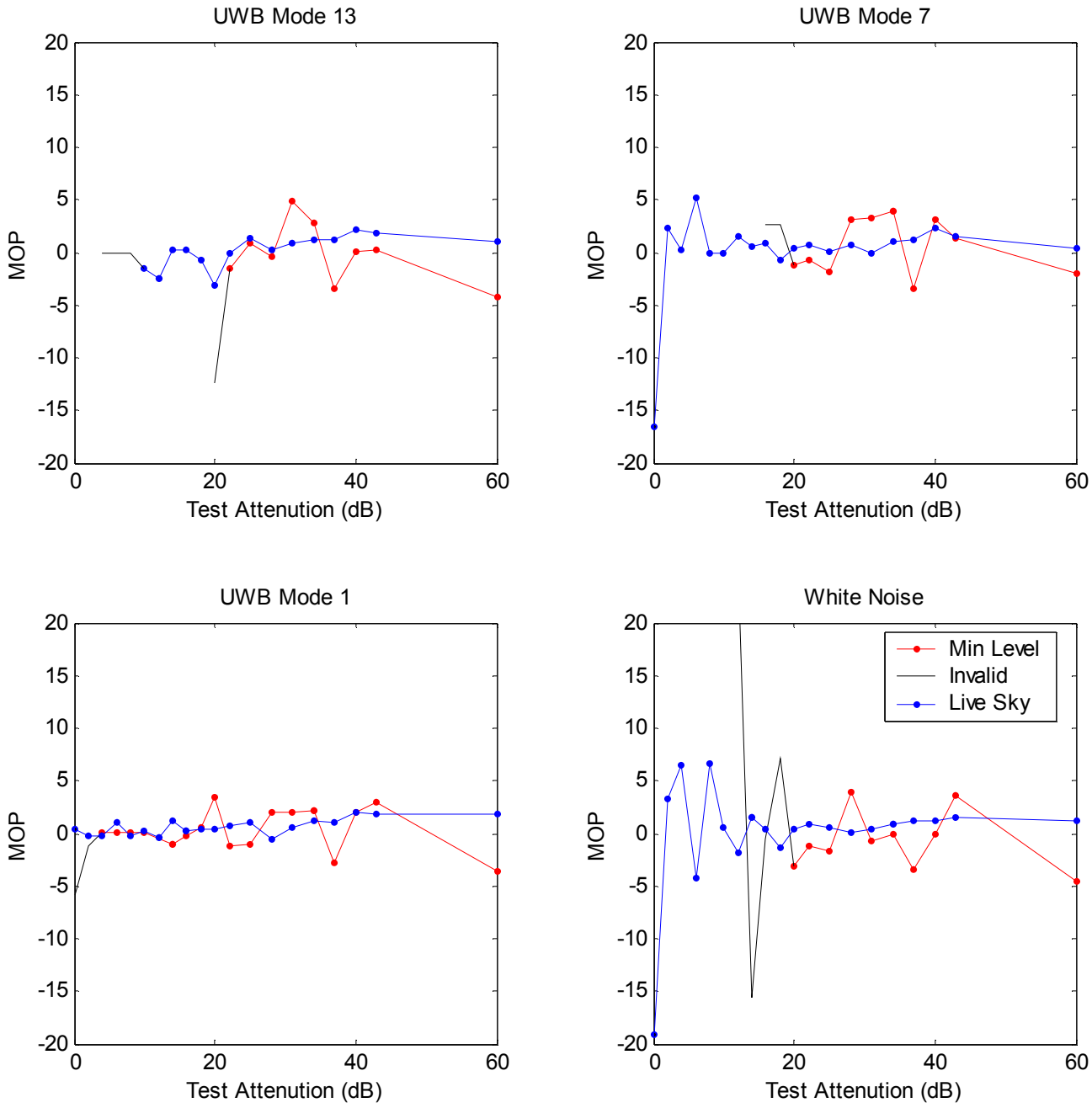

Ashtech Z-12 Double Difference Noise (cm)

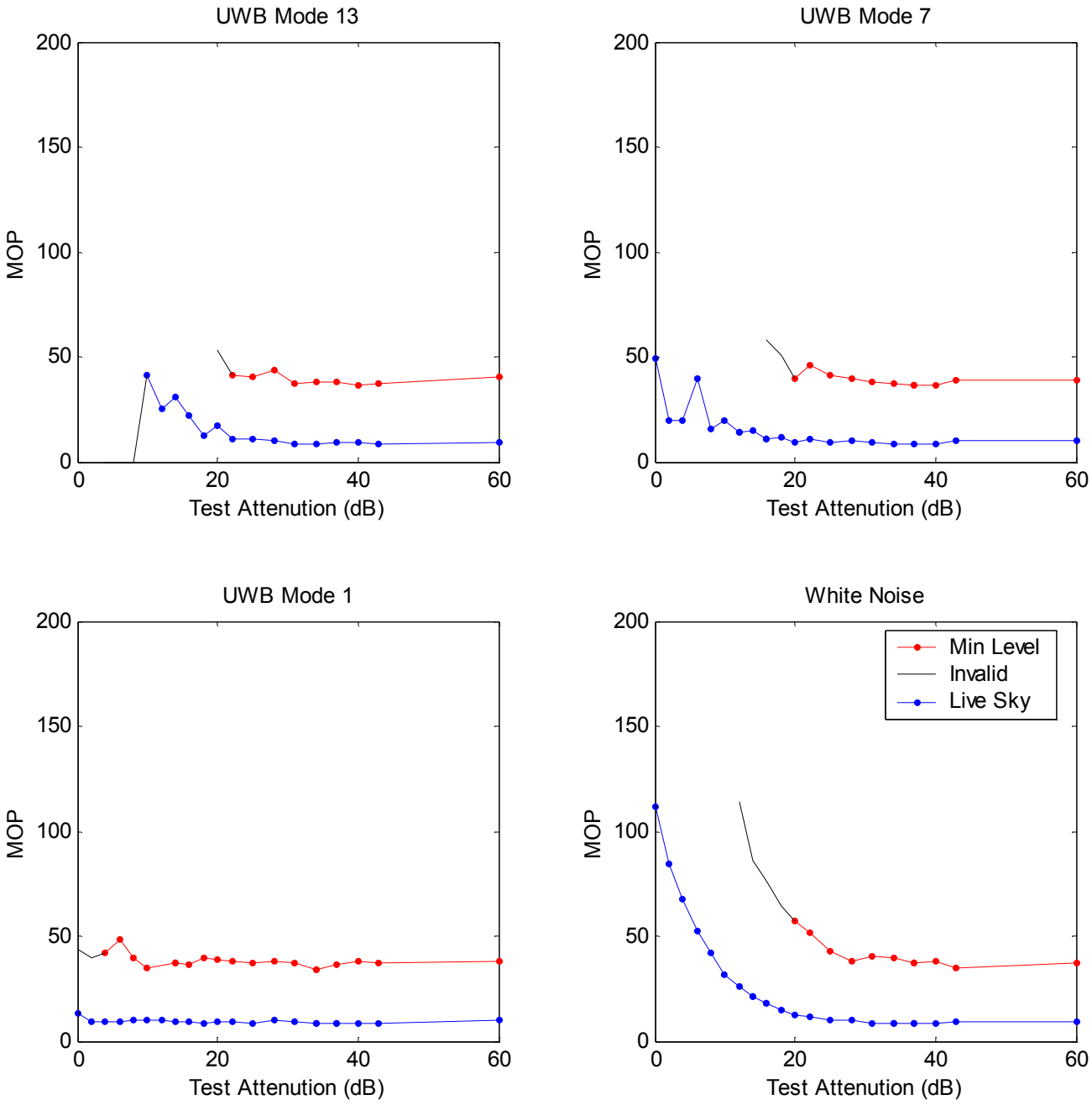

Ashtech Z-12 Incr. Time To Reacq. 1 tk'd sat. (sec)

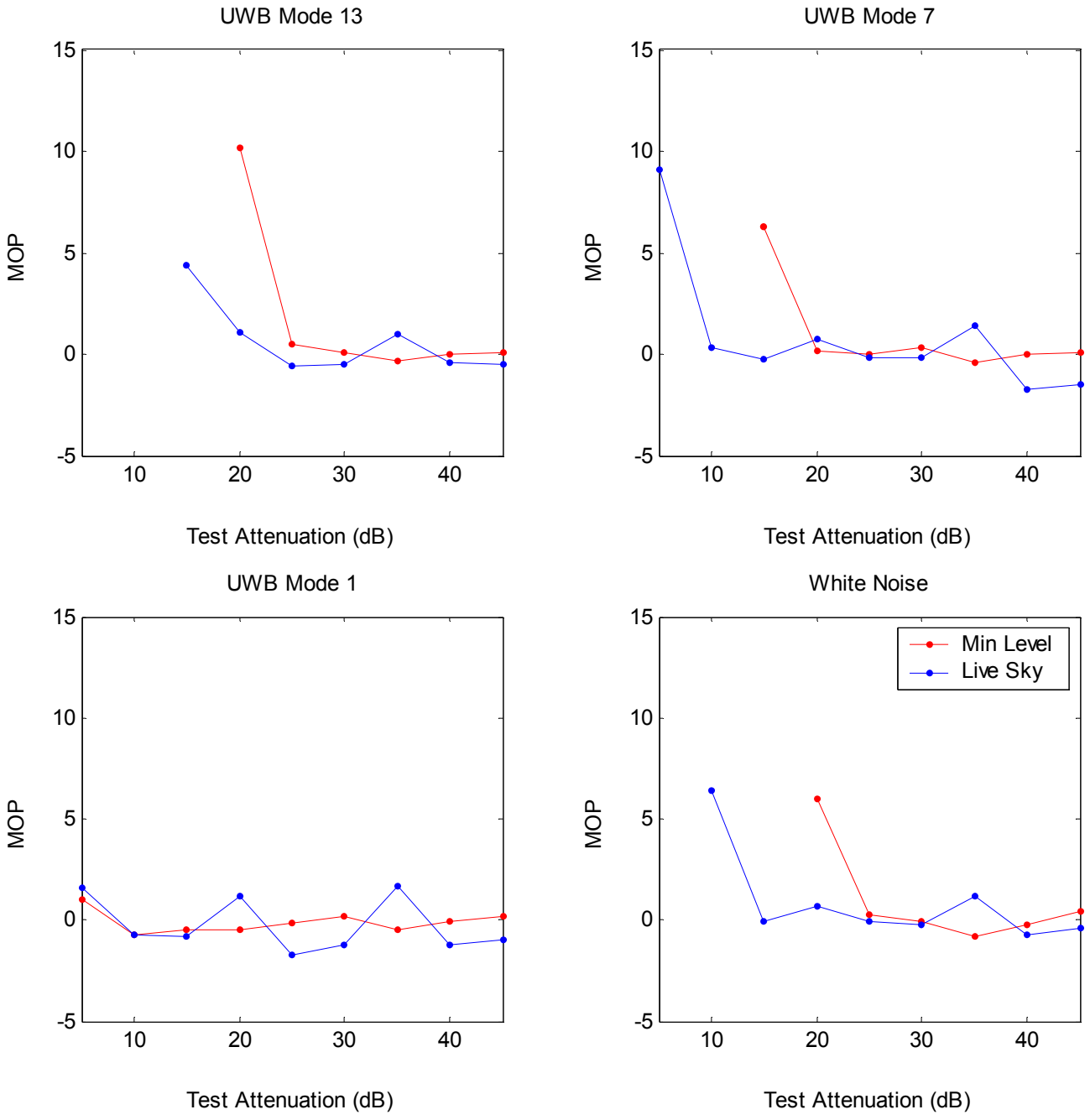

Ashtech Z-12 Incr. Time To Reacq. N tk'd sat's. (sec)

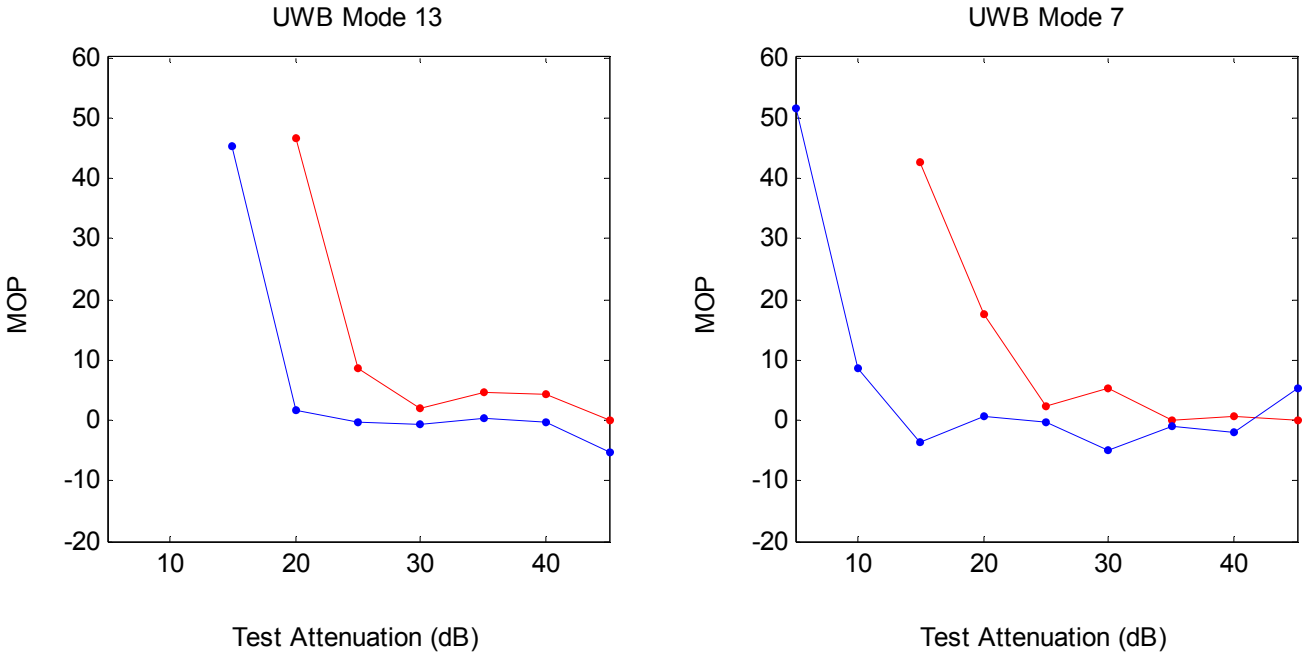

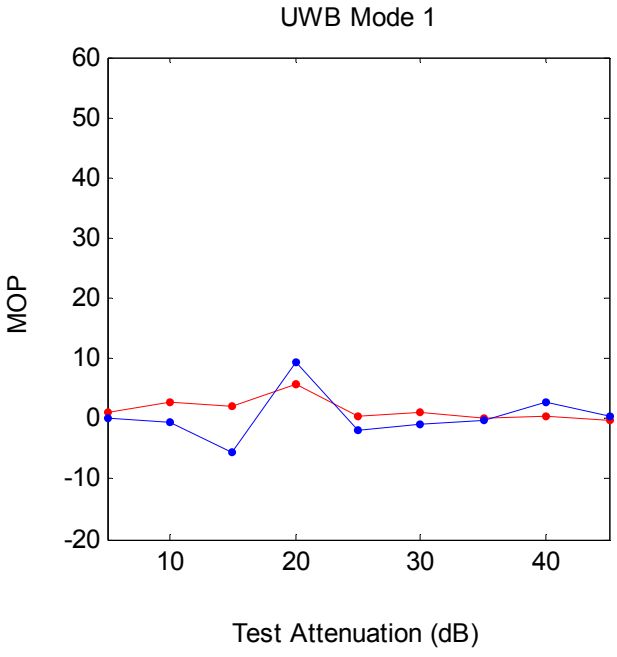

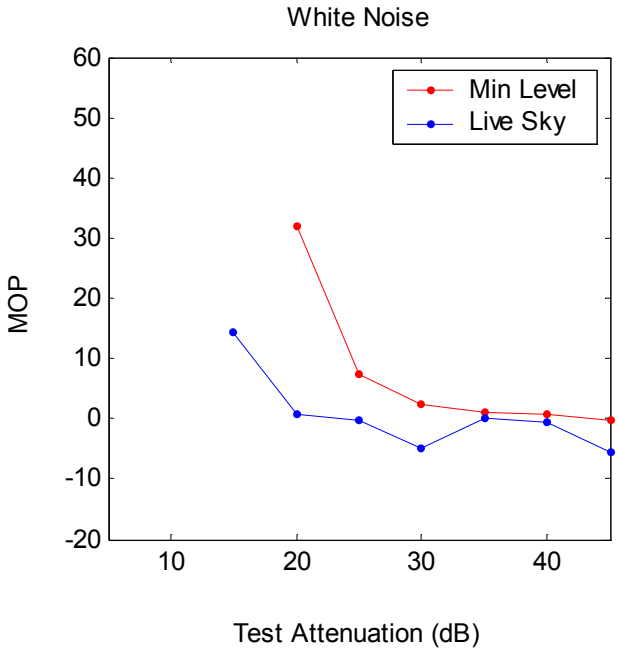

Ashtech Z-12 Incr. Time To Reacq. 4 nav'd sat's. (sec)

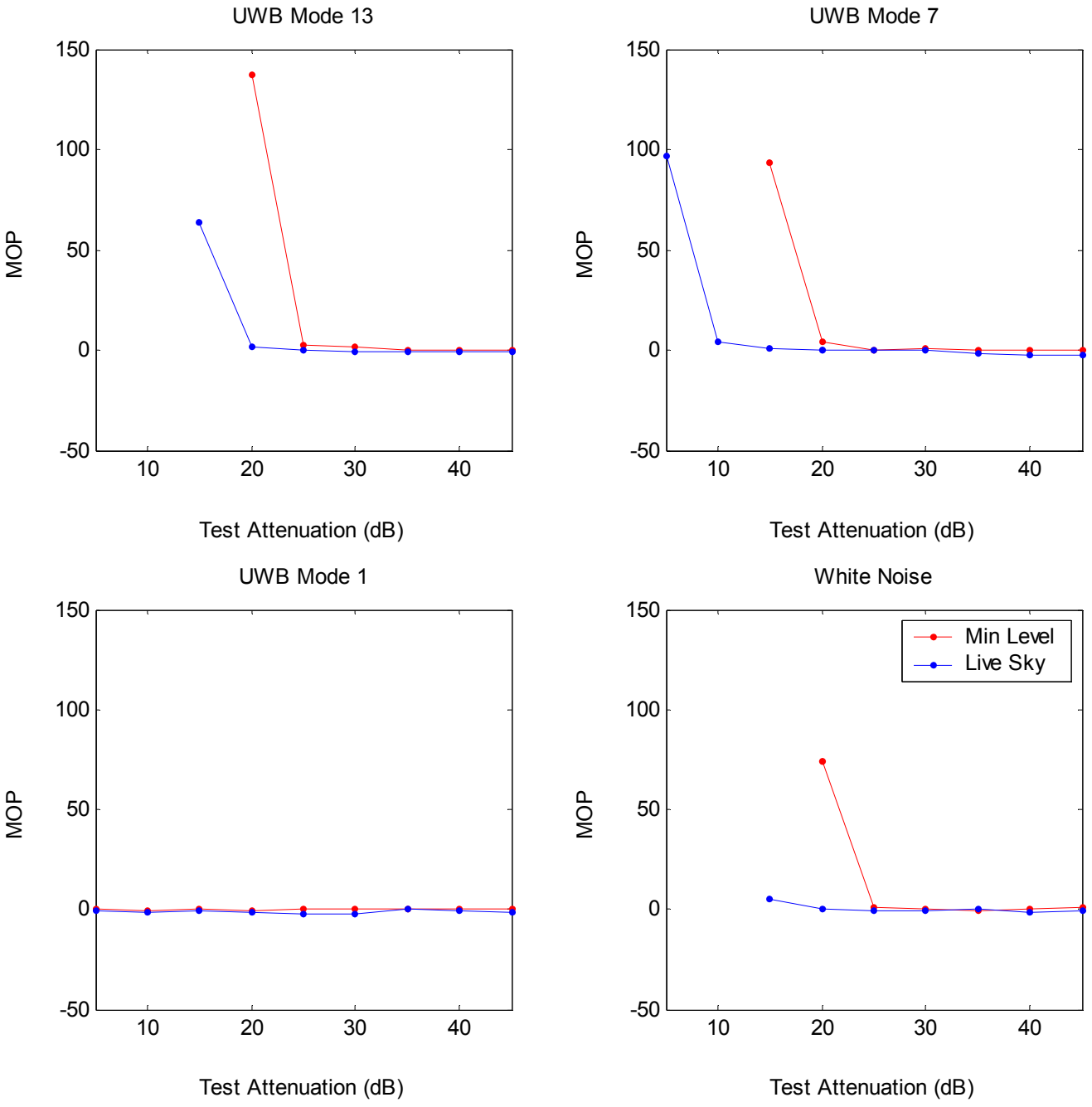

Ashtech Z-12 Trials Used to Reacq. 4 navd sat's. (sec)

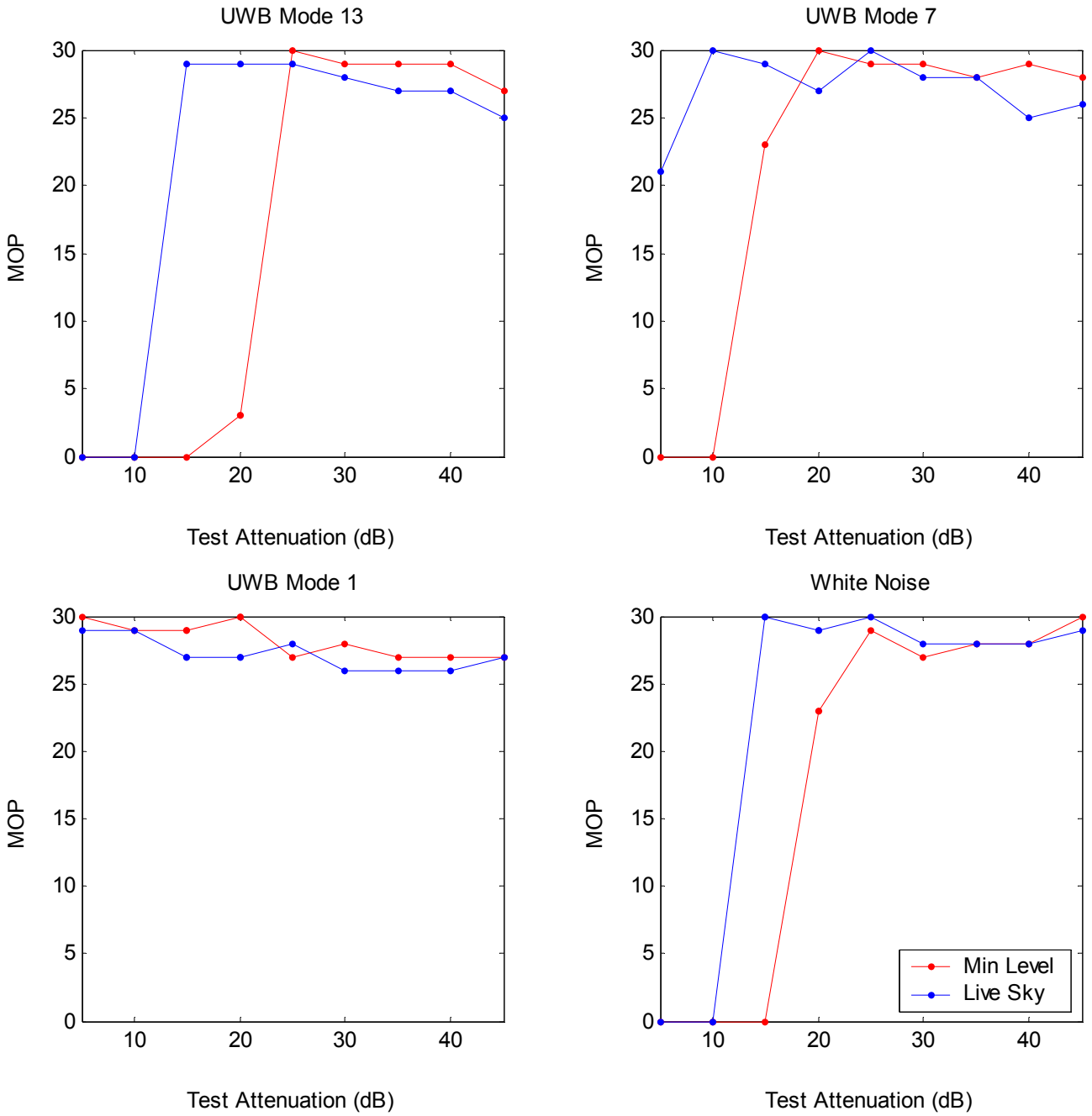

A.4 Garmin 155XL

Receiver 3 is a Model 155XL manufactured by Garmin Corporation. This receiver is an aviation quality receiver with imbedded navigation applications and user interfaces, but no ability to output raw measurement data. The Garmin 155XL uses 12 channels to track C/A code only. The pertinent performance specifications for this receiver are:

- Autonomous position accuracy = 15 m RMS without Selective Availability
- Cold start acquisition time = 150 sec[5]
- Warm start acquisition time = 15 sec
- Reacquisition time = 20 sec[5]

During the radiated testing, a Model GA56 GPS antenna manufactured by Garmin Corporation was connected to Receiver 3. Both the L1 and L2 frequency bands are appropriate for this antenna. This antenna incorporates a low noise amplifier with the following specifications:

- 20.0 dB dB gain
- 3.0 dB noise factor

Throughout the conducted, radiated, and aggregate testing, this receiver was configured to output receiver generated navigation solutions in the standard NMEA 0183 format.

A.4.1 Receiver Specific Measures of Performance

All Garmin 155XL data collected during the ARL:UT test program were successfully processed as described in the beginning of this Appendix. Data were processed for both simulated GPS power levels with UWB modes 1, 7, and 13 and with the white noise source. Unfortunately, the NMEA 0183 format does not support the output of raw measurement data; therefore, only the C/N_0 measure of performance has been computed for the Garmin 155XL when assessing the pseudorange quality. This gap in the analysis severely hampers the ability of an analyst to assess the performance of this receiver. In addition, the Garmin 155XL is noted to output seemingly good navigation data when the receiver is known to not be tracking any satellites. These suspect data are tagged as "invalid" per the definition in the first section of this appendix and are not carried forward into Chapter 6. Other analysts are encouraged to apply similar data screening of the Garmin 155XL data.

[5] *"GPS World Receiver Survey," January 2001.*

To compute the number of satellites tracked, a satellite was considered to be tracked by the GPS receiver when the SV was listed in the GPSSV record, and the record contained a non-zero C/N_0 value. The number of satellites used in the navigation solution was based on those SV's listed in the GPGSA record. Finally, all time tags are based on UTC time in the GPGGA record.

A detailed analysis of the Garmin reacquisition times indicates that both the number of satellites tracked and the number of satellites navigated do not correlate with the description of the test setup. Whereas the test setup describes disconnecting the GPS signal 10 seconds after the start of the trial, all plots of number of satellites tracked versus time and of number of satellites navigated versus time show valid satellite counts out to at least epoch 18. There can be two explanations for this. First, the GPS signals were, in fact, not turned off 10 seconds after the trial start, but 18 seconds. This cannot be true since acquisition tests for receivers one through four were run in parallel, and detailed analysis of the other three receivers all show satellite counts dropping to zero ten seconds into the trials. The other explanation is that the receiver output data stream does not accurately represent the satellite counts of the receiver during the time period near where GPS input is lost. A second discrepancy in the plots of number of satellites tracked versus time and of number of satellites navigated versus time shows that, for certain tests and during the time when the GPS signal is disconnected from the receiver, the satellite counts do not drop to zero. Some of these trials in question show no degradation at all in the satellite count, and some show only a minimal drop. For these reasons, the Garmin reacquisition times are only presented here in Appendix A as a function of attenuation setting, and are not carried forward to Chapter 6.

The available MOPs are depicted in the following nine figures. The reader is directed to the NovAtel 3151 section for a description of the specific content of these figures.

Garmin 155XL Decreased Satellites Tracked

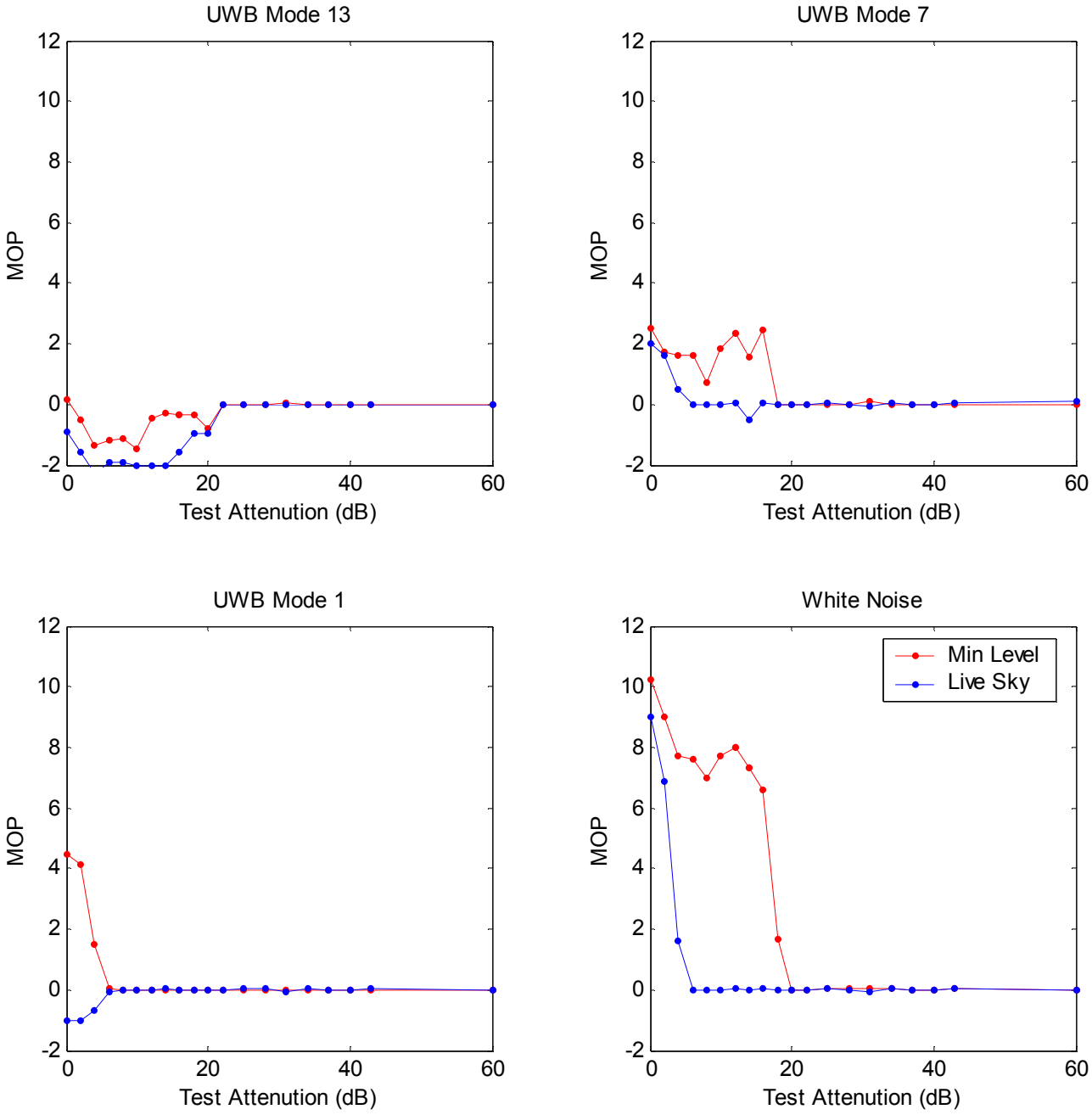

Garmin 155XL Decreased Satellites Used

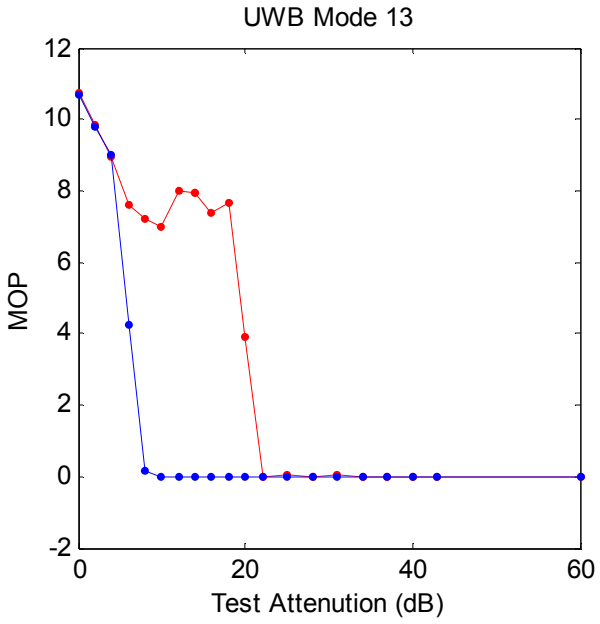

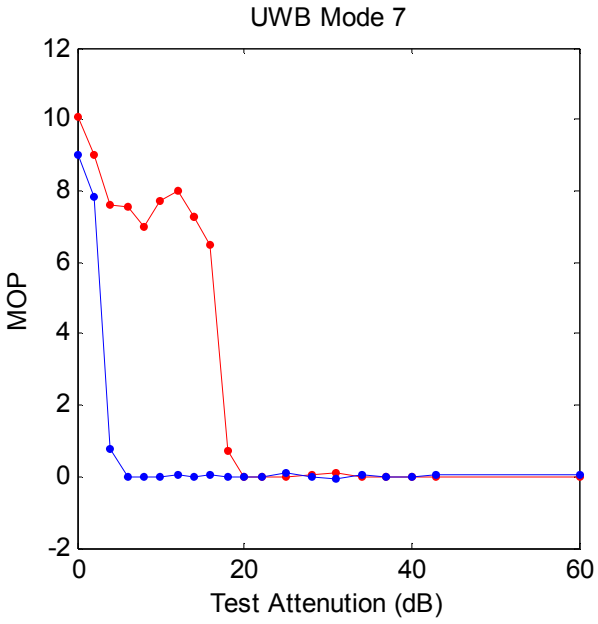

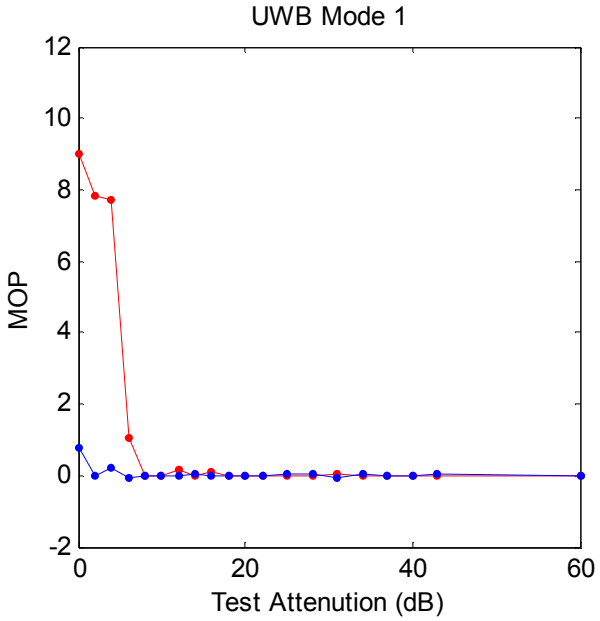

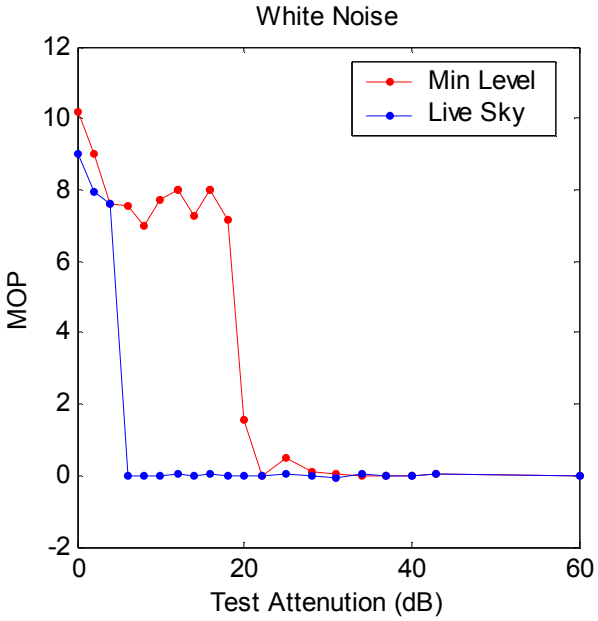

Garmin 155XL Normalized PDOP

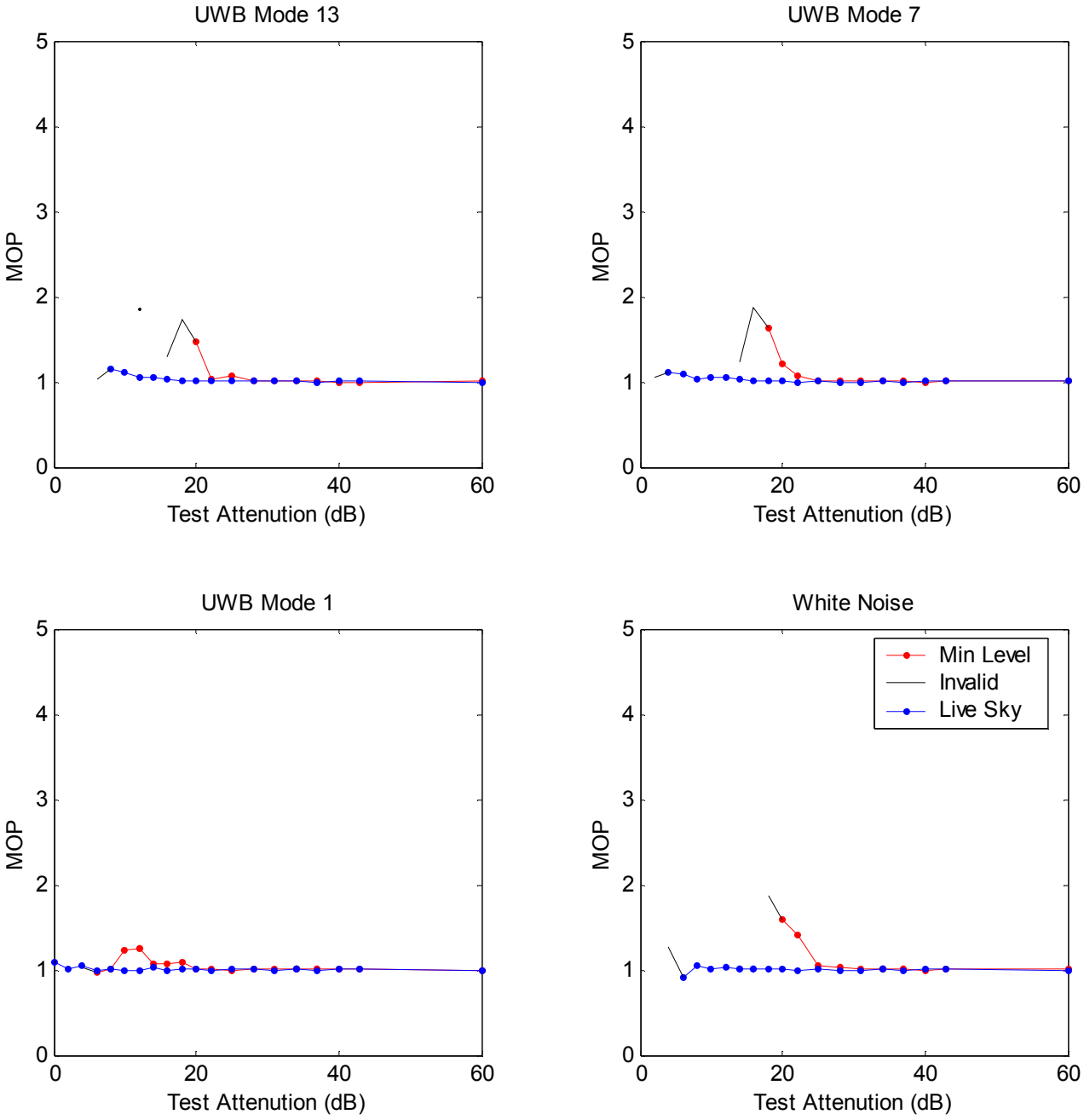

Garmin 155XL Increased Position Error (m)

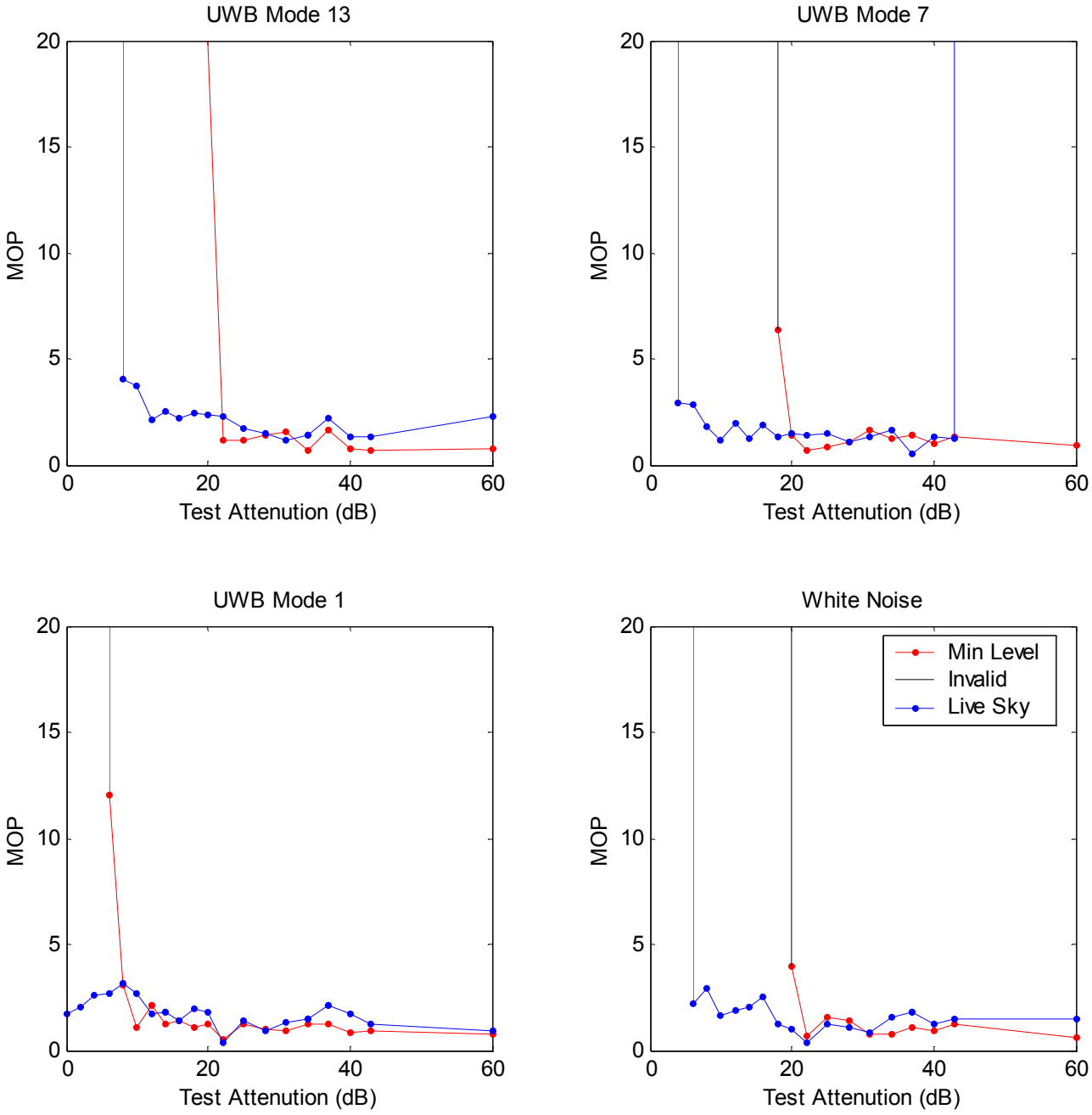

Garmin 155XL Normalized C/NO

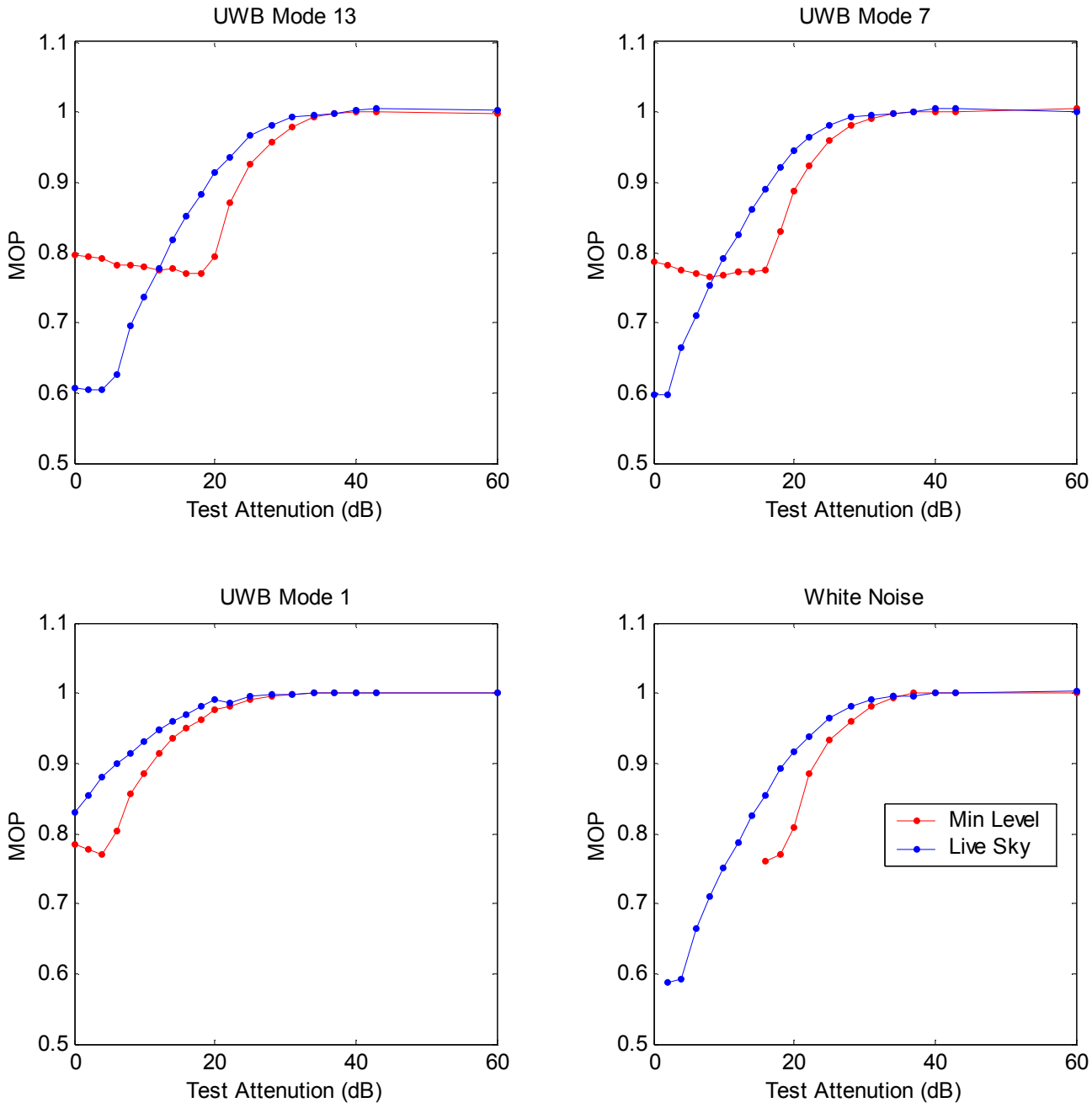

Garmin 155XL Incr. Time To Reacq. 1 tk'd sat. (sec)

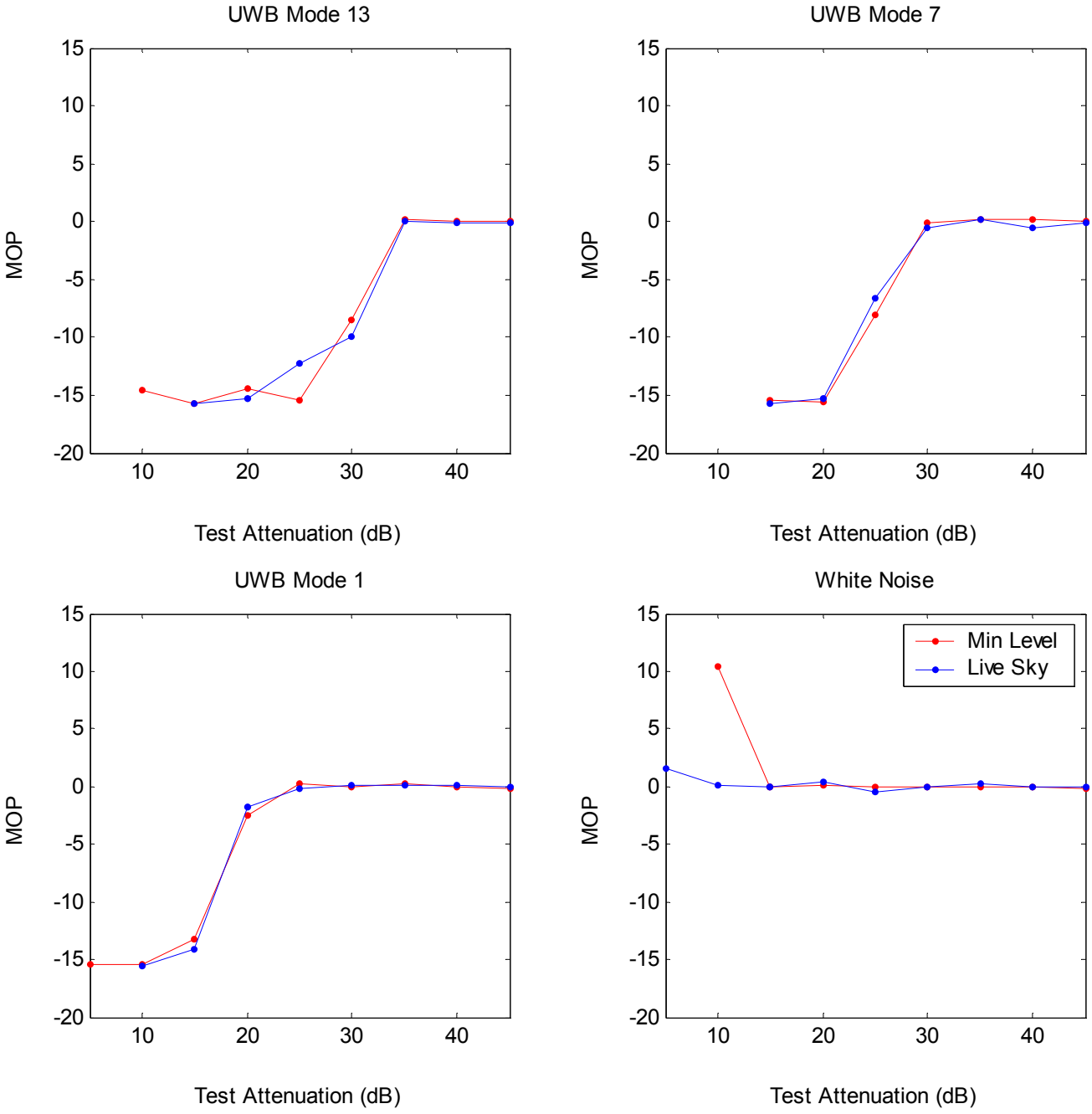

Garmin 155XL Incr. Time To Reacq. N tk'd sat's. (sec)

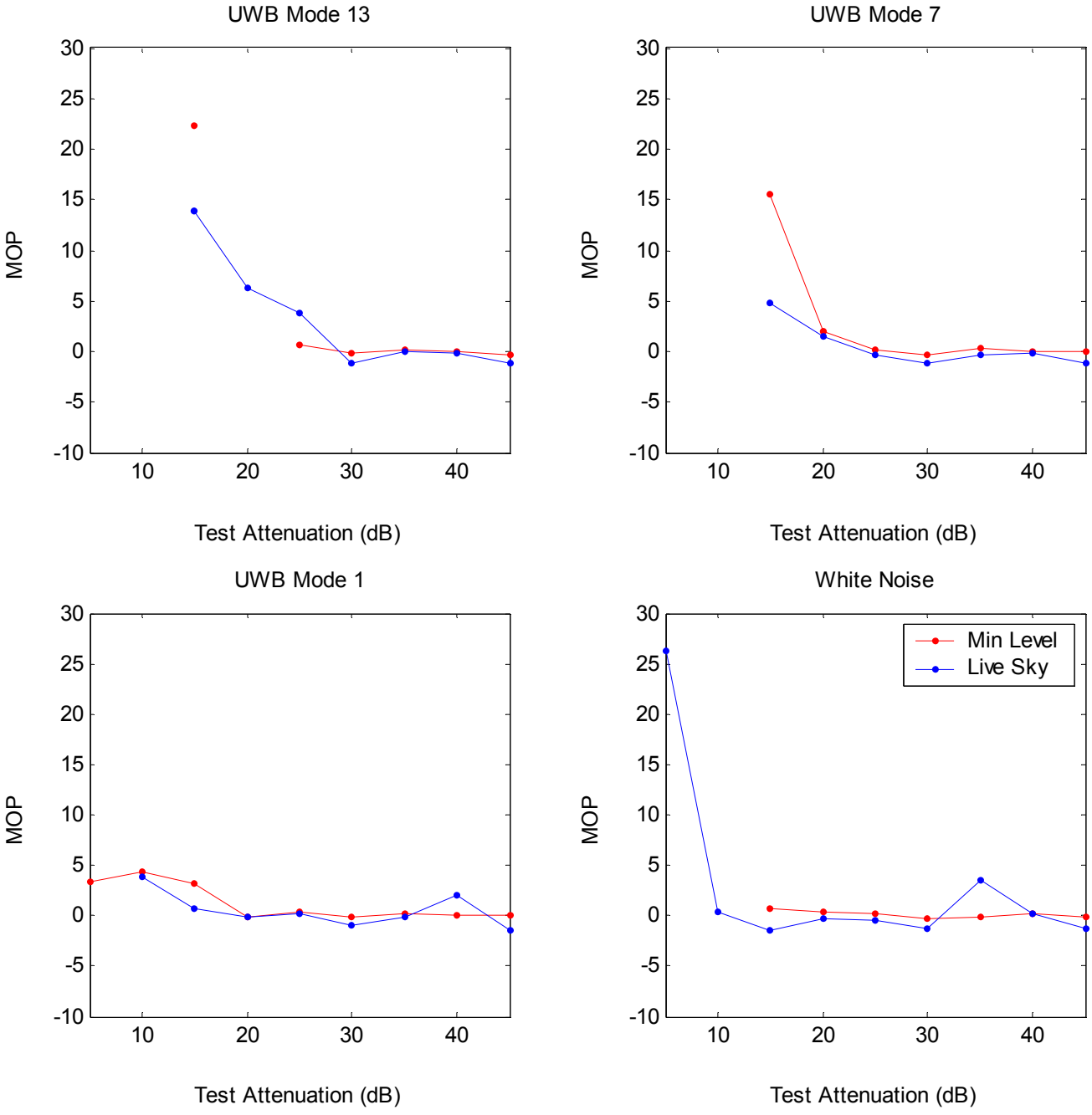

Garmin 155XL Incr. Time To Reacq. 4 nav'd sat's. (sec)

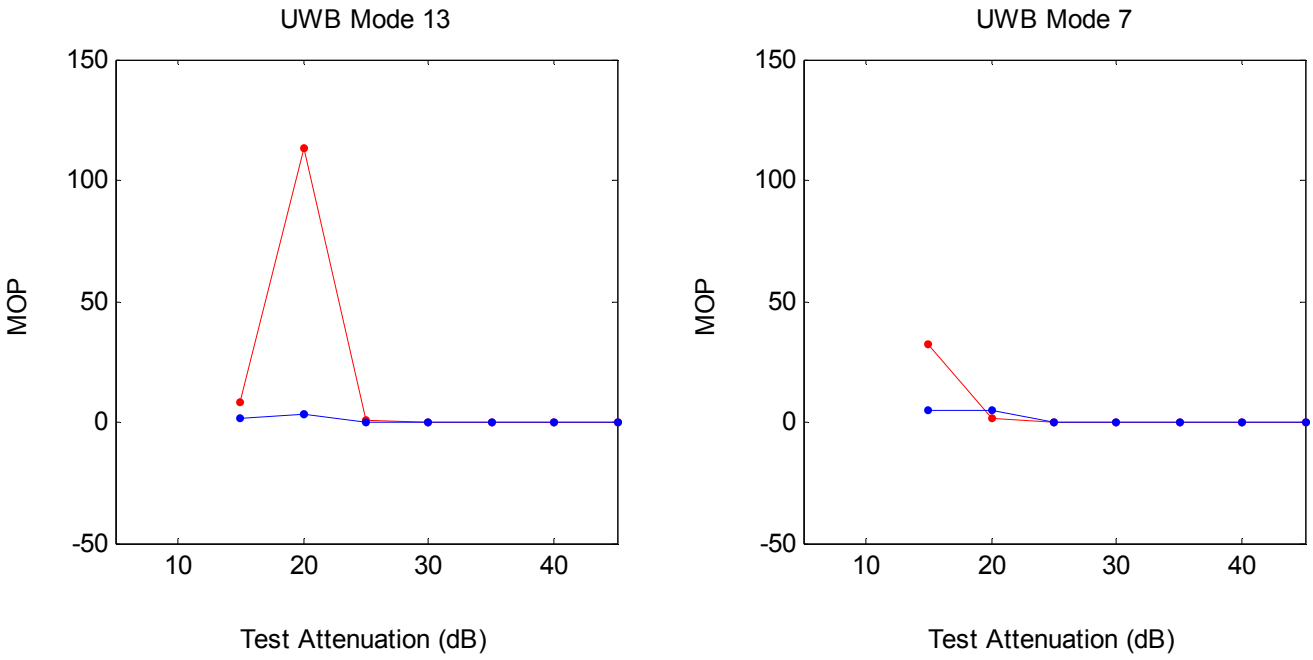

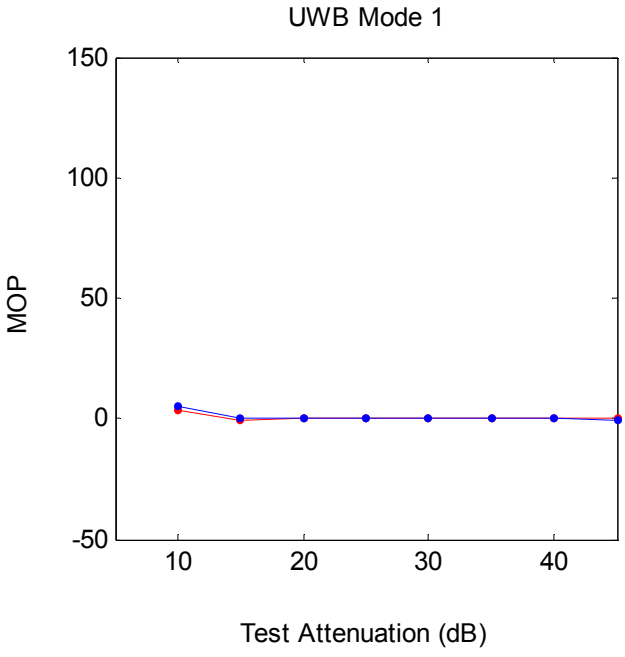

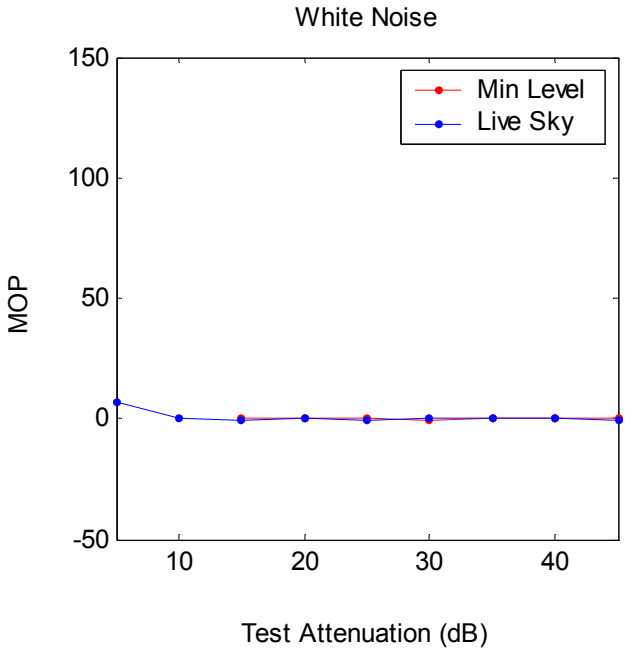

Garmin 155XL Trials Used to Reacq. 4 navd sat's. (sec)

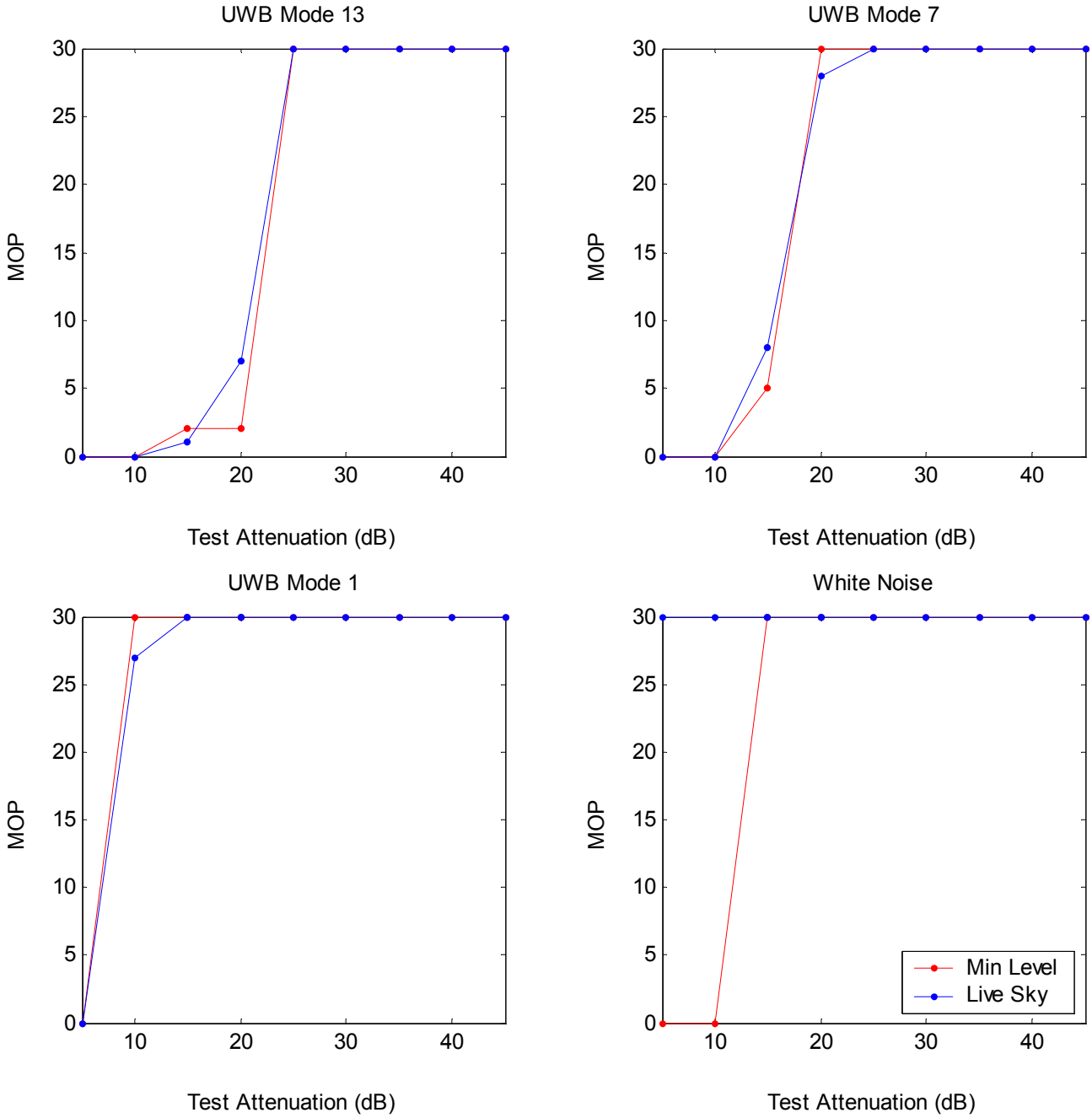

A.5 Ashtech Z-Sensor

Receiver 4 is a Model Z-Sensor GPS receiver manufactured by the Ashtech Precision Products division of Magellan Corporation. This receiver is a survey quality receiver with numerous with numerous stand-alone and rover differential applications. The Z-Sensor is essentially the Z-12 technology adapted to a single circuit board with limited user interfaces. The Z-Sensor tracks C/A code and carrier phase, L1 P code and carrier phase, and L2 P code and carrier phase, but with 36 channels instead of the 12 channels used with the Z-12. With Anti-Spoofing activated, this receiver employs the Ashtech Z tracking technology to mitigate the effects of the encryption and successfully track the P/Y code. The pertinent performance specifications for this receiver are:

- Autonomous position accuracy = 3.0 m CEP without Selective Availability
- Cold start acquisition time = 150 sec[6]
- Warm start acquisition time = 15 sec[6]
- Reacquisition time = 5 sec[6]

During the radiated and aggregate testing, a Model 701945-01 GPS antenna manufactured by Ashtech was connected to Receiver 2. Both the L1 and L2 frequency bands are appropriate for this antenna. This antenna incorporates a low noise amplifier with the following specifications:

- 37.5 dB ± 3.0 dB gain for L1
- 42.0 dB ± 3.0 dB gain for L2
- 2.4 dB noise factor for both L1 and L2

Throughout the conducted, radiated, and aggregate testing, this receiver was configured to output data in the Ashtech proprietary real-time binary output format described in Reference (20). Identical to the case with the Z-12, this format is typically used for real-time processing via a computer connected to the receiver's RS-232 serial post, rather than real-time recording and subsequent post test analysis.

A.5.1 Receiver Specific Measures of Performance

All Ashtech Z-Sensor data collected during the ARL:UT test program were successfully processed as described in Appendix C and the beginning of this Appendix. This data included both simulated GPS power levels with UWB modes 1, 7, and 13 and with the white noise source. All MOPs could be computed, and all combinations of GPS power level and UWB modes are

[6] *"GPS World Receiver Survey," January 2001*

presented in this Appendix and carried forward to Chapter 6. Along with the Ashtech Z-12, this receiver contains the most complete picture of the overall performance.

To compute the number of satellites tracked, a satellite was considered to be tracked by the GPS receiver when a MBEN record existed for that SV. The number of satellites used in the navigation solution was inferred from the above tracking plus a value of 24 for the good-bad indicator included with the measurement data in the MBEN record for that SV. All time tags in seconds of week were extracted from the PBN records.

The MOPs are depicted in the following 12 figures. The reader is directed to the NovAtel 3151 section for a description of the content of these figures.

Ashtech Z-Sensor Decreased Satellites Tracked

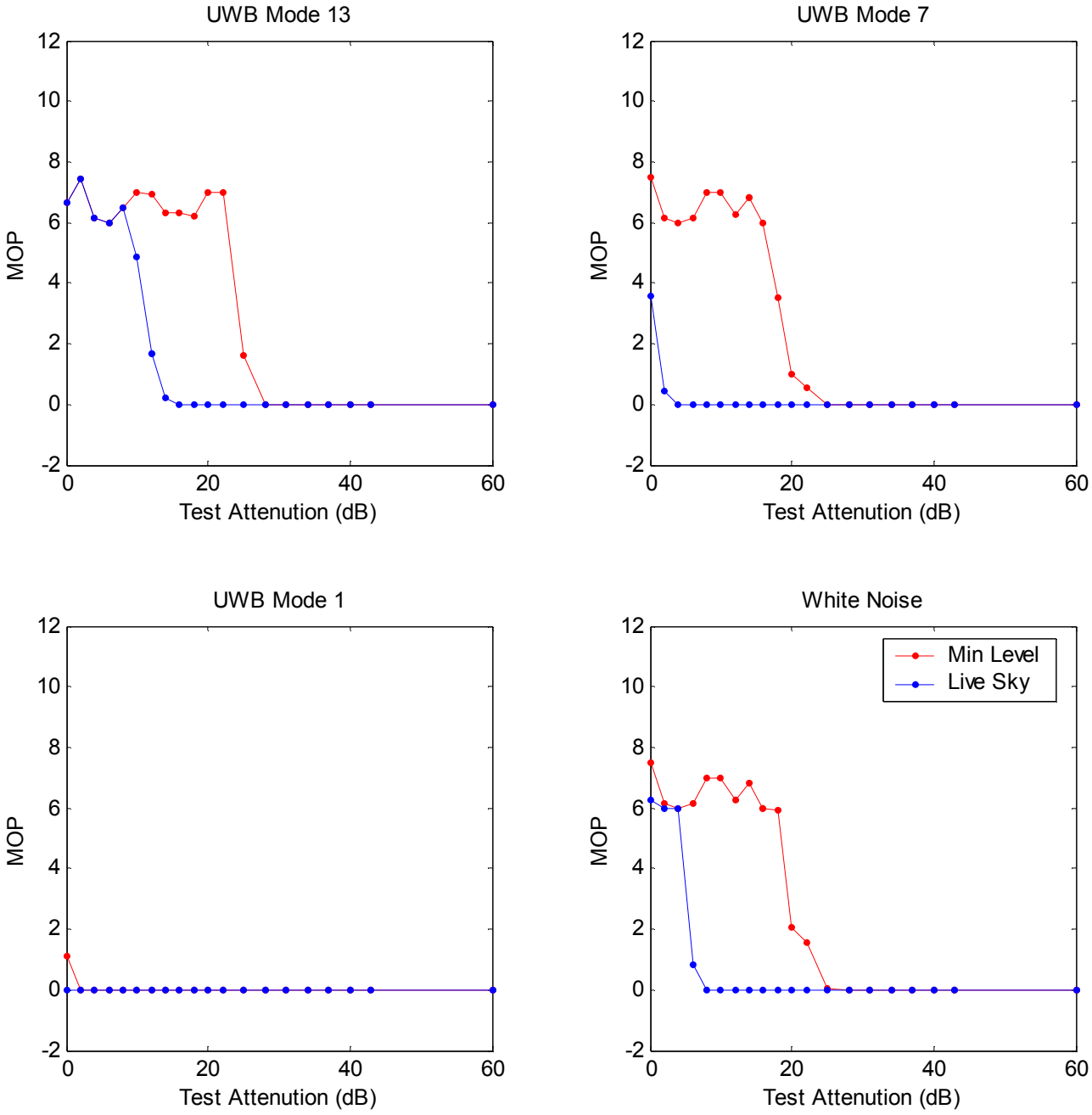

Ashtech Z-Sensor Decreased Satellites Used

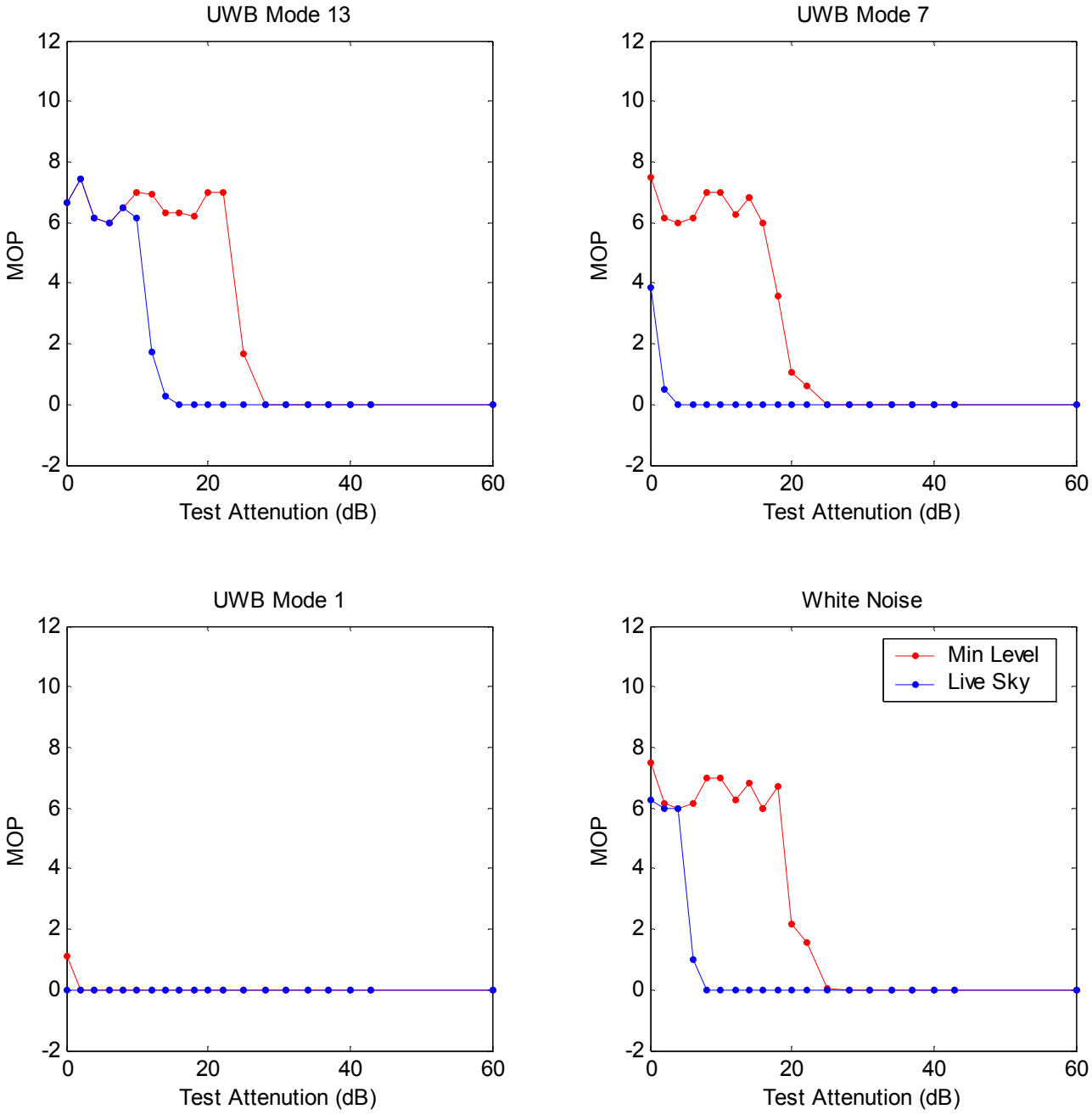

Ashtech Z-Sensor Normalized PDOP

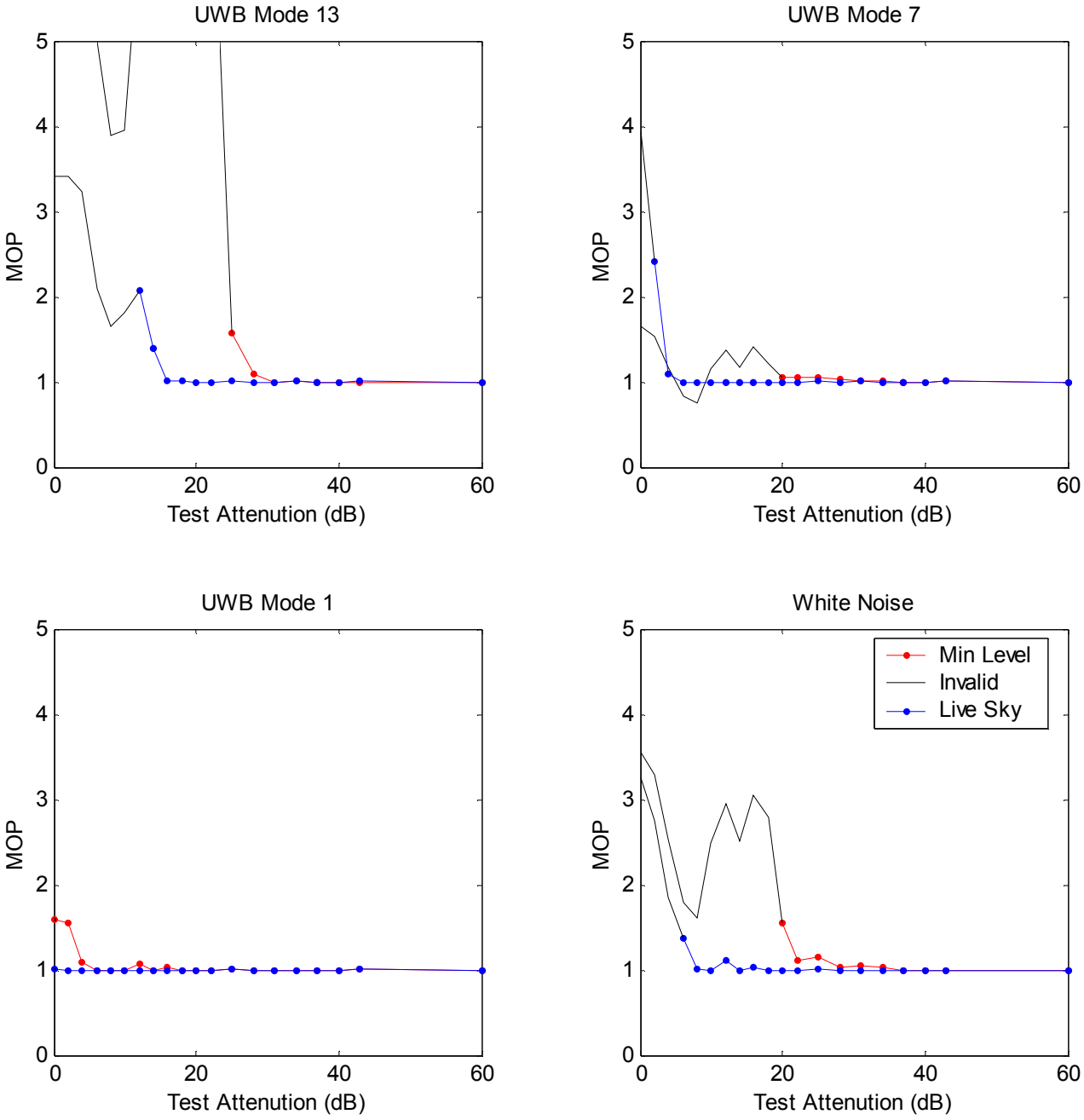

Ashtech Z-Sensor Increased Position Error (m)

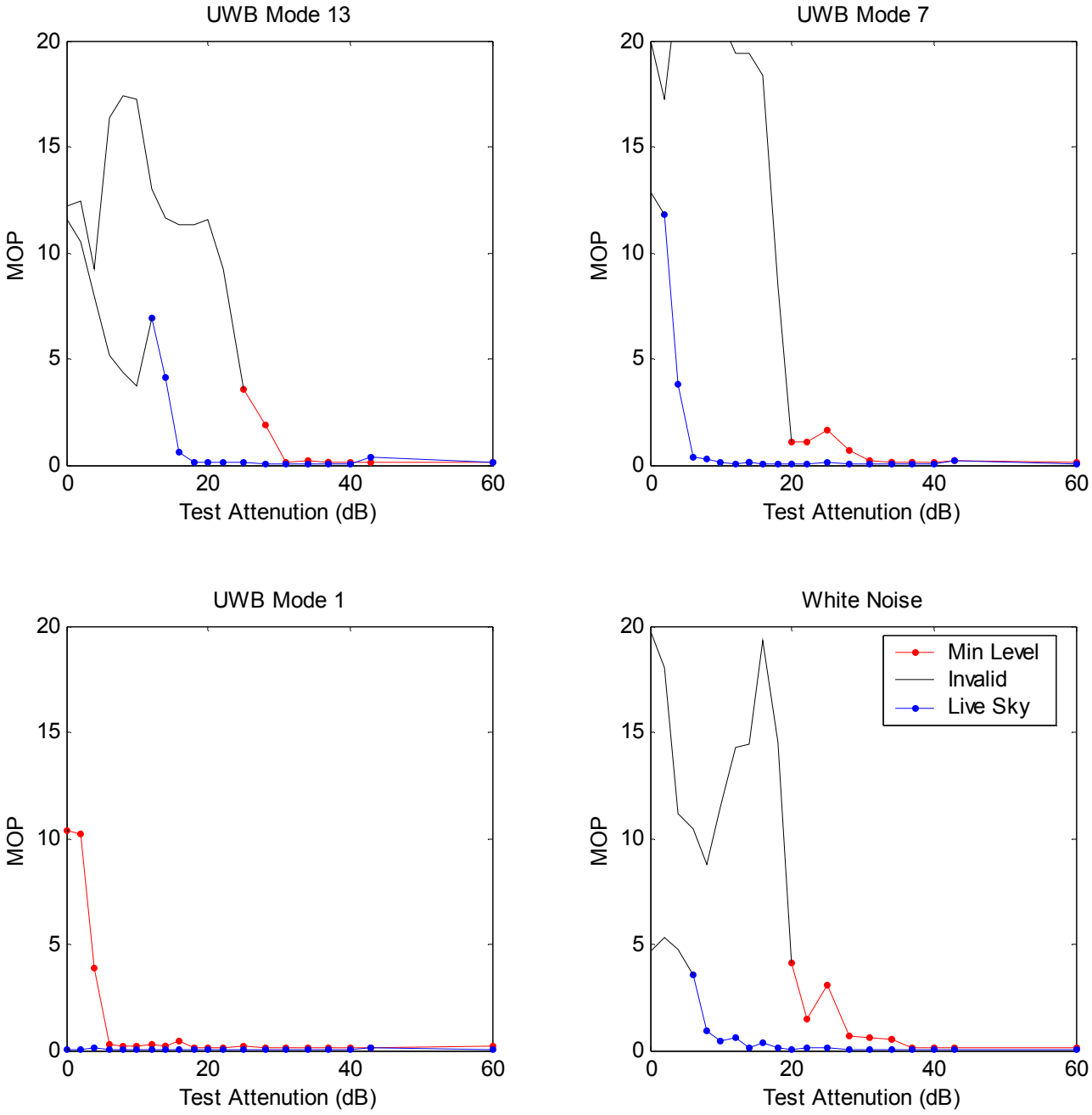

Ashtech Z-Sensor Normalized C/NO

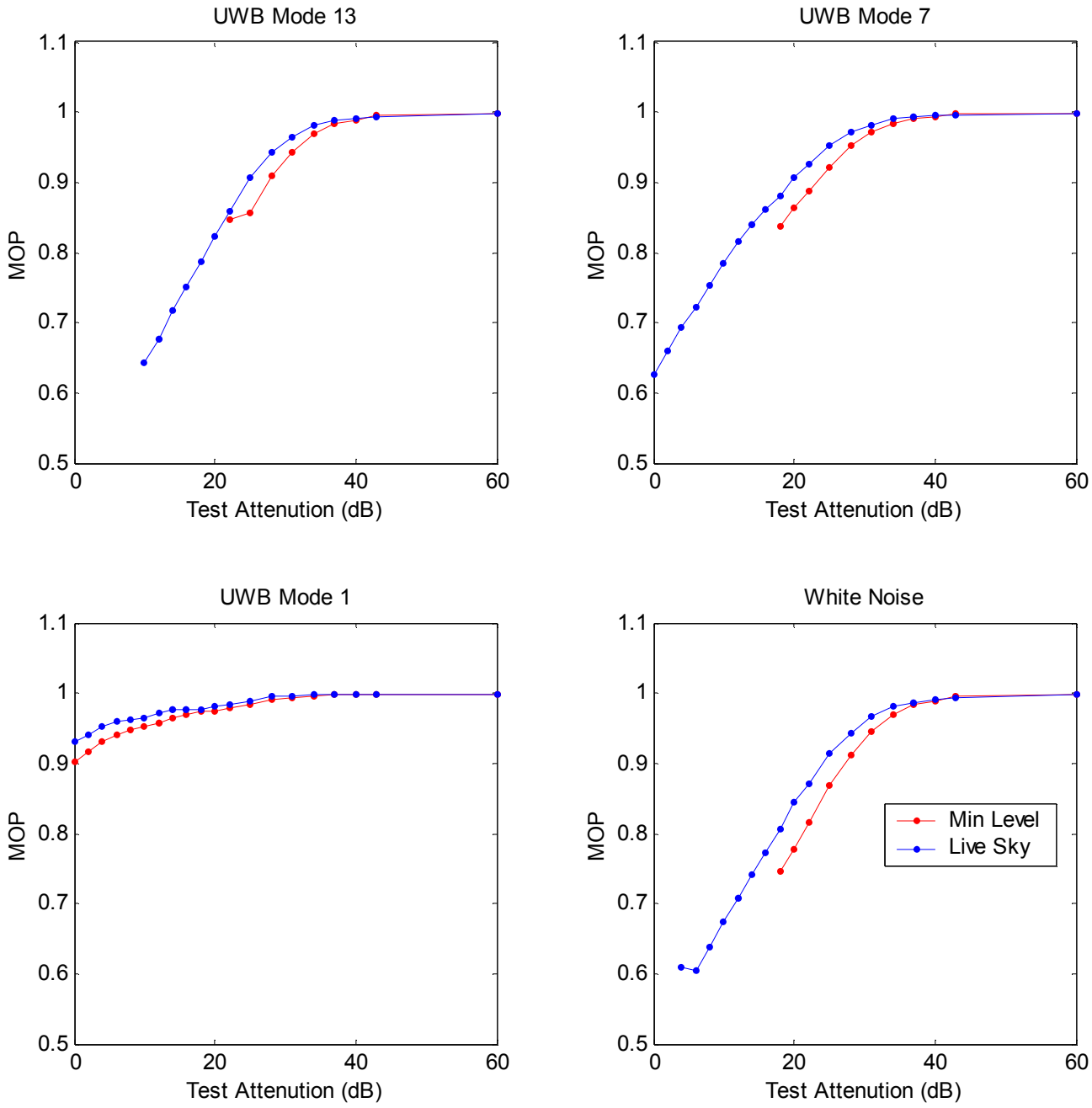

Ashtech Z-Sensor Normalized Pseudorange Noise

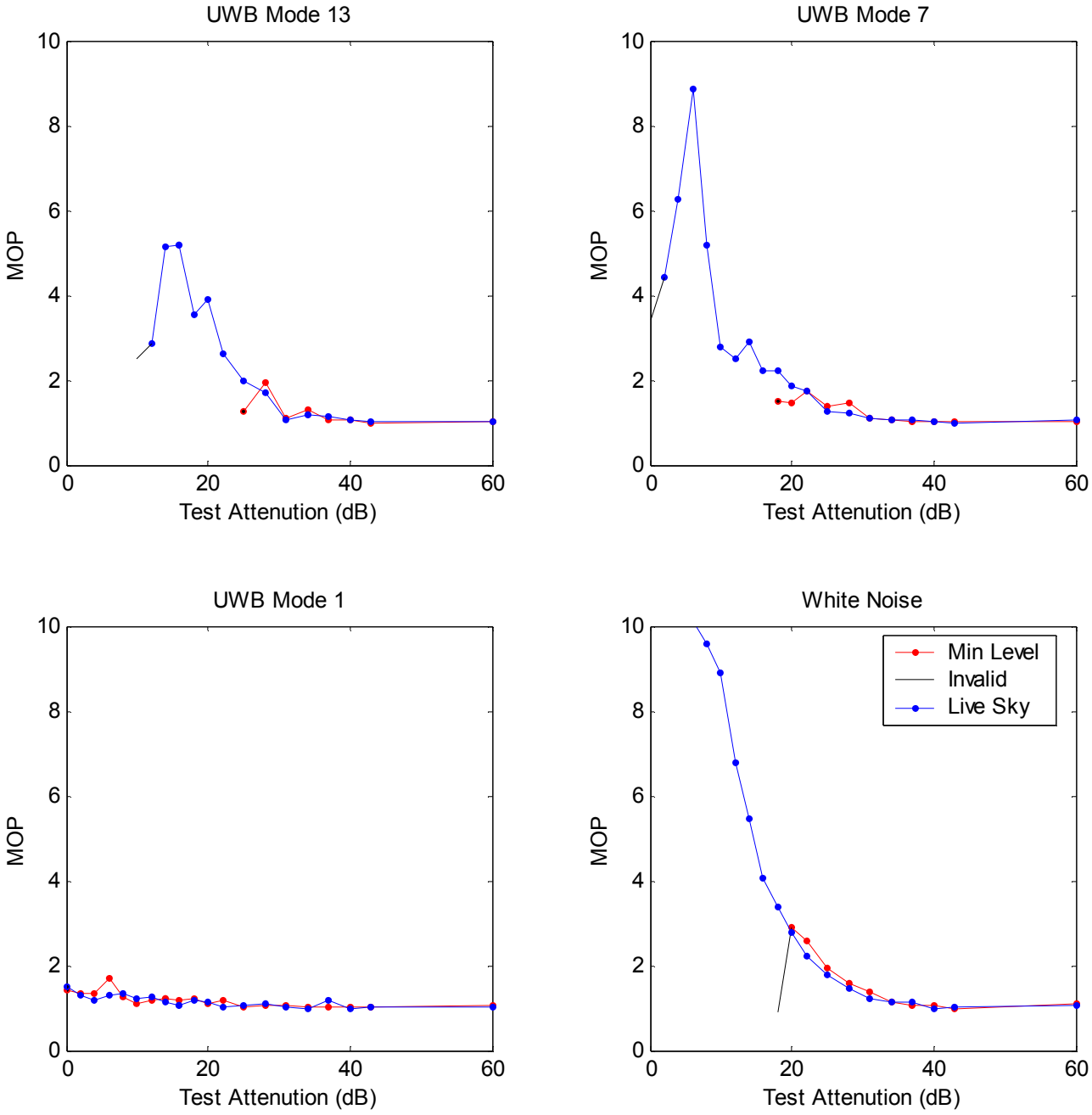

Ashtech Z-Sensor Double Difference Bias (cm)

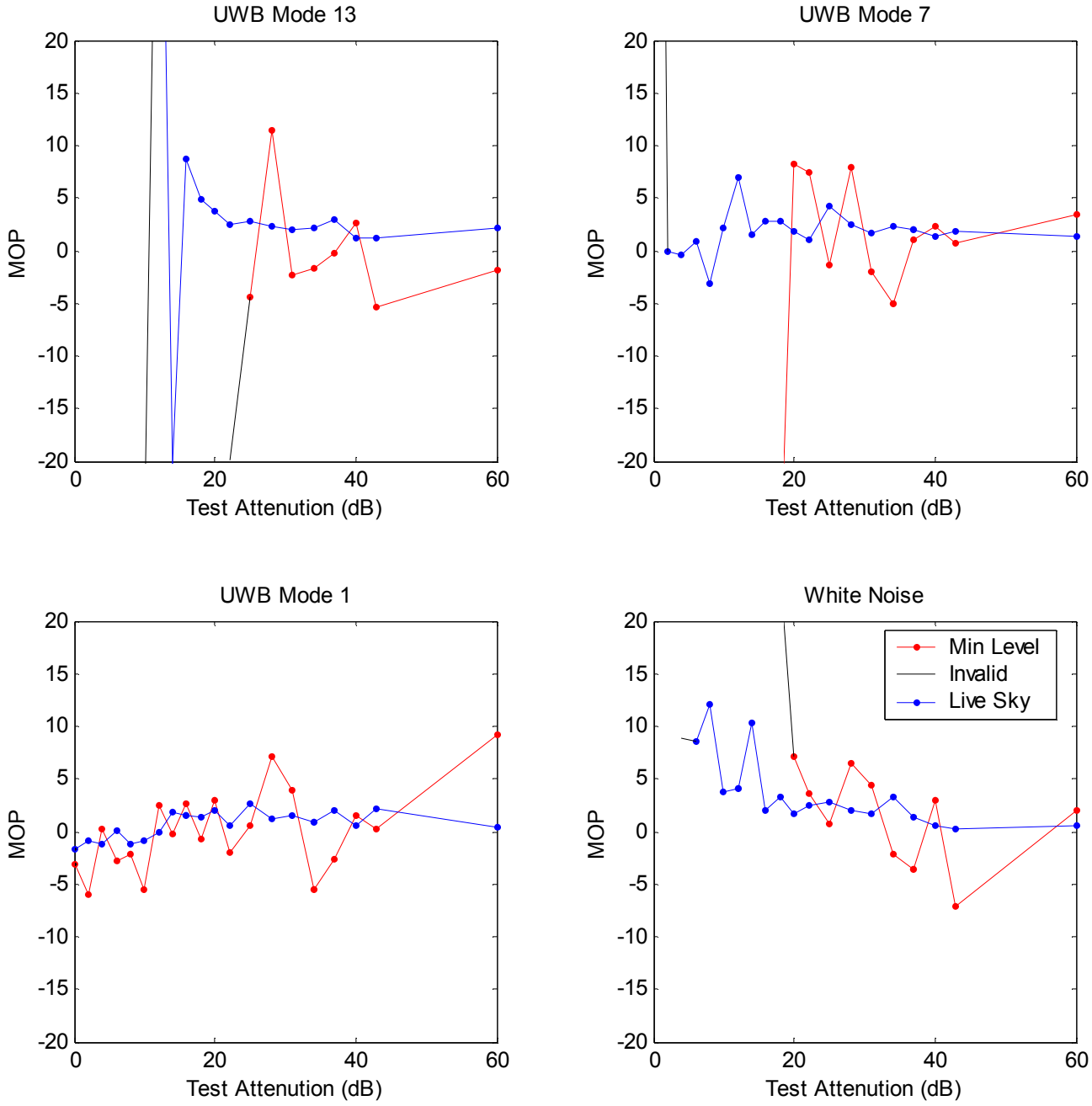

Ashtech Z-Sensor Double Difference Noise (cm)

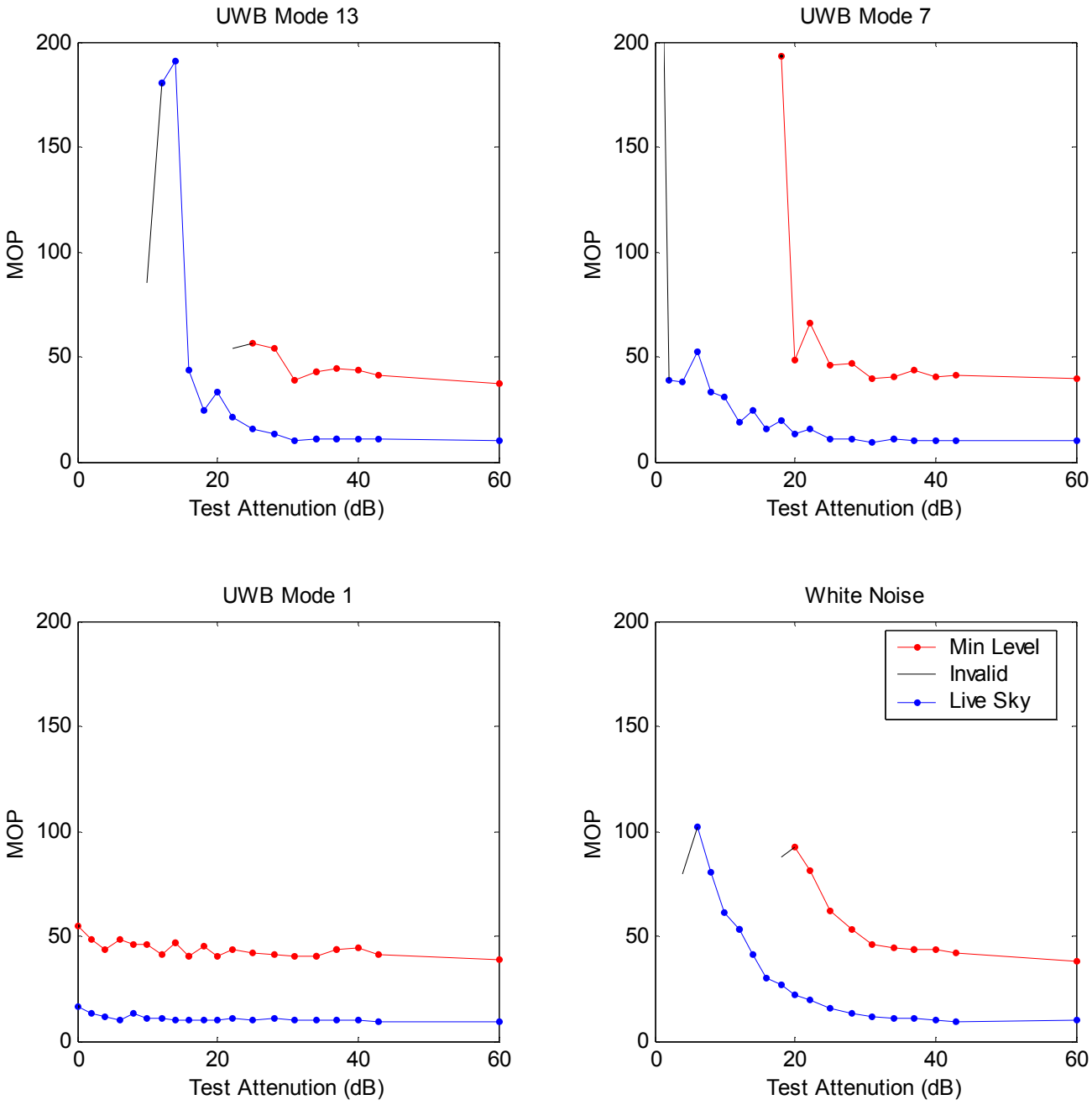

Ashtech Z-Sensor Incr. Time To Reacq. 1 tk'd sat. (sec)

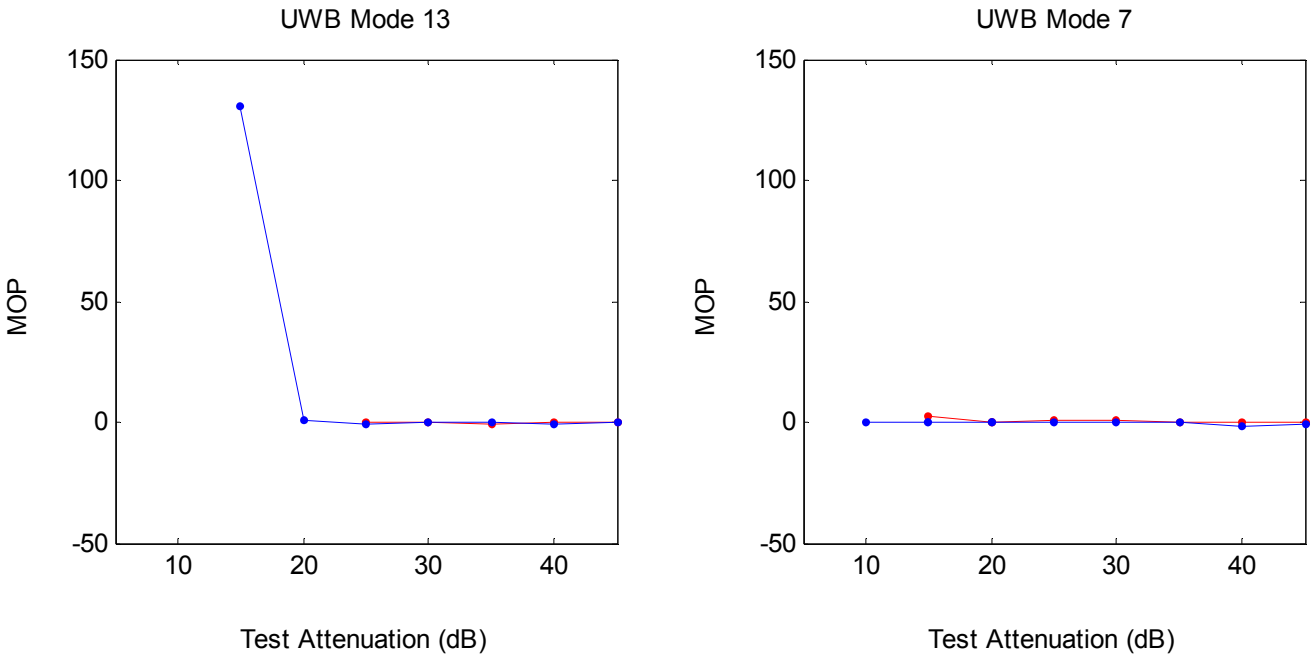

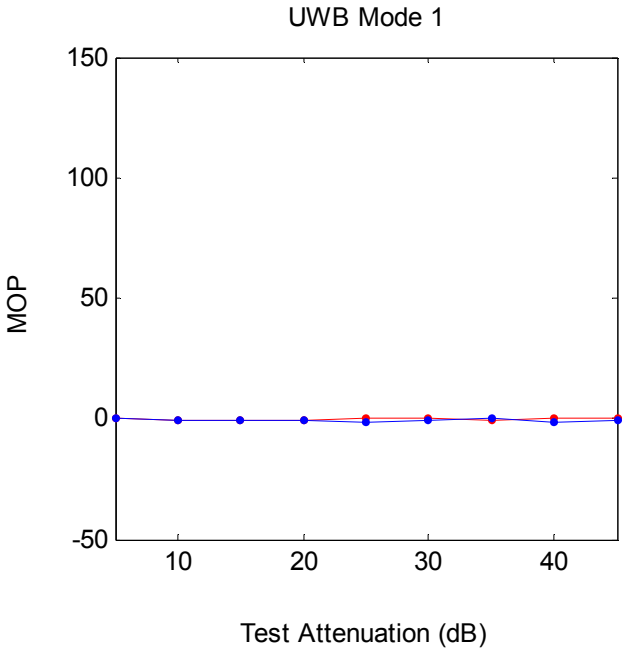

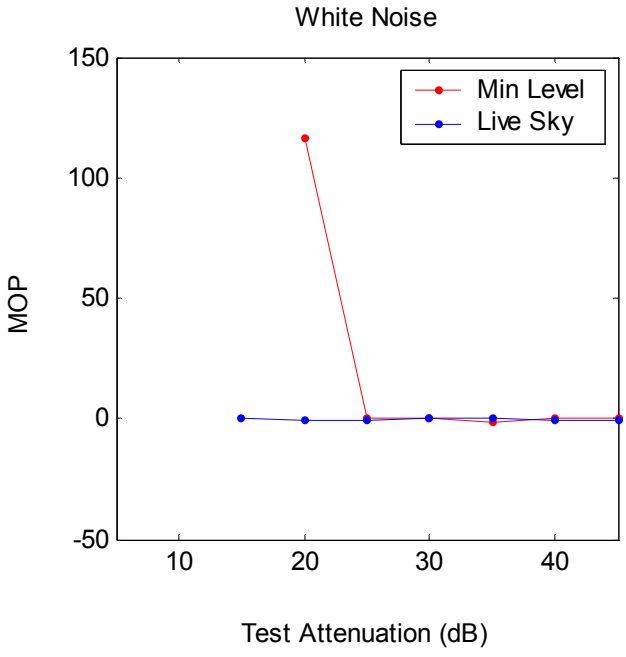

Ashtech Z-Sensor Incr. Time To Reacq. N tk'd sat's. (sec)

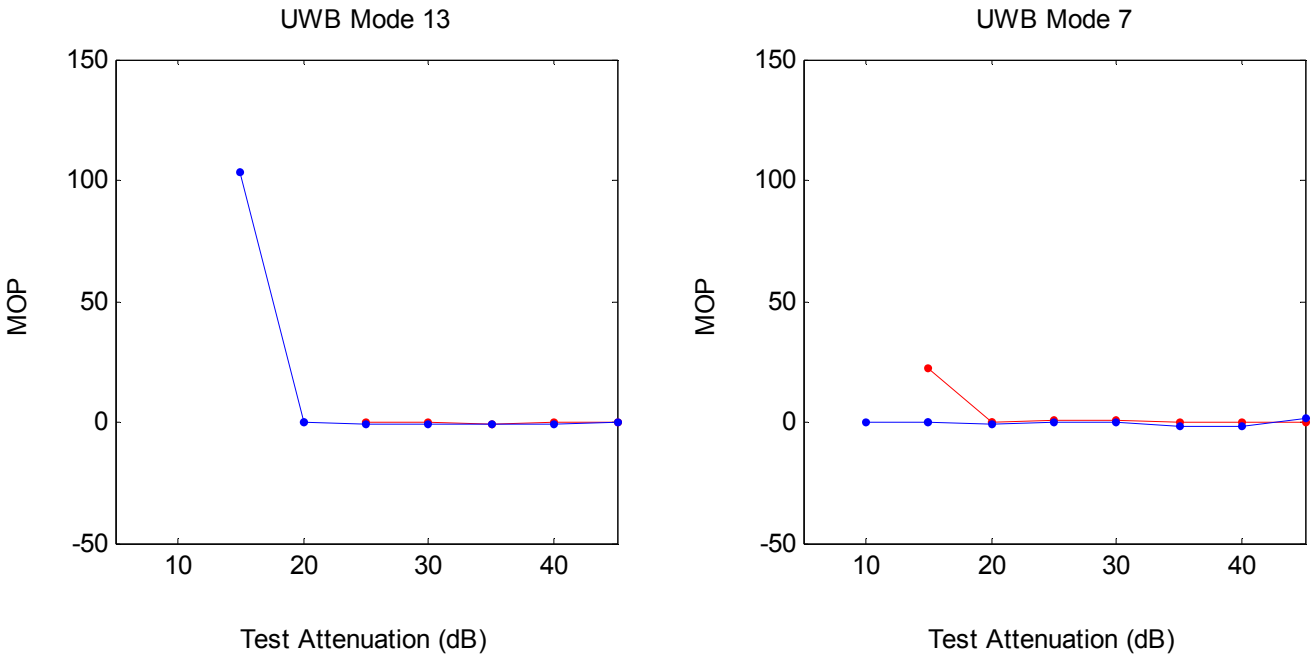

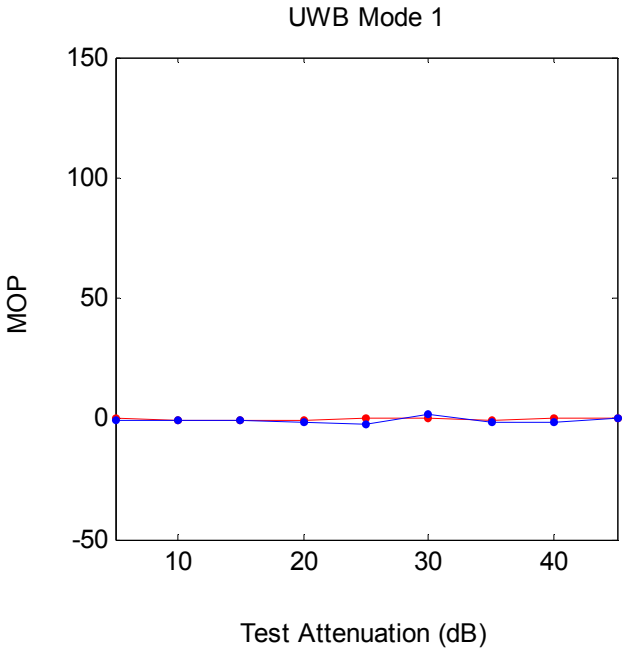

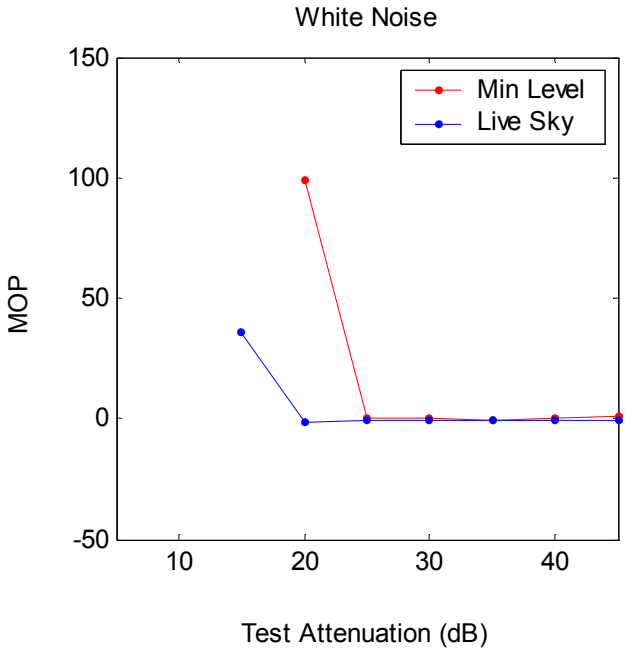

Ashtech Z-Sensor Incr. Time To Reacq. 4 navd sat's. (sec)

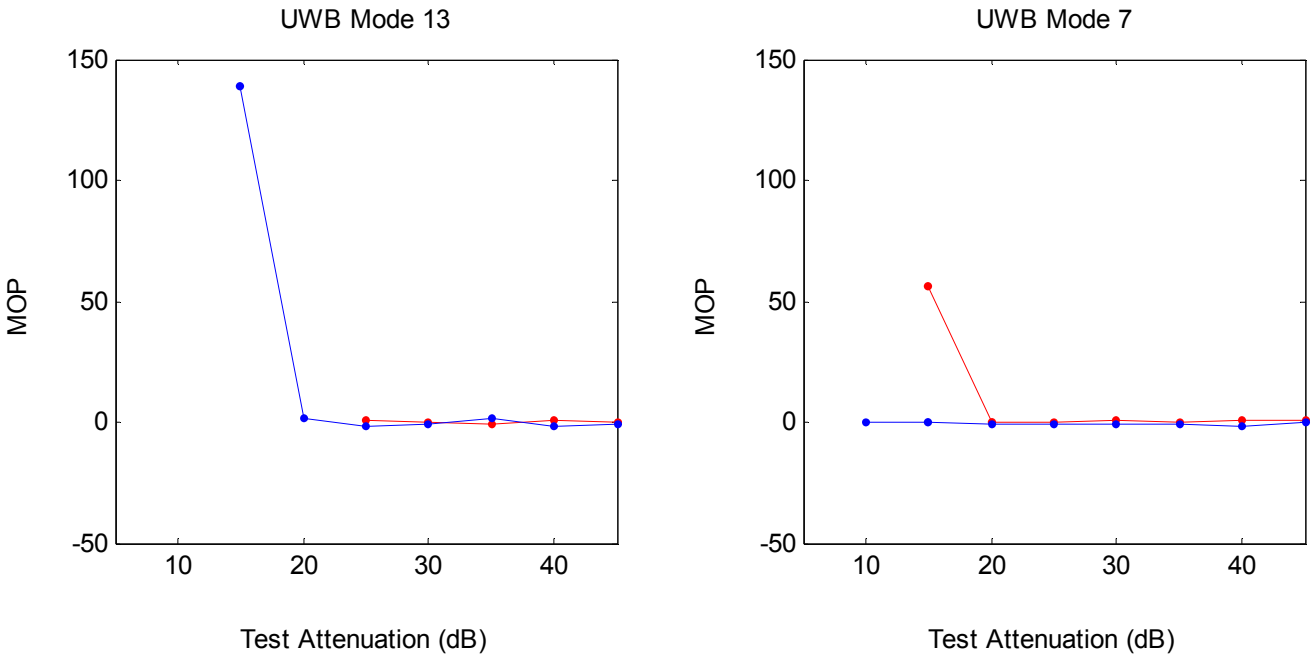

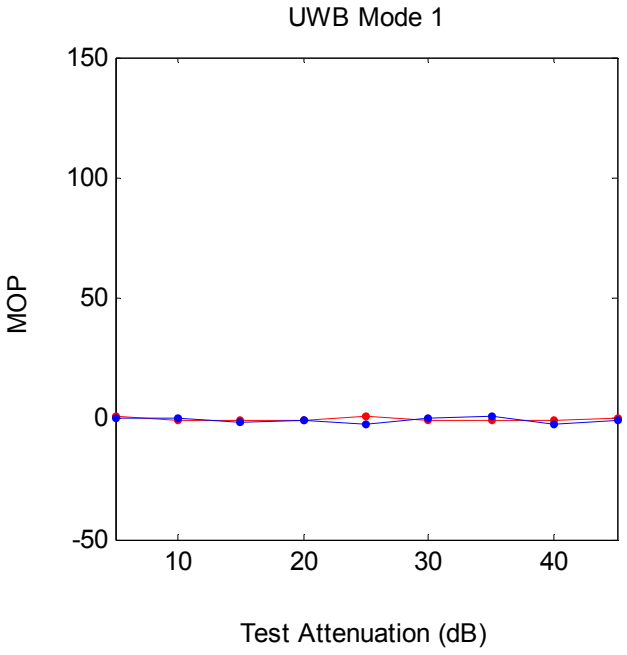

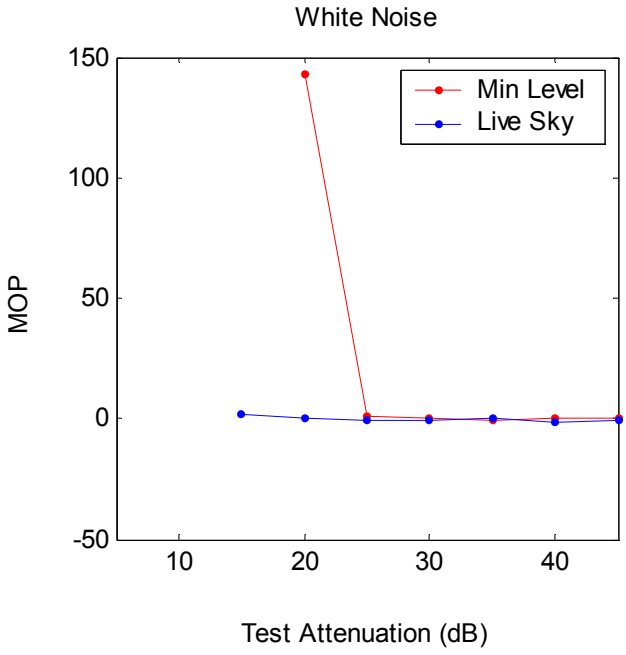

Ashtech Z-Sensor Trials Used to Reacq. 4 navd sat's. (sec)

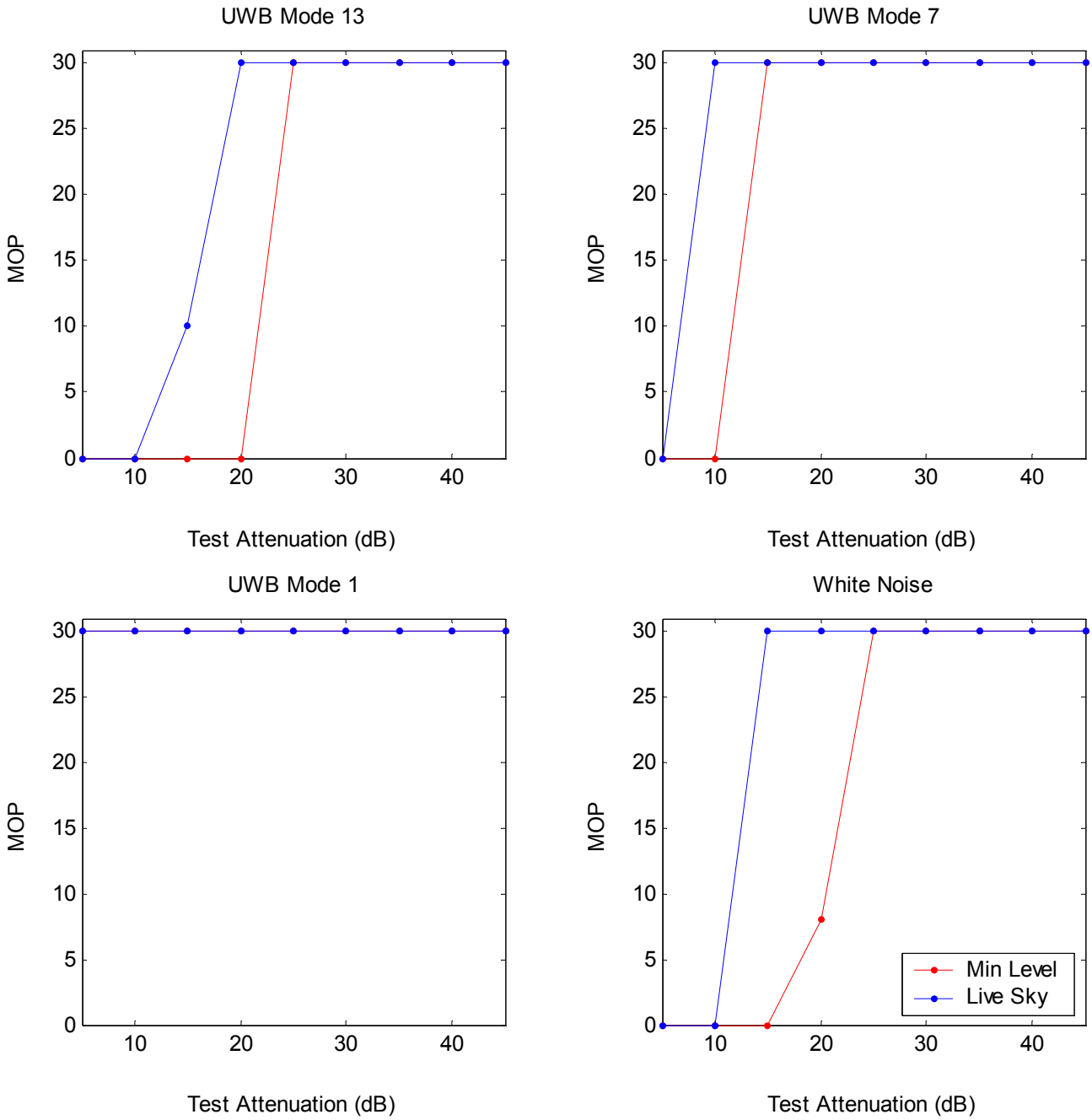

A.6 NovAtel MiLLenium

Receiver 6 is a MiLLenium GPS receiver manufactured by NovAtel Communications Ltd.. More specifically, the standard OEM3 GPS Card version enclosed in a ProPak II housing was used during the testing. This receiver is an aviation quality receiver that allows numerous autonomous and differential applications. Twelve channels are used to track L1 C/A code, L1 and L2 carrier phase, and L2 P code. To increase its accuracy performance, this receiver employs both a narrow correlator. The pertinent performance specifications for this receiver are:

- Autonomous position accuracy = 15 m CEP without Selective Availability
- Pseudorange accuracy = 15 cm RMS
- Cold start acquisition time = 70 sec
- Warm start acquisition time = 60 sec[7]
- Reacquisition time = 5 sec[7]

During the radiated and aggregate testing, a Model 503 GPS antenna manufactured by NovAtel Communications Ltd. was connected to Receiver 6. Both the L1 and L2 frequency bands are appropriate for this antenna. This antenna incorporates a low noise amplifier with the following specifications:

- ±10 MHz bandwidth
- 26.0 dB ±2.0 dB gain
- 2.5 dB noise factor

Throughout the conducted, radiated, and aggregate testing, this receiver was configured to output only measurement data in the NovAtel proprietary binary output format described in Reference (18). No receiver generated navigation solutions were output as part of the data stream.

A.6.1 Receiver Specific Measures of Performance

All NovAtel Millenium data collected during the ARL:UT test program were successfully processed as described in Appendix C and the beginning of this Appendix. It is noted that like the NovAtel 3151, these data are time tagged with GPS week 48 instead of GPS week 1072 as with the other GPS receivers. Although both simulated GPS power levels were initially processed, anomalies were observed in the measurement data for the live sky case that are not attributed to the injected UWB signal. However, they remain unexplained without being able to examine the original test setup at ARL:UT. For this setup, only the Trimble 4700 receiver was tested simultaneously, and since these data were not analyzed, the source of the anomalies cannot

[7] *"GPS World Receiver Survey," January 2001*

be narrowed to a GPS simulator or receiver. Similar anomalies are not observed in the minimum level data.

In addition, the NovAtel Millenium and Trimble 4700 were tested simultaneously and required an unusual test setup. The test setup "required that a unusually large amount of fixed attenuation be placed in the signal path of the Novatel Millenium so as not to over-drive the receiver front end, and so that it operated near its average live sky value. This large attenuation was also in-line between the receiver and the UWB source so that injected UWB signal for some test conditions could be quite low. It is possible, therefore, that the data collected for the NovAtel Millenium does not indicate the full range of UWB impacts on that receiver."[8] Indeed, the JHU/APL analysis demonstrates that the performance of this receiver is not affected by the injected UWB signal as severely as the other receivers are.

Therefore, the NovAtel Millenium data are not considered to be truly representative of an injected scenario, and these data have not been carried forward to Chapter 6. This appendix does present the minimum level and live sky data as a function of attenuation setting for all those MOPs where the aforementioned data anomalies were not observed. Finally, as with the NovAtel 3151, the PDOP and receiver position MOPs have not been computed because the appropriate NovAtel records were not recorded as a part of the ARL:UT test program.

To compute the number of satellites tracked, a satellite was considered to be tracked by the GPS receiver when an observation existed in the RGEC record for that SV. The number of satellites used in the navigation solution was inferred from the above tracking plus a zero-valued reject code in the SATB record for that SV. Finally, all time tags in seconds of week and measurement data were extracted from the RGEC records.

The following ten figures depict the available receiver navigation outputs, receiver measurement output, and receiver reacquisition MOPs. The reader is directed to the NovAtel 3151 section for a description of the content of these figures.

[8] *Draft of the ARL:UT Test Report, page 35*

NovAtel MiLLenium Decreased Satellites Tracked

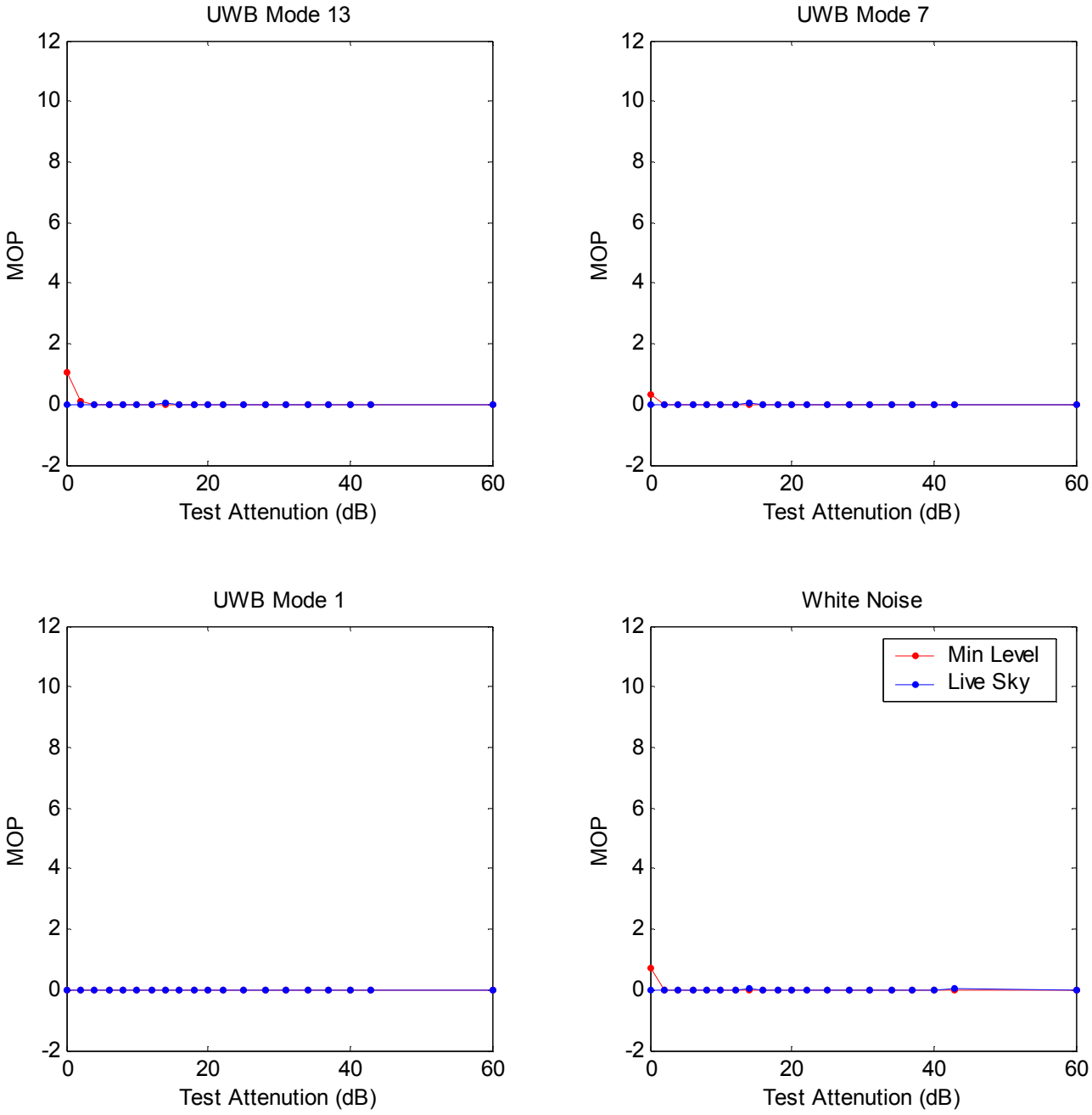

NovAtel MiLLenium Decreased Satellites Used

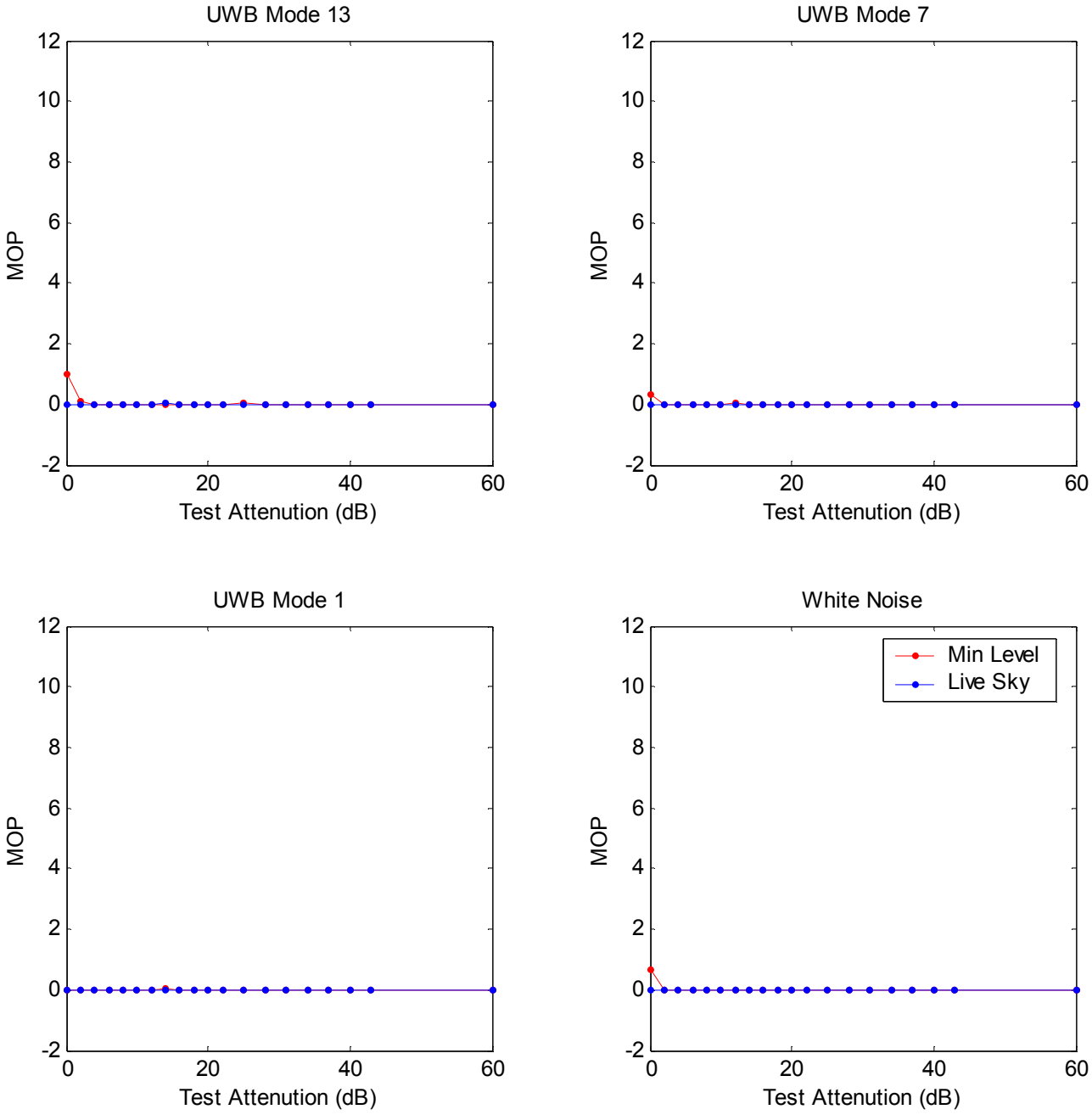

NovAtel MiLLenium Decreased Satellites Used

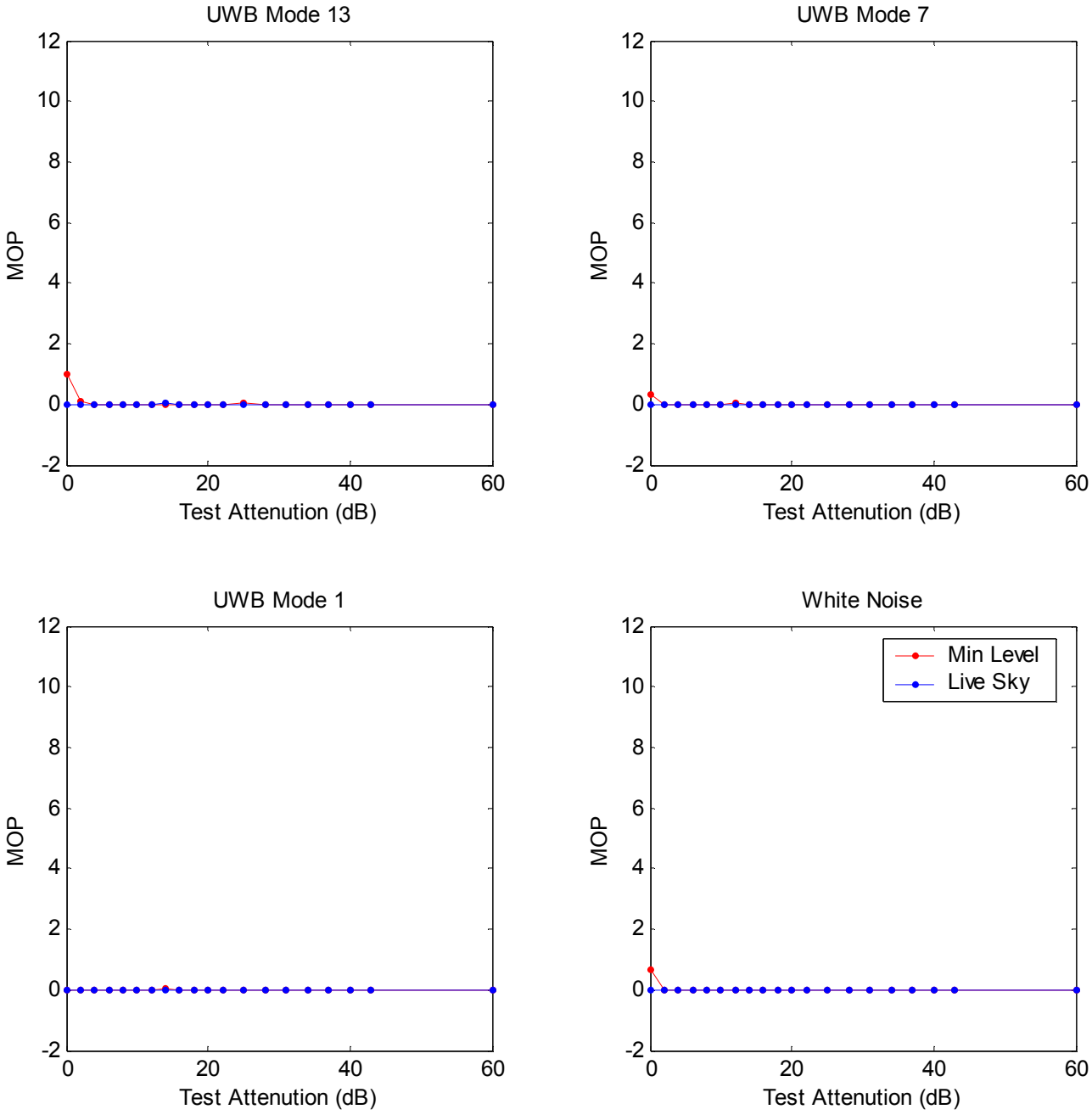

NovAtel MiLLenium Normalized Pseudorange Noise

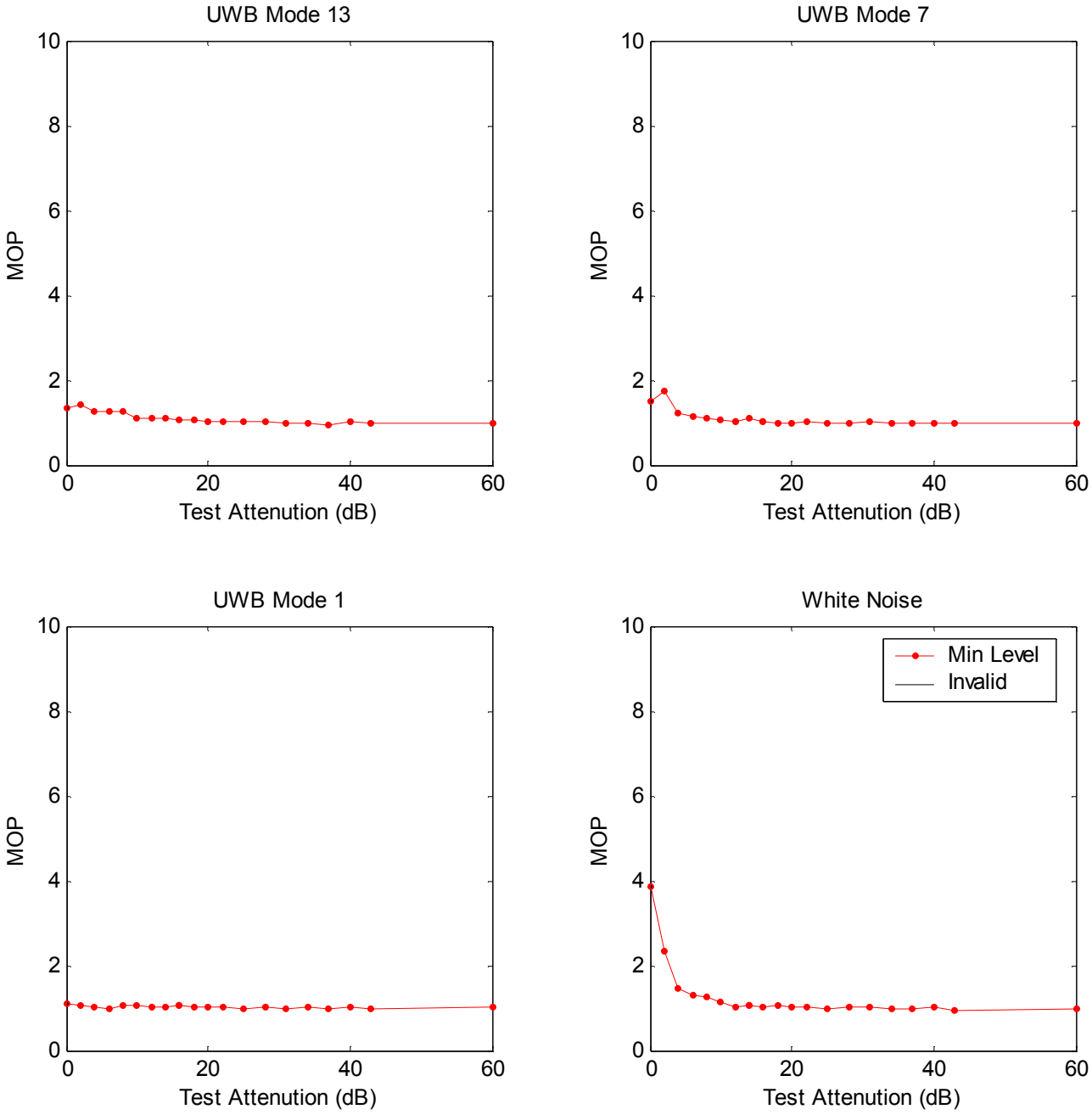

NovAtel MiLLenium Double Difference Bias (cm)

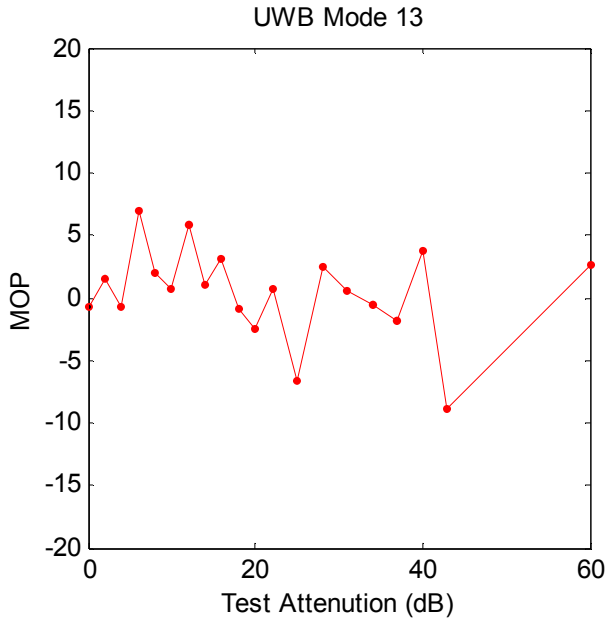

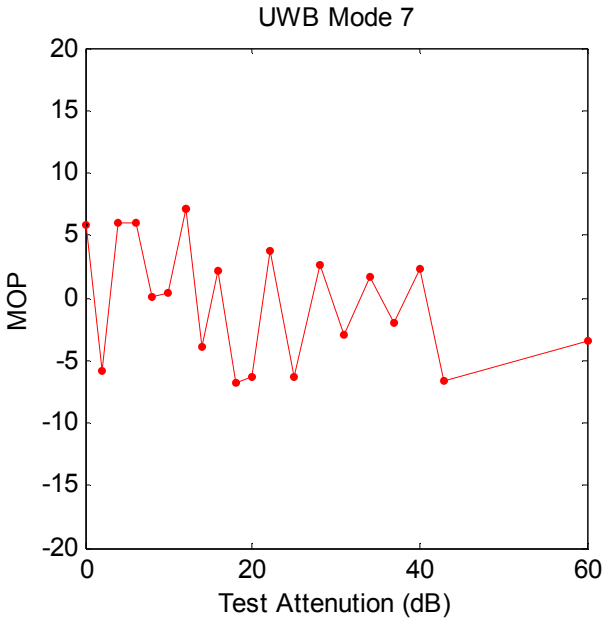

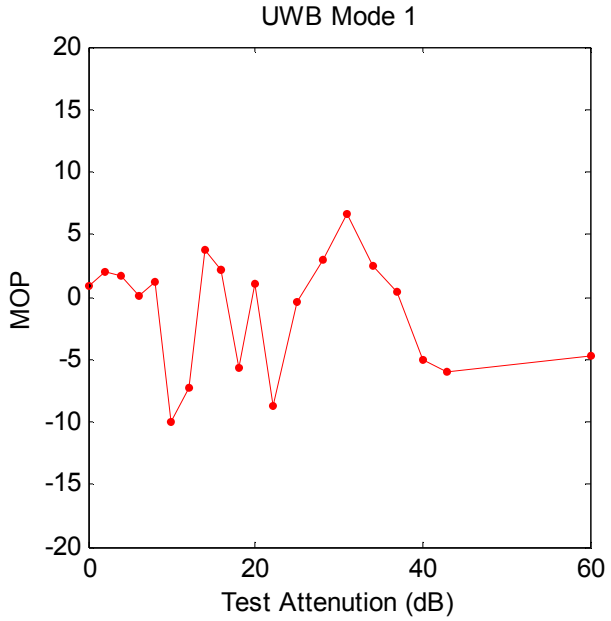

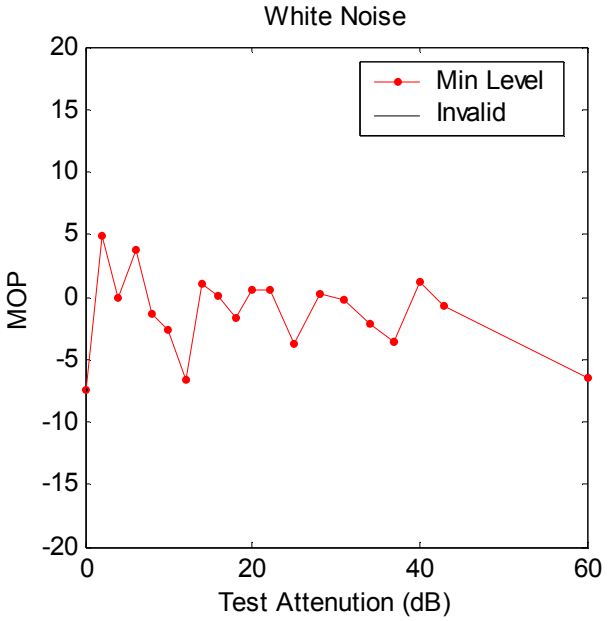

NovAtel MiLLenium Double Difference Noise (cm)

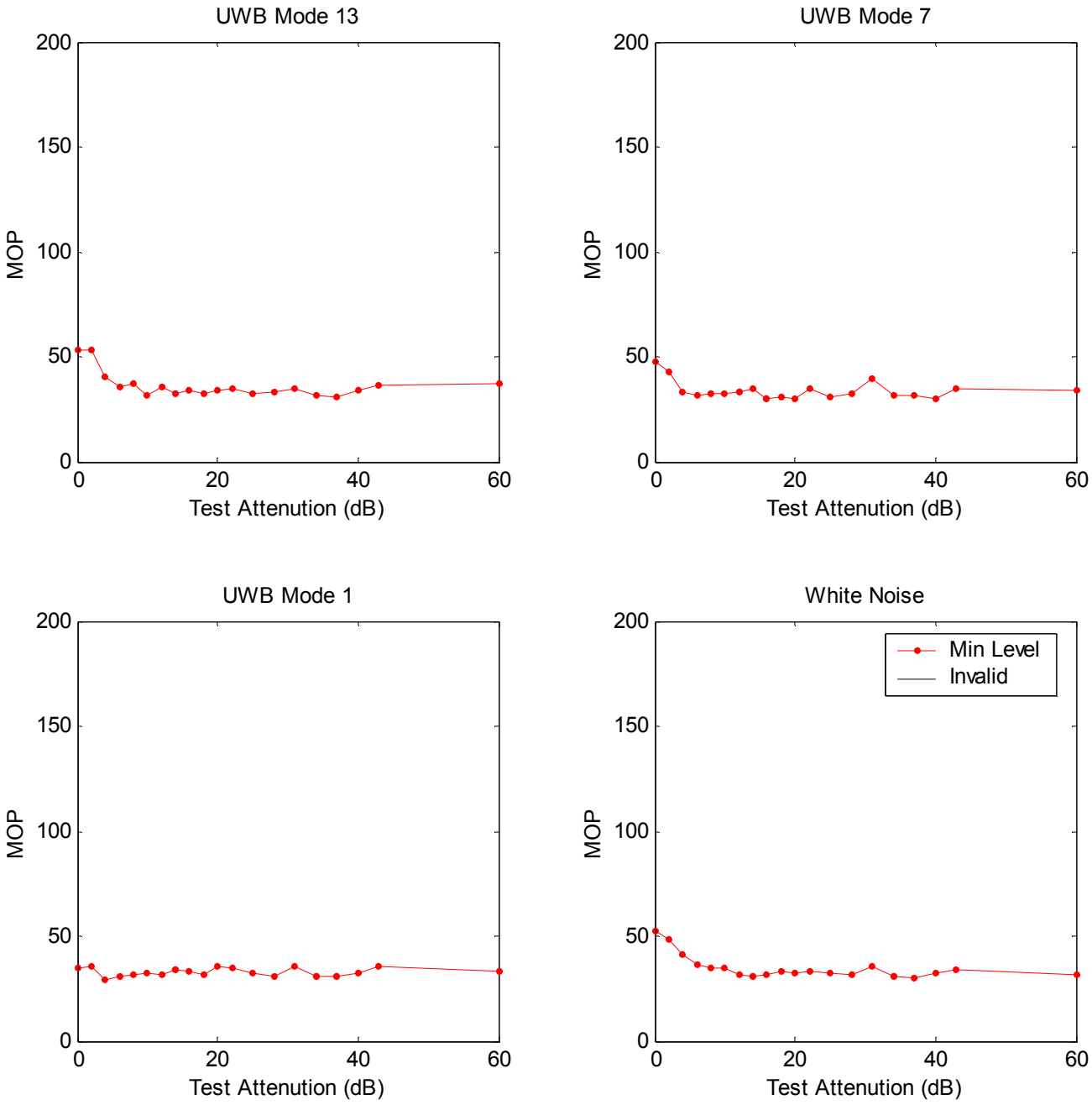

NovAtel MiLLenium Incr. Time To Reacq. 1 tk'd sat. (sec)

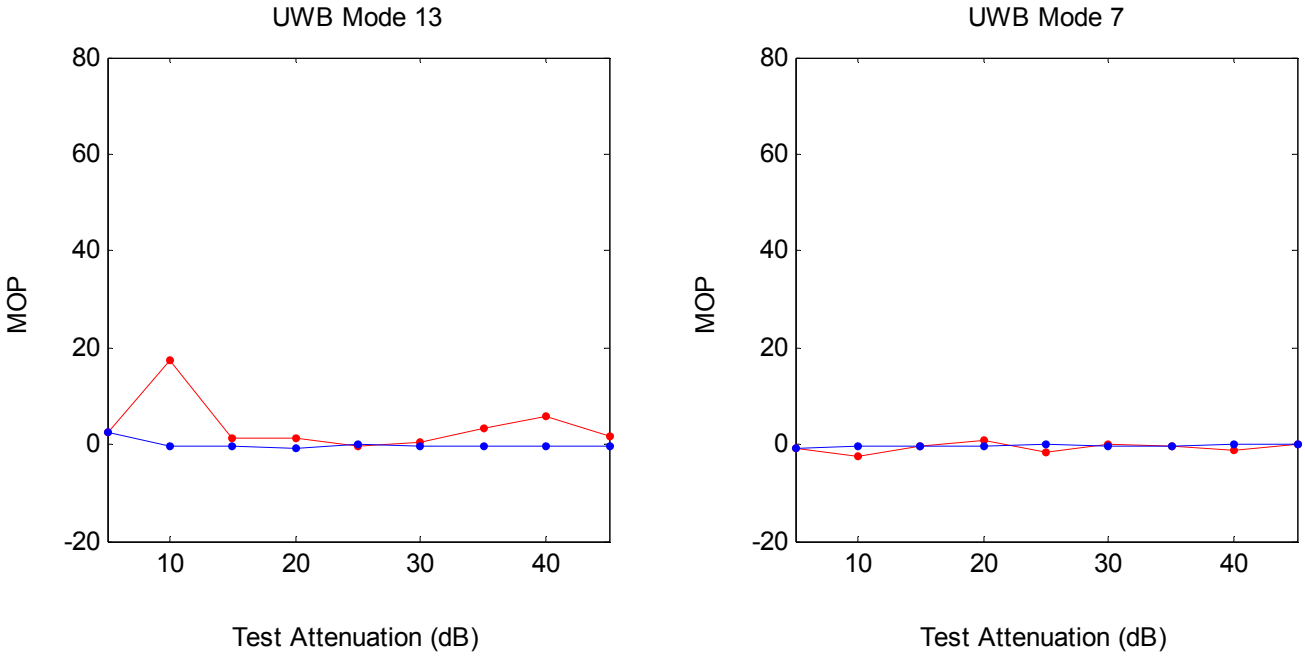

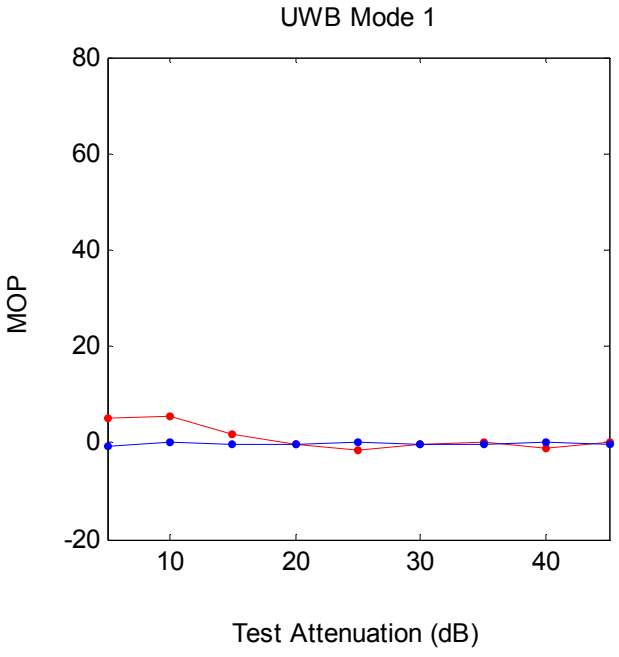

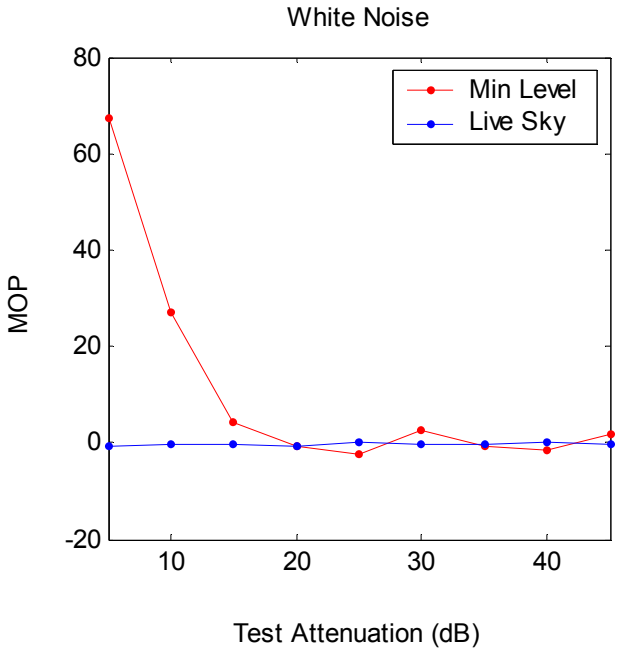

NovAtel MiLLenium Incr. Time To Reacq. N tk'd sat's. (sec)

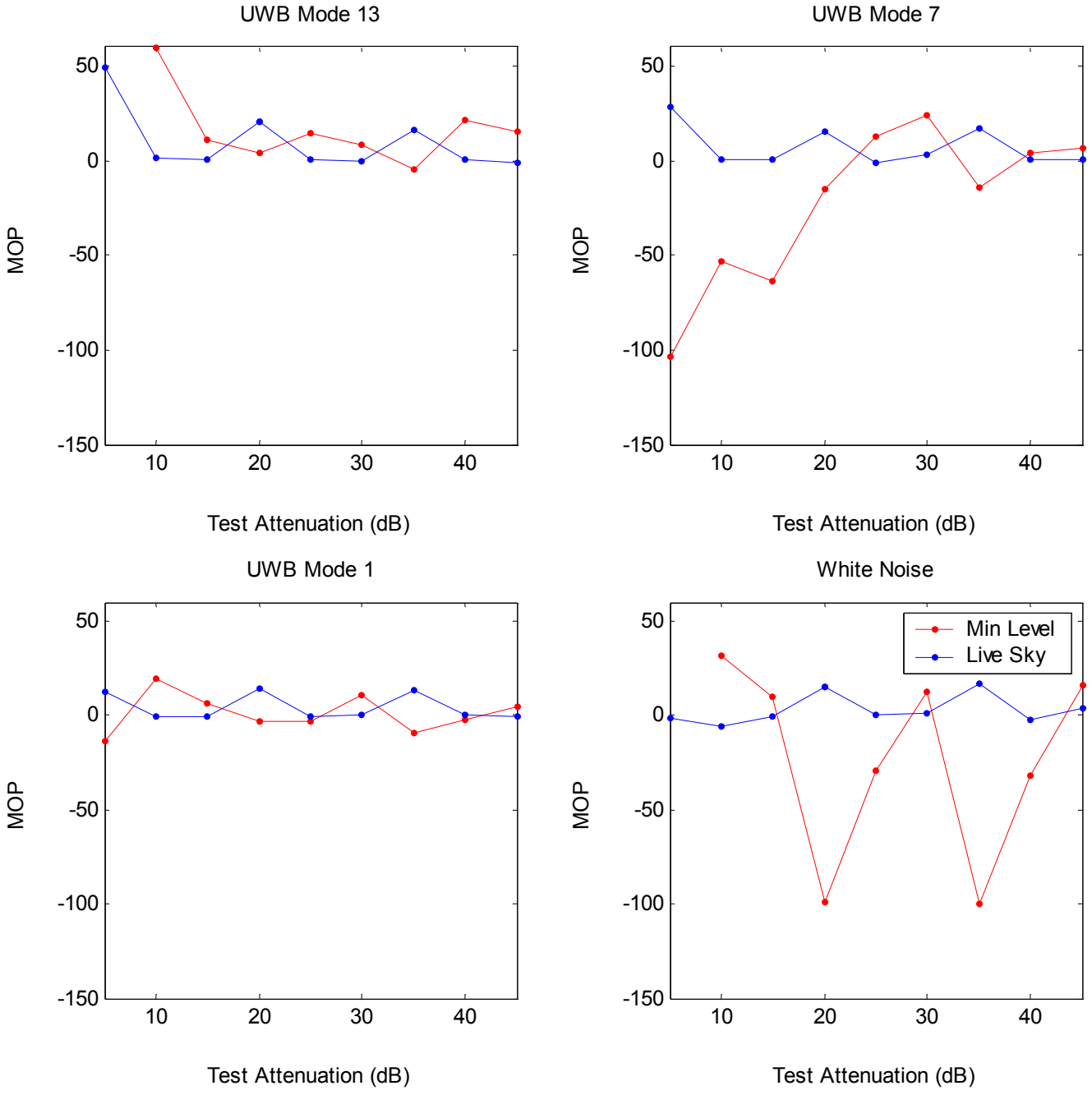

NovAtel MiLLenium Incr. Time To Reacq. 4 navd sat's. (sec)

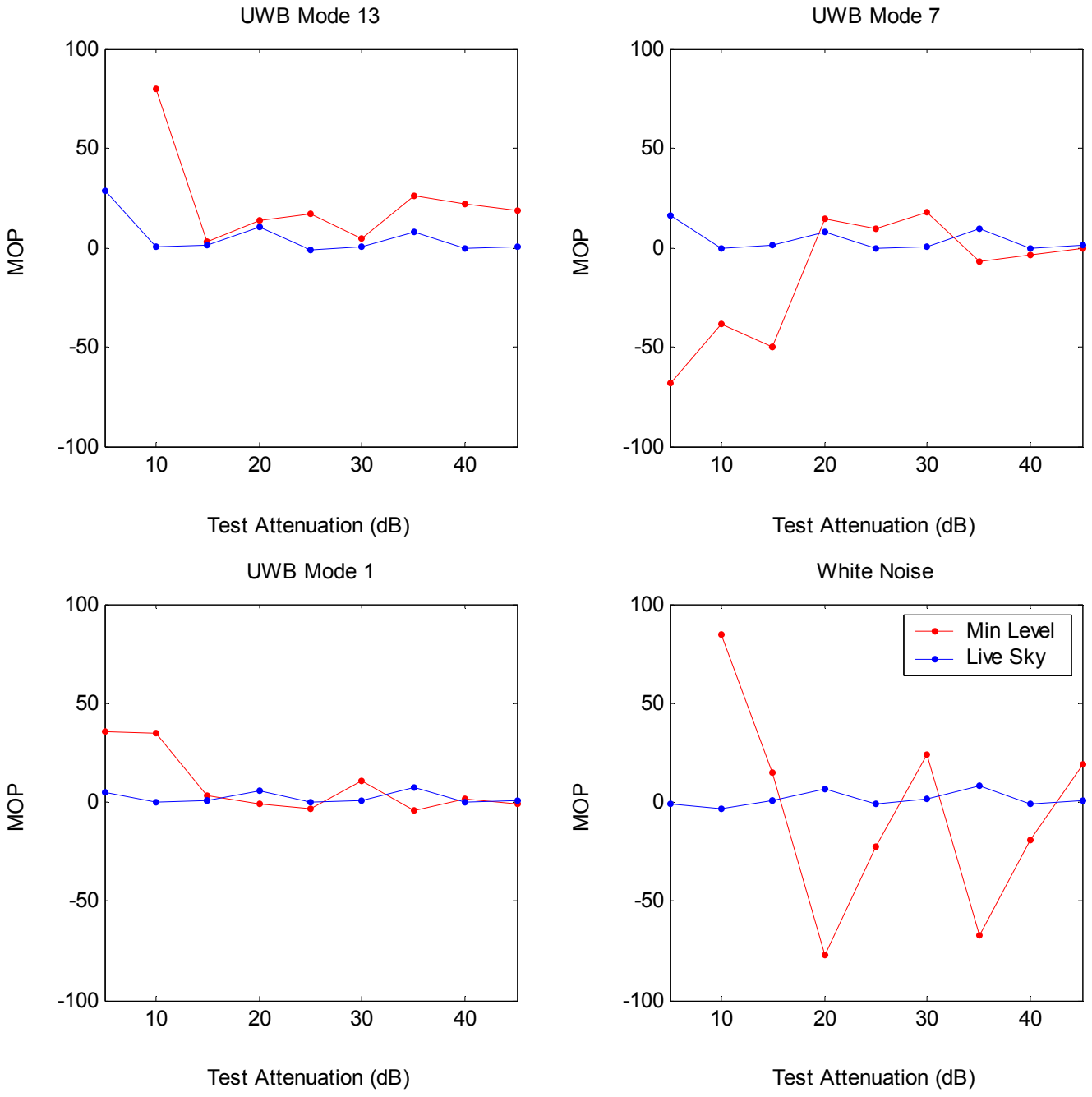

NovAtel MiLLenium Trials Used to Reacq. 4 navd sat's. (sec)

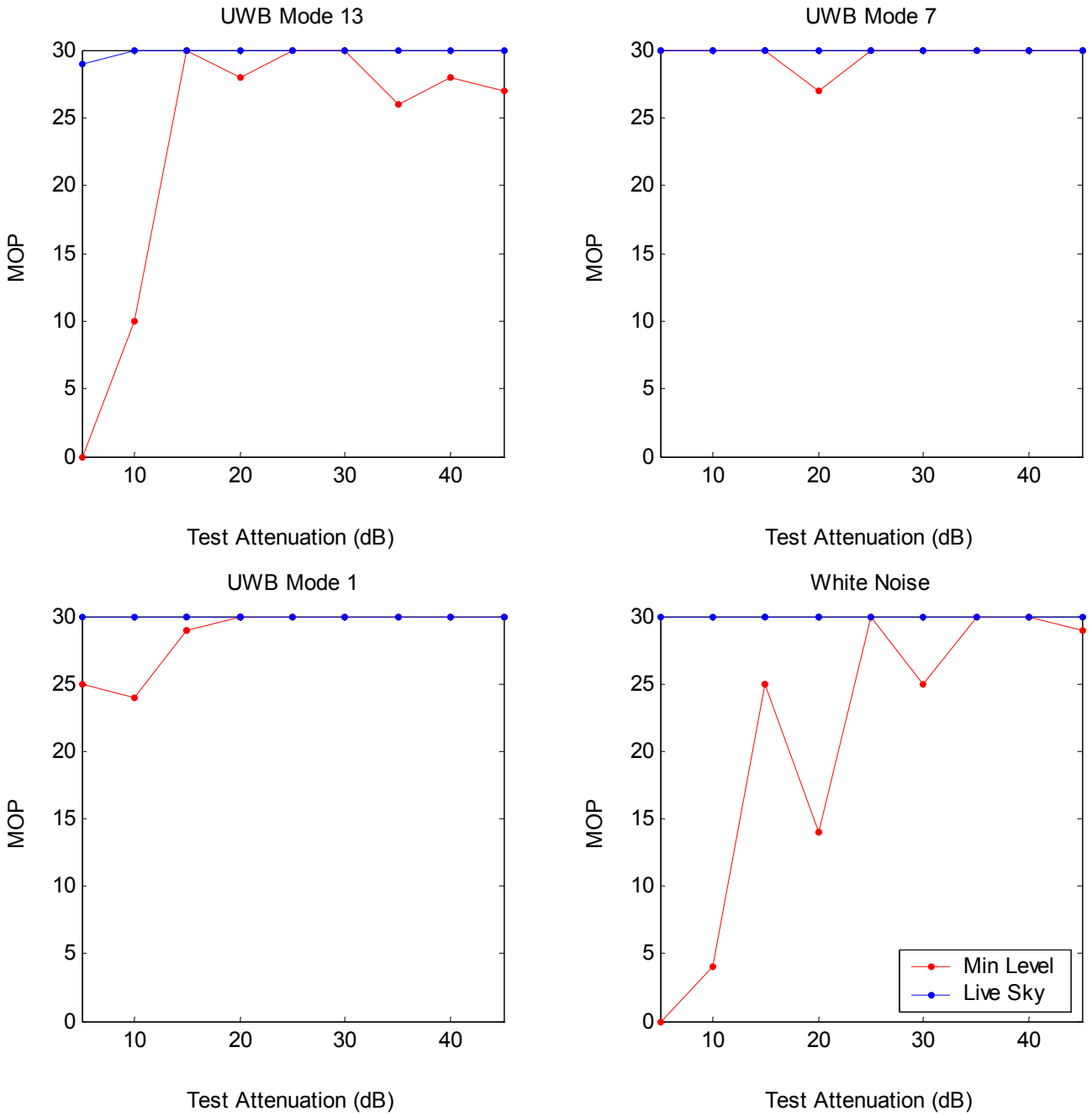

APPENDIX B
EQUIVALENT RANGE COMPUTATION

B.0 Introduction

The conducted interference testing is based on simulated Global Positioning System (GPS) signals that are directly combined with ultra-wideband (UWB) interference in a radio frequency network. This testing naturally bypasses actual antenna effects and also bypasses the GPS antenna-mounted preamplifiers. For the purposes of this calculation, we will consider both the UWB and the GPS antennas to have 0-dB gain except for the inclusion of a 3-dB loss due to polarization mismatch. The calculation will establish a basis for comparison with results from the radiated tests. We have no means to account for the band limiting aspects of the two antennas or the GPS preamplifiers in the conducted test setup. However, the conducted test equivalent range will be adjusted for a best match to the radiated test results before the test data are reported in terms of equivalent range and compared with the theoretical analysis. The differences between receivers will be accommodated in this final adjustment process.

B.1 Path Loss Computation

The basis for computation is shown in Figure B-1. The computation is based on a model of the radiated test setup with parameters determined from the conducted test setup.

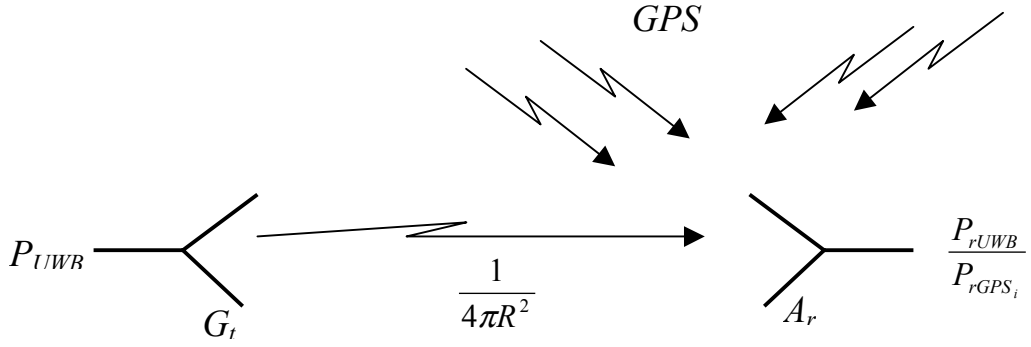

$$\frac{P_{rUWB}}{P_{rGPS_i}} = \frac{P_{UWB} G_t A_r}{P_{rGPS_i} 4\pi R^2}$$

$$R = \sqrt{\frac{P_{UWB} G_t A_r}{4\pi P_{rGPS_i} \left(\frac{P_{rUWB}}{P_{rGPS_i}} \right)}} \; ; \; A_r = \frac{\lambda^2}{8\pi} \textit{(including polarization loss)}$$

Figure B-1 Computation of Equivalent Range for Conducted Interference Tests

It should be noted that the power density (i.e., watts/meter) for the UWB power at the GPS antenna location is properly represented by the above range equation, but the receive aperture area is only valid at (or in the region of) the L1 wavelength used in the equation. In this analysis we will consider P_{UWB} as an equivalent noise spectral density (i.e., N_{I0} in watts/Hz), and only consider it as a total power when multiplied by one of the two GPS signal bandwidths of 2 MHz and 20 MHz. In that way, the band limited UWB spatial power density at the GPS antenna is properly converted to received power when multiplied by the formulated GPS antenna aperture area. While this power representation is convenient for analysis purposes, it must be remembered that the average UWB power is considerably larger than this value. In this test setup, the 20 MHz GPS limited power is about 18 dB less than the total UWB power level.

B.2 Conducted Test Setup for Receivers 1-4 (Holloman AFB)

The test setup is shown in Figure B-2. The illustration was copied from the Applied Research Laboratories, University of Texas (ARL:UT) test report with annotations added for this discussion. As noted in Figure B-2, the interference-to-signal ratio (ISR) is set at the point where the two signals are combined. Attenuation measurements were made from points A and B to each receiver. We can compute the ISR as:

$$ISR = \frac{k_{B-C} P_{UWB}}{k_{A-C} P_{GPS}}$$

where :

$P_{UWB} = Average\ UWB\ Power\ at\ point\ B$

$k_{B\text{-}C} = Attenuation\ factor\ from\ B\ to\ C$

$P_{GPS} = Average\ GPS\ Power\ at\ point\ A$

$k_{A\text{-}C} = Attenuation\ factor\ from\ A\ to\ C$

Inspection of the test setup diagram shows that the attenuation difference [UWB path (B-to-C) minus GPS path (A-to-C)] should be the same for each receiver measurement. That is, the ratio of $k_{B\text{-}C}$ to $k_{A\text{-}C}$ is constant; in dB-terms it is equal to the attenuation difference in the two paths. The path loss measurements from points A and B to each receiver are provided as network analyzer measurement files in Appendix A of the report documentation at the ARL:UT web site. Figure B-3 shows the path differences (UWB-GPS) for the four receiver paths. The variations between paths are attributed to measurement error. The average path difference of 6.67 dB (with a variance of 0.12 dB) is shown in Table B-1 for all receivers over the 20-MHz measurement bandwidth.

The attenuation difference measured over a very large bandwidth (50 MHz to 10 GHz) is essentially constant up to about 3 GHz and then it tapers slowly to about 9 dB at 10 GHz. The 20-MHz measurement was taken as the most representative value for this test setup. We use the total GPS signal power at point A and the spectral power density at L1 times 20 MHz as the maximum UWB power at point B reduced by the path attenuation difference in the ISR.

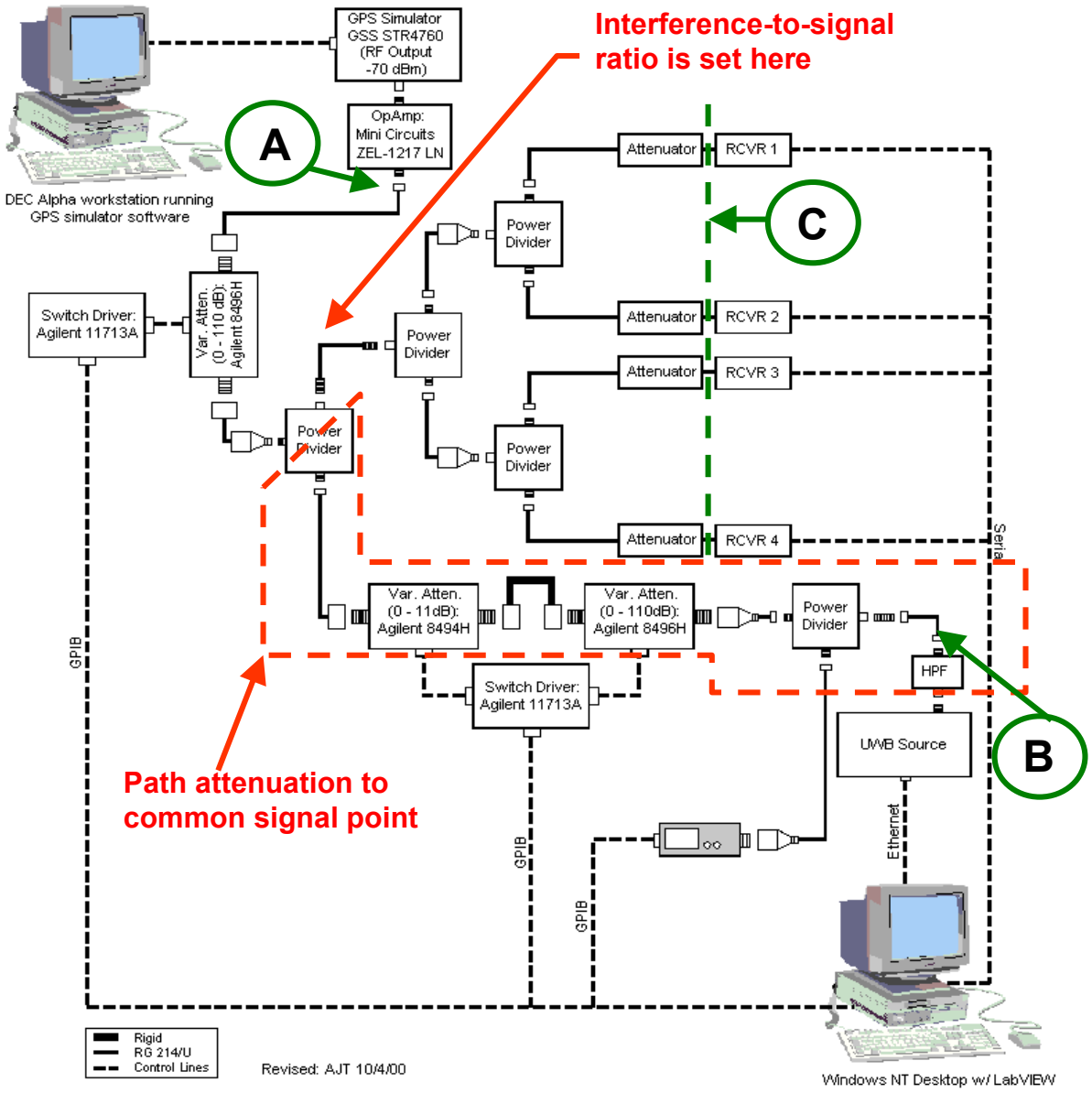

GPS signal attenuation measured from (A) to each receiver (C), and UWB signal attenuation measured from (B) to each receiver (C)

Figure B-2 Conducted Interface Test Setup at Holloman AFB

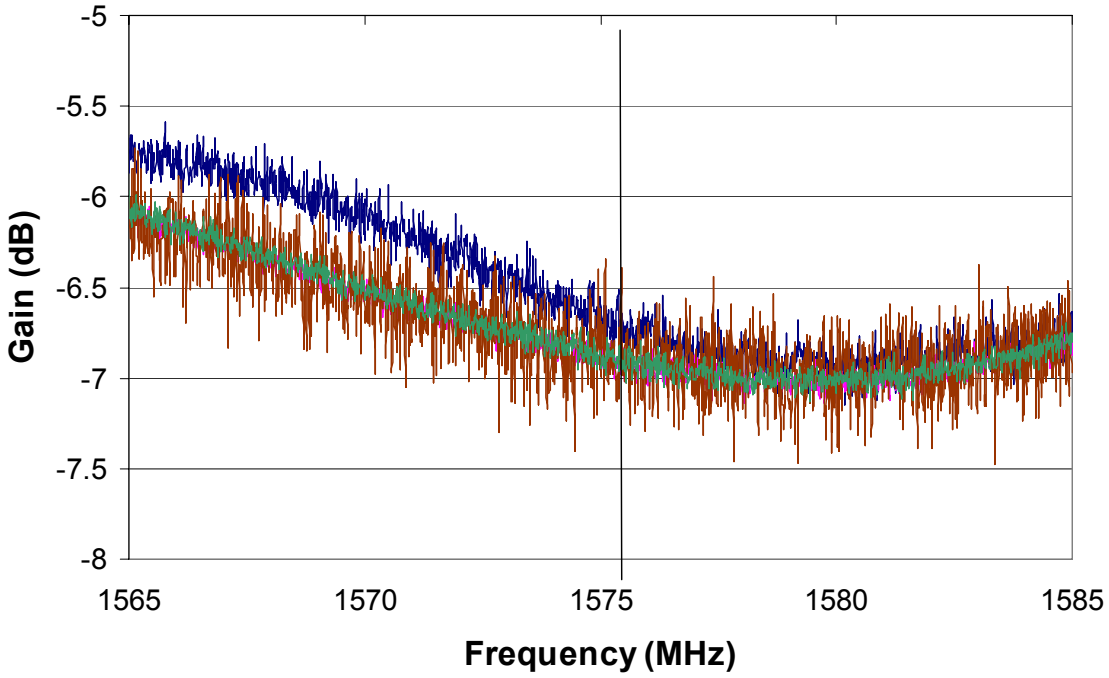

Figure B-3 UWB-GPS Attenuation Path Differences for Receivers 1-4 at L1

Table B-1
Conducted Test Setup Average Path Attenuation for Receivers 1 – 4 (over 20 MHz) at L1

Receiver	UWB Path (dB)	GPS Path (dB)	Difference (dB)
1	33.55	27.05	6.50
2	27.80	21.06	6.74
3	40.33	33.60	6.72
4	27.82	21.10	6.72
		Average of all path differences	6.67

We are now ready to define the range equation in terms of the conducted test setup. The ISR in the conducted test setup can be expressed as:

$$ISR = \frac{P_{rUWB_C}}{P_{rGPS\,iC}} = \left(\frac{P_{rUWB\,C}}{P_{rGPS\,iC}} \right)_0 k_{attn}$$

where :

$$\left(\frac{P_{rUWB_C}}{P_{rGPS\,iC}} \right)_0 = \text{Ratio with } k_{attn} = 1 \quad (i.e.,\ 0\ dB)$$

$$\text{and } k_{attn} = \text{attenuation setting factor}$$

The subscript *C* used on each power term is to indicate they are the values that set ISR in the conducted test setup. Our expression for range then becomes:

$$R = \sqrt{\frac{P_{UWB} G_t A_r}{4\pi P_{rGPS_i} \left(\frac{P_{rUWB_C}}{P_{rGPS_{iC}}} \right)_0 k_{attn}}}$$

The P_{rGPS_i} in the ranging equation is computed from the carrier to noise ratio (C/N_0) value that the setup was normalized for, using an estimated value of N_0. To be perfectly rigorous this number may be slightly different for each receiver, but the variations in noise figure are small enough that we will consider a single noise density of –171 dBm/Hz for all receivers. Similarly, the actual GPS aperture area may be different for each receiver, but these differences (at least at reasonable satellite elevation angles) will also be small enough to ignore in this part of the analysis.

It should be noted that P_{UWB} changes with the selected UWB operating mode. However, the ISR in the ranging equation changes by the same amount, therefore the range calculation is independent of UWB mode. The other condition changed during the conducted test is the level of the GPS signal (P_{GPS}). However, when this value is reduced, the C/N_0 and the P_{rGPS_i} will decrease by the same factor and the ISR will increase by that factor. Therefore the product of the two terms will remain constant and the computed range will not change. The conducted test setup will provide a variety of ISR values as a function of UWB mode and simulated GPS signal power, but the calculated range for the setup is independent of these changes.

The spectrum analyzer shown in Figure B-2 was used to monitor UWB transmissions during all tests. A 20-MHz sweep of the UWB transmissions for the three 100-percent duty factor transmissions (i.e., Modes 1, 7, and 13) are shown in Figure B-4. The levels are average power densities in dBm/MHz, and they were plotted directly from the data files from the ARL:UT web site. The average powers were increased by 7.98 dB to account for the loss between the power source and the spectrum analyzer. The power densities for all other modes were reduced in direct proportion to their duty factors.

The P_{GPS} *(live-sky)* at point A is –90.5 dBm. P_{GPS} *(live-sky)* is computed by noting that the simulator signal was set at 17.5 dB above –130 dBm, and the amplifier at the output of the simulator has 22-dB gain. The power at the minimum GPS level was set 13 dB below the live-sky condition (i.e., –103.5 dBm at point A). Table B-2 shows the average UWB power (using the above densities and a 20-MHz bandwidth) and the ISR for each UWB mode and GPS signal condition with the UWB attenuation set to zero. Using the reported UWB spectral power density at L1, the power in 20 MHz is –34.9 dBm (Mode 13). The ratio values shown in the table also include the path attenuation difference indicated by the ISR equations. Finally, the P_{rGPS_i} not in the ISR computation is computed from the setup C/N_0, and for the live-sky and minimum level is –119 dBm and –132 dBm, respectively, (based on an average of receivers 1 and 4, there was

9-dB variation in the data). One final adjustment is required to account for the UWB source having a 6 dB lower power into the antenna than the value used in the conducted test setup. Therefore, P_{UWB} in the equivalent range equation is set at –40.9 dBm (again this is the GPS bandwidth limited power). Also note that the two powers, in the equation, outside the ISR represent the values for a radiated test that match the expected UWB transmit power in that test and the GPS power that would produce the C/N_0 value of the conducted test normalization. While the ISR is the value set in the conducted test.

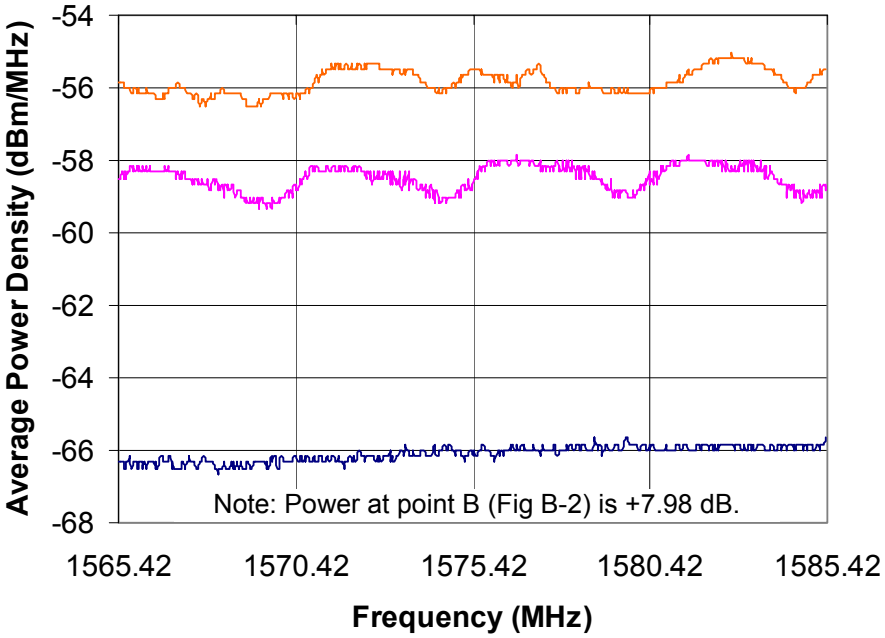

Figure B-4 UWB Average Power Densities for Modes 1, 7, and 13

As noted previously the ratio of P_{UWB}-to-$\left(\frac{P_{rUWBC}}{P_{rGPS_{iC}}}\right)$ remains constant as the mode changes, such that, the equivalent range is mode independent. This ratio for all modes is equal to –89.8 dB for the live sky condition and for the minimum level condition is –102.8 dB (includes the 6 dB radiated power reduction). When multiplied by $\left(\frac{G_t A_r}{4\pi}\right)$ and divided by the GPS power

level for each condition the value in the square root is –10.2 dB for both cases. We can now restate the equivalent range equation for all conducted test conditions (for receivers 1-4) as:

$$R_L = \sqrt{\frac{0.095}{k_{attn}}} = 0.31\sqrt{\frac{1}{k_{attn}}} \quad meters$$

$$or:$$

$$R_{LdB} = \left(-5.1 + \frac{Attenuator\ Setting}{2}\right) \ dB\text{-}meters$$

Table B-2
Average UWB Power and Interference Ratio – Conducted Test Setup (Receivers 1-4)

UWB Mode	PRF (MHz)	Duty Cycle (%)	P_{UWB} (dBm)	Live-sky GPS $\left(\frac{P_{rUWB_C}}{P_{rGPS_{iC}}}\right)_0$ (dB)	Minimum GPS $\left(\frac{P_{rUWB_C}}{P_{rGPS_{iC}}}\right)_0$ (dB)
1	1	100	-45.1	38.7	51.7
2-4	1	50	-48.1	35.7	48.7
5	1	25	-51.1	32.7	45.7
6	1	66	-46.9	36.9	49.9
7	5	100	-37.5	46.3	59.3
8-10	5	50	-40.5	43.3	56.3
11	5	25	-43.5	40.3	53.3
12	5	66	-39.3	44.5	57.5
13	10	100	-34.9	49.0	62.0
14-16	10	50	-37.9	46.0	59.0
17	10	25	-40.9	43.0	56.0
18	10	66	-36.7	47.2	60.2

The above equivalent range equation is an approximation based on a simple model that makes no distinction relative to the individual performance factors of the four receivers in the setup. As noted earlier the receivers may have different noise figures and different antenna characteristics. Additionally, they are unlikely to have the same response characteristics with regard to their reported C/N_0, and since this receiver data will be used later to compute the conducted-to-radiated adjustment factor, these will also be accommodated in the final fitting process. This range equation is simply the means for estimating the initial value used in the final fitting process. However, before discussing the final fit, the initial estimate for the other conducted test setup will be defined.

B.3 Test Setup for Receivers 6 and 7

The test setup for receivers 6 and 7 was basically the same with a less capable simulator (limited to 10 satellites). It used a different amplifier at the output of the simulator, there were some cable and adapter changes, and the fixed receiver attenuation values were changed to achieve the normalized GPS power levels. The attenuation path differences for this setup are shown in Figure B-5 and the path attenuation is shown in Table B-3. The extra noise is due to higher measurement errors at the large attenuation values for receiver 6. The variance of all differences for this setup was 0.37 dB. The ISR, at 0-dB attenuation, for each UWB mode and GPS power level are shown in Table B-4. Receiver 6 C/N_0 for the conducted baseline was used to set the GPS power level. The same bandwidth reduction ratio was used, but the live-sky to minimum level powers was different by only 12 dB in this test setup.

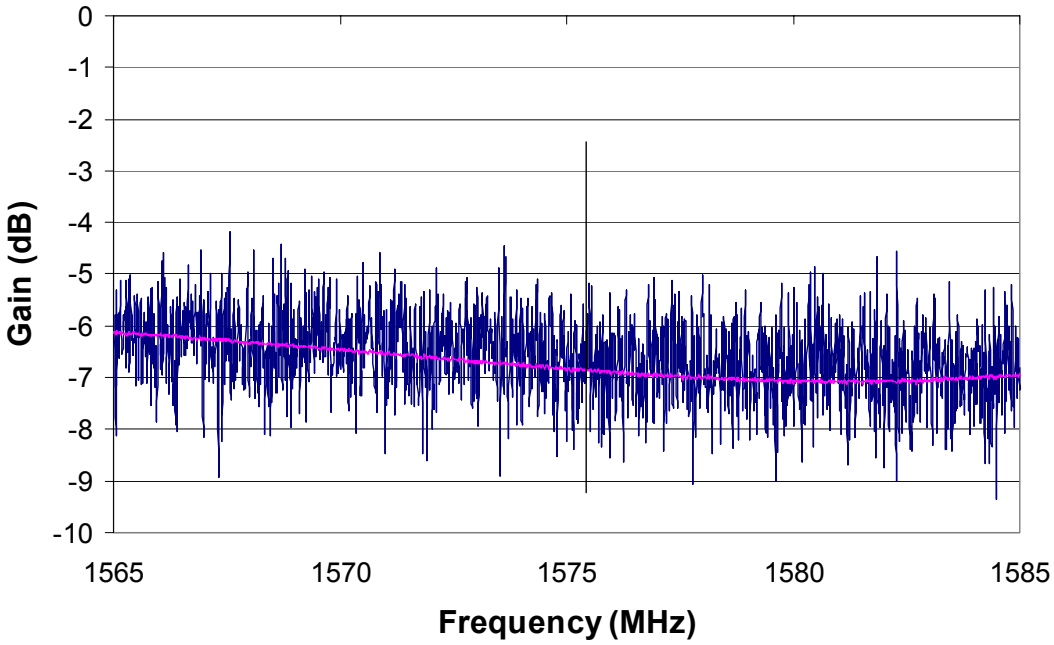

Figure B-5 UWB-GPS Attenuation Path Differences for Receivers 6 and 7 at L1

Table B-3
Conducted Test Setup Average Path Attenuations for Receivers 6 and 7 (over 20 MHz) at L1

Receiver	UWB Path (dB)	GPS Path (dB)	Difference (dB)
6	52.98	46.40	6.58
7	21.55	14.81	6.73
		Average of all path differences	6.66

The values for live-sky and minimum GPS signal levels in this setup are –87.1 dBm and –99.1 dBm, respectively. The UWB power setup was the same as it was for receivers 1-4. The equivalent C/N_0 GPS power was taken from the receiver 6 values, they were –124 dBm and –136 dBm for live-sky and minimum level respectively. The equivalent range equation for this setup is:

$$R_L = \sqrt{\frac{0.66}{k_{attn}}} = 0.81\sqrt{\frac{1}{k_{attn}}} \quad meters$$

or :

$$R_{LdB} = \left(-1.8 + \frac{Attenuator\ Setting}{2}\right) \ dB\text{-}meters$$

Table B-4
Average UWB Power and Interference Ratio – Conducted Test Setup (Receivers 6 and 7)

UWB Mode	PRF (MHz)	Duty Cycle (%)	P_{UWB} (dBm)	Live-sky GPS $\left(\frac{P_{rUWBC}}{P_{rGPS_{iC}}}\right)_0$ (dB)	Minimum GPS $\left(\frac{P_{rUWBC}}{P_{rGPS_{iC}}}\right)_0$ (dB)
1	1	100	-45.1	35.3	47.3
2-4	1	50	-48.1	32.3	44.3
5	1	25	-51.1	29.3	41.3
6	1	66	-46.9	33.5	45.5
7	5	100	-37.5	42.9	54.9
8-10	5	50	-40.5	39.9	51.9
11	5	25	-43.5	36.9	48.9
12	5	66	-39.3	41.1	53.1
13	10	100	-34.9	45.6	57.6
14-16	10	50	-37.9	42.6	54.6
17	10	25	-40.9	39.6	51.6
18	10	66	-36.7	43.8	55.8

Although the above calculations, for both test setups, were carried out with fractional dB precision, the numbers have an uncertainty of at least several dB. The largest uncertainties are in the range of C/N_0 values experienced in the conducted baseline ranging tests. The variations in simulated signal powers for all GPS satellites appeared to be considerably smaller than the variations in C/N_0 values output by the receivers during the baseline test run (i.e., the test run without any interference). A single average value was subsequently used to define the GPS signal power condition used in calculating the conducted test equivalent range.

B.4 Adjusting Ranges by Comparison with Radiated Tests

The primary limitation of the conducted test setup is that several assumptions are required to estimate the actual transmission coupling between the UWB and GPS antennas and the assumption of equal noise figures in both test conditions. The radiated tests will provide realistic transmission coupling and the actual noise figures, but these tests are limited by the unknown impact of signal multipath and other possible interference sources. This section describes the process for adjusting the equivalent range of the conducted tests to best match the data collected in the radiated tests. The quality of the match will provide an indication of whether the radiated tests were seriously impacted by multipath or other interference. The conducted data sets with the necessary adjustments will provide the final performance data for all the tested conditions using the equivalent range produced by this process. The process is based on a comparison of the ratio of C/N_0 with and without interference between the two test conditions. Formulating this ratio with equal values of C removes the GPS signal from the data used to compare UWB standoff ranges observed from radiated tests to those calculated for conducted tests where both produced equivalent degradations.

We can observe each satellite C/N_0 as a function of satellite elevation angle without UWB radiation. Since this parameter exhibits good repeatability from day-to-day, we can have a confident estimate of its value in a subsequent test period when we introduce UWB interference. That is, as long as the elevation history over an interference test interval is matched up with a non-interference test interval, the C values are removed in the ratio. This is easily accomplished by simply fitting a quadratic function to C/N_0 as a function of elevation angle using the conducted and radiated baseline data sets and the other radiated test segments without interference. With these analytic functions the C/N_0 with interference is simply divided by the analytic baseline value having the same elevation angle (see Appendix F for additional details). Having removed the GPS signal power, the ratio provides a direct measure of the interference density to the receiver noise density. That is:

$$R_{C/N} = \frac{\dfrac{C}{N_{I0} + N_0}}{\dfrac{C}{N_0}} = \frac{N_0}{N_{I0} + N_0}$$

or :

$$\frac{N_{I0}}{N_0} = \frac{1 - R_{C/N}}{R_{C/N}}$$

This ratio provides a relatively straightforward means for comparing conducted to radiated tests and for computing the equivalent range adjustment factors. Figure B-6 shows the N_{I0}/N_0 ratio for the conducted Mode 1, Mode 7, and Mode 13 UWB transmission modes for both the live-sky and minimum GPS signal levels and their average value (e.g., in the legend, Mode1-LC = Mode 1, live-sky, conducted data). These data were taken using Receiver 1, shown as the means of the ratios for each conducted interference C/N_0 data point divided by the C/N_0 taken

from the quadratic function of elevation angle for the corresponding conducted noninterference C/N_0 data points. Note that the live-sky and minimum levels for each mode are very nearly identical, demonstrating that this performance ratio is insensitive to GPS signal power (13-dB difference between live-sky and minimum level, in this test setup).

It can also be seen that the data do separate by mode. Referring back to Table B-2, the Mode 1 average UWB power is 10.2 dB less than Mode 13 and the Mode 7 is less by 2.6 dB. Figure B-7 shows the same plot with the Mode 1 data increased by 10.2 dB and with the Mode 7 data increased by 2.6 dB. This shows that the N_{I0}/N_0 ratio is directly proportional to the average UWB power level. The baseline conducted test data also provide a direct measure of the receiver-indicated C/N_0 difference between the live-sky and minimum levels without interference. This provides a direct calibration of this receiver's C/N_0 response. When this adjustment is made, it produces the results shown in Figure B-8. This correction factor was applied for each receiver. It should be noted that the higher values of N_{I0}/N_0 are only possible through the multiplication factors applied to Modes 1 and 7. The receiver would not actually produce an output with those values of interference. A value 10 to 20 times N0 are not likely, but the primary purpose of this process is to extract an equivalent range factor. Normalization to Mode 13 provides the maximum data for estimating the range factor.

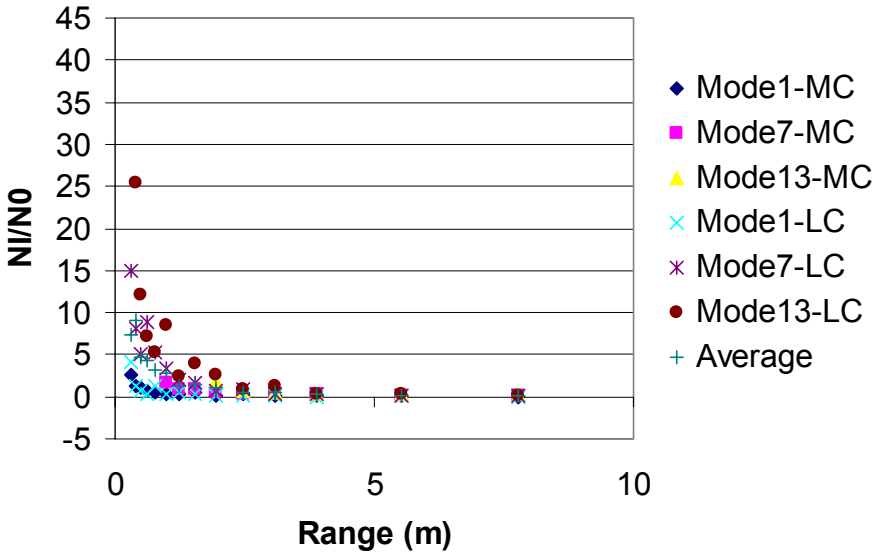

Figure B-6 Receiver 1 Conducted Test Data – Modes 1,7, and 13 – Live-Sky and Minimum Levels

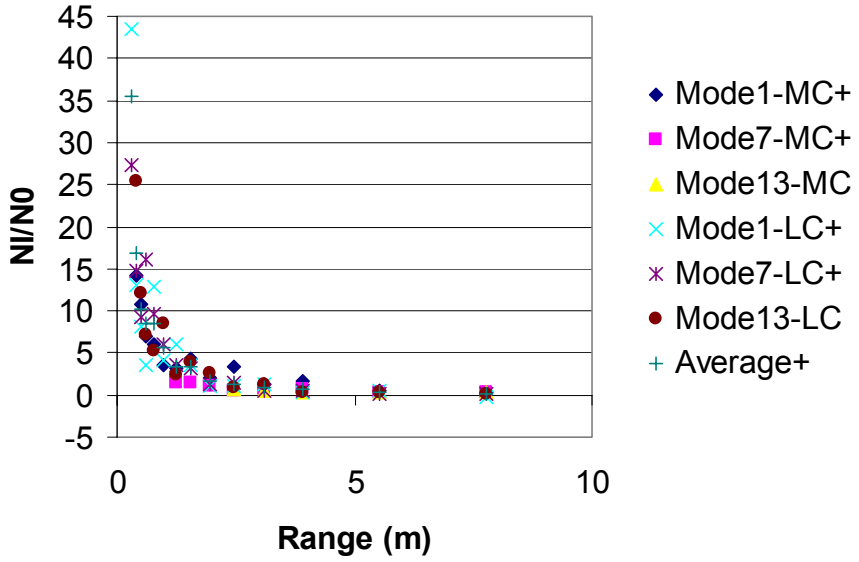

Figure B-7 Data in Figure B-6 Normalized to Mode 13 Average Power

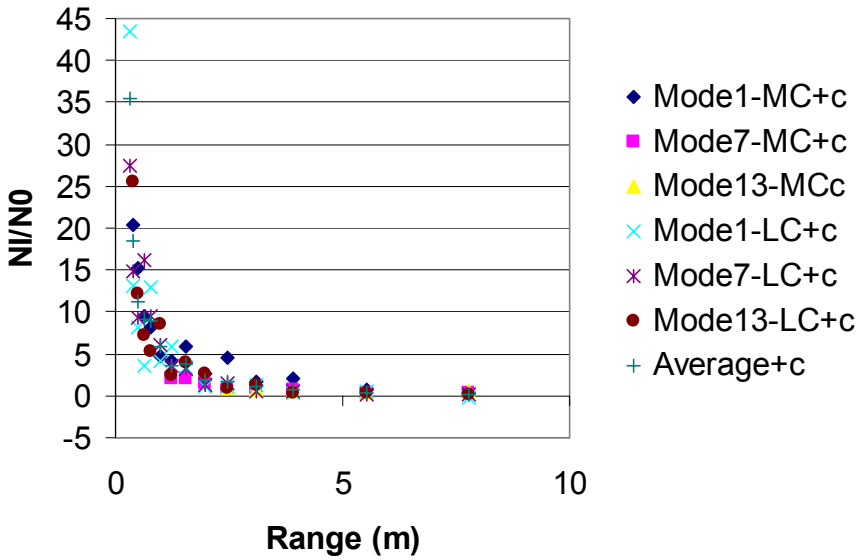

Figure B-8 Data in Figure B-7 Normalized for Receiver C/N_0 Response

The same factors (average power normalization and C/N_0 response for this receiver) apply to the radiated test data. Receiver 1 only included measurements for Mode 1 and Mode 7. The uncorrected radiated test data for the two modes and the average are shown in Figure B-9. Again the average power difference between the two modes is apparent. Figure B-10 is the same data normalized to Mode 13 power and with the C/N_0 response adjustment.

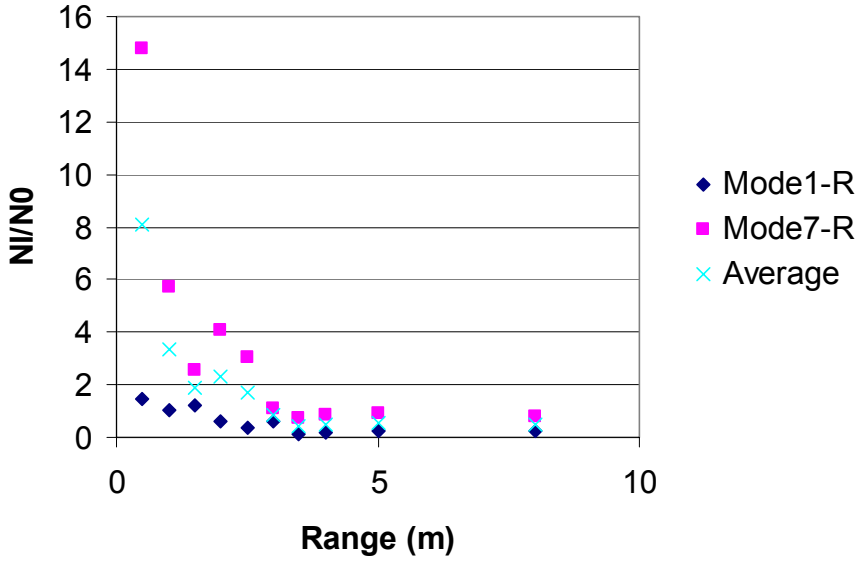

Figure B-9 Receiver 1 Radiated Test Data – Modes 1 and 7

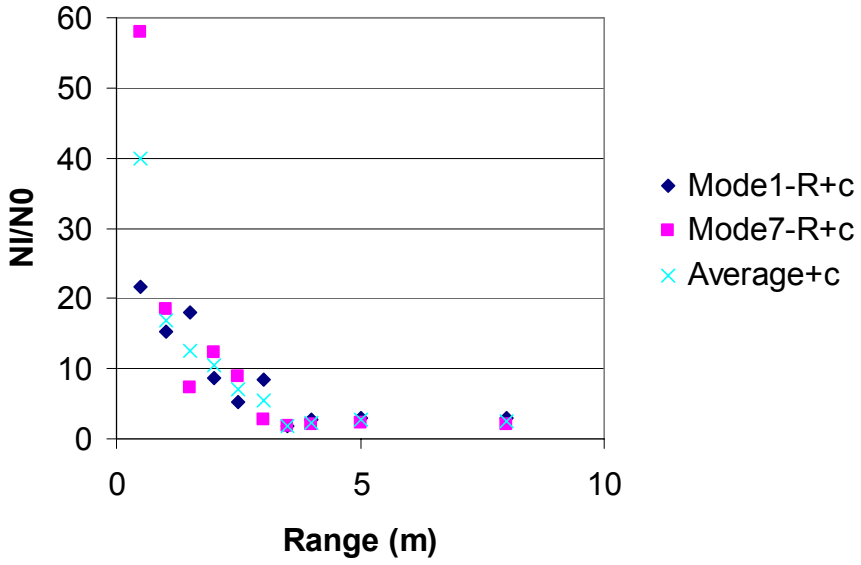

Figure B-10 Receiver 1 Radiated Test Data Normalized for Power and C/N_0 Response

Figure B-11 shows the average radiated and conducted N_{I0}/N_0 data, with corrections, for Receiver 1. These are the data used to compute adjustment factors for the conducted data set, from which the final equivalent range factor for Receiver 1 is derived.

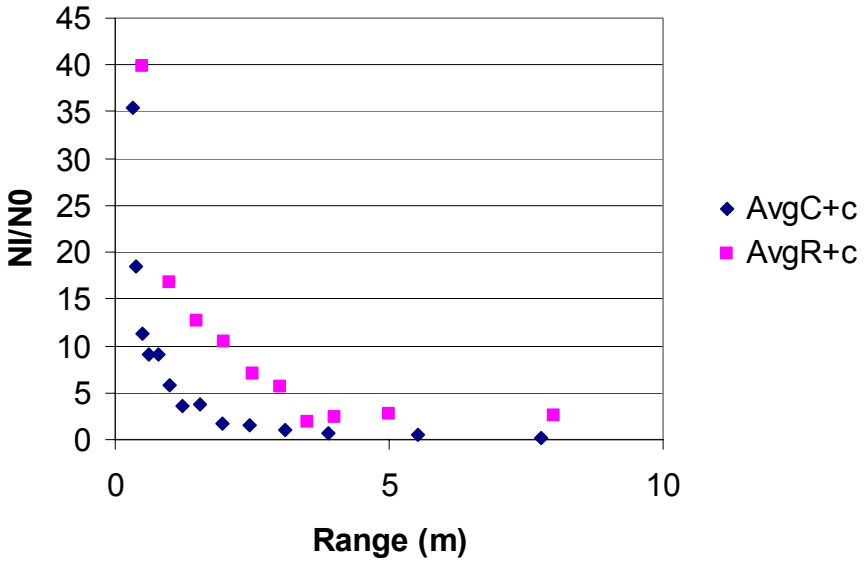

Figure B-11 Receiver 1 Conducted and Radiated N_{I0}/N_0 Measurements (Corrected)

The conducted data shown in Figure B-11 is adjusted with two factors. One factor adjusts the N_{I0}/N_0 data points to account for the difference between the power coupling and N_0 differences of the two test setups. The other factor adjusts the 0.31-meter 0-dB range value determined from the previous model calculation. The fitting process for this receiver produced the results shown in Figure B-12.

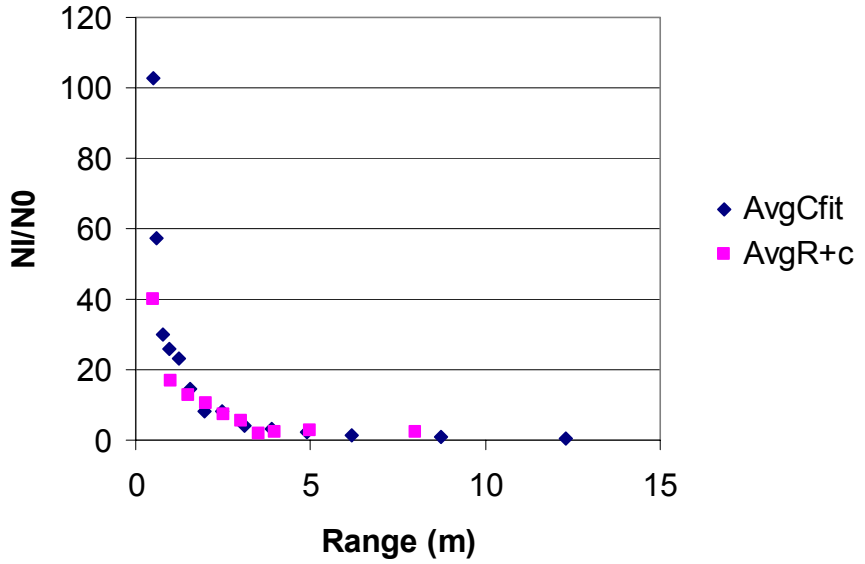

Figure B-12 Adjusted N_{I0}/N_0 Conducted Test Data for Receiver 1

With all corrections made the 0-dB range value for Receiver 1 changed from 0.31 meters to 0.49 meters. This process was repeated for receivers 2-4 and 6. The data fits for those receivers are shown in Figure B-13. The final range equations are:

$$R = (0.49\,m)\sqrt{UWB\ \ Attenuator\ \ Setting\ \ Factor} \quad (Receiver\ \ 1)$$

$$R = (0.31\,m)\sqrt{UWB\ \ Attenuator\ \ Setting\ \ Factor} \quad (Receiver\ \ 2)$$

$$R = (0.69\,m)\sqrt{UWB\ \ Attenuator\ \ Setting\ \ Factor} \quad (Receiver\ \ 3)$$

$$R = (0.49\,m)\sqrt{UWB\ \ Attenuator\ \ Setting\ \ Factor} \quad (Receiver\ \ 4)$$

$$R = (1.14\,m)\sqrt{UWB\ \ Attenuator\ \ Setting\ \ Factor} \quad (Receiver\ \ 6)$$

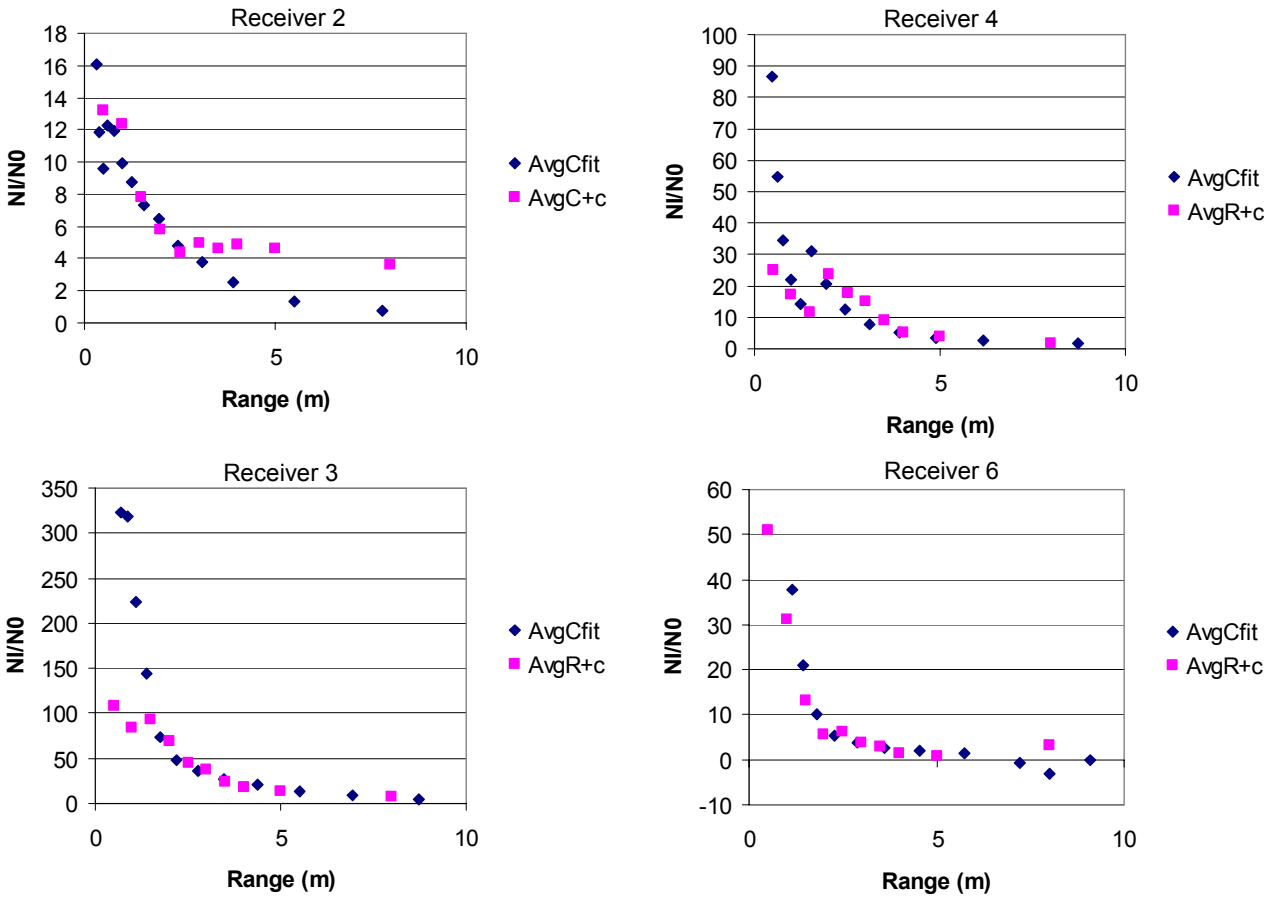

Figure B-13 Adjusted N_{I0}/N_0 Conducted Test Data for Receivers 2, 3, 4, and 6

APPENDIX C
GLOBAL POSITIONING SYSTEM (GPS) MEASUREMENT PROCESSING

C.0 Introduction

Appendix A describes how receiver-generated outputs were distilled into normalized Measures of Performance (MOPs) across different receivers, modes, and GPS power levels. These outputs required no additional processing prior to their normalization and subsequent mapping from attenuation space to standoff distance between the GPS receiver and the ultra-wideband (UWB) device. This appendix describes how more fundamental outputs of the GPS receivers (i.e., receiver measurement data) were processed and transformed into condensed MOPs. Three areas are addressed herein: reacquisition times, double difference residuals (DDRs) and pseudorange noise. This appendix is meant to supplement the methodology presented in Chapter 6 and Appendix A. For complete validation purposes, subsets of recorded measurement and ephemeris data were used to renavigate the receiver position, Appendix E.

C.1 Reacquisition Methodology

The ultimate data developed from the Conducted, Acquisition test are plots showing the increase in reacquisition time between injected tests (with GPS simulator signals and UWB PulsON Application Developer (PAD) signals) and baseline tests (with only GPS simulator signals) as a function of range. The raw data used to compute these plots are contained in the baseline and injected trial data files. Unlike the basic receiver MOPs, which utilize parameters extracted directly from the data file records, reacquisition processing reduces the data file contents to an intermediate set of parameters before computing their respective MOPs. Each reacquisition trial will produce three intermediate parameters that indicate when, if at all, the receiver reacquired the following satellite thresholds: four navigated satellites, one tracked satellite, and the number of tracked satellites present at the start of the trial. The intermediate parameters from trials of a specific test (i.e., a specific sky, receiver, UWB Mode, and UWB attenuation configuration) are combined to yield two values per threshold that characterize the reacquisition performance for the entire test (average reacquisition time and reacquisition probability). The specific sequence of events that produces the average reacquisition time and reacquisition probability for all UWB modes and attenuations of a particular sky and receiver configuration is outlined below.

Each (approximately 3½ minute) trial contains a nominal 10-second acquisition period, followed by a nominal 30-second loss-of-lock period, followed by a nominal 3-minute reacquisition period. A test is made up of 30 trials run contiguously over a 2-hour period. For baseline trials, only GPS simulator signal is input during the initial acquisition and reacquisition periods, and no signal is input during the loss-of-lock period. For injected trials, a mix of GPS simulator and UWB signals are input during the initial acquisition and reacquisition periods, and

only UWB signal is input during the loss-of-lock period. All injected tests were run with the GPS simulator generating signals for one of the following 2-hour periods: 0600 to 0800 Zulu, July 26, 2000; 0800 to 1000 Zulu, July 26, 2000; or 1000 to1200 Zulu, July 26, 2000. One baseline test was also run for each of these 2-hour periods. The receivers nominally output their data streams during the entire trial duration. There are instances where the data stream output is suspended during loss-of-lock, then resumes (with correct time tags) when the GPS signal is restored.

The first portion of the MOP computation parses the receiver data files, and extracts the time tag of each record, the number of satellites that were being tracked at that time and the number of satellites that were being navigated at that time. Figure C-1 shows a plot of these data for a Live-Sky Ashtech Z-12 baseline trial. The actual satellite counts are plotted as dots, with a linearly interpolation overlay plotted as a line. The number of satellites tracked was computed by counting the number of measurement records per time epoch. The number of satellites navigated was computed by counting the number of measurement records per time epoch with a measurement quality indicating that the measurement was used to compute position. Loss-of-lock onset is clearly visible by the sudden drop in both tracked and navigated satellite counts occurring when the GPS input was removed from the receivers. Reacquisition is also clearly visible as a gradual increase in satellite counts after the GPS input was restored. Also visible is how the receiver stops outputting data between approximately 7:25:55 and 7:26:25 (note the absence of actual data, i.e., dots, in this region). The satellite counts are assumed to be zero in the time regions where there are no data.

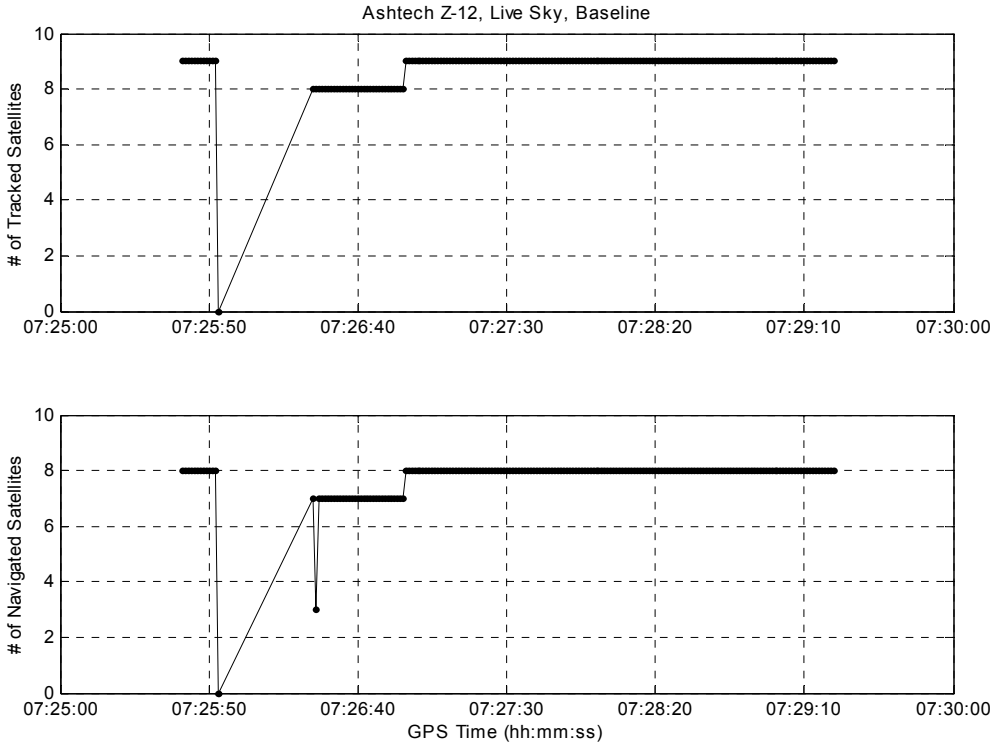

Figure C-1 Tracked and Navigated Satellite Plots of a Baseline Acquisition Trial

Figure C-2 shows a representative plot of tracked and navigated satellite counts versus time for a Live-Sky Ashtech Z-12 injected trial (UWB Mode 13 at 10 dB attenuation). Again, loss-of-lock onset is clearly visible by the sudden drop in both satellite counts occurring when the GPS input was removed from the receivers, and reacquisition is also clearly visible as a gradual increase in satellite counts after the GPS input was restored.

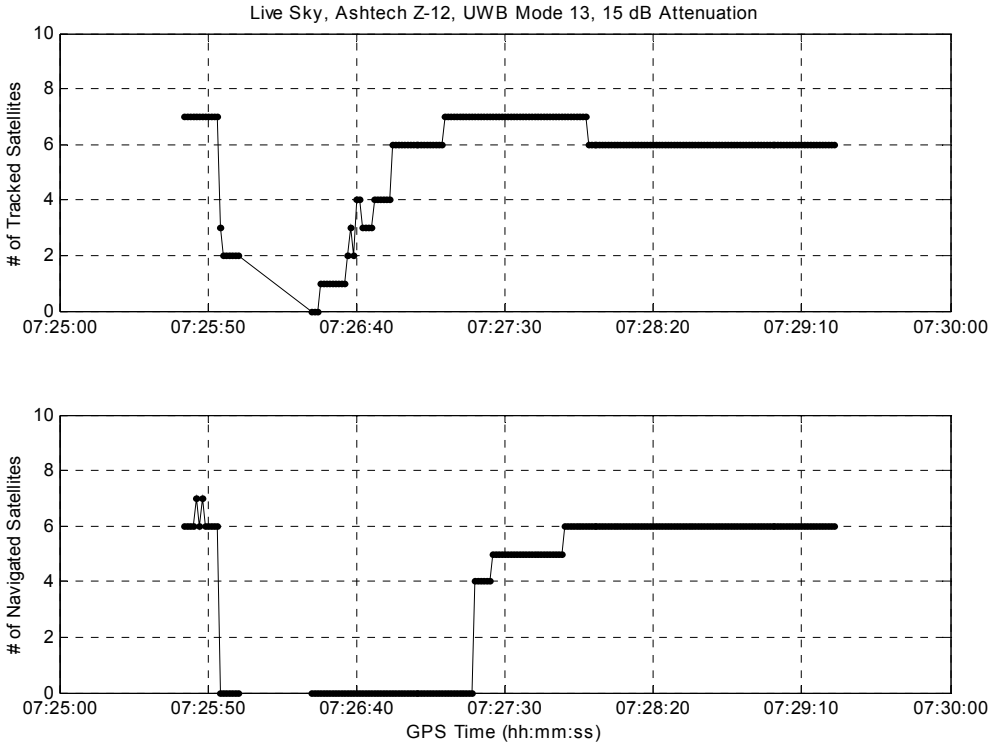

Figure C-2 Tracked and Navigated Satellites Plot of an Injected Acquisition Trial

The next step is the extraction of the times at which reacquisition occur. Three different reacquisition thresholds are considered for each trial; one indicating when at least four navigated satellites are continually reacquired (the minimum number of satellites required to compute a position/time solution), one indicating when at least one tracked satellite is continually reacquired (necessary to compute time), and one indicating when the pre-loss-of-lock number of tracked satellites plus/minus one is continually reacquired (indicating total recovery). The over/under specification in the pre-loss-of-lock number of tracked satellites accounts for potential changes in the satellite constellation during the trial. Figures C-3 and C-4 highlight the reacquisition times for the same two Ashtech Z-12 trials used in the preceding figures. Figure C-3 illustrates how the first instance when at least four navigated satellites is reacquired is not selected since the count subsequently drops below four before rising again to its steady state value. It also shows how the same time epoch can be selected for two reacquisition thresholds [one tracked satellite and N (+/- 1) tracked satellite]. All three reacquisition thresholds were present in these examples. If the time for a reacquisition threshold does not exist, the time associated with that threshold is flagged as invalid (by setting the value to –1).

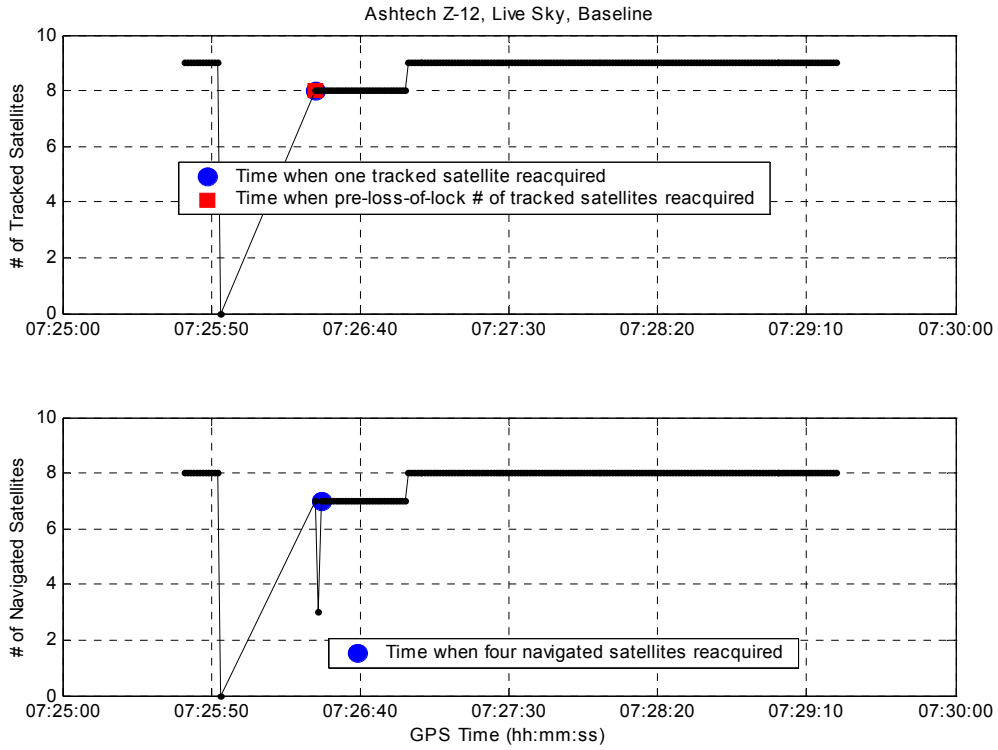

Figure C-3 Time of Reacquisition for a Baseline Acquisition Trial

The next step is to convert the times at which reacquisition occurs to actual reacquisition times. This requires computing the time at which the GPS signal was reintroduced to the receivers (t_rie) and subtracting it from the times at which reacquisition occur. The ARL:UT Test Plan/Report specifies that the GPS simulator signal was input to the receivers for 10 seconds, then removed from the receivers for 30 seconds, then input to the receiver for remainder of the trial. There are no specific indications of these events in any of the receiver data files, nor is there a reliable method of discerning the times at which these events occur from the available data. Some data files show the effects of the GPS simulator signal being removed by a sudden drop in the number of satellite measurement records. Other data files simply contain a variable length time gap that is generally between data records gathered during the initial acquisition period and those gathered after the loss-of-lock period. We therefore assume that the time at which the GPS signal is reintroduced to the receivers is equal to the time of the first epoch in the data file plus the nominal time the GPS signal was first input to the receivers (10 seconds) plus the nominal time the GPS signal was removed from the receivers (30 seconds). The equations below show the reacquisition time calculations for the injected trials. Parameters in lower-case are absolute times (i.e., start of a trial, time one tracked satellite was reacquired). Parameters in uppercase are time-spans (i.e., the time to reacquire one tracked satellite).

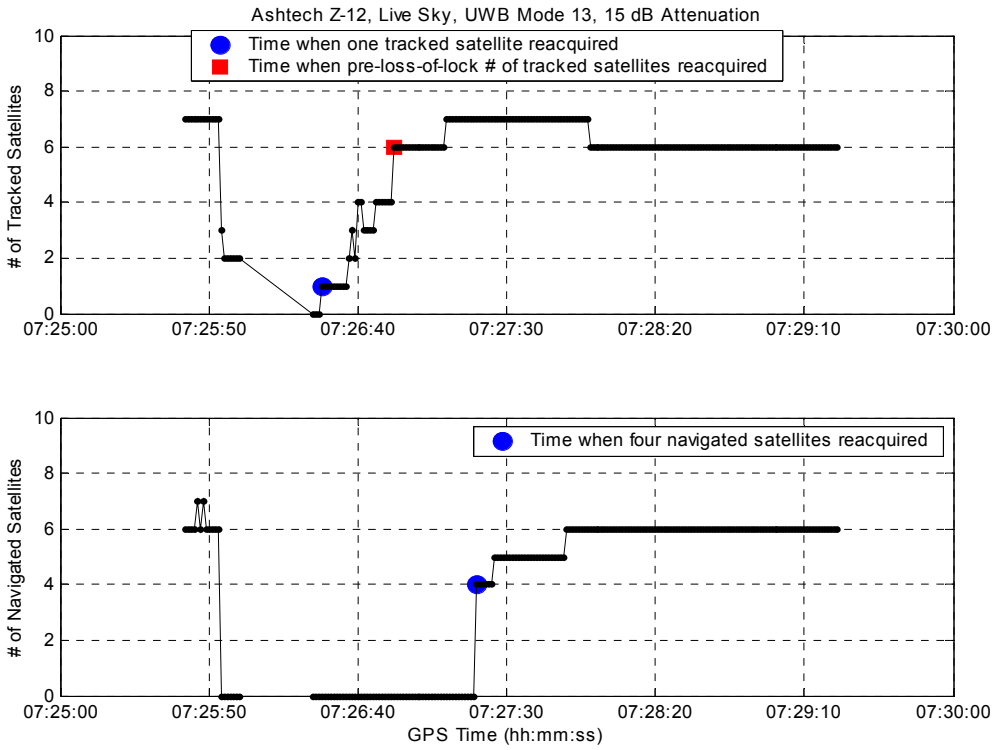

Figure C-4 Time of Reacquisition for an Injected Acquisition Trial

$$t\_rie_{m,a,i} = t\_sot_{m,a,i} + NIACQ\_T + NLL\_T \ [sec]$$

$$REACQ\_T\_4N_{m,a,i} = t\_reacq\_4n_{m,a,i} - t\_rie_{m,a,i} \ [sec]$$

$$REACQ\_T\_1T_{m,a,i} = t\_reacq\_1t_{m,a,i} - t\_rie_{m,a,i} \ [sec]$$

$$REACQ\_T\_NT_{m,a,i} = t\_reacq\_nt_{m,a,i} - t\_rie_{m,a,i} \ [sec]$$

where,

i	=	trial index (1 … NT)
NT	=	Number of trials (30)
m	=	UWB mode index (1…3 for UWB modes 1, 7, 13)
a	=	Attenuation index (1…9 for attenuations 5, 10, …45 dB)
t_rie	=	Time GPS signal is reintroduced to receiver
t_sot	=	Time of trial start
NIACQ_T	=	Nominal initial acquisition time (= 10 sec)
NLL_T	=	Nominal loss-of-lock time (= 30 sec)

t_reacq_4n	=	Time at which 4 navigated satellites reacquired
t_reacq_1t	=	Time at which 1 tracked satellites reacquired
t_reacq_nt	=	Time at which N (+/- 1) satellites reacquired
REACQ_T_4N	=	Time to reacquire 4 navigated satellites
REACQ_T_1T	=	Time to reacquire 1 tracked satellites
REACQ_T_NT	=	Time to reacquire N (+/- 1) tracked satellites

Up to 30 reacquisition times per specification exist for each injected test (i.e., UWB Mode/Attenuation) from which the averages are computed as shown in the equation below. Invalid times are not used to compute average reacquisition times, but instead are used to develop parameters indicating the probability that reacquisition occurred as shown in the equation below:

$$\mathrm{AVG\_REACQ\_T\_4N}_{m,a} = \frac{\sum_i \left(\mathrm{REACQ\_T\_4N}_{m,a,i} * \mathrm{TF}(\mathrm{t\_reacq\_4n}_{m,a,i} \neq -1)\right)}{\mathrm{NT}} \ [\mathrm{sec}]$$

$$\mathrm{AVG\_REACQ\_T\_1T}_{m,a} = \frac{\sum_i \left(\mathrm{REACQ\_T\_1T}_{m,a,i} * \mathrm{TF}(\mathrm{t\_reacq\_1t}_{m,a,i} \neq -1)\right)}{\mathrm{NT}} \ [\mathrm{sec}]$$

$$\mathrm{AVG\_REACQ\_T\_NT}_{m,a} = \frac{\sum_i \left(\mathrm{REACQ\_T\_NT}_{m,a,i} * \mathrm{TF}(\mathrm{t\_reacq\_nt}_{m,a,i} \neq -1)\right)}{\mathrm{NT}} \ [\mathrm{sec}]$$

$$\mathrm{P\_4N\_R}_{m,a} = \frac{100 * \sum_i \mathrm{TF}(\mathrm{t\_reacq\_4n}_{m,a,i} \neq -1)}{\mathrm{NT}} \%$$

$$\mathrm{P\_1T\_R}_{m,a} = \frac{100 * \sum_i \mathrm{TF}(\mathrm{t\_reacq\_1t}_{m,a,i} \neq -1)}{\mathrm{NT}} \%$$

$$\mathrm{P\_NT\_R}_{m,a} = \frac{100 * \sum_i \mathrm{TF}(\mathrm{t\_reacq\_nt}_{m,a,i} \neq -1)}{\mathrm{NT}} \%$$

where,

TF(arg)	=	1 if arg is true, otherwise 0
AVG_REACQ_T_4N	=	Average time to reacquire 4 navigated satellites
AVG_REACQ_T_1T	=	Average time to reacquire 1 tracked satellite
AVG_REACQ_T_NT	=	Average time to reacquire N(+/- 1) tracked satellites

P_4N_R	=	Probability that 4 navigated satellites were reacquired
P_1T_R	=	Probability that 1 tracked satellite was reacquired
P_NT_R	=	Probability that N (+/- 1) tracked satellites were reacquired

Figure C-5 shows the average reacquisition times for the Live-Sky Ashtech Z-12 receiver of each UWB PAD mode plotted as a function of attenuation. Figure C-6 shows the probability that any as the average reacquisition times for the Live-Sky Ashtech Z-12 receiver of each UWB PAD mode plotted as a function of attenuation.

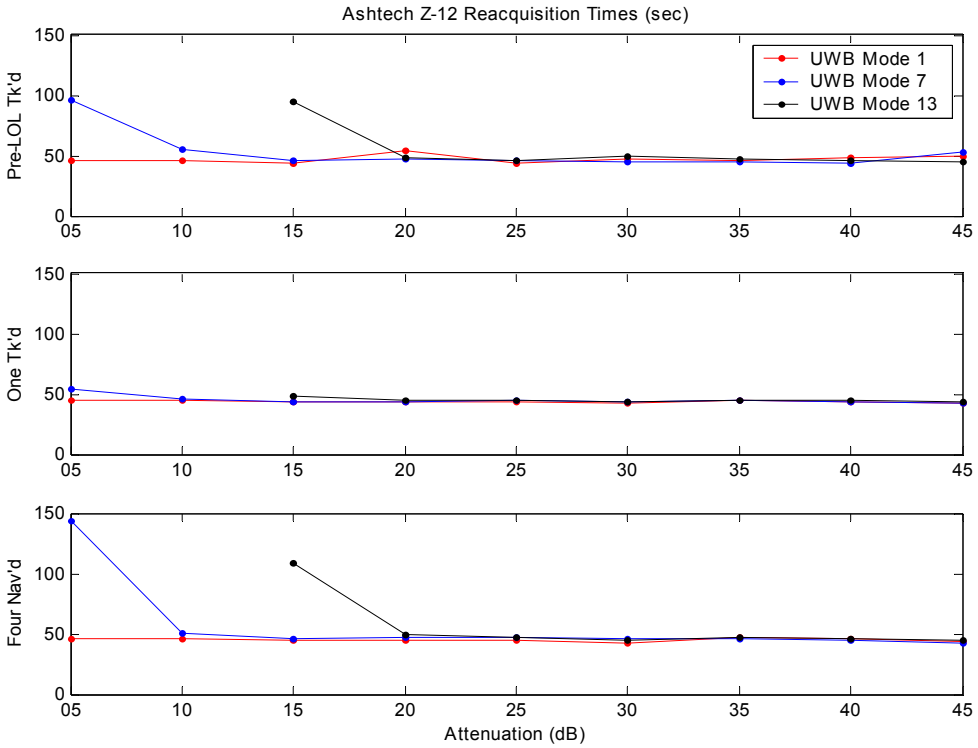

Figure C-5 Average Reacquisition Times for Individual Injected Tests

The final step is to normalize the reacquisition times for the injected tests by those in the baseline tests. The trials of baseline tests were run with the GPS simulator outputting data for the same time frames as it did for the injected cases, and without UWB signal contribution. The equations to compute the reacquisition times for the baselines are similar to the ones described above for the injected trials, but are not indexed by UWB Mode and attenuation. Also, reacquisition probabilities are not computed for the baselines.

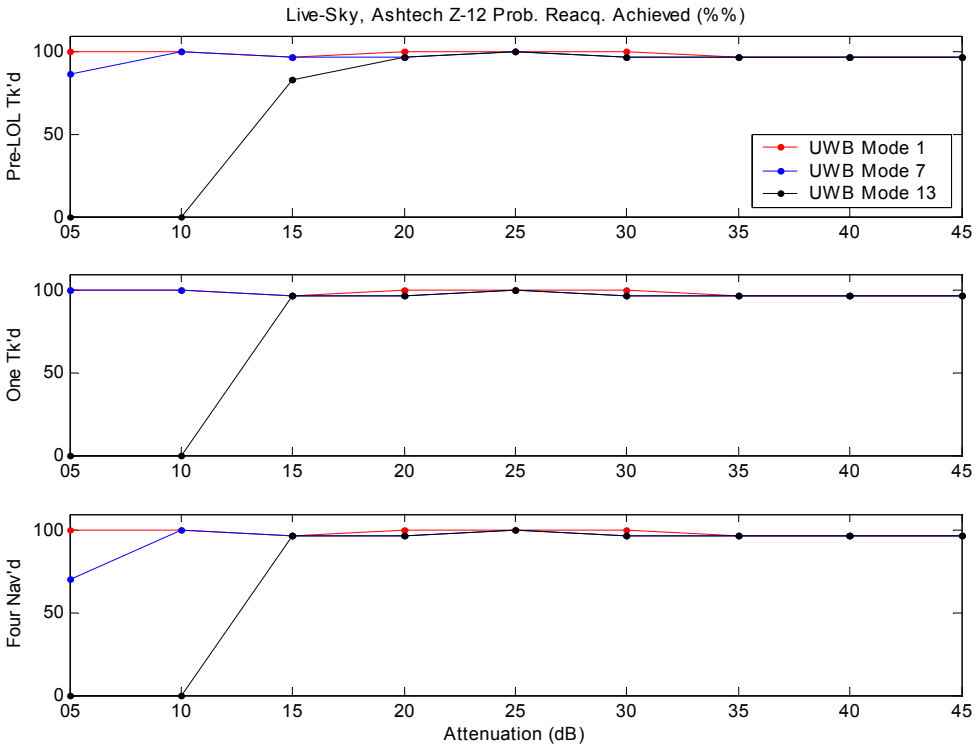

Figure C-6 Probability of Achieving Reacquisition Time for Individual Injected Tests

Subtracting the average baseline reacquisition times for the same sky, receiver, time period, and threshold normalizes the injected average reacquisition times. The resulting data are then ready for compliant device correction, conducted range normalization, and radiated range normalization as described in Chapter 6. Figure C-7 shows the average increase in reacquisition times for the Live-Sky Ashtech Z-12 receiver of each UWB PAD mode over the baseline times plotted as a function of attenuation.

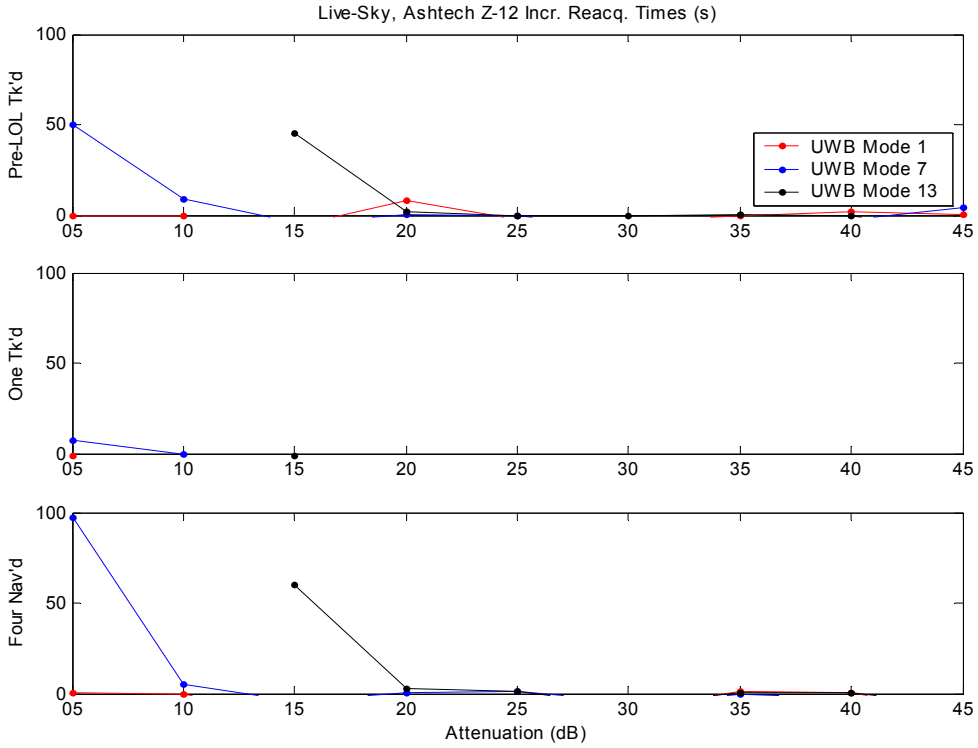

Figure C-7 Reacquisition Times Increase Over Baseline for Individual Injected Tests

C.2 Receiver Double Difference Processing

This section describes the process required to derive the double difference observable. The data presented in this section were generated with the Ashtech Z-12 receiver. Due to the design of this device, processing these measurements was more challenging then for the other receivers. However, the methodology was the same for each data set that was analyzed. Due to the lack of baseline measurements for the radiated experiments, the double difference MOP was evaluated for the conducted tests only.

C.2.1 Double Difference MOP

The double difference MOP provides a measure of the following:

- Systematic code ranging errors induced by the UWB.
- The double difference code noise. Note that the single link code noise may be inferred from this measurement.

The general formulation for the receiver pseudorange measurement [Reference (22)] is given by

$$\rho_i(\tau) = | p_{s_i} - p_u | + \tau_u - \tau_{s_i} + \varepsilon + \upsilon_i$$

where ρ_i = measured pseudorange to GPS satellite i, τ = GPS time, p_{s_i} = position of GPS satellite i, p_u = receiver position, τ_u = receiver clock error, τ_{s_i} = GPS satellite i clock error, ε =error sources (ionosphere, troposphere, ephemeris errors, etc), υ_i = measurement noise.

In order to formulate the double difference, measurements from the baseline experiment as well as the UWB injected experiment are combined. The double difference is then defined as

$$\nabla\Delta\rho(\tau_{injected}, \tau_{baseline}) = (\rho_i(\tau_{injected}) - \rho_j(\tau_{injected}))|_{injected} - (\rho_i(\tau_{baseline}) - \rho_j(\tau_{baseline}))|_{baseline}$$

where the measured pseudoranges to GPS satellites i and j are used. Note that the measurements from the baseline experiment and injected experiment may be combined at different GPS times $\tau_{baseline}$ and $\tau_{injected}$. However, if $\tau_{baseline} = \tau_{injected}$, the state of the GPS constellation observed by the receiver in the injected experiment and baseline experiment is the same. The principle result is that almost all of the terms appearing in the pseudoranges are eliminated. This includes the receiver and GPS satellite clock errors, as well as the effects of the ionosphere, troposphere, and GPS ephemeris errors. Further, since the receivers for both the injected and baseline experiments were simulated to be at the same location, the terms due to receiver and GPS satellite locations are eliminated.

The double difference observable then reduces to (with $\tau \equiv \tau_{baseline} = \tau_{injected}$)

$$\nabla\Delta\rho(\tau,\tau) = (\upsilon_i - \upsilon_j)|_{injected} - (\upsilon_i - \upsilon_j)|_{baseline} + B_{uwb}$$

where B_{uwb} would be any systematic error resulting from the impact of the UWB signal on the measured pseudoranges. Note that systematic code ranging errors translate into biased position estimates, and would therefore indicate degraded receiver performance.

In order to distill the data down to simple metrics, the mean and standard deviation of the computed double difference measurements were evaluated for each receiver/UWB attenuation level/sky level/mode combination. Note that if the receiver in the baseline and injected experiments tracked N (common) GPS satellites, there would be N -1 independent double difference measurements that may be formed at any given epoch. For example, given that each attenuation level was simulated for 20 minutes, and data were output at 1 Hz, there would be 1200-Hz epochs of data for each test attenuation. Assuming the receiver in the baseline and injected experiment each tracked eight common GPS satellites, there would be a total of seven independent double differences that could be formed. Therefore, there would be a total of 8,400

double difference measurements of which the mean and standard deviation would be computed. The computed mean is an estimate of B_{uwb}, and should be nearly zero if the UWB signal does not cause systematic code tracking errors.

The following algorithm was used to compute the statistics for each receiver/UWB attenuation level/sky level/mode combination:

1. The double differences must be formed using measurements evaluated at the same GPS time. The data files for the baseline and injected experiments are searched in order to match up those measurements that correspond to the same *receiver* time. The receiver times of interest are those associated with the particular attenuation level being evaluated.

2. The GPS satellite that was tracked most often by the receiver is identified, and the pseudorange measurement from this satellite is used with the pseudoranges from each of the other satellites to form all the double differences.

3. The double difference measurements computed in (2) are preprocessed. The preprocessing is described later in this appendix.

4. The mean and standard deviation of all the double difference measurements are computed for the given mode/attenuation/sky/receiver combination.

C.2.2 Experimental Setup Limitations

The receivers used in this study did not output raw (unsmoothed) pseudorange measurements. Therefore, the double differences were computed with smoothed-code measurements. This limitation does not severely impact the utility of this MOP, since the mean of the double difference measurements are principally the same whether smoothed or raw (unsmoothed) pseudorange measurements are used.

C.2.3 Double Difference Preprocessing

Preprocessing of the double difference measurements was required prior to computing the mean and standard deviation to account for several effects:

1. The impact of sample time errors between the receiver in the baseline and injected experiments.

2. The impact of the filter dynamics that occur when a new satellite is acquired.

C.2.4 Receiver Sampling Time Errors

GPS receivers output data measurements at some designated rate as determined by their internal clocks. In order to identify the precise time that these measurements occurred, the data

are typically time stamped using either GPS or receiver time. In the event that receiver time is used, receivers also output a clock bias measurement, which is the difference between GPS time and the receiver time. Note that this clock bias may become significant depending on the particular receiver implementation.

As described in Subsection C.2.1, the double difference measurements are formed using data from each receiver, and that data must be referenced to the same moment in time. The Ashtech Z-12 (as well as the other receivers in this study) outputs data time stamped with the receiver time. Therefore, when comparing the measurements from the baseline and injected experimental data that are referenced to identical receiver times, non-zero clock biases imply that these measurements did not occur at the same GPS time. This must be accounted for when the double difference measurements are computed.

Reference Subsection C.2.1, the double difference measurement is defined to be

$$\nabla\Delta\rho(\tau_{injected},\tau_{baseline}) = (\rho_i(\tau_{injected}) - \rho_j(\tau_{injected}))\,|_{injected} - (\rho_i(\tau_{baseline}) - \rho_j(\tau_{baseline}))\,|_{baseline}$$

$$= \nabla\rho(\tau_{injected})\,|_{injected} - \nabla\rho(\tau_{baseline})\,|_{baseline}$$

The clock bias is defined by

$$\tau_{GPS} = t_{receiver} + \tau_{bias}$$

where τ_{GPS} = GPS time, $t_{receiver}$ = receiver time, and τ_{bias} = clock bias.

Let $\bar{\tau}_{GPS} = t_{baseline} + \tau_{bias}\,|_{baseline}$, and $\tilde{\tau}_{GPS} = t_{injected} + \tau_{bias}\,|_{injected}$. To first order then, the double difference measurement referred to a common GPS time is given by

$$\nabla\Delta\rho(\tilde{\tau}_{GPS},\bar{\tau}_{GPS}) = \nabla\rho(\tilde{\tau}_{GPS})\,|_{injected} - \nabla\rho(\bar{\tau}_{GPS})\,|_{baseline}$$

$$= \nabla\rho(\tilde{\tau}_{GPS})\,|_{injected} + \nabla\dot{\rho}(\tilde{\tau}_{GPS})\,|_{injected}\,(t_{injected} - t_{baseline}$$

$$+ \tau_{bias}\,|_{injected} - \tau_{bias}\,|_{baseline}) - \nabla\rho(\bar{\tau}_{GPS})\,|_{baseline}$$

$$= \nabla\Delta\rho(\tilde{\tau}_{GPS},\bar{\tau}_{GPS}) + \nabla\dot{\rho}(\tilde{\tau}_{GPS})\,|_{injected}\,(t_{injected} - t_{baseline}$$

$$+ \tau_{bias}\,|_{injected} - \tau_{bias}\,|_{baseline})$$

$$= \nabla\Delta\rho(\tilde{\tau}_{GPS},\bar{\tau}_{GPS}) + time\_correction$$

where

$$\nabla\dot{\rho} = \dot{\rho}_i - \dot{\rho}_j$$

and $\dot{\rho}$ = receiver Doppler measurement.

Indexing into the injected and baseline data files and forming the double difference with the pseudoranges time stamped with the same receiver times yields $\nabla\Delta\rho(\tilde{\tau}_{GPS}, \bar{\tau}_{GPS})$. A "time correction" factor, $time\_correction$, must then be applied using the clock bias and Doppler measurements provided by the receivers to yield the corrected double difference ($\nabla\Delta\rho(\bar{\tau}_{GPS}, \bar{\tau}_{GPS})$) measurement. The corrected measurement is used to generate the required statistics for the MOP. Note that since $t_{injected} = t_{baseline}$, the time correction reduces to a function of the Doppler measurements and the clock bias difference between the injected and baseline experiments. The time correction is thus proportional to the true sample time error.

The Ashtech Z-12 is implemented with a free running clock, so that the clock bias generally grows as the receiver runs, and will approach 1 milliseconds prior to a "leap millisecond" being introduced. The "leap millisecond" effectively realigns the receiver clock to GPS time (reducing the clock bias). Given that typical observed Doppler rates for a fixed receiver are on the order of several KHz, the time correction necessary to account for the true sample time offsets can approach several meters for the Ashtech Z-12.

Note that many receivers actively control their clocks to keep them closely aligned to GPS time. This is the case for the NovAtel receivers used in this study. In this case, the clock biases are small enough that the time correction may be effectively ignored. As a practical matter, the formulation as presented breaks down as the true sample time error becomes large. However, the sample time misalignment is bounded by 2 ms in this study, so that the formulation here is perfectly adequate.

C.2.5 Receiver Filter Dynamics

The receivers used in this study did not output raw (unsmoothed) code measurements. Therefore, the double difference was computed using the available measurement (e.g., smoothed code). When the receiver first acquires a GPS satellite, the smoothing filter requires some period of time to converge. The principle result is that the smoothed code noise is significantly higher as the filter undergoes transients. This effect was particularly observable in the Ashtech Z-12, and the filter typically required 2 minutes to converge. In order to accurately convey the impact of UWB, it was felt that the measurements should be used only after steady state had been reached. Therefore, the data preprocessing eliminated the double difference measurement from the final statistic if it was computed using a GPS satellite that had been acquired within the past 120 seconds.

C.2.6 Double Difference Experimental Data

This section presents several snapshots of experimental data to illustrate the processing that was undertaken to develop the MOP. The data presented here are for the Ashtech Z-12 receiver. The data for the other receivers are similar in nature, and the methodology described was applied to those data sets as well.

Figure C-8 (top subplot) shows the unedited (e.g., prior to accounting for the sample time error or filter transients) double differences computed using the pseudoranges corresponding to identical receiver time stamps for the injected/baseline pair. This data are for a conducted test, live sky, UWB Mode 13, attenuation of 25 dB, Ashtech Z-12 receiver. The bottom subplot (Edited DD Residuals) corresponds to the double differences after the time stamp error was accounted for and the transient filter dynamics were eliminated. The transient filter dynamics are clearly visible near t=50 seconds (top subplot).

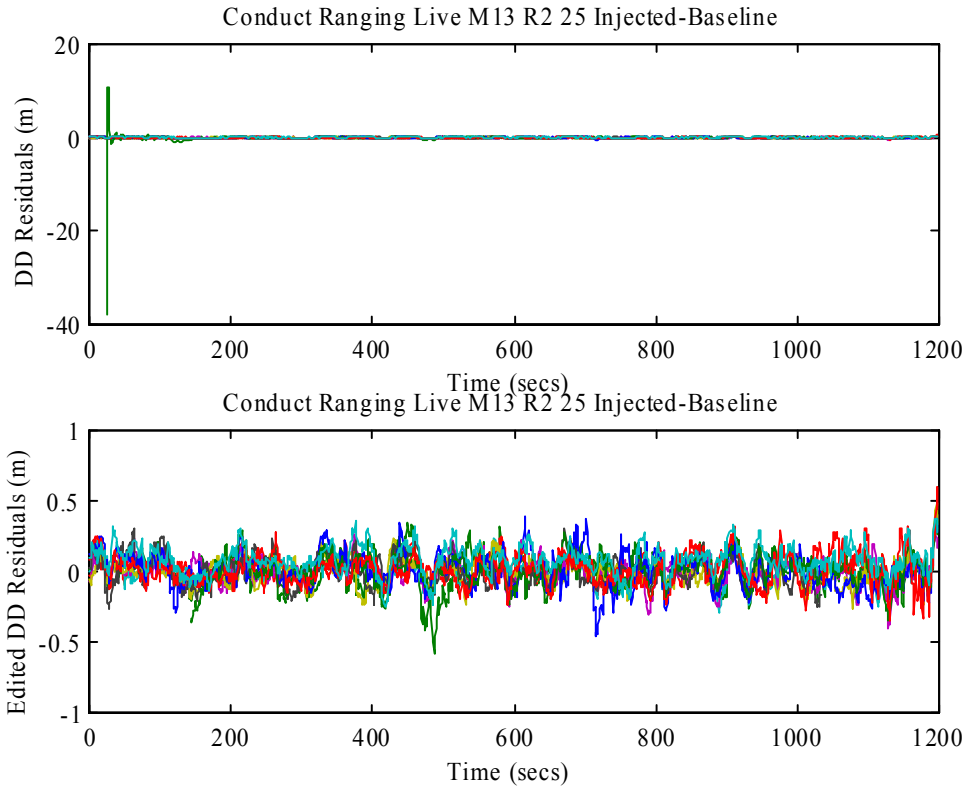

Figure C-8 Unedited and Edited Double Difference Measurements

Figure C-9 shows a close-up of the same double difference data presented in Figure C-8. The figure shows the data prior to editing. Visible near t=1000 sec is the impact the introduction of a "leap millisecond" that occurred on the receiver during a 20-minute interval. The "leap

millisecond" effectively introduces a discontinuity in the sample time error, which results in the discontinuity observed in the data. This effect has nothing to do with the impact of UWB. The "time correction" factor eliminates this effect from the final double difference measurements that are used to compute the statistics.

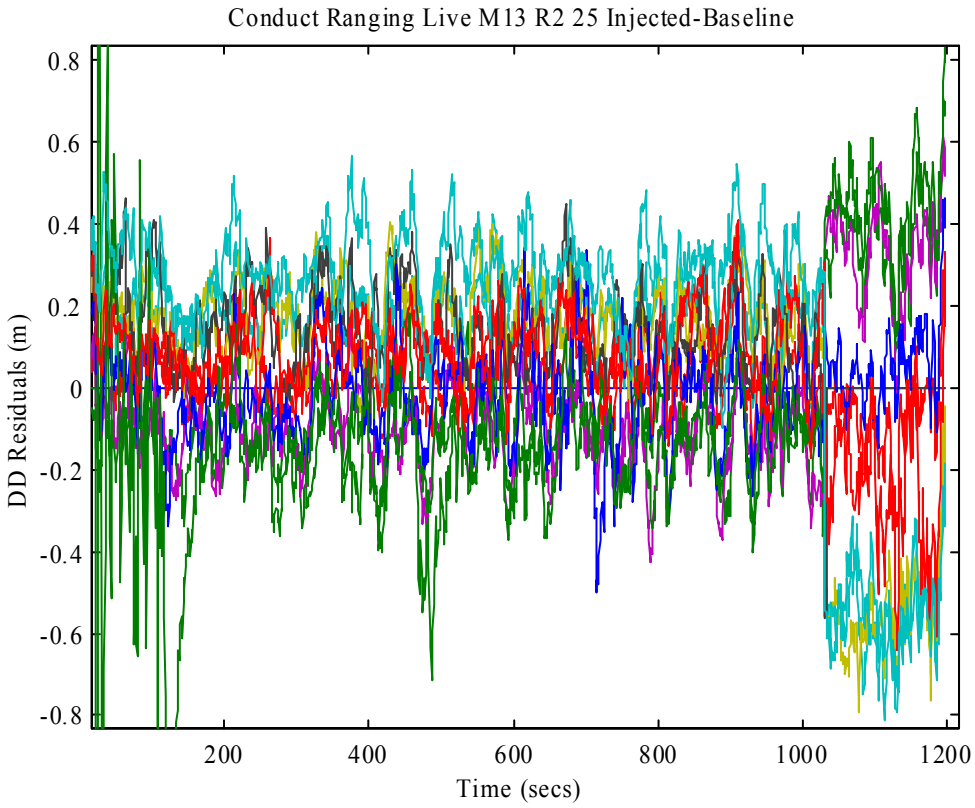

Figure C-9 Double Difference Residuals

Figure C-10 shows the difference in the reported clock biases between the receiver during the injected and baseline experiments. These data correspond to the Mode 13, live sky, 60-dB attenuation, Ashtech Z-12 experiments. Note that although the double differences are formed using measurements from the same receiver, the receiver for the injected and baseline experiments are run at different times. Therefore, the clock biases for the separate injected and baseline experiments corresponding to a particular mode/sky/attenuation are generally different. Reference section C.2.4, the difference in clock biases between the receiver in the baseline and injected experiment is used to determine the time correction.

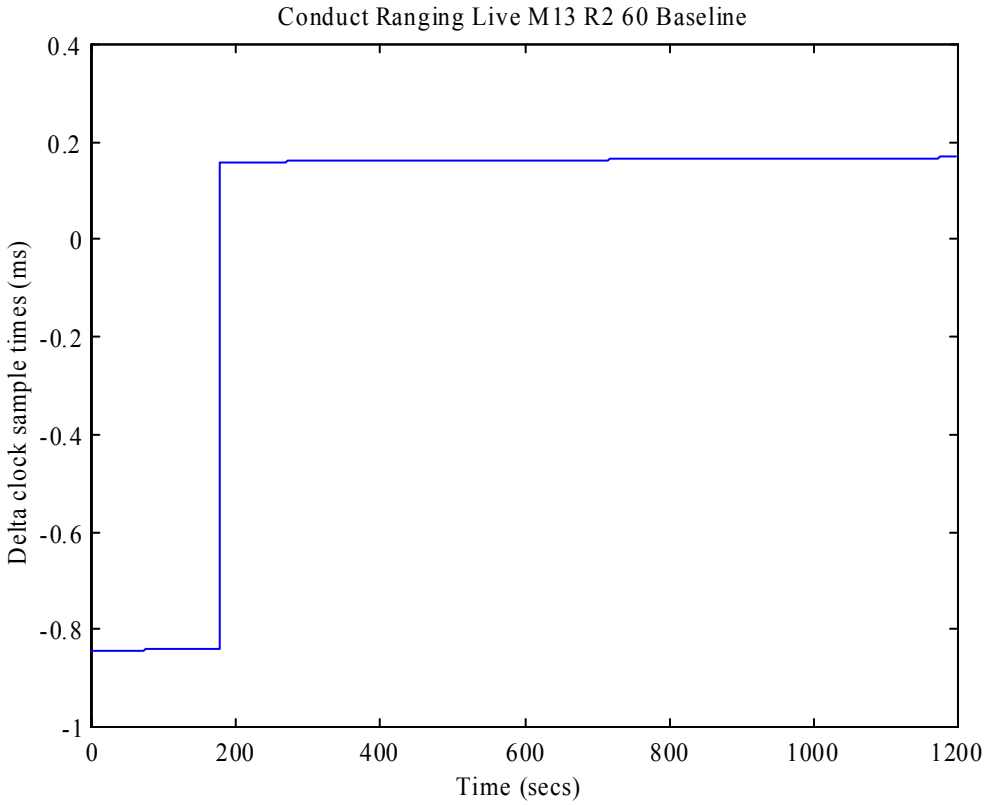

Figure C-10 Ashtech Z-12 Clock Biases

Figure C-11 shows the time corrections corresponding to the data presented in Figures C-8 and C-9. The discontinuity visible at t=1000 seconds is due to the introduction of the leap millisecond. The single discontinuity visible at t=50 seconds is due to a satellite acquisition. The double difference prior to that point was not being used to compute the statistics and no time correction was computed.

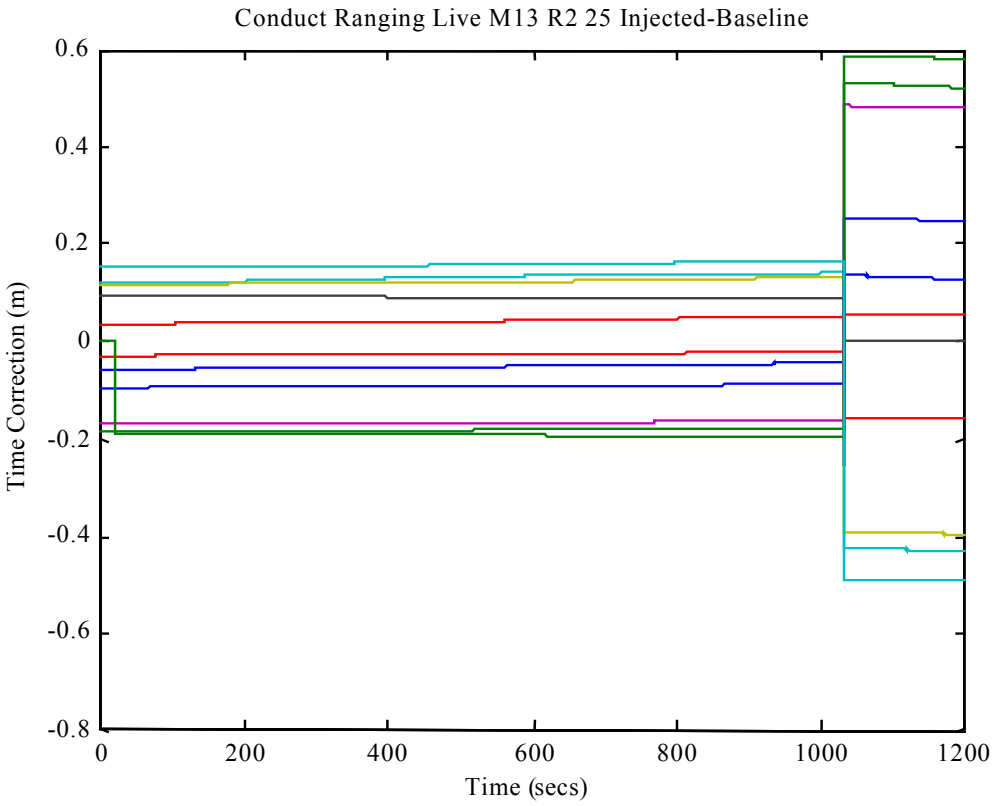

Figure C-11 Time Correction

Figure C-12 shows the final results for the Mode 13, live sky, Ashtech Z-12 experiment. Indicated in the plot is the mean and standard deviation of all the double differences for each attenuation level. The mean is quite small (a few centimeters) over all attenuations, and could be attributed to possible inconsistencies in the GPS simulator set-up. These results indicate that UWB did not induce a systematic receiver tracking error. The plot shows that the receiver noise increased as the attenuation of the UWB signal was reduced. The fact that the noise level at 12 dB is less then that at 14 dB is a statistical aberration. The receiver was having trouble tracking and acquiring satellites at these attenuation levels, and this impacted the computed statistics. The absence of data indicates that at attenuations below 10 dB no data were present to analyze.

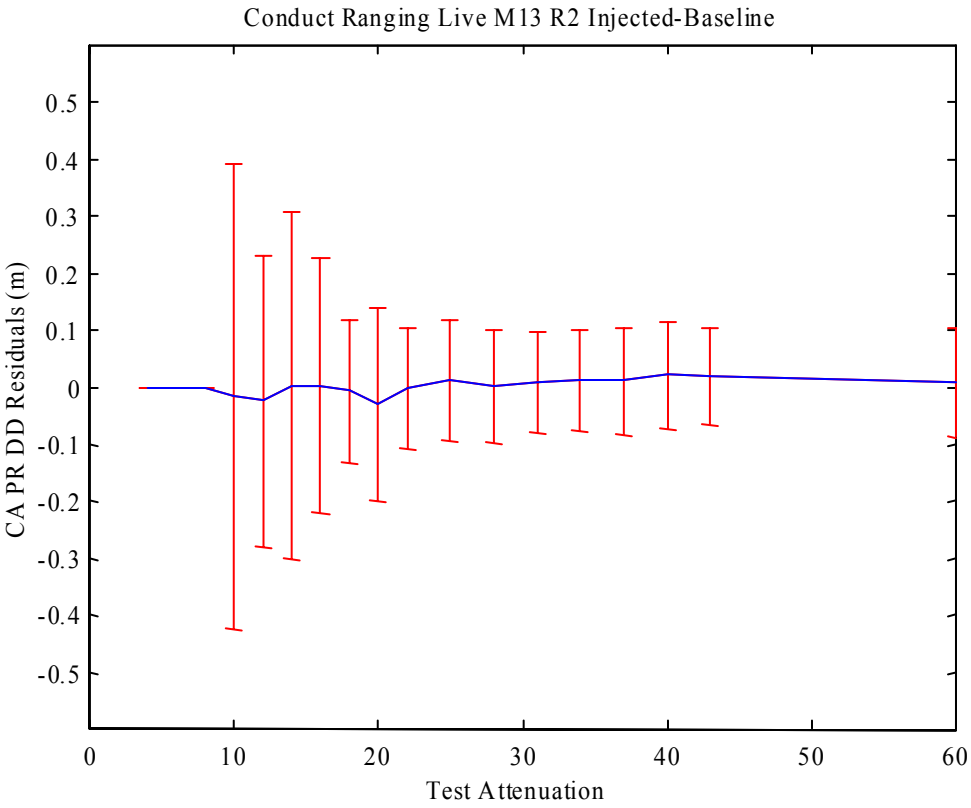

Figure C-12 Conducted Ranging Results

C.3 Receiver Code Noise Processing

This section describes the processing required to derive the receiver code noise from the experimental data. The data presented in this section were generated with the Ashtech Z-12 receiver. The methodology described here was applied to all the experimental data.

C.3.1 Receiver Code Noise MOP

The receiver noise MOP provides a measure of the following: The *relative* noise ratio of a receiver undergoing injected UWB to the same receiver under baseline conditions (e.g., no injected UWB).

For purposes of this section, define the code and carrier phase [Reference (22)] measurements as

$$\rho_i(\tau) = \rho_{iT} + \varepsilon + I + \upsilon_{\rho i}$$
$$\phi_i(\tau) = \rho_{iT} + \varepsilon - I + N + \upsilon_{\phi i}$$

where ρ_i = measured pseudorange to satellite i, ϕ_i = integrated carrier phase measurement for satellite i, ρ_{iT} = true pseudorange (range plus receiver clock), ε = measurement errors exclusive of ionosphere, N = integer ambiguity, I = ionospheric error, $\upsilon_{\rho i}$ = code noise, $\upsilon_{\phi i}$ =carrier noise. In these equations, all of the quantities are expressed in equivalent range units.

The equations express the fact that the ionosphere induces a group delay and a carrier advance. This is typically referred to as code-carrier divergence. The code minus carrier measurement is then given by

$$\rho_i(\tau) - \phi_i(\tau) = 2I - N + \upsilon_{\rho i} - \upsilon_{\phi i}$$

The usual assumption is that the code noise is significantly larger then the carrier noise. Therefore, a standard approach to measuring the code noise is to perform the following:

1. Compute the code minus carrier measurement for each GPS satellite that was tracked over the duration of the experiment.

2. Detrend each satellite's data to remove the integer ambiguity and effects of the code-carrier divergence.

3. Compute the statistics of the resulting measurements to generate the standard deviation of the code noise over the entire experiment. The standard deviation is generated using the data from every satellite that was tracked.

This was done for each receiver/sky level/attenuation level/mode, as well as for the baseline experiment wherein the receiver operated under non-injected (no UWB) conditions. The receiver code noise MOP was then defined as the ratio of the noise of the receiver under injected conditions to the noise of the receiver under baseline conditions. The MOP is given by

$$MOP = \frac{\sigma|_{injected}}{\sigma|_{baseline}}$$

C.3.2 Experimental Setup Limitations

The receivers used in this study did not output raw (unsmoothed) pseudorange measurements. Therefore, the receiver noise MOP was computed using the smoothed code measurements. The utility of this measure is not greatly affected because the code noise for the injected experiment is normalized with respect to the code noise for the baseline (e.g., no UWB) experiment.

C.3.3 Code Minus Carrier Detrending

In order to detrend the measured code minus carrier measurement, a polynomial (1st or 2nd order) was fit to the code minus carrier data for a given receiver/sky/attenuation/mode (as well as baseline cases). The polynomial fit was then subtracted from the code minus carrier measurement, and the statistics of the resulting data was computed to yield the code noise.

This algorithm was complicated by several factors.

- The introduction of the leap millisecond by the Ashtech Z-12 results in a discontinuity in the clock bias. However, the change in the clock bias as measured by the code is different then that as measured by the carrier. This may be explicitly accounted for so that the navigation solution is not affected, but the relevant result is that the observed code minus carrier undergoes a large jump at that point.

- The acquisition or loss of a satellite during a 20-minute data run causes jumps in the code minus carrier (since it is set to zero when the satellite is not being tracked).

- The smoothed code filter transients during a satellite acquisition need to be excluded from the statistic.

These effects typically make it impossible to fit a single polynomial to each satellite's data over the entire 20-minute data window. Therefore, logic was built into the software to detect occurrences of the events described, and separate polynomials were fit over the contiguous data segments between these events.

C.3.4 Code Minus Carrier Experimental Data

Figures C-13 and C-14 show the unedited (prior to detrending) code minus carrier measurement (top subplot), and the resulting measurement after detrending (bottom subplot) for both an injected and baseline experiment. These data correspond to the live sky/31 dB attenuation/mode 13/Ashtech receiver runs. Clearly visible in both figures is a discontinuity in the measurement due to a "leap millisecond." The integer ambiguity is not included in the unedited code minus carrier difference (top subplot), which results in the large discrepancies in the measurements. Detrending eliminates these discrepancies.

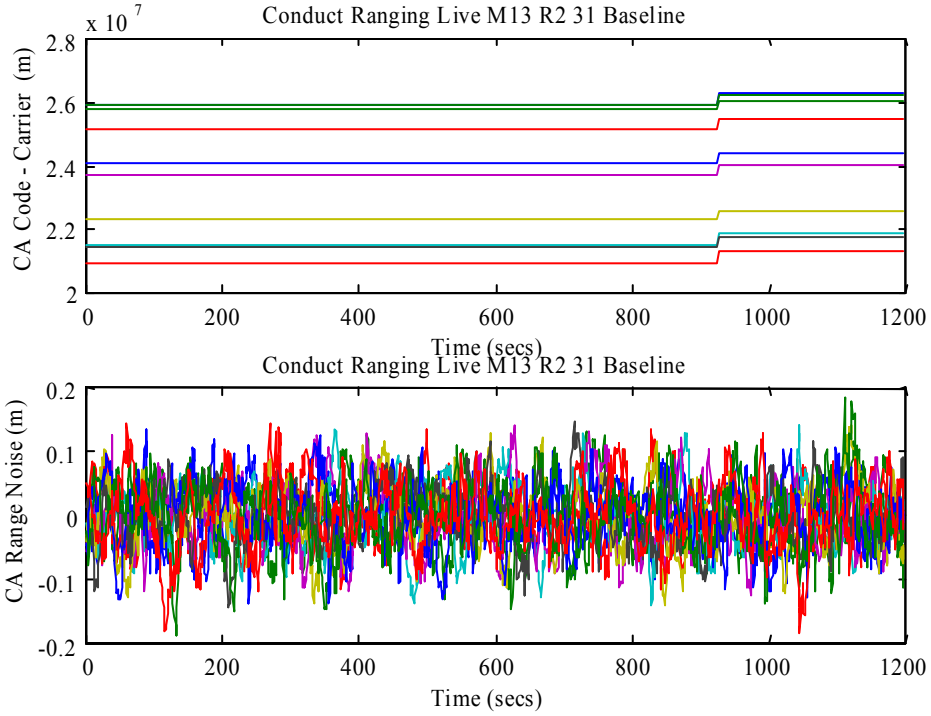

Figure C-13 Baseline Code Noise

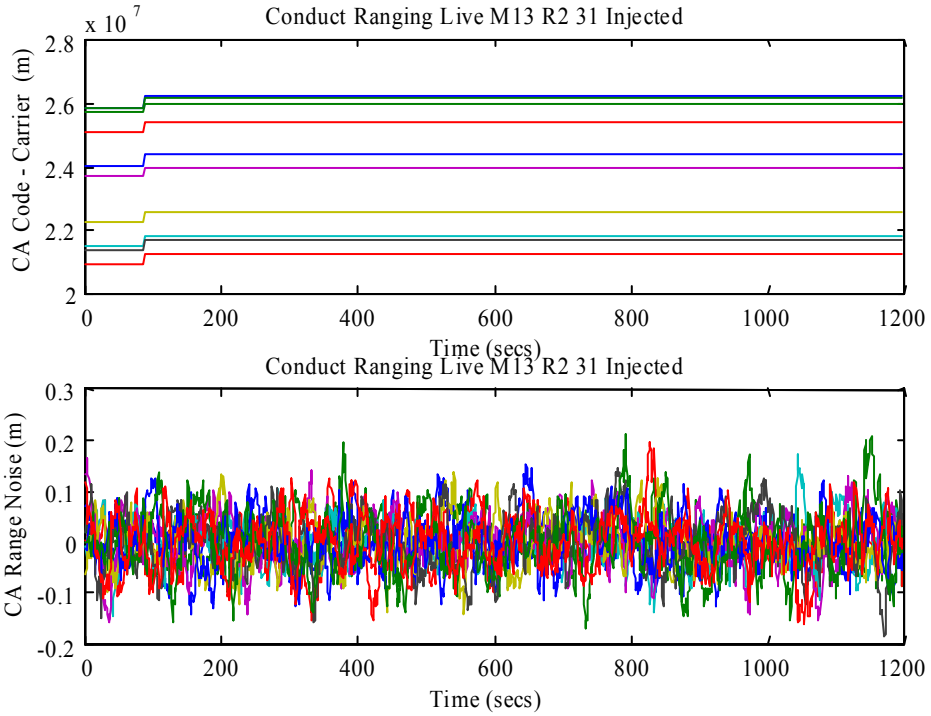

Figure C-14 Injected Code Noise

Figure C-15 shows the code minus carrier measurement prior to detrending. For clarity, the carrier phase ambiguity has been removed. Note the clear trend in the data over the 20-minute interval. This is a result of the code-carrier divergence induced by the ionosphere. The noise that is visible is clearly not white, and is a result of the filter used to smooth the code.

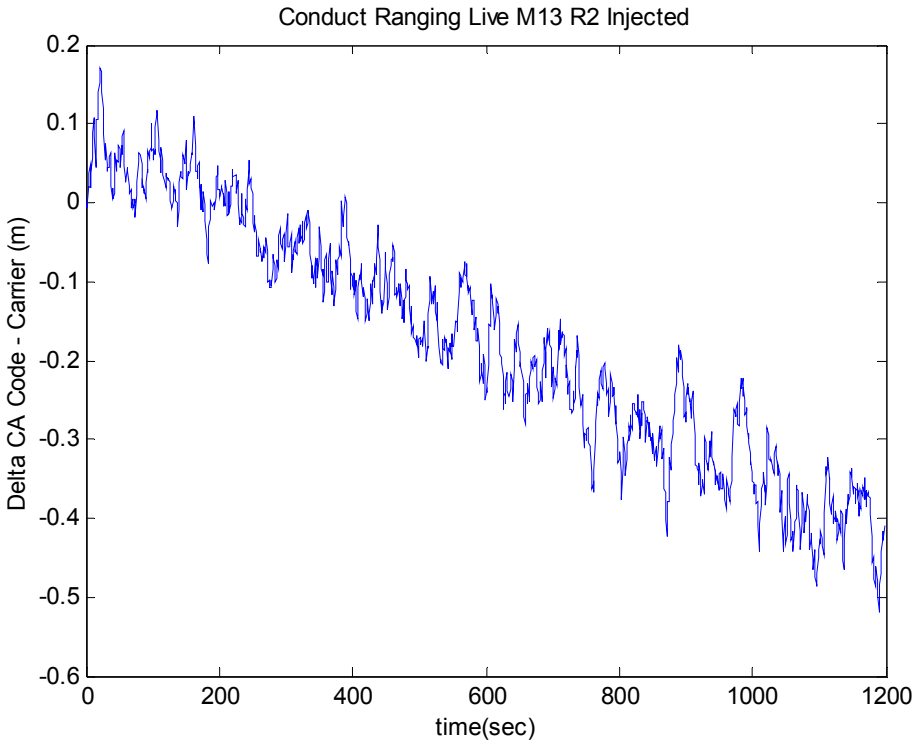

Figure C-15 Code minus Carrier

Figure C-16 shows the computed noise levels for the baseline experiment corresponding to Mode 13/live sky/Ashtech experiments. As the receiver in the baseline experiments did not receive any injected UWB signal, the noise level is effectively constant across the entire experiment, as would be expected. The absence of statistics for dB levels below 10 dB indicates an absence of data to analyze.

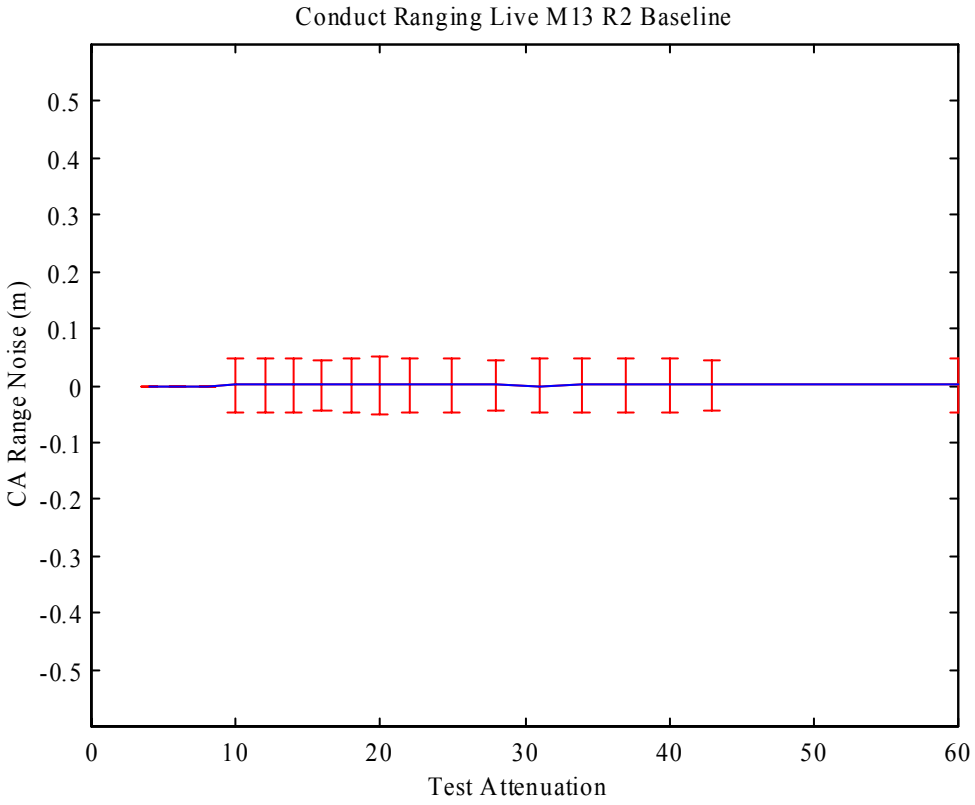

Figure C-16 Baseline Noise Results

Figure C-17 show the computed noise levels for the injected experiment (Mode 13/Live Sky/Ashtech). The noise is constant at the higher attenuations, indicating that the UWB signal had no impact on the receiver performance. As the attenuation level decreases, the receiver noise becomes larger as expected. The fact that the noise level at 12 dB is less then that at 14 dB attenuation is a statistical aberration. The receiver was having trouble tracking and acquiring satellites at these attenuation levels, and this impacted the computed statistics.

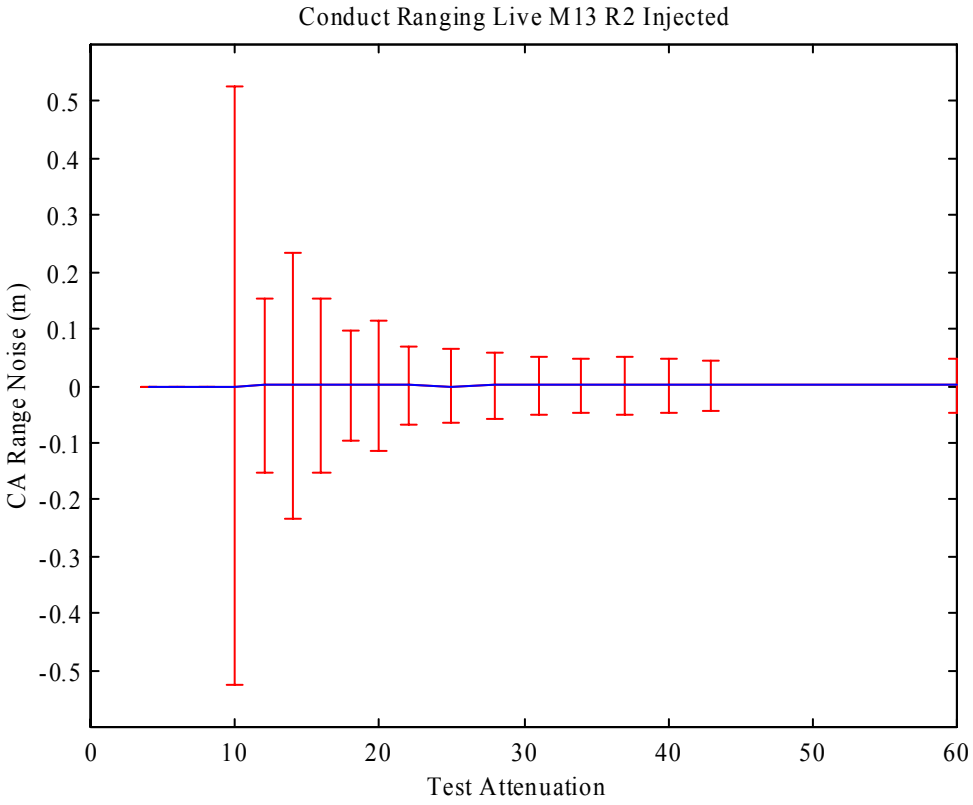

Figure C-17 Injected Noise Results

Figure C-18 shows the ratio of the receiver noise for the injected experiment versus the baseline experiment across all attenuations. The ratio is unity for high attenuation levels as would be expected, and increases as the attenuation level decreases. The data here indicate that the receiver suffered some degradation as the attenuation dropped below 30 dB. See the main report for a discussion of equivalent range.

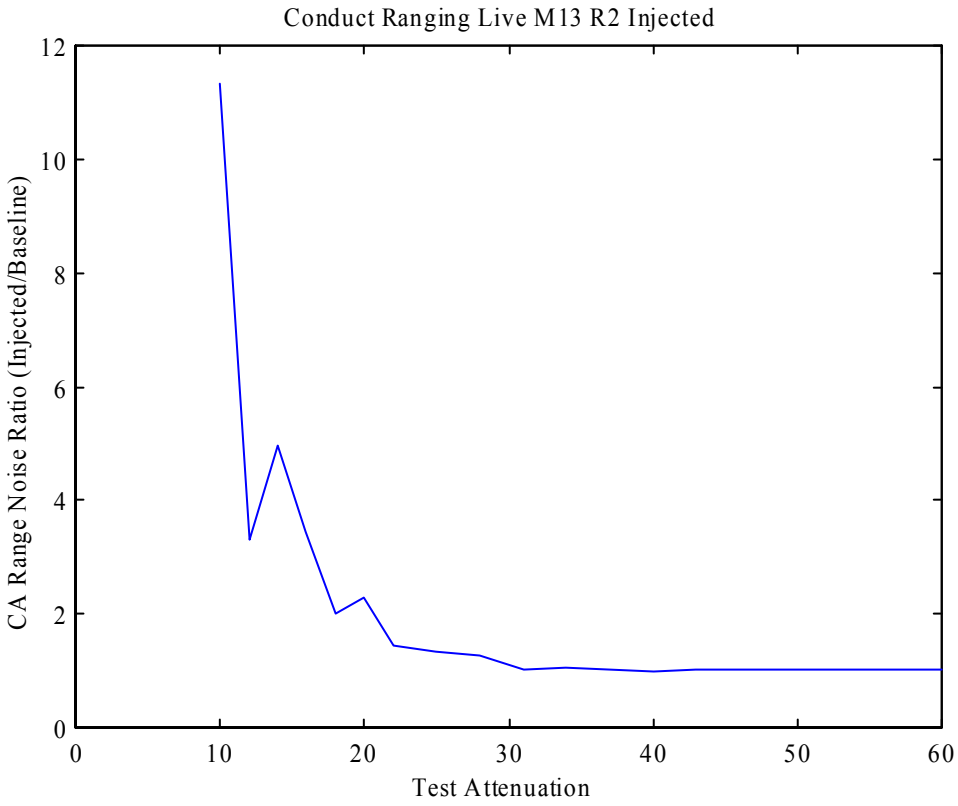

Figure C-18 Receiver Noise Ratio

APPENDIX D
NAVIGATION MESSAGE RECOVERY

D.0 Introduction

This appendix describes the results of the navigation message recovery analysis. The intent of the message recovery analysis was to determine the impact of ultra-wideband (UWB) injection on the ability of the receiver to recover the message bits. The navigation message is critical to accurate measurement and position determination.

D.1 Message Recovery

An analysis of the message bit recovery was performed for both the Ashtech and NovAtel receivers. Verification of the message recovery was done in three ways: (1) file verification, (2) orbital parameters or satellite position comparisons with a reliable source or from a baseline test, (3) receiver renavigation. All files were checked for completeness (i.e. parity checksum). Comparisons of the data files generated by the receivers in the baseline and injected experiment were performed. Verification methods (2) and (3) are described in Appendix E. The receivers analyzed in this study output subsets of the entire navigation message in receiver proprietary formats. These records were recorded as part of the experiments performed by Applied Research Laboratories, University of Texas (ARL:UT). This offered a limited opportunity to analyze the impact of UWB on the ability of the receiver to recover the navigation message bits. Statistics on bit error rates could not be computed.

D.1.1 Ashtech Receivers

The binary SNV records containing the orbital ephemeris parameters were output by the Ashtech receivers and stored during the experimental runs. Comparisons of these records for all conducted injected and baseline tests were performed. Injected and baseline orbital parameters were compared by matching the same week number, time-of-ephemeris (TOE), and satellite pseudorandom number (PRN). The injected and baseline parameters agreed exactly for all cases.

D.1.2 NovAtel Receivers

The ephemeris message (subframes 1-3) were recorded in hexadecimal 60-character length records (REPA/B format) during the experiments performed by ARL:UT. The data records for both the injected and baseline experiments were compared and were found to agree except for a few cases. However, it is likely that the inconsistency in the stored message files was the result of the Novatel implementation as well as the test setup, and not UWB injection. In particular, the Novatel did not output ephemeris data whose TOE was stale and/or it only reported ephemeris data for all satellites nominally every 2 hours and did not duplicate those

already reported. This caused some disagreement in the output records at the start of each experiment, during the period of time where the attenuation of the UWB signal was at its highest.

D.2 Conclusions

Verification of the navigation message recovery was done in three ways. All methods show no indication that the message was impacted by UWB injection. Test set-up limitations prevented a though analysis of the resultant bit error rates due to not having access to the entire navigation message.

APPENDIX E
TEST DATA UNDERSTANDING

E.0 Introduction

The Global Positioning System (GPS) is very complex and so is the setup and operation of the GPS simulators and receivers used in the Applied Research Laboratory, University of Texas (ARL:UT) testing. These devices can be operated under numerous parameters, modes and conditions, which affect the resultant data. The understanding of the simulators' and receivers' operation and their settings for incorporating errors into the measurements is critical to understanding degradations in the GPS receiver performance – i.e., are effects simulator-induced or caused by the UWB signals. In order to ensure confidence in the results contained in this report, the data were thoroughly checked as part of the analysis.

This appendix has three primary topics: (1) simulator test understanding, (2) analyses to validate the conducted and radiated test data, and (3) conclusions. Section E.1 describes briefly our understandings of the Global Simulation System (GSS) simulators used during the conducted ranging and conducted acquisition tests. Section E.2 describes the various approaches to confirm the quality and accuracy of the data, and Section E.3 provides the major conclusions that resulted from thorough investigation of the ARL:UT test setup and data collected.

E.1 Simulator Test Understanding

The "Conducted" testing by ARL:UT was performed in a laboratory environment using an instrumented radio frequency (RF) network with a GPS simulator providing the "satellite" signals processed by the receivers under test. This testing was actually carried out at two locations, one at ARL:UT in Austin Texas and the other at Holloman AFB, New Mexico. Testing of receivers 1 through 4 was conducted at Holloman AFB using a 12-channel GSS 4760 GPS simulator. Testing at ARL:UT used a 10-channel GSS 2760 GPS simulator to test receivers 6 and 7. The input to the GPS receiver was hardwired and consists of the sum of the RF output from a GPS simulator and the output signal from an ultra-wideband (UWB) device. Each test was run at a fixed signal ratio for 20-minuite intervals during which time the receiver navigation message was captured. The "Radiated" testing was conducted outside near ARL:UT facilities. In the radiated tests, the input to the GPS receiver was the real GPS system signals injected by a UWB device. Each test was run at a fixed range during which time the receiver outputs, including the navigation message, were captured. GPS ephemeris and almanac parameters are well defined in Reference (23). An objective of the ARL:UT testing was to set up the simulators to simulate the same date and time and satellite constellation as existed for the live sky radiated testing. This would allow the radiated and conducted test results to be compared. However, differences in the date and time of the test and ephemeris cannot be compared within reasonable precision. Chapter 4 has more details about the test collection procedure and data.

Some important facts about the simulator are summarized below. Conclusions drawn from the analyses described in the next section confirm these simulator understandings. A partial list of the GPS 4760 simulator input files and settings are shown in Table E-1. The simulator settings were not all set to default settings as indicated below and in Reference (16). In some cases, not all information was known about the test, so independent validation was necessary. These input files and settings will be referenced throughout this section.

Table E-1 GSS 4760 Simulator Inputs and Settings

File type: GPS_CONSTELLATION	File name: AUSTIN_WEEK_49.NAV_SAT;7
Satellite Enable	= 28
Obscuration Angle	= 0 degrees
Obscuration Type	= Earth Tangent
Satellite Selection Sampling Interval	= 6s (default 30 seconds)
Satellite Selection Criterion	= PDOP
Satellite Selection Sampling Interval	= 6s (default 30 seconds)
Diverge Ephemeris	= Enabled (default Disabled)
Diverge Clocks	= Enabled (default Disabled)
GPS to UTC Time Difference – Delta tls	= 13 sec (default 0 seconds)
Pseudorange Logging Rate	= 1.0 seconds
Clock Noise	= Disabled
Update Interval for Clock Noise	= 60 (100 msec ticks)
Surface Refractivity Index @ msl	= ? (default 324.8)
Signal Strength	= Modeled
L1 - L2 Delay	= Modeled
Tropospheric Delay	= STANAG
File type: System Setup	File name: DEF.SETUP;6
L1L2	= yes
Pseudo-Y	= no
File type: Static_Position	File name: AUSTIN_REF_COM;2
File Header	= Holloman
Initial Latitude	= North 30 degrees 23.045468817 minutes
Initial Longitude	= West 97 degrees 43.6368709832 minutes
Height	= 207.601948868 m
File type: Antenna_Pattern	File name: Default.Ant;

The simulator was set in a static mode (File type: Static_Position and File name: AUSTIN_REF_COM;2) by providing fixed Latitude-Longitude-Height (LLH) coordinates. Visible satellites set are calculated for elevations above the horizon (Satellites Enable=28, Obscuration Angle=0 and Obscuration Type=Earth Tangent) using a spherical earth model from Almanac data, date and time reference, antenna aperture angle and positional data. The best selection of satellites are chosen with the Satellite Selection Criteria=PDOP. The satellite signal power levels will vary slightly per satellite depending on elevation and is based on the modeling

(Signal Strength=Modeled). No antenna gain pattern file was used, so no antenna effects were simulated. Selective availability was turned off for the conducted (Pseudo-Y=no) and radiated tests. No external reference oscillator or timing sources were used.

The simulator produces Almanac data and Ephemeris data from a Constellation File and a start date and time for all specified satellites. The Constellation File was created with default satellite constellations (orbital parameters) and was determined to be closer to GPS week-49 despite the test day being in the middle of week-48 (i.e., AUSTIN_WEEK_49.NAV_SAT;7). The almanac and ephemeris data were derived from the orbit data in the GPS Constellation file by scaling appropriately and modifying the time dependent terms (Longitude of Ascending Node, Mean Anomaly and Inclination) for the difference between the almanac reference time and the orbit reference time. The harmonic correction order and timing group delay (TGD) terms are zero in the simulated ephemeris and differs significantly from Broadcast (BC) for the simulated test day (see Subsection E.2.1).

Relative dynamics, navigation data, signal level, L1/L2 delays, antenna arrival angle data, and other scenarios source information were produced to drive the RF Signal Generator based on all the above information. The ephemeris data may change throughout the simulation, which causes the ephemeris and clock data reference times to change; hence the time-dependent parameters will change. The time dependent terms are modified accordingly whenever TOE (TOC) changes. The simulator ephemeris was shown in Subsections E.2.1 to have time delays, therefore the measurements are not consistent with measurements generated from other ephemeris sources for that day (i.e., live testing). This means simulator and live testing can not be compared within any reasonable precision unless these errors are estimated. Section E.2.2 estimates and corrects for these timing delays, however the ephemeris and clock errors were undeterminably perturbed to generate measurements with errors other than timing delays (i.e., Diverge Ephemeris and Clocks). Diverge Ephemeris and Diverge Clock are Enabled so errors are applied to the ephemeris parameters to simulate degradation in ranging accuracy due to time since upload and inherent system errors. The parameters perturbed are Mean Anomaly, Longitude of Ascending Node and Inclination. In addition, the Mean Motion Difference, Rate of Right Ascension and Inclination Rate are perturbed in order to effect a smooth transition between data sets. The Diverge Ephemeris and Diverge Clock errors are unknown and uncorrectable, so receiver position errors will be evident, Subsection E.2.2.

The pseudorange and pseudorange rate are calculated by taking an estimate of signal transit time from the satellite to the receiver and calculating the corresponding satellite position at time of transmission. The satellite-receiver range is calculated and converted to a corresponding signal propagation time. Calculated troposphere and ionosphere delays are added to this to give a total signal transit time, which is compared with the original estimate. The original estimate is adjusted and the calculation repeated until the solution converges to the required accuracy.

Software was developed to understand the simulator outputs (i.e., time, site location, satellite position, azimuth, elevation, slant range, and pseudorange) and to compute true and predicted slant ranges. Radiated pseudorange measurements could be compared to predicted

slant ranges. The simulator's pseudorange measurements includes L1 and L2 ionosphere and troposphere delays, relativistic clock error, satellite clock bias and drift (provided on the navigation message), satellite ephemeris and clock errors (noise and divergence terms). The pseudorange errors would include any of the terms above not accounted for by the receiver. The pseudorange errors are independently determined by re-navigating the receiver, Subsection E.2.2. The receivers presumably were set in their default parameter setting with the data output rate at 1-Hz rate. More information can be found in the GSS Simulator Manuals, Reference (24).

E.2 Data Validation Analyses

This section summarizes analyses performed in support of understanding the test setup and evaluating the data recorded. The analyses are addressed in two sections: (1) Ephemeris Investigations (Subsection E.2.1), and (2) Receiver Re-navigation (Subsection E.2.2)

E.2.1 Ephemeris Investigations

Investigations include comparisons of satellite position, visibility, elevation and ground track time delay for radiated and conducted recorded messages and post-processed ephemerides. These analyses check the data quality, consistency, and simulated generation of the collected ephemeris data.

Ephemeris data collected during the conducted tests by the Ashtech and Novatel receivers were evaluated by performing receiver-to-receiver and injected-to-baseline comparisons. Conducted test ephemeris data were compared to reliable post-processing ephemeris sources to further understand the origin of the data. Also, Radiated test ephemeris data were compared to reliable post-processing ephemeris sources to verify data quality. United States Coast Guard (USCG) provides almanac parameters every week per satellite in YUMA format. International GPS Service for Geodynamics Service (IGS)/Crustal Dynamics Data Information System (CDDIS) and National Geodetic Survey (NGS)/Continuously Operating Reference Station (CORS) provide BC parameters in Receiver Independent Exchange Format (RINEX) format [Reference (25)]. National Imagery and Mapping Agency (NIMA) and NGS provide precise satellite position, velocity and clock data for ECEF coordinates in SP3 format. These post-processed sources were compared to one another as a reference. Satellite positions and velocities are computed for ephemeris sources containing orbital parameters based on Reference (23). A few examples of ephemeris comparisons are plotted showing RSS satellite position and satellite clock bias differences in ECEF coordinates. Satellite velocity and clock drift differences are not shown.

Post-processed sources of ephemeris products for the conducted test day (26 July 2000) are consistent and compare to the expected uncertainties. NGS/CORS BC and NIMA precise ephemeris agree nominally within 4 m, 0.001 m/sec and 1 nsec in position, velocity and clock bias, respectively. Satellite positions computed from ephemeris (orbital parameters) are good for only ~4 hours and the reference is at the center of the 4 hours. BC accuracy has improved over time, especially due to more frequent updates (every 1 hour rather than every 2 hours); however, the position degrades rapidly beyond 1½ hours rather than 2 hours from the time of interest.

CORS BC and week 48 almanac (YUMA48) almanac ephemeris compare within thousands of meters in position and a clock bias on the order of μsec.

The simulated ephemerides recorded by the various receivers are consistent as expected due to the fact the receivers are receiving the same RF signal. There were some discrepancies among all the ephemeris sources regarding PRNs 16 and 18 data. CORS, NIMA, and NGS sources believed PRN 18 ephemeris was bad (not included on the files) and PRN 16 data were good for that day. YUMA48 and week-49 almanac (YUMA49) had both satellite ephemerides marked bad, which means anytime in the week those satellites were bad. The "Health" flag for PRN 18 was marked unhealthy. Receivers handled the satellites that were marked unhealthy differently. The Novatel did not output ephemeris for satellites PRN 16 and 18, whereas the Ashtech receivers marked the ephemeris unhealthy. There were few occurrences due to precision issues where some parameters were slightly different among receivers causing small RSS position differences.

The simulated and real messages are not the same and yield significant position differences. CORS BC and simulated BC (Ashtech Z-Sensor) position differences are shown in Figure E-1. A ½ hour time delay was artificially inducted when computing the simulator satellite positions producing closer agreement to the CORS BC, Figure E-2. Simulated BC comparisons to YUMA48 (Figures E-3-E-4) and YUMA49 (Figures E-5 and E-6) show simulated BC agrees better with YUMA49 than with YUMA48. A satellite ground-track advances about 4 minute/day so it is reasonable that in a week the time delay is 28 minutes or around ½ hr.

Satellite elevation and visibility for conducted and radiated tests were compared over various times of interest to baseline or expected values. Satellite visibility was shown for any satellite above zero-degree mask. For conducted tests, receiver-to-receiver and injected-to-baseline comparisons were done to test for consistency. Example plots for a 2-hour span, centered at 6 hours into the day are shown for YUMA49 and simulated BC, Figures E-7 through E-10. They agree exactly, except for PRN 3, which differs by ¼ hour. This supports the fact mentioned above that the simulated ephemeris generation is based on YUMA49. CORS BC and YUMA48 have similar satellite visibility and elevations. The satellite elevations and visibility based on simulated ephemeris do not agree with CORS BC by different time delays and are estimated below.

An investigation on the simulator ephemeris was conducted to determine whether by applying appropriate time delays the simulator (conducted) data and live (radiated) test data could be compared. The simulator generates ephemeris and clock data derived from a Satellite Configuration File. The ephemeris only consists of almanac parameters (no higher order terms) and differs significantly from CORS BC for the same day. A comparison between the simulator and BC ephemeris was made in the HLC-frame in order to estimate any timing delays. Satellite positions were generated in the ECEF-frame, converted to ECI; the ephemeris sources were differenced, and then converted to the HLC-frame. The Long Track component (dL) was used to compute a delta angle (dtheta) by dtheta = dL/A, where A is the semi-major axis. Then a time delay (dt) was determined by dtheta/wdot, where wdot is the satellite's angular velocity.

Uncorrected satellite position differences in the HLC-frame are shown in Figures E-13 through E-15. After a few iterations, these timing delays were estimated (Table E-2 and Figure E-16), and the satellite positions were corrected. The hope was that if all the error was timing differences, then this effect could be accounted for when post-processing and equivalent simulator and live testing could be compared. Figure E-17 shows the remaining error is not due to a timing delay. This confirms that the simulated measurements were perturbed with ephemeris and clock errors other than timing delays.

Table E-2 Timing Corrections

PRN	Timing Delays (seconds)
1	-1213.4
2	-1183.2
3	-0933.5
4	-1248.3
7	-1245.0
8	-1215.3
11	-1225.7
13	-1843.8
15	-1403.9
19	-1227.5
20	-1022.1
26	-1170.8
27	-1297.2
31	-1170.4

Also, satellite visibility for simulated BC was compared to expected values derived from post-processed ephemeris sources to gain understanding of the ephemeris generation. Example plots during a 2-hr span centered at 6 hours and 14 hours into the day are shown in Figures E-8-E-12. Satellite elevations computed from various conducted test ephemerides agree with each other. According to the simulated ephemeris, satellites PRN 1, 3, 15 drop out early and PRN 6, 17, 25, 30 come in late. The Ashtech receivers have a default elevation mask of 10 degrees, which explains some of the discrepancies in satellite tracking between live-sky and minimum power levels. Also, satellite elevation and visibility were compared to expected values to verify radiated tests.

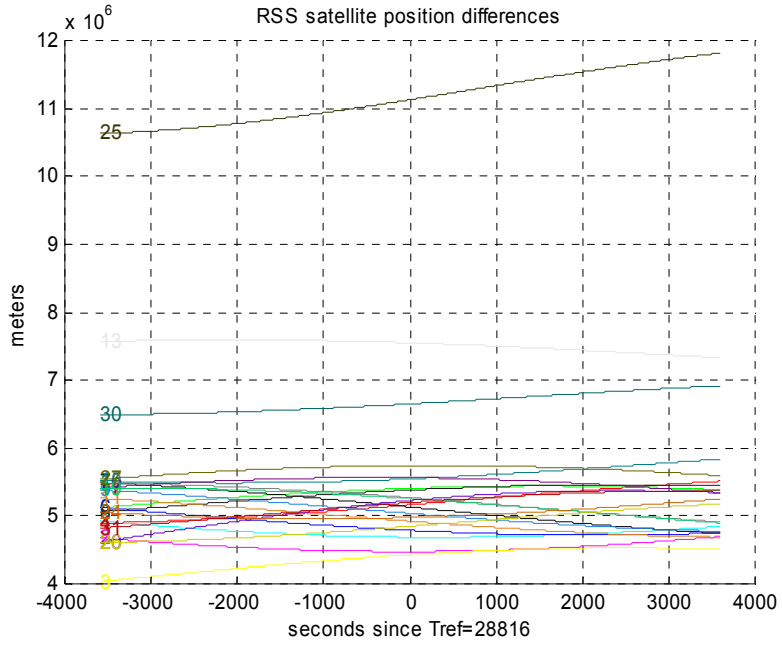

Figure E-1 CORS BC and Simulator Satellite Position Comparisons

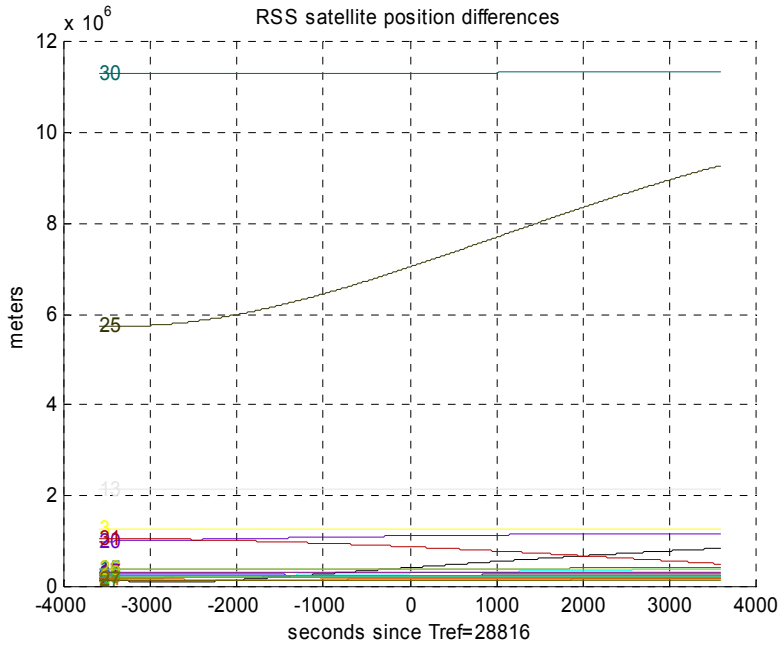

Figure E-2 CORS BC and Simulator Satellite Position with ½ hour Time Delay Comparisons

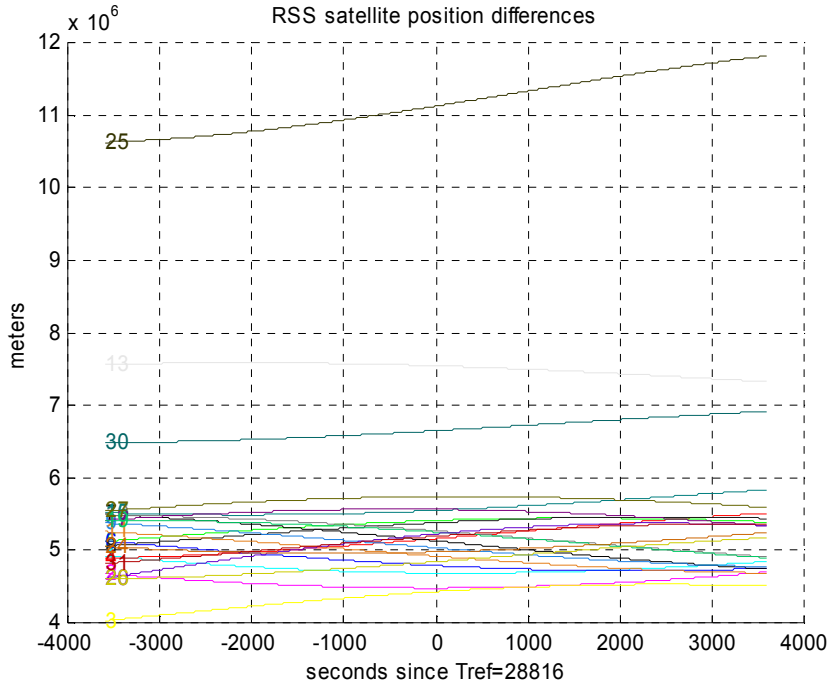

Figure E-3 Simulator BC and YUMA48 Satellite Position Comparisons

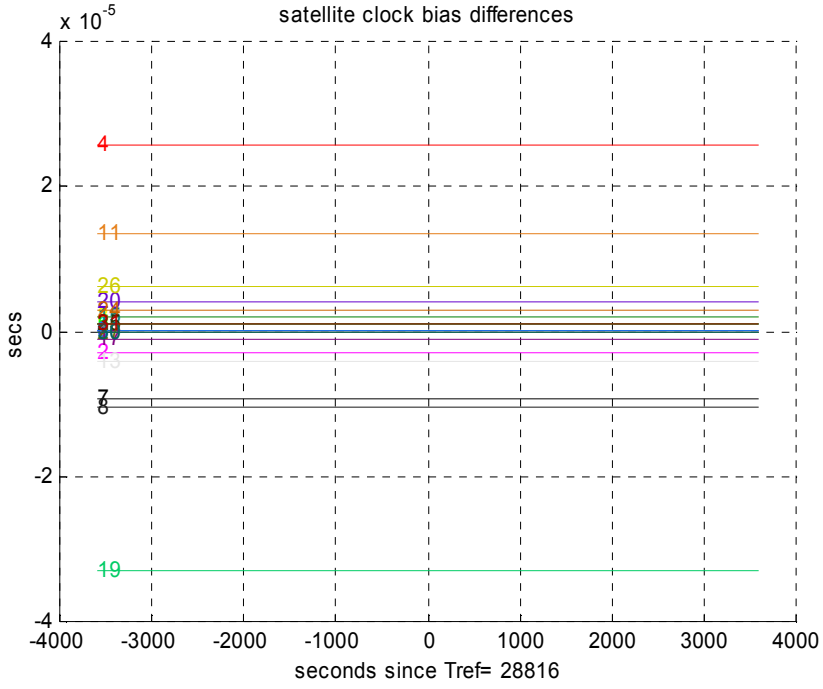

Figure E-4 Simulator BC and YUMA48 Clock Bias Comparisons

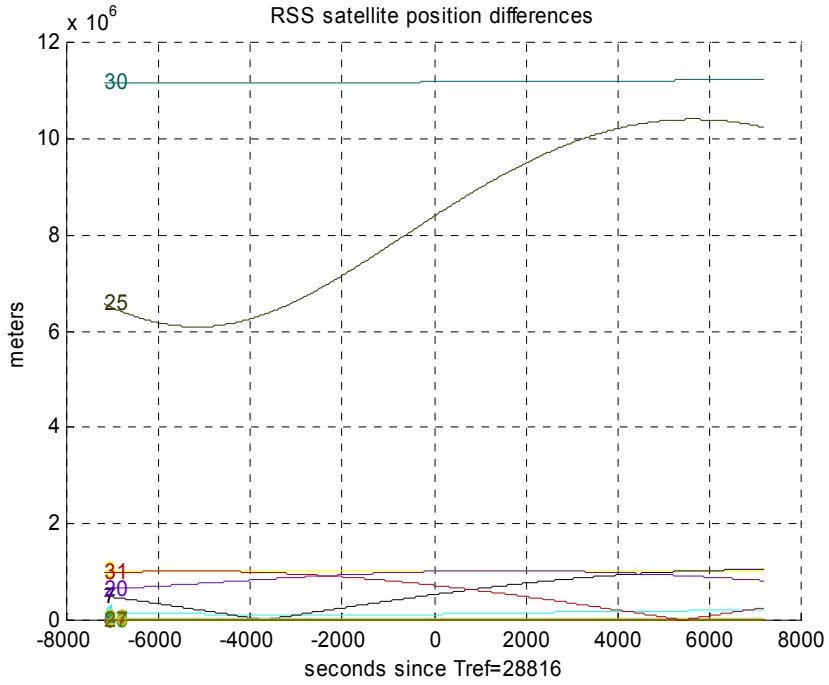

Figure E-5 Simulator BC and YUMA49 Satellite Position Comparisons

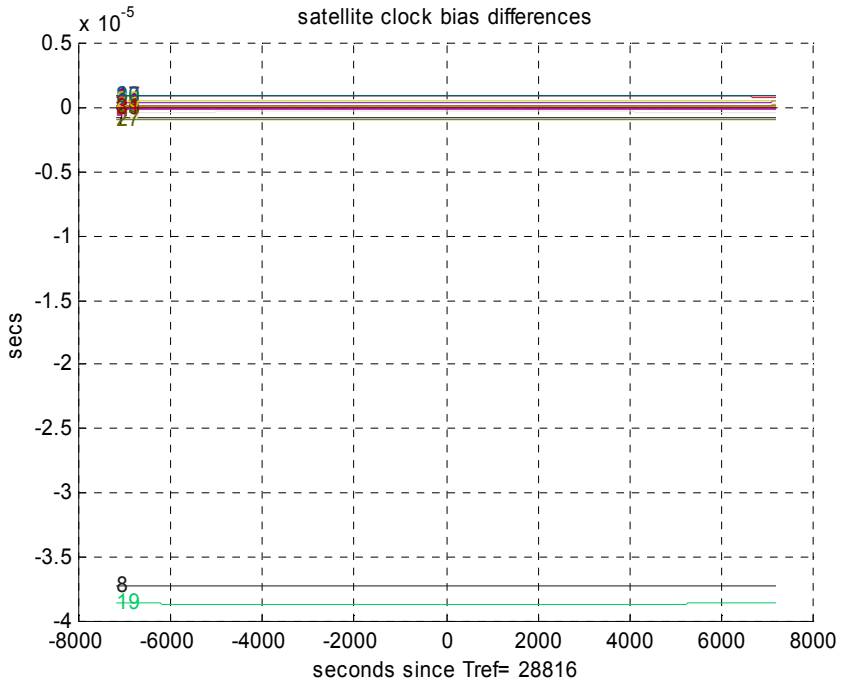

Figure E-6 Simulator BC and YUMA49 Clock Bias Comparisons

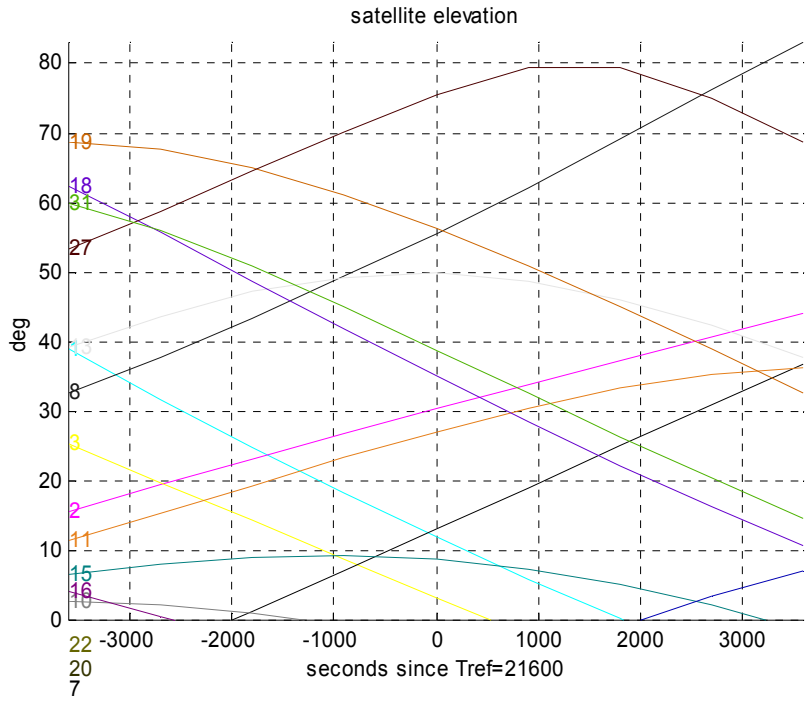

Figure E-7 YUMA49 Satellite Elevations Centered at 6-hour Epoch

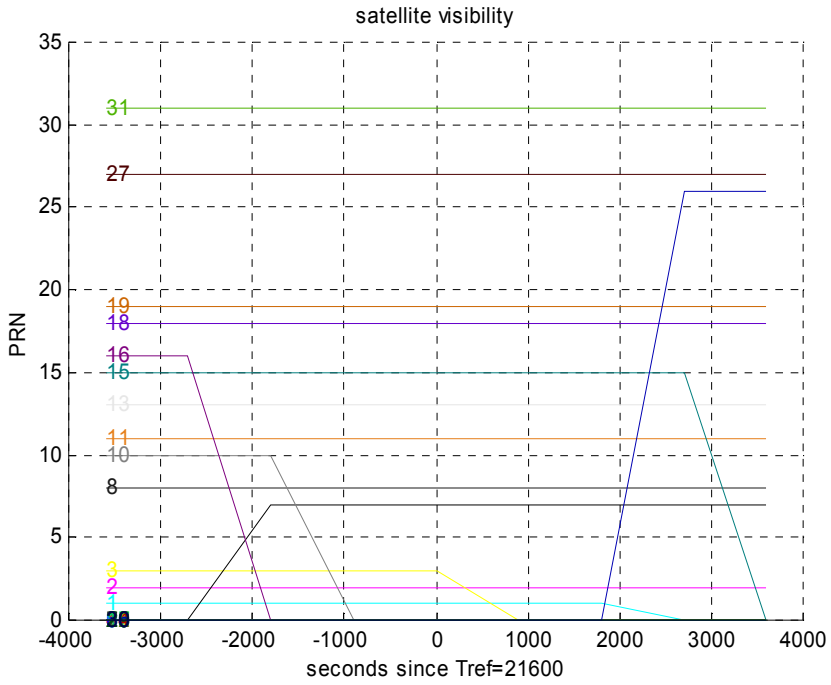

Figure E-8 YUMA49 Satellite Visibility Centered at 6-hour Epoch

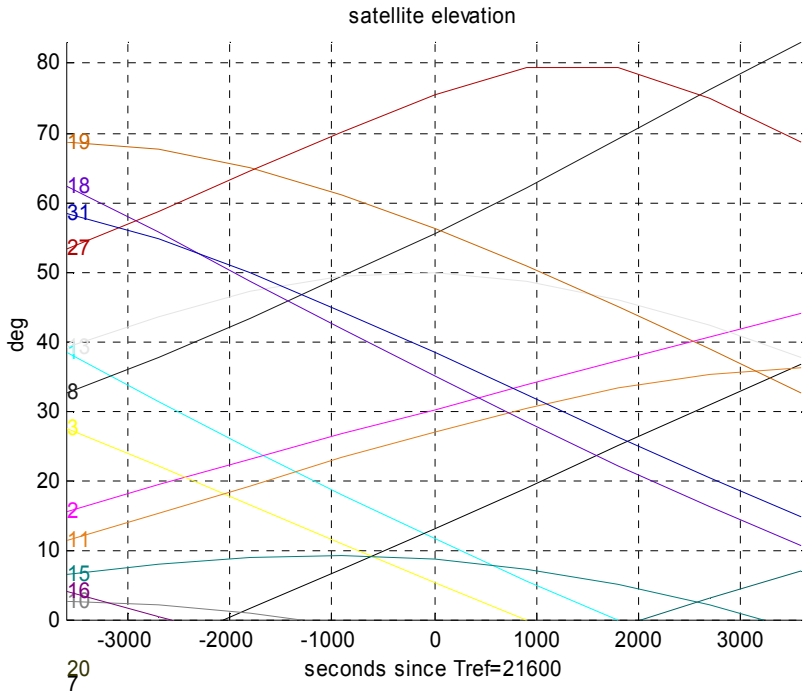

Figure E-9 Simulator Satellite Elevations Centered at 6-hour Epoch

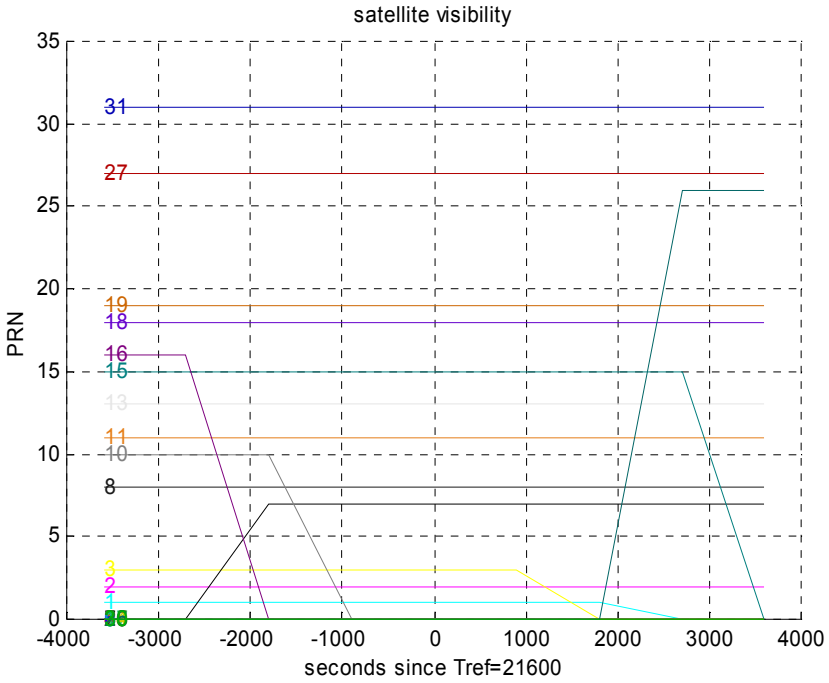

Figure E-10 Simulator Satellite Visibility Centered at 6-hour Epoch

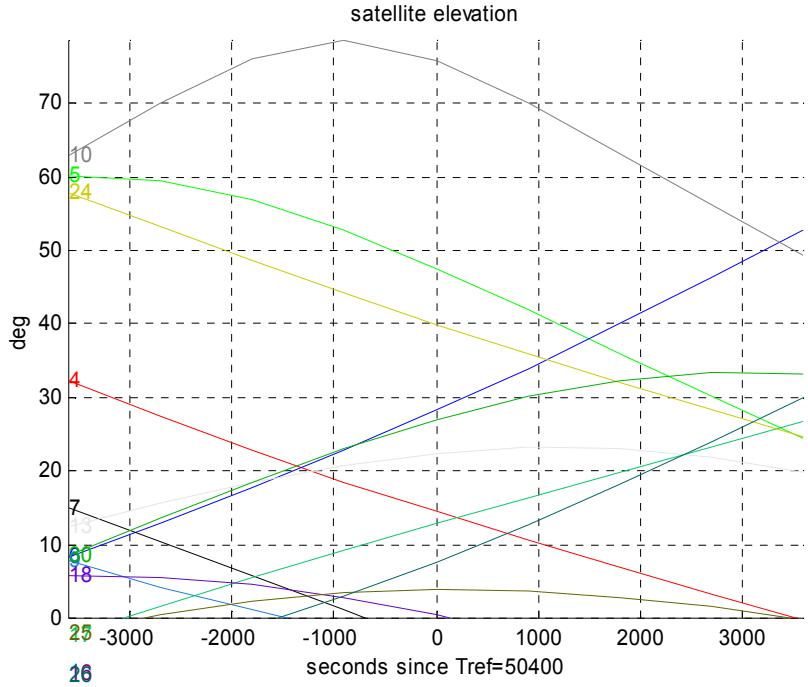

Figure E-11 Simulator Satellite Elevations Centered at 14-hour Epoch

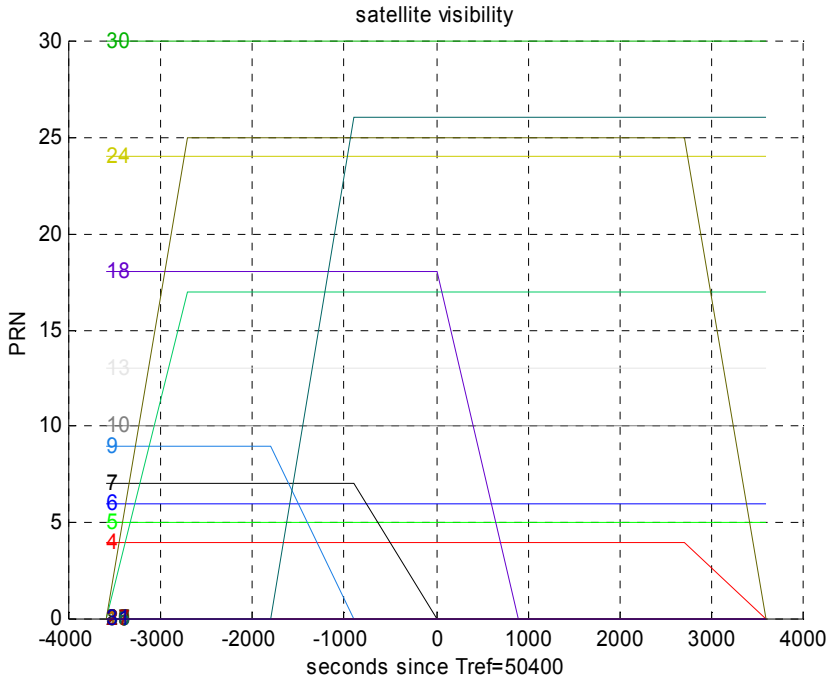

Figure E-12 Simulator Satellite Visibility Centered at 14-hour Epoch

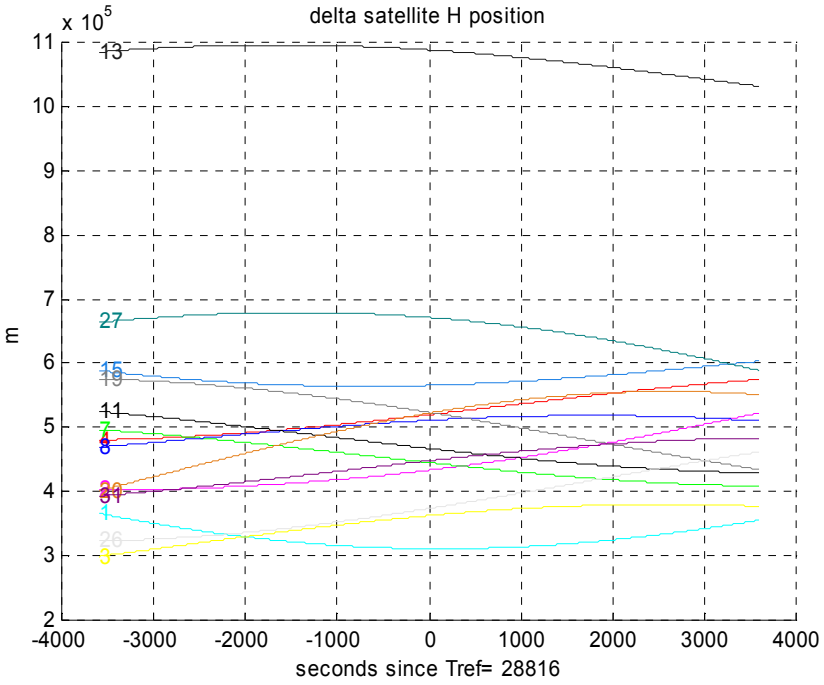

Figure E-13 Uncorrected Satellite H Position Differences

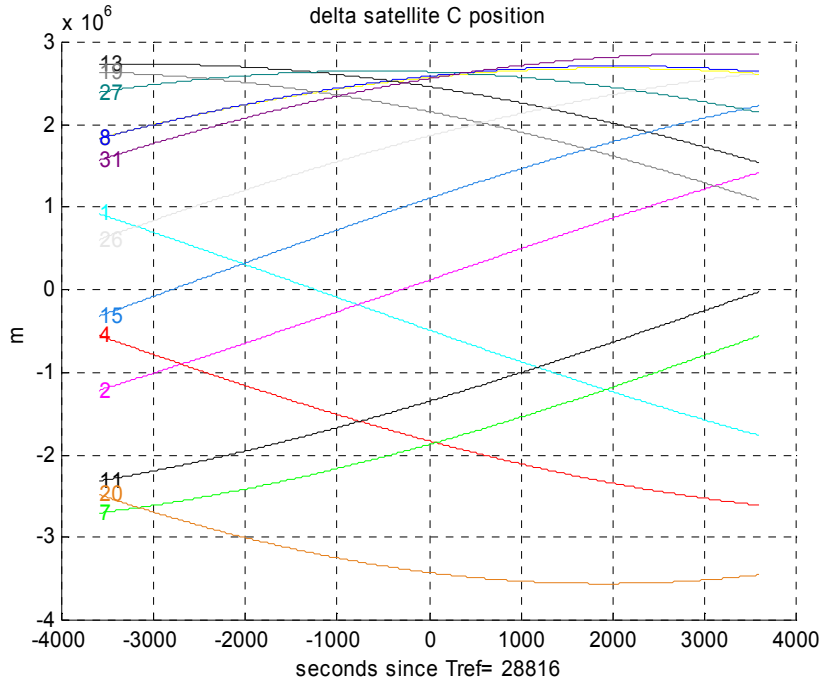

Figure E-14 Uncorrected Satellite C Position Differences

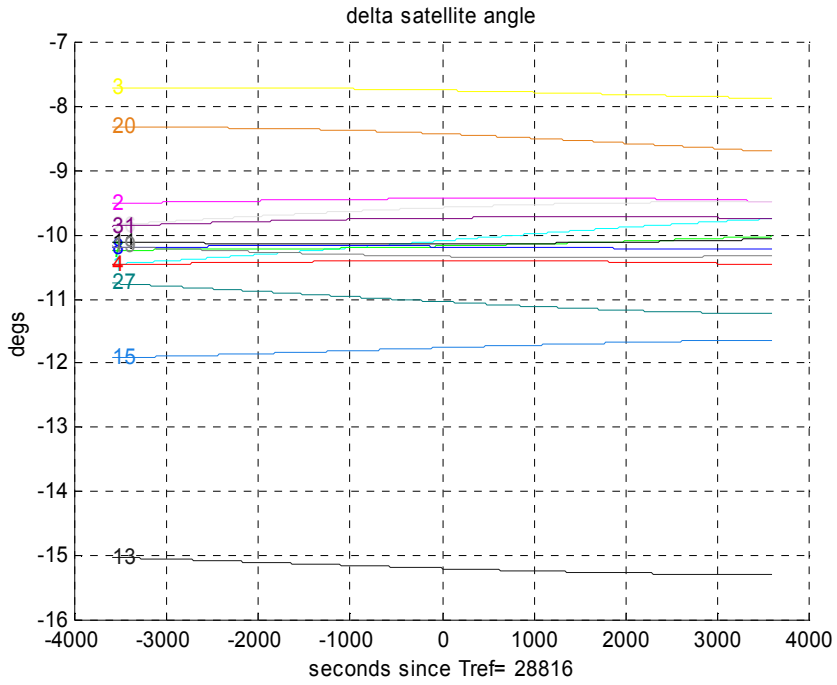

Figure E-15 Uncorrected Satellite Angle Differences

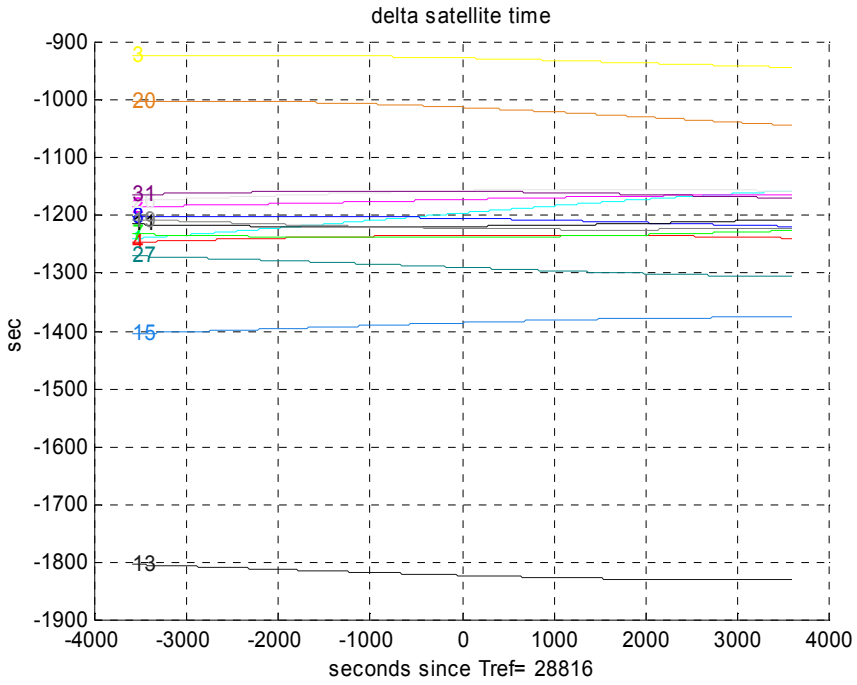

Figure E-16 Time Correction Differences

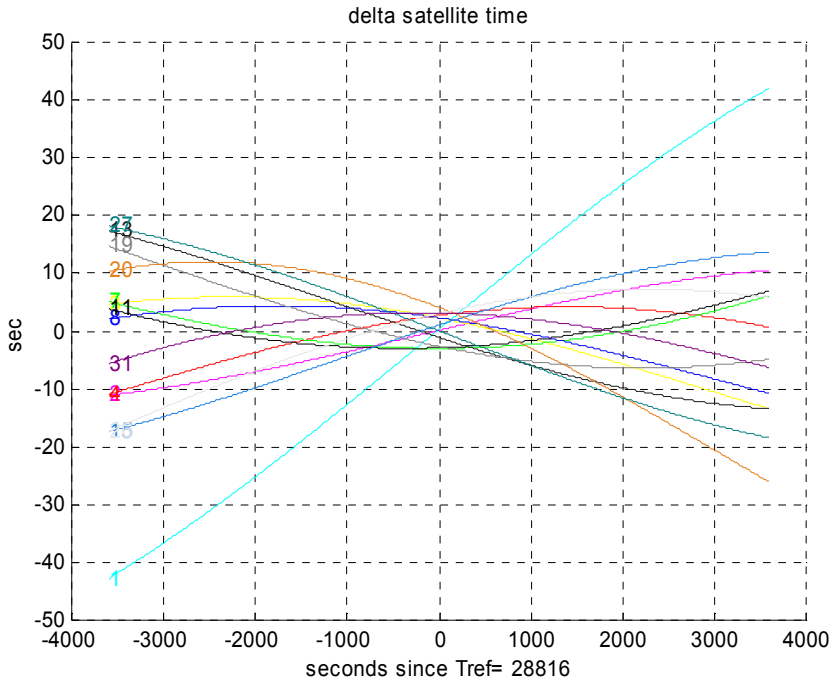

Figure E-17 Remaining Error

E.2.2 Receiver Re-navigation

This section describes the methodology to navigate a static receiver, provides some conducted and radiated test results, and draws conclusions. Receiver re-navigation is an end-to-end validation. It provides an understanding of the test plan and simulator, receiver, and UWB devices/settlings; and verification of end-user outputs, receiver measurements and model conclusions. The measurement and ephemeris data; are used to re-navigate the receiver relative to ARL's surveyed fixed test site to produce a position error and uncertainty. For conducted tests, examples of single (one receiver data) and differential (receiver-to-receiver or injected-to-baseline) navigation position errors (and uncertainty), single and double difference link measurements and residuals are shown. The comparison of baseline performance to UWB/WN injected performance is the most relevant. Simulator generated message data (and not post-processed ephemerides) must be used due to the differences in ephemeris data, however, small navigation position errors confirm the consistency of the measurement and ephemeris data, Section E.2 through E.4. For radiated testing, precise ephemeris was used to obtain the best solution. Each receiver and scenario of the radiated testing was done at different times, therefore the right precise ephemeris data must be obtained. A post-processed navigation solution is more time-consuming than the other levels of analysis, but post-processing should yield a better navigation solution than the real-time receiver solution.

ARL collected and processed an Ashtech data file to produce survey coordinates for the GPS antenna site used in the radiated testing and the static position used to initialize the simulator in the conducted testing. ARL:UT utilized data from the nearby NIMA GPS

monitoring station to provide a differential GPS survey reference coordinate for the fixed sites. The survey results were in World Geodetic Survey (WGS)-84 Earth-Centered, Earth-Fixed (ECEF) or LLH, Reference (16). All heights are measured as height in meters above the ellipsoid. All GPS antennas were not mounted with the same hardware due to differences in antenna design, however, according to ARL, all GPS antenna phase centers should be within +/- 20 cm of the survey coordinates. Therefore, the receiver antenna variations will cause relative static navigation error to be about 20 cm instead of in the millimeters.

E.2.2.1 Analytical Method

Specialized MATLAB code was developed to process RINEX converted files. The navigation solution is computed from raw measurement data based on best knowledge of the "conditions". In particular, L1 C/A or P-code and L2 P-code and carrier phase, and clock offset (if available) data will be used to obtain the most accurate solution. Exhaustive data editing procedures ensures the quality of the range or phase measurements including detection of any cycle slips. Some of the data quality techniques are described in Appendix C. Data corrections applied are listed below, References (bb, cc, and dd).

- Phase Cycle-Slips and Spikes
- Relativity
- GPS Clock Error/Epoch
- Satellite Lever Arm
- Dual Frequency Ionosphere
- Troposphere
- Receiver Clock Error or Residual Error.

The data corrections are applied to the L1 observations to make corrected pseudorange and phase measurements. Phase-derived range (PDR) measurements are computed from the corrected range and phase measurements. The measurement noise varies per satellite depending on the satellite geometry and data quality. Satellites with larger troposphere error had the measurement noise increased in order to cover any residual error. PDR residuals are computed using the surveyed position, BC or precise ephemeris and the PDR measurements. Link-differences of these measurements will remove all common user errors. The receiver clock error is estimated by computing single link measurement residuals from the otherwise corrected L1 PDR measurements. For the Ashtech Z-12, the receiver clock sample time differences between receivers must be corrected, see Appendix C. A single-step least-squares filter estimates the receiver clock and the receiver navigation position error using an iterative technique to correct for the measurement for the receiver clock bias. Position errors are calculated with and without error sources to confirm the simulator and receiver setups. For example, the simulator generated

L1 and L2 ionosphere and troposphere delays, relativity, GPS clock bias, and perturbed ephemeris and clock errors. The filter output is fully corrected single-link range (PDR) measurements and residuals. Double difference measurements are computed and the procedure is described in Appendix C. A batch filter estimates the receiver's position, and satellite ephemeris, clock and clock bias errors. Real ephemeris and clock errors for dual-frequency P-code are typically around 4 meters. Additional runs are done to ensure the results are insensitive. Various sensitivity runs show little change in the results.

E.2.2.2 Conducted Test Example

This section shows some examples of receiver navigation results for the conducted testing. Prior to the execution of the conducted tests, an Ashtech Z-12 GPS receiver was taken to a surveyed point at ARL:UT and data were collected for a period of 8 hours. The coordinates calculated from the collected data were used as the fixed point input to the GPS simulator for all conducted tests, Table E-1. The conducted test data were collected on July 26, 2000 and the simulator reference time was 05:54:00 GPS, Zulu. Data were collected from about 06:00:03 GPS, Zulu and ended approximately 8 hours later. Navigation message and measurement data recorded by the receivers were converted to RINEX format for processing.

In particular, the Conducted, Ranging, Live-sky, Baseline, ASHTEH Z-12 (C_R_L_BASELINE_R2) and ASHTEH Z-Sensor (C_R_L_BASELINE_R4) cases were processed and results of the Z-12 are described below. The first 1197 seconds of the conducted test had eleven satellites visible, Figure E-18. Satellite elevations and orbital positions are given in Figures E-19-E-20. Three satellites were removed from the solution due to them being low elevation satellites and having large tropospheric errors. Data quality checks are depicted by Figure E-21. PDR measurements were formed from eight satellites with continuous range and phase data throughout the processing span. Figures E-22 through E-24 show the atmospheric delays. Two tropospheric models were tried. A BC satellite model was used to more appropriately represent simulated errors. The receiver clock error and navigation position errors were estimated by using a single-step least squares filter. Figure E-25 shows the receiver position error in the North-East-Down (NED) coordinates. The single-link residuals are shown in Figure E-26. Single-link and link-difference range measurements show negligible common-mode errors remaining, Figures E-27 and E-28. The batch filter link residuals are shown in Figure E-29. Satellite PRN 7 had a large enough estimated troposphere error to increase the measurement noise in order to cover any residual error. The RSS receiver position error is 7 m with an uncertainty of less than 2 m per axis. The position error can be contributed to three reasons: (1) the simulated diverged ephemeris/clock errors, (2) simulator errors due to producing realistic measurement and ephemeris data, and (3) modeling discrepancies, such as troposphere.

Differential processing results of the C_R_L_BASELINE_R2 and C_R_L_BASELINE_R4 cases are shown in Figures E-30-E-31. Double-link difference residuals are ~0.01 m per link error between runs, which is caused by residual tropospheric errors due to simulator and GPS processing modeling discrepancies. Differential processing shows the data are consistent. Injected-to-baseline double difference residuals were slightly higher due to simulated error sources not being identically equivalent.

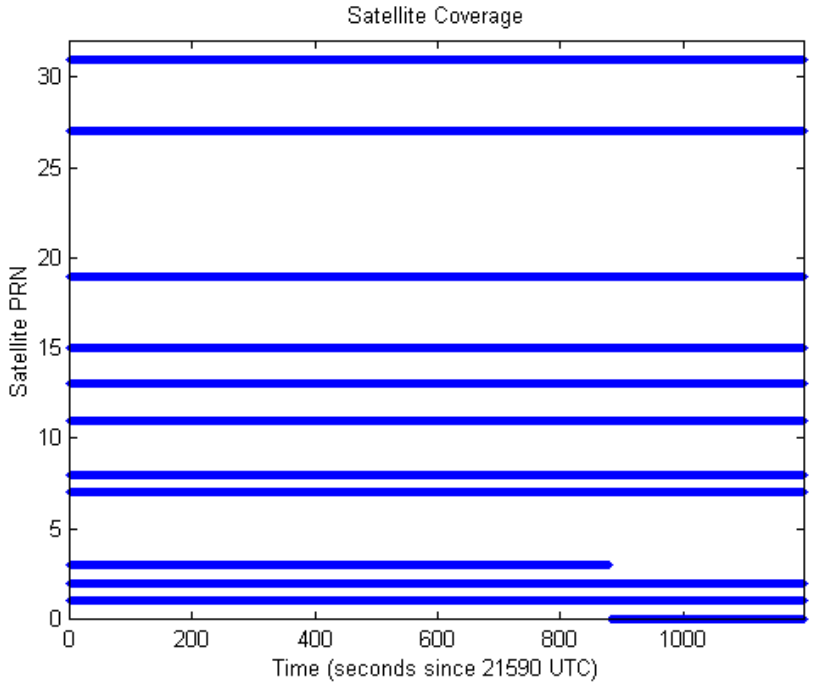

Figure E-18 C_R_L_BASELINE_R2 Satellite Availability

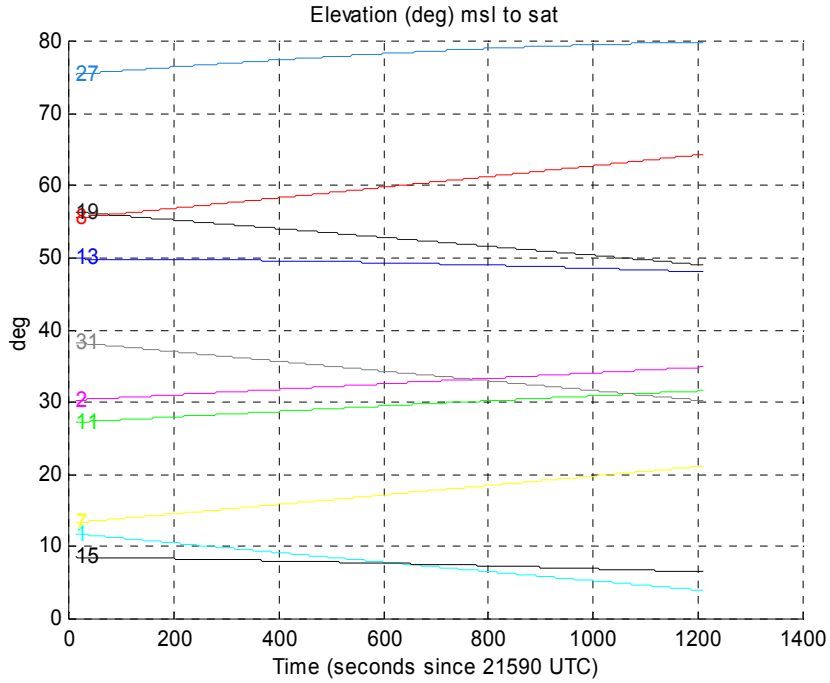

Figure E-19 C_R_L_BASELINE_R2 Satellite Elevation

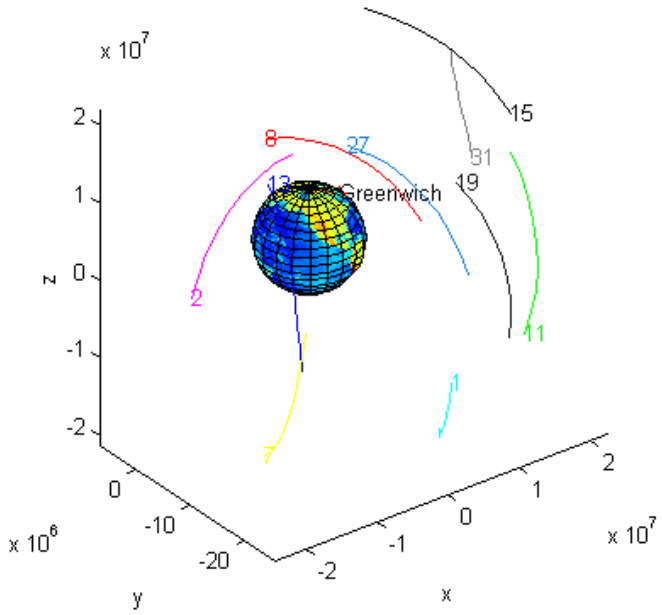

Figure E-20 C_R_L_BASELINE_R2 Satellite Orbits

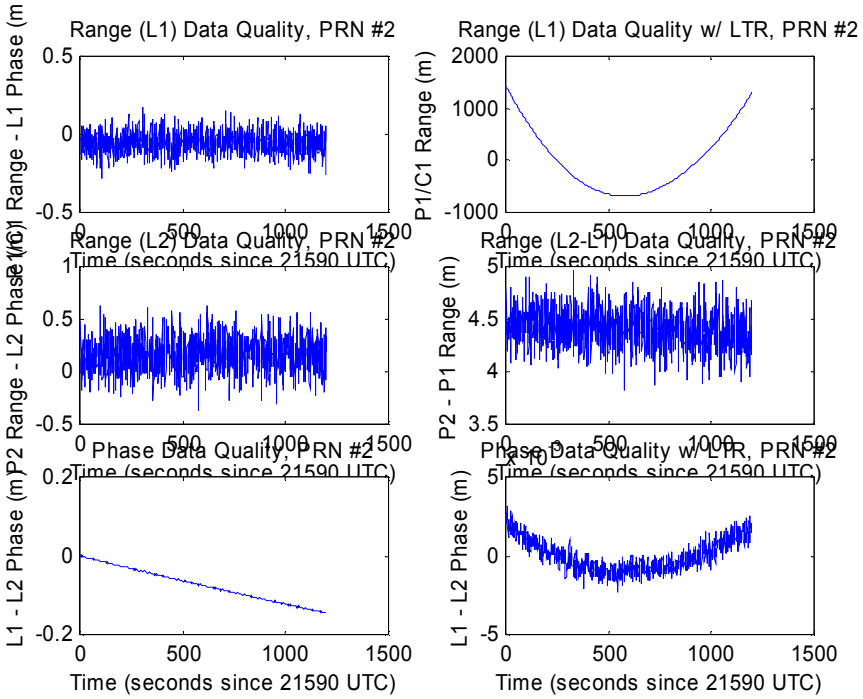

Figure E-21 C_R_L_BASELINE_R2 Data Quality

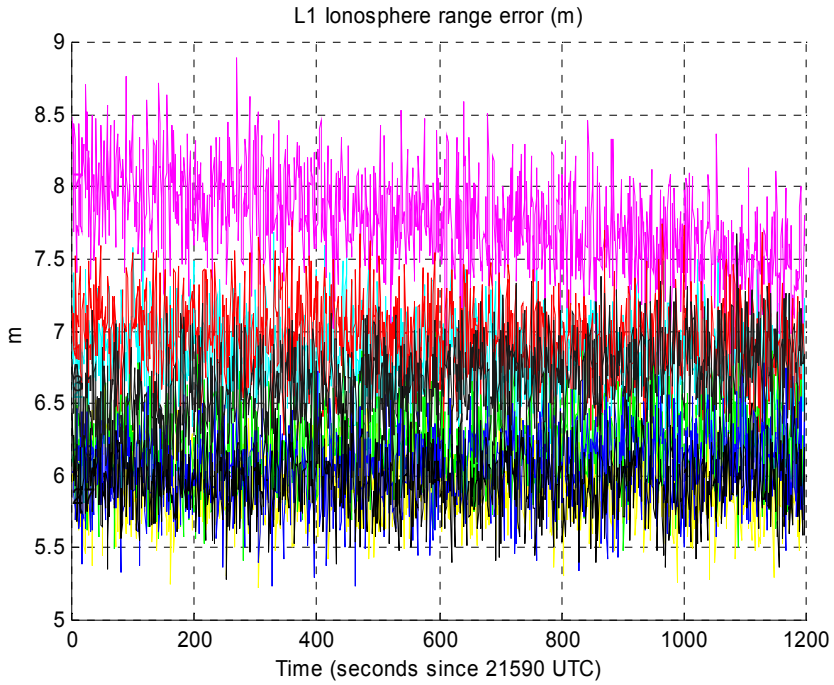

Figure E-22 C_R_L_BASELINE_R2 L1 DF Ionosphere Range Error

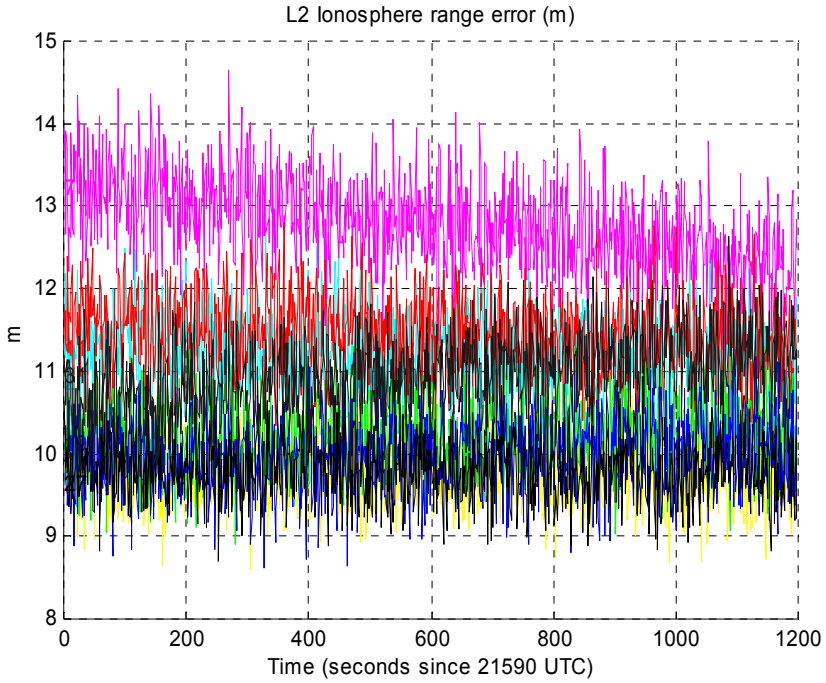

Figure E-23 C_R_L_BASELINE_R2 L2 DF Ionosphere Range Error

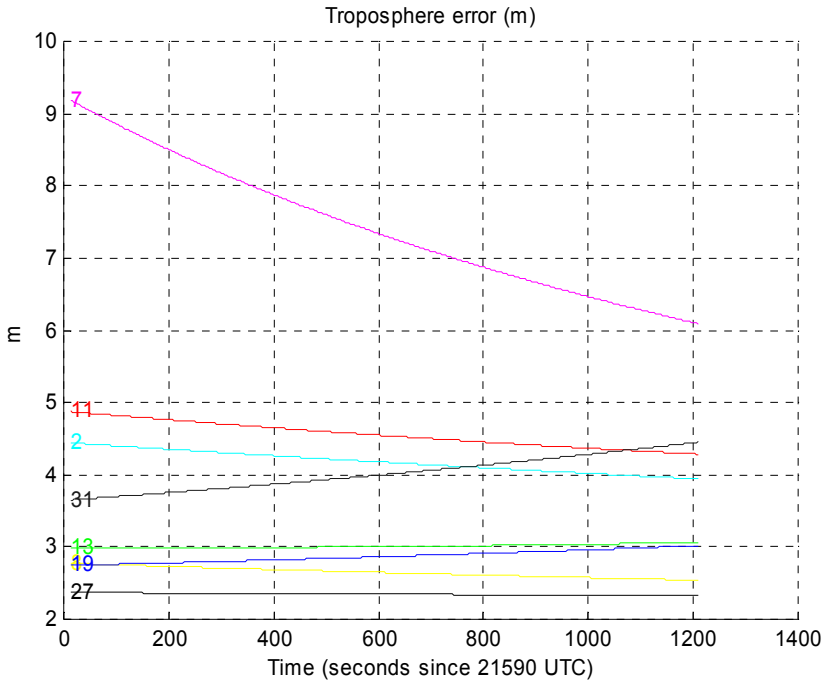

Figure E-24 C_R_L_BASELINE_R2 Troposphere Error

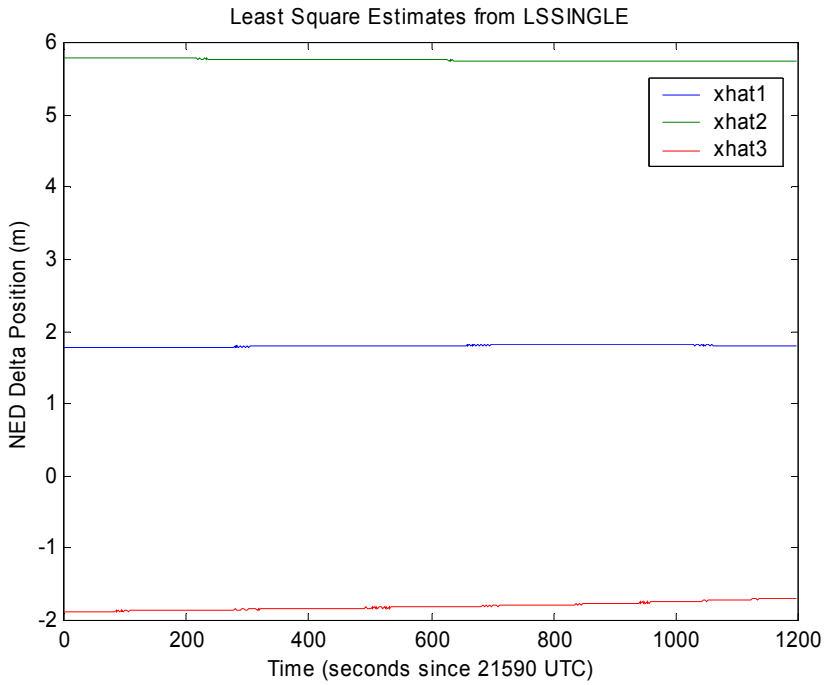

Figure E-25 C_R_L_BASELINE_R2 NED Position Error

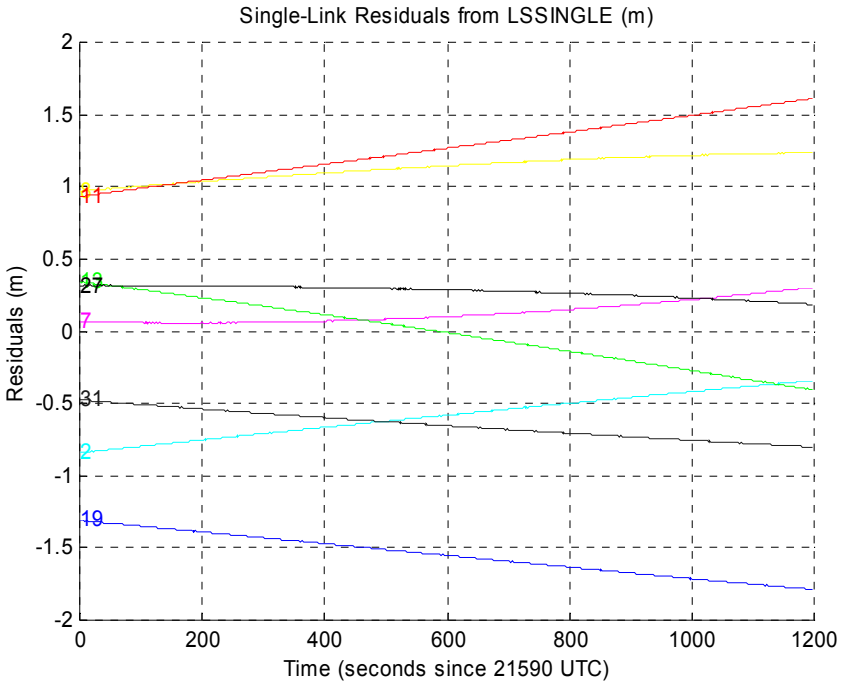

Figure E-26 C_R_L_BASELINE_R2 Single-link Residuals

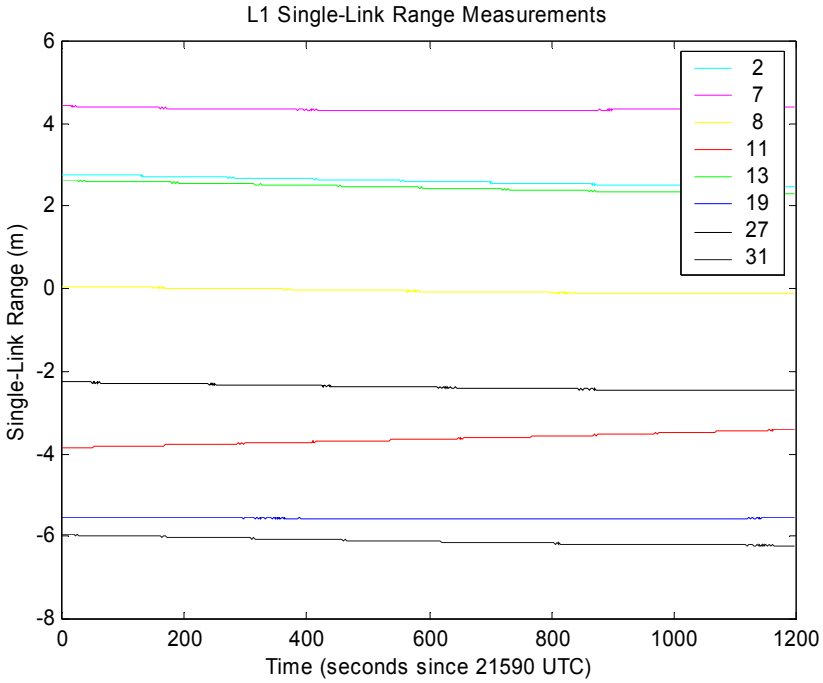

Figure E-27 C_R_L_BASELINE_R2 Single-link Range Measurements

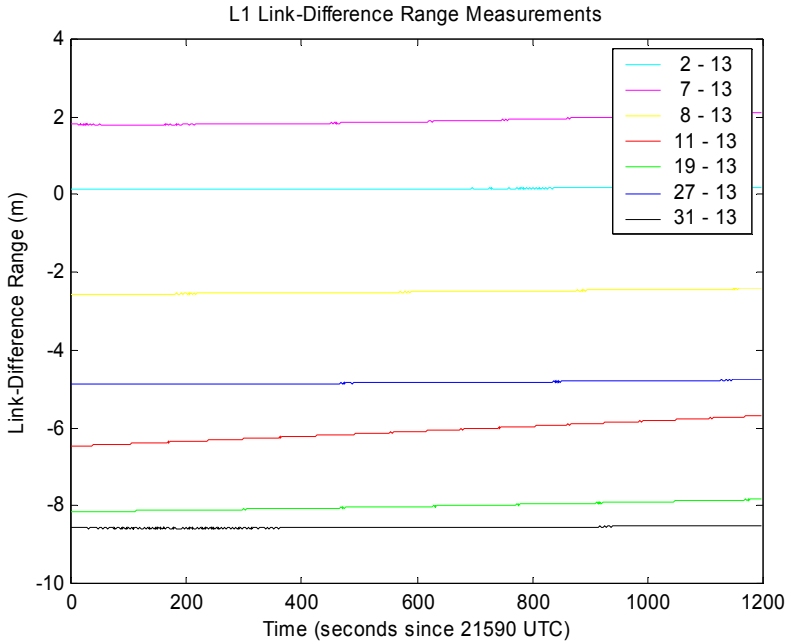

Figure E-28 C_R_L_BASELINE_R2 Link Difference Range Measurements

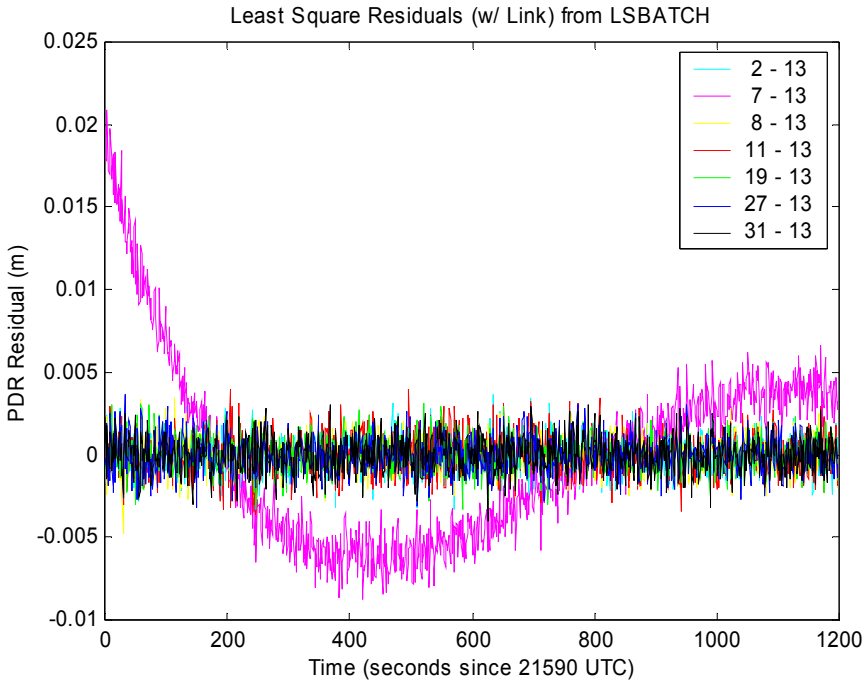

Figure E-29 C_R_L_BASELINE_R2 PDR Residuals

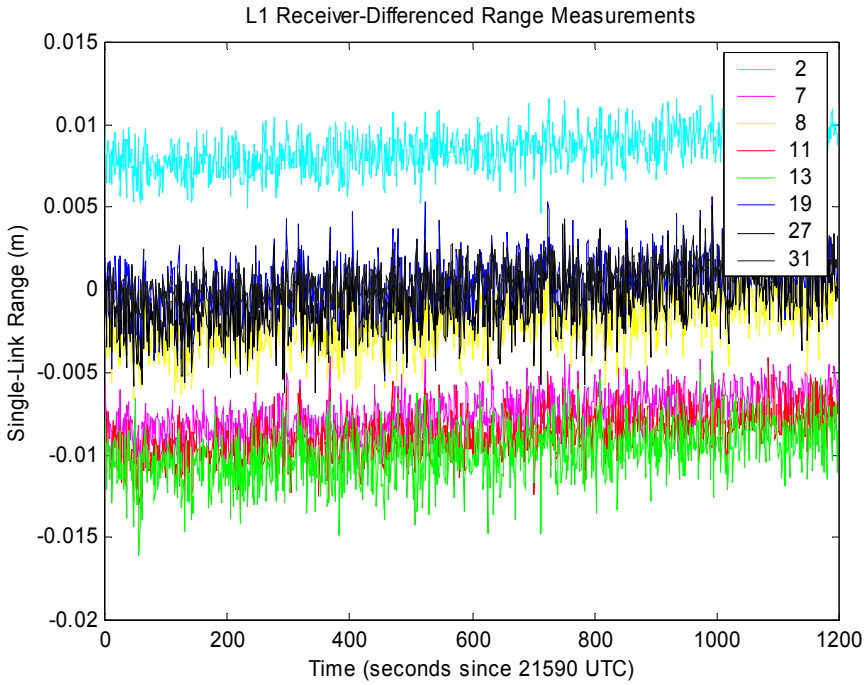

Figure E-30 BASELINE_R2 – BASELINE_R4 Single-Link Range Measurements

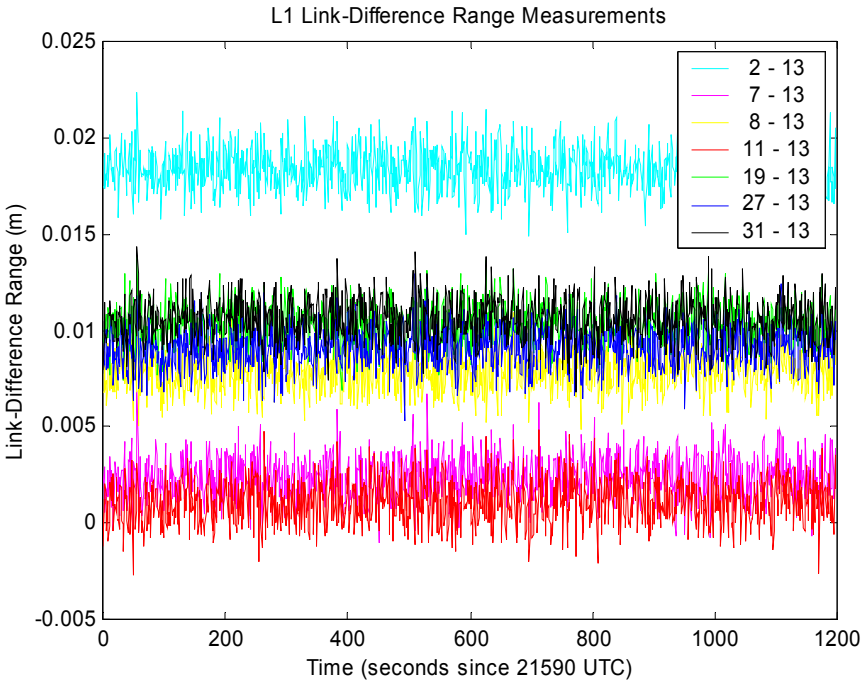

Figure E-31 BASELINE_R2 – BASELINE_R4 Link-Difference Range Measurements

E.2.2.3 Radiated Test Example

This section shows some of the receiver navigation results for radiated testing. The radiated tests were conducted at various times, so the appropriate NIMA/NGS precise ephemeris in SP3 format and the NGS/CORS global message were downloaded via the Internet. A continuously operating, GPS monitor ground station, operated for the NIMA, was used as the GPS performance baseline during the radiated interference testing. The GPS antenna survey location provided by ARL:UT is 30.38412946 degrees latitude, -97.72729702 degrees longitude and 226.192 m above the ellipsoid.

In particular, the radiated, UWB MODE 13, 8-meter, ASHTECH Z-12 (R_U_M13_8M_R2) results are described next. The radiated test data for this scenario were collected on October 17, 2000, and the reference time was 13:24:28 GPS, Zulu. There were nine satellites visible during 135 to 1333 seconds into this radiated test. Satellite elevations are given in Figure E-32. Four satellites were removed from the solution due to them being low elevation satellites and having large tropospheric errors. Data quality checks are depicted by Figure E-33. PDR measurements were formed from seven satellites with continuous range and phase data throughout the processing span. Figures E-34-E-35 show the real atmospheric delays. A more accurate satellite model was used in conjunction with the NIMA precise ephemerides. The receiver clock error and navigation position errors were estimated by using a single-step least squares filter. Figure E-36 shows the receiver position error in NED coordinates. The single-link residuals are shown in, Figure E-37. Single-link and link-difference range measurements show negligible common user errors remaining, Figures E-38-E-39. The batch filter link residuals are shown in Figure E-40. The RSS receiver position error is 15 m with an uncertainty of less than 1.5 m per axis. A 14-m height bias error can be explained by three reasons: (1) real ephemeris/clock errors, (2) incorrect survey, and (3) modeling discrepancies, such as troposphere. Results were noticeably improved when the survey point to initialize the simulator was used as a reference.

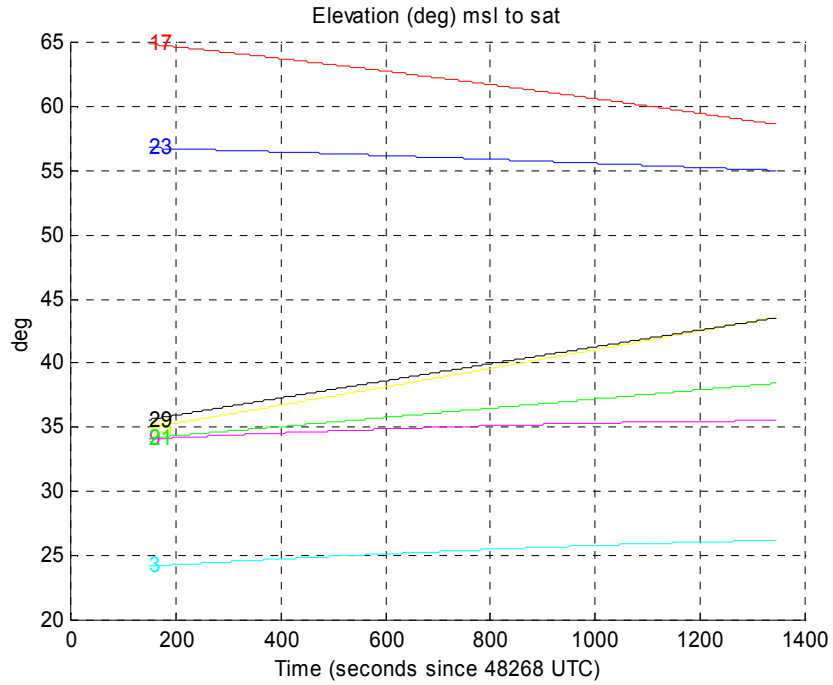

Figure E-32 R_U_M13_8M_R2 Satellite Elevations

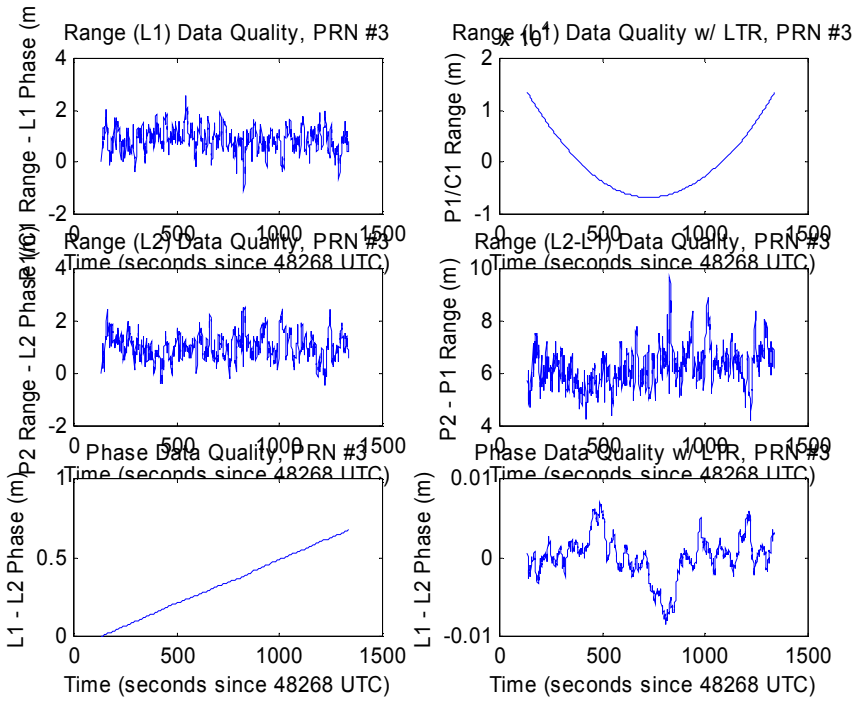

Figure E-33 R_U_M13_8M_R2 Data Quality

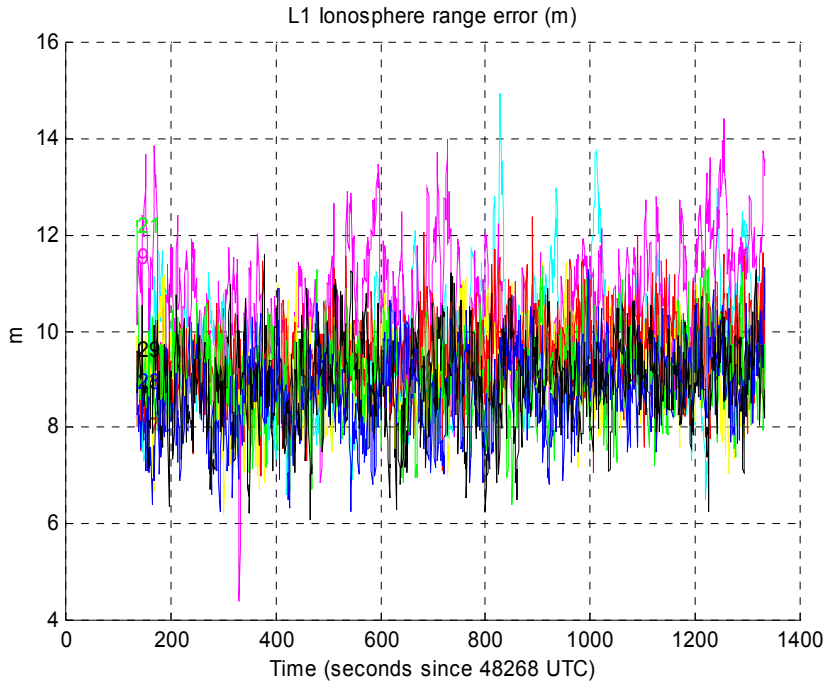

Figure E-34 R_U_M13_8M_R2 L1 DF Ionosphere Range Error

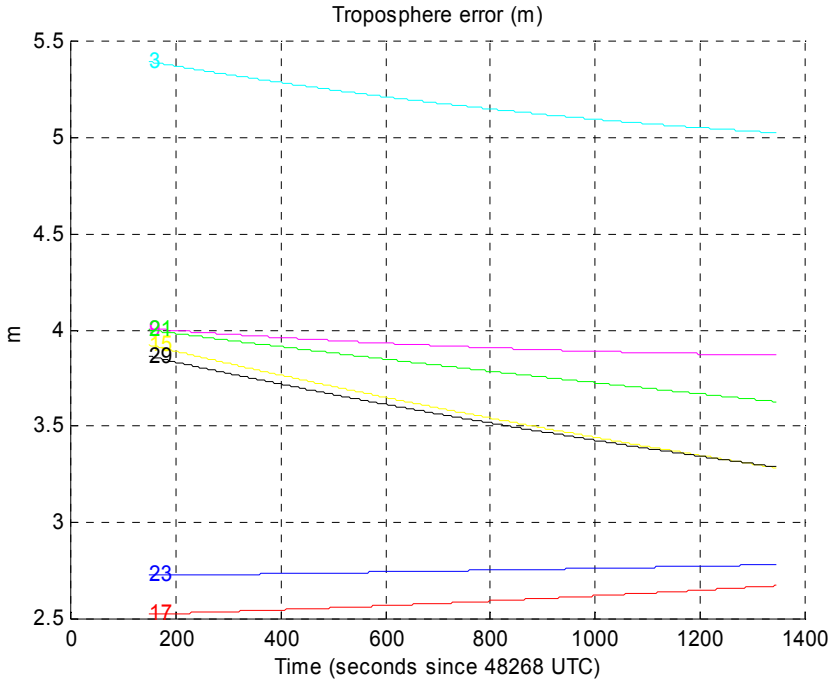

Figure E-35 R_U_M13_8M_R2 Troposphere Error

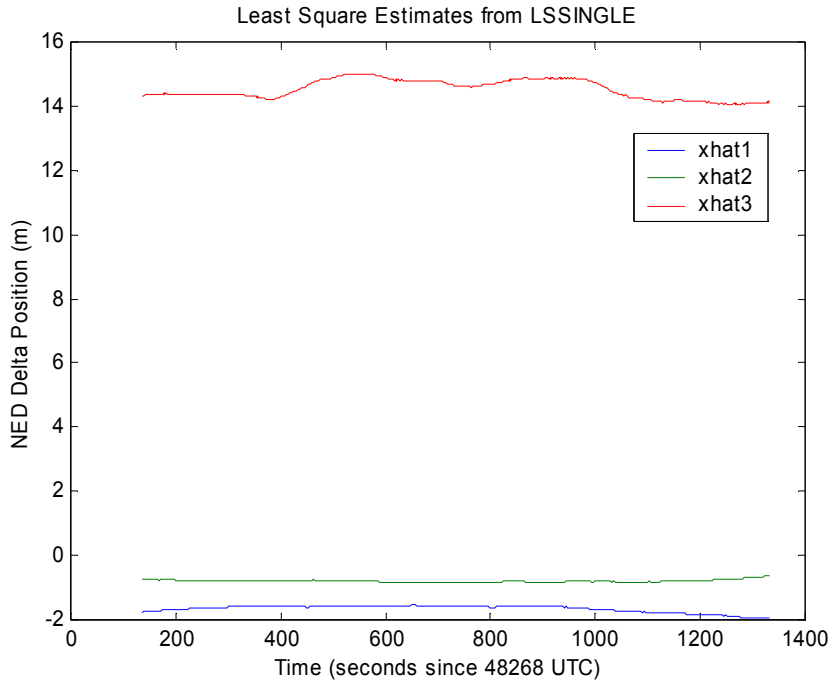

Figure E-36 R_U_M13_8M_R2 NED Position Error

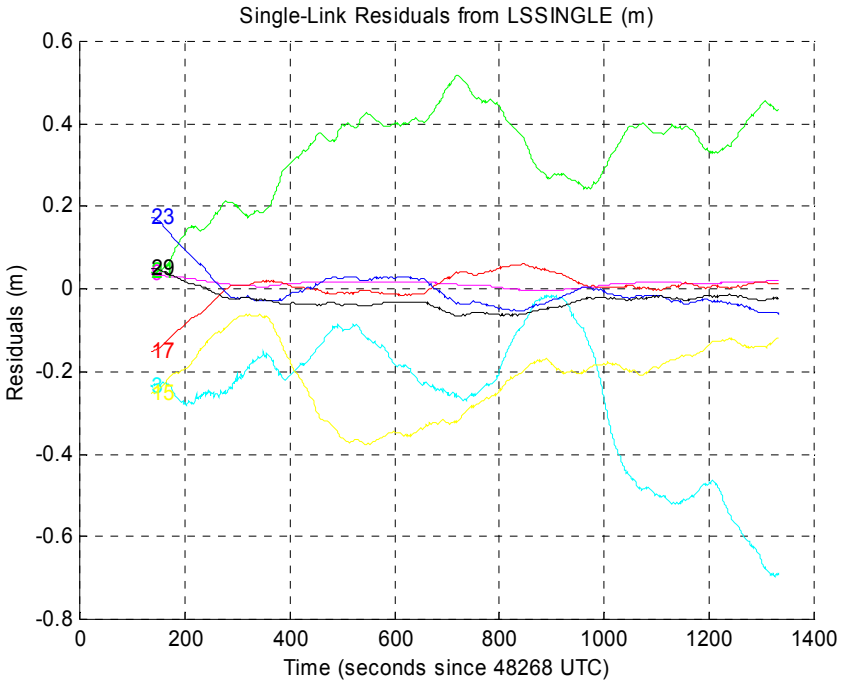

Figure E-37 R_U_M13_8M_R2 Single-Link Residuals

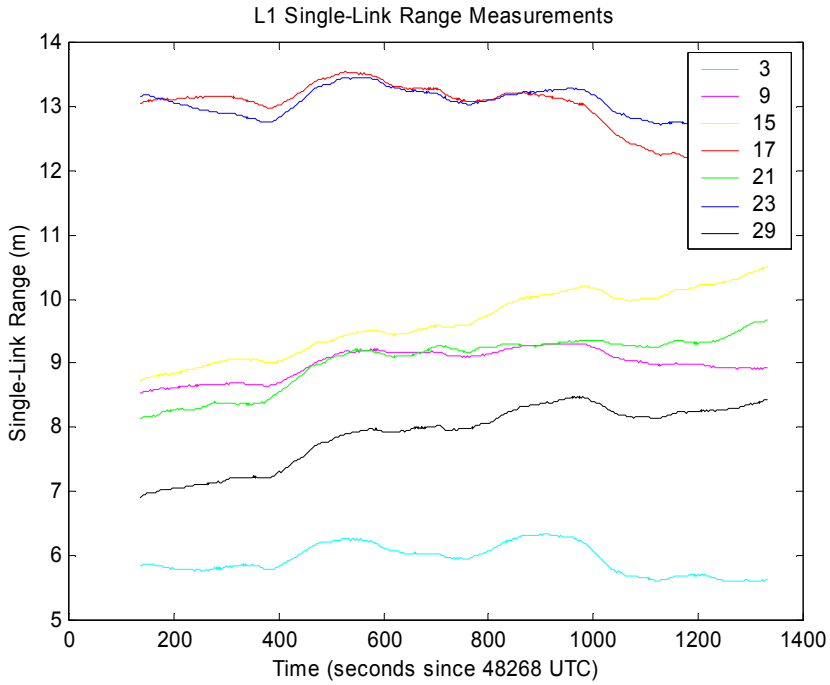

Figure E-38 R_U_M13_8M_R2 Single-Link Range Measurements

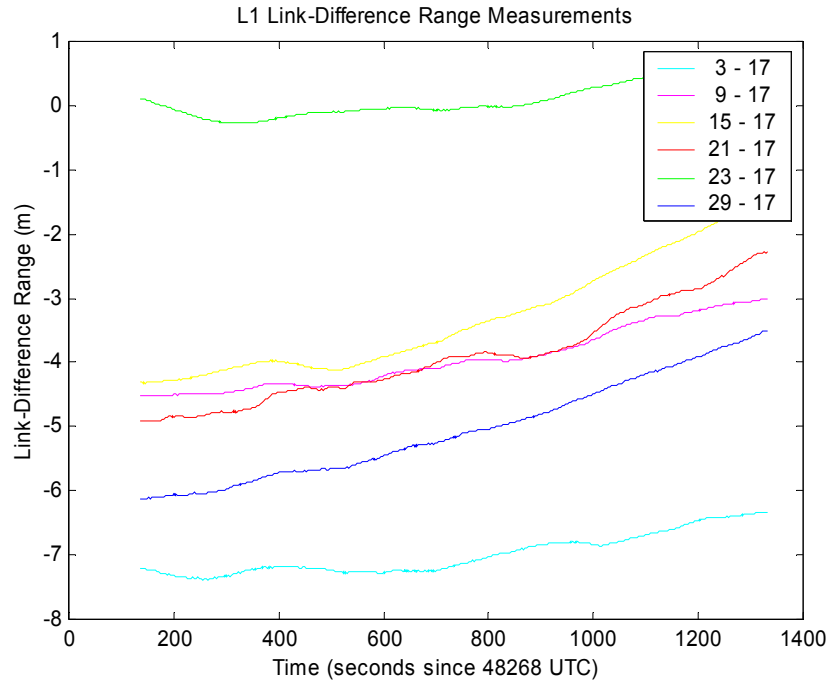

Figure E-39 R_U_M13_8M_R2 Link-Difference Range Measurements

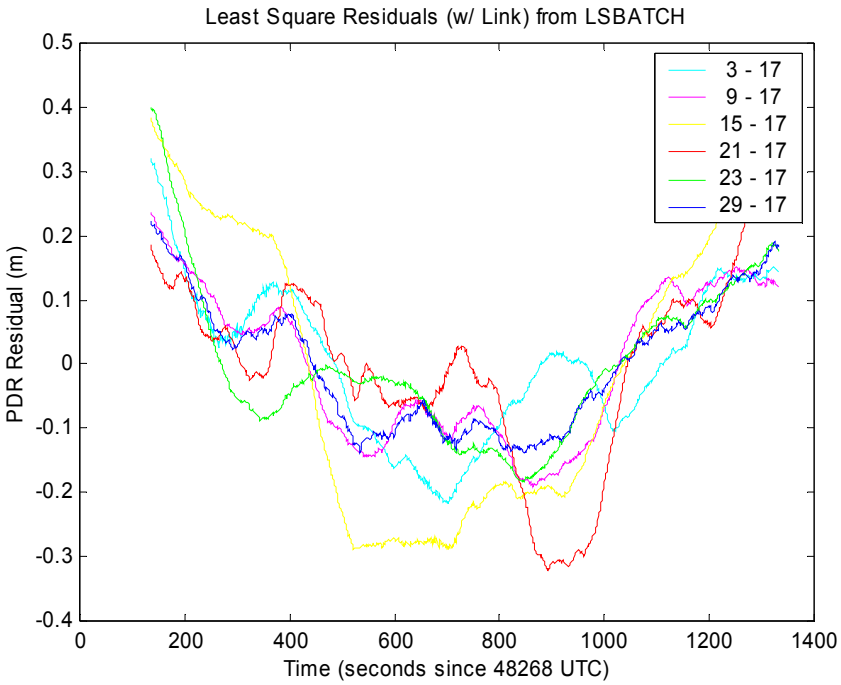

Figure E-40 R_U_M13_8M_R2 PDR Link Residuals

E.3 Conclusions

This section provides the major conclusions that resulted from a thorough investigation of the ARL:UT test setup and valid the data collected.

- The simulators and receivers were not entirely set in default mode as indicated by ARL:UT.

- The simulated ephemeris was generated based on default satellite constellations or orbital parameters and was determined to be closer to GPS week-49 despite the test day being in the middle of week-48. Therefore, the satellite positions differ significantly from real broadcast messages for the simulated test day. Also, the simulator-generated ephemeris was perturbed with additional time-dependent ephemeris and clock errors. The perturbed ephemeris and clock errors were unpredictable and uncorrectable, so receiver position errors were evident in the renavigation results. The simulated measurements are not consistent with measurement generated from other ephemeris sources for that day (i.e., live testing). So, the radiated and conducted test data can not be compared.

- The pseudorange errors were independently determined by re-navigating the receiver. The pseudorange measurements generated by the simulator contained L1 and L2

ionosphere and troposphere delays, relativity, GPS clock bias, and perturbed ephemeris and clock errors

- The simulated ephemeris data recorded for various receivers and attenuation settings are consistent as expected. Also the ephemeris and the measurements self-consistent. The RSS receiver position error was 7 m with an uncertainty of less than 2 m per axis. The position error can be contributed to three reasons: (1) the simulated diverged ephemeris/clock errors, (2) simulator errors due to producing realistic measurement and ephemeris data, and (3) modeling discrepancies, such as troposphere. Double-link difference residuals were ~0.01 m per link between runs, which is caused by residual tropospheric error due to simulator and GPS processing modeling discrepancies. Differential processing shows the ephemeris and measurement data collected are self-consistent. Injected-to-baseline double difference residuals were slightly higher due to simulated error sources not being identically equivalent.

- The radiated test ephemeris and data recorded and the measurements are self-consistent. A height bias error of 14-m was estimated with an uncertainty of less than 1.5 m and can be explained by three reasons: (1) real ephemeris/clock errors, (2) incorrect survey, and (3) modeling discrepancies, such as troposphere. Real ephemeris and clock errors for dual-frequency P-code are typically around 4 meters. It was noted that the receiver position error was improved when the survey point used by the simulator was used as a reference.

APPENDIX F
COMPARISON TO RADIATED TESTING

F.0 Introduction

To validate and extend the results of the conducted testing, the Applied Research Laboratories, University of Texas (ARL:UT) test program included a segment where the Global Position System (GPS) receivers were exposed to a live GPS satellite constellation, and the strength of the injected ultra-wideband (UWB) signal was varied with actual physical separation rather than attenuation. The separation or range between the GPS receiver and UWB device varied from 8.0 to 0.5 meters. Obviously, this test setup required real antennas for both the GPS receivers and the UWB PulseON Application Developer (PAD). This segment of the ARL:UT test program is denoted as radiated testing. Due to problems with breaking tracking or lock with the GPS signals, only the ranging (and not the reacquisition) tests were performed. Similar to the conducted testing, five GPS receivers were evaluated with the UWB device configured in various modes to reflect the three pulse repetition frequencies (PRFs) and various duty cycles. Obviously, only one GPS signal power can be realized. As expected, the GPS power is observed to vary more dramatically with satellite elevation angle due to the beam patterns of the GPS antennas. The simulated GPS signals were only reduced for propagation losses but not GPS antenna beam patterns.

The data collected during the radiated testing are more difficult to rigorously analyze than the conducted data since no adequate baseline data exist with which to normalize the MOPs and remove any apparent degradation that actually should be attributed to naturally occurring variations in performance. Baseline data are defined to be GPS data collected in the total absence of an injected UWB signal. The ARL:UT test program did include some baseline data sets. For the first three receivers, 16 hours of baseline data were collected before the entire test, and for the remaining three receivers, 20 minutes of baseline data were collected just prior to changing UWB modes. These baselines can be used to predict general receiver performance with a live GPS satellite constellation. However, since they were not gathered with the exact same conditions (e.g., satellite geometry and outside sources of interference) as the injected data, these baselines do not provide a sound basis for normalization or statistical comparison with the current measure of performance. Even a measure of performance (MOP) as simple as receiver position, which might be compared to the surveyed receiver location, is a poor measure because the radiated testing was performed over several weeks and not contiguously due to inclement weather. Significant jumps are noted in the receiver position between range settings due to different satellite geometries and initializations of the navigation solution.

One could attempt to predict other simple baselines, such as satellites tracked, based on the almanac, broadcast ephemeris or precise ephemeris – these predictions would have to be matched to the exact times that each portion of the test was performed. Unfortunately, not only is

this process tedious, but it does not account for the natural variations within a receiver nor its satellite selection criteria. Therefore, the analyst would like an MOP where the exact time and satellite constellation is not relevant and baseline performance can be inferred from the above data collections. Ideally, degradation in this MOP would also be predictive of degradation in the other MOPs.

F.1 Carrier-To-Noise (C/N_0) Ratio

With a little adaptation, the C/N_0 MOPs can be a good choice. In the radiated test setup, the GPS satellites have nearly repeating ground tracks, and the geometry relative to a fixed site antenna repeats every orbit. Furthermore, the satellite's effective radiated power is very nearly the same for all satellites. Thus the satellite power at the GPS antenna port is mostly a function of the antenna's vertical beam pattern (most GPS antenna are nearly omni-directional). Therefore, independent of the exact satellite, C/N_0 as a function of the satellite elevation angle is repeatable at the fixed antenna site. An example of this is shown in Figure F-1 for the Ashtech Z-Sensor using data collected during several concatenated 20-minute baselines. Figure F-1, C/N_0 is graphed versus the satellite elevation angle, where the different colors represent different satellites. The increased variation at low elevation angles is typical of multipath effects, but for elevations above 15 degrees, the data are quite predictable. The solid blue line is a quadratic representation of C/N_0 as a function of 90 degrees minus the elevation angle as given in the following equation:

$$C/N_0 = c_0 + c_1 * (90 - elev) + c_2 * (90 - elev)^2$$

The quadratic coefficients have been determined via a least-squares fit to the data. Each GPS receiver requires a unique set of coefficients due to different GPS antennas and computations of C/N_0. Table F-1 contains these quadratic coefficients for each GPS receiver. With this functionalized baseline, the normalization of C/N_0 is simply dividing the C/N_0 measured in the injected case by that predicted with the corresponding satellite's elevation angle. For any specific range setting, this ratio is then averaged over all epochs and satellites tracked. The data are considered to be from a single distribution across all satellites, and no ANOVA statistic is computed.

Table F-1 Elevation Polynomial Coefficients

GPS Receiver	c_2	c_1	c_0
NovAtel 3151	-0.003054	0.151090	44.6081
Ashtech Z-12	-0.011380	0.679353	229.812
Garmin 155XL	-0.002379	0.102489	48.5151
Ashtech Z-Sensor	-0.003494	0.117634	54.7542
NovAtel Millenium	-0.004189	0.212600	48.4867

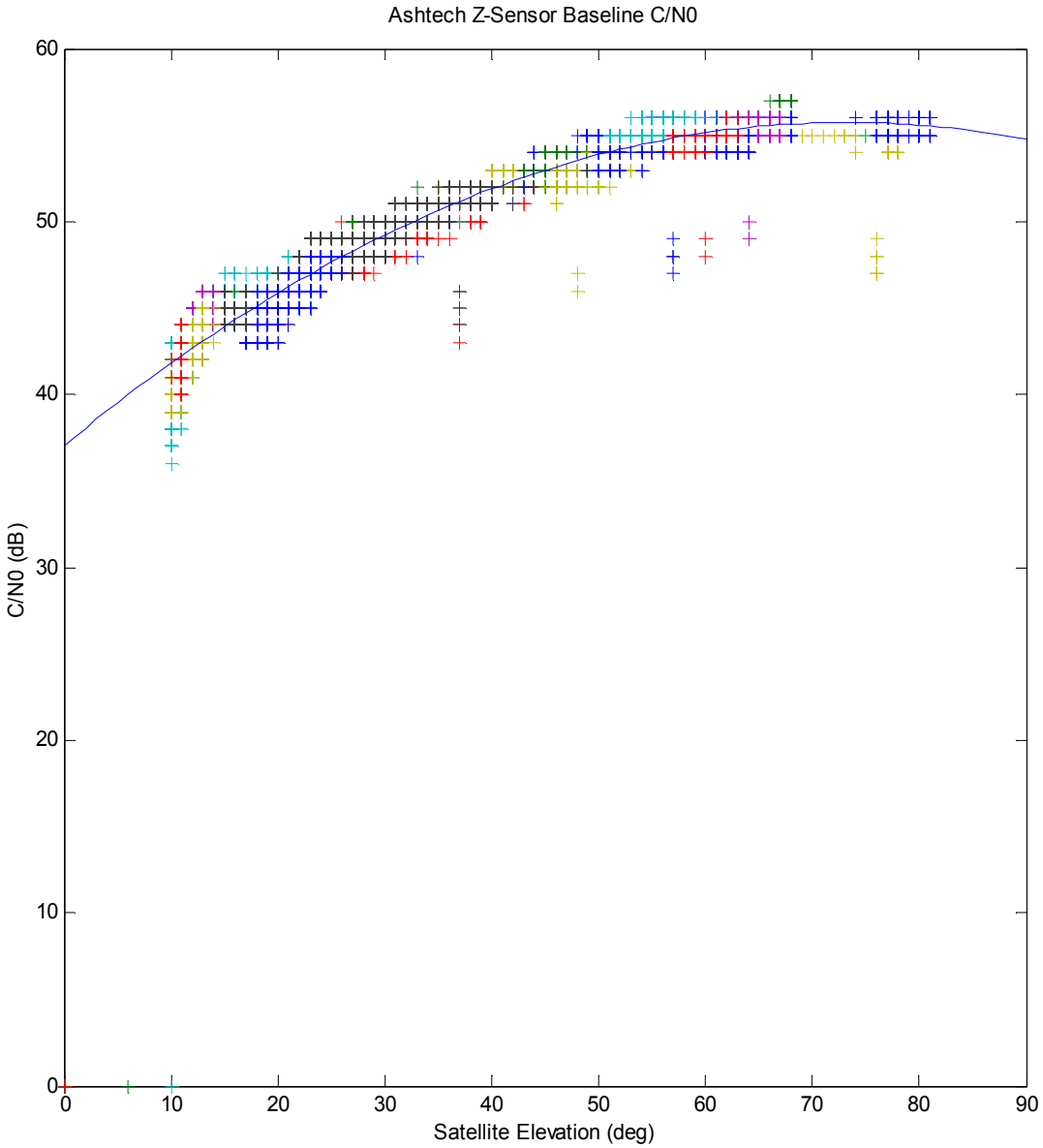

Figure F-1 Satellite C/N_0 Versus Elevation Angle

Figure F-2 contains two graphs that depict the results when the radiated C/N_0 data are normalized by the value predicted by above equation and coefficients. All five GPS receivers and UWB modes 1, 7, and 13 are included in the graph. These modes represent the continuous duty cycles for the three pulse repetition frequencies. In the left-hand graph, each color represents a single GPS receiver with all three UWB modes. They are shown simultaneously to depict both the similarities in the general trend and the dispersion across receivers. None of the data for the lower pulse repetition frequencies have been mapped to represent "compliant devices" in terms of average power as was the case with the conducted data.

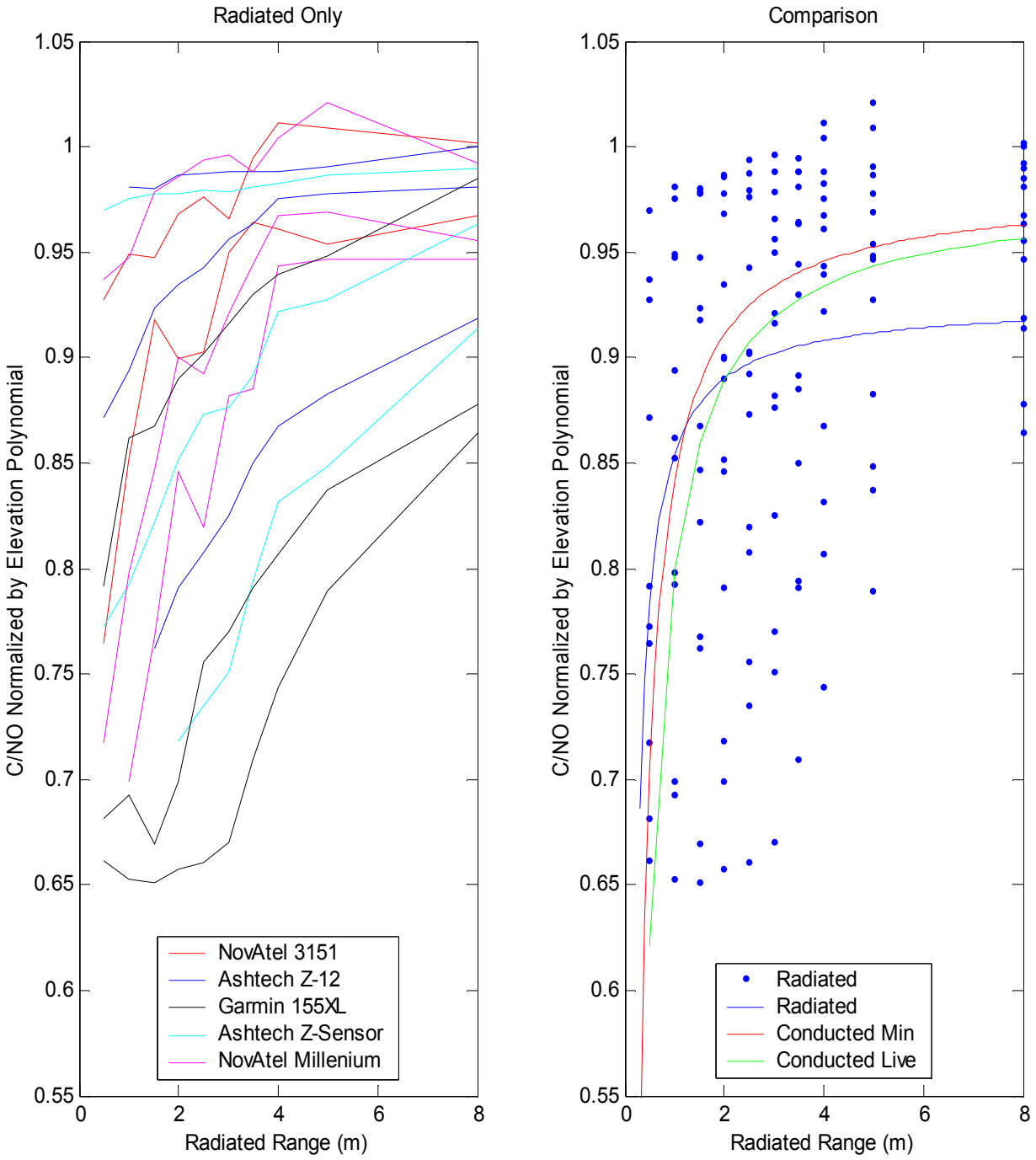

Figure F-2 Radiated C/N_0 Normalized by Elevation Polynomial

The right-hand graph in Figure F-2 displays all points regardless of GPS receiver or UWB mode. The blue curve is a hyperbola computed from a least squares fit to all of these data. For comparison, the hyperbolas computed from the conducted data for the minimum level and live sky GPS signal powers are shown in Figure F-2 as the red and green curves, respectively. Recall that these curves do not include the NovAtel Millenium data in the least squares fit but do include the mapping to compliant devices with regard to average power.

To validate this alternative process, the original conducted C/N_0 data were normalized by a baseline C/N_0 computed solely by a quadratric derived from the original conducted baseline data, which were collected during an eight-hour period. The resulting degradation in C/N_0 was found to be very consistent with that observed when the normalization is based on the actual baseline C/N_0 values.

As shown in Figure F-2, the radiated and conducted tests show the same trends and levels of degradation. This favorable comparison lends tremendous credibility to the applicability of the conducted testing and the mapping from attenuation setting to equivalent range. As in the conducted case, the radiated results show more variation in the C/N_0 MOP across GPS receivers than across UWB modes. Furthermore, the receiver to receiver variation is much larger in the radiated case. This difference can be attributed to the different GPS antennas used in the radiated testing and their varying performance characteristics (e.g., noise factor and gain). The reader is directed to Appendix I for more discussion on the variation across receivers versus UWB modes.

F.2 Pseudorange Measurement Noise

The raw pseudorange measurement noise could also be a good choice for assessing the radiated data even when not normalized. The C/A code minus carrier phase measurement was computed for the radiated data using the exact same methodology that was applied to the conducted data as described in Appendix C. This MOP was computed for both NovAtel and both Ashtech receivers when injected with UWB signal from modes 1, 7, and 13. After detrending the data, the radiated results differ from the conducted results in that the remaining error signature does not consist only of range noise – instead it is predominated by large damped oscillations. This error signature has been termed “detrended C/A code minus carrier.” These oscillations are not observed in the data for every satellite, but they are observed for every combination of GPS receiver, UWB mode, and physical separation. Figures F-1 and F-2 contain graphs that depict the “detrended C/A code minus carrier” for several combinations of GPS receiver, UWB mode, and physical separation. These examples span the worst case to nominal realizations, respectively. In each set of graphs, the upper graph is the code minus carrier prior to the applying the detrending. The results for every satellite tracked during the 20-minute time period have been overlaid to demonstrate the range in the amplitudes of these oscillations. Note that the range of the y-axes in Figure F-3 is much larger than that in Figure F-4.

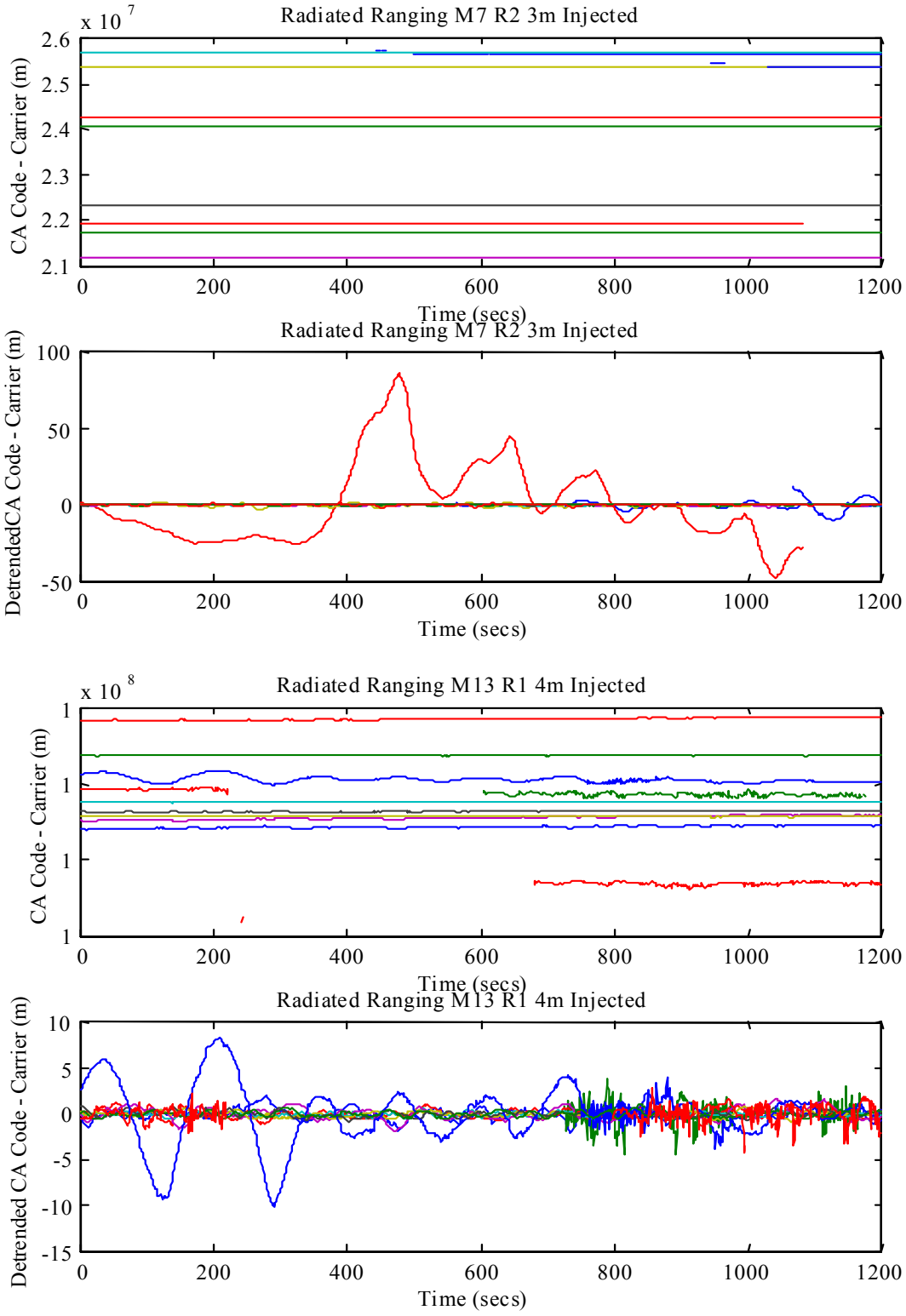

Figure F-3 Worst Case Oscillations in Code Minus Carrier

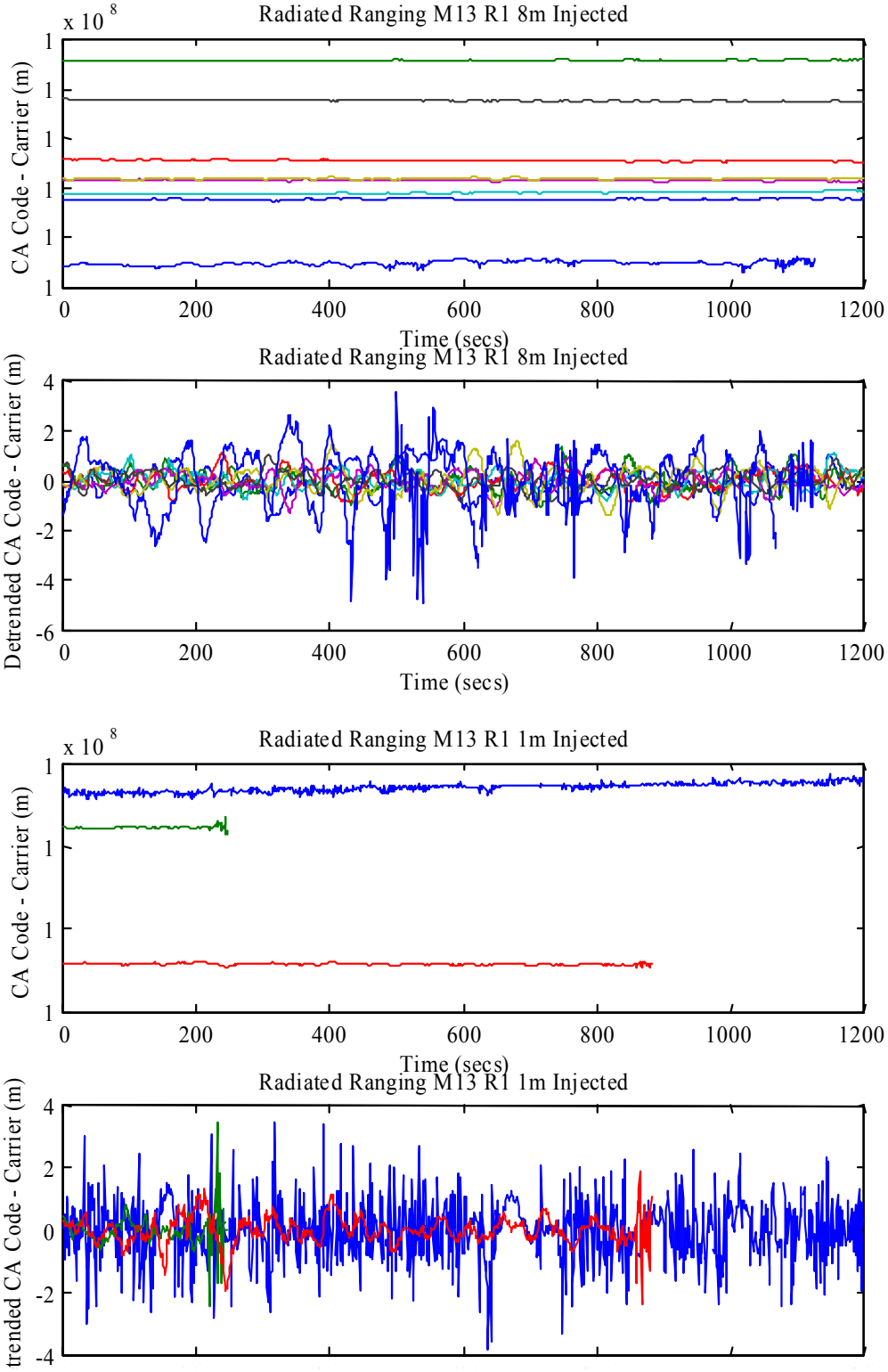

Figure F-4 Nominal Oscillations in Code Minus Carrier

A definitive explanation of these oscillations has not been found; therefore, these results are presented only for information and not as validated analysis conclusions. Possible explanations of these oscillations include the following. It is noted that the setting times of these damped oscillatory trends appear to be from newly acquired satellites, but the amplitude is too large to be attributed to tracking loop or filter responses.

- Tracking loop or filter responses to newly acquired satellites
- Satellite geometry relative to the UWB device
- Multipath

The measurement data collected with these GPS receivers only included smoothed code pseudoranges. The raw C/A code pseudorange noise is typically a few meters, whereas smoothed pseudorange noise it typically at the sub-meter level. In the analysis, the nominal C/A pseudorange noise (using smoothed code) has about a 0.5 meter one-sigma value. The worst case has larger values. However, the "detrended C/A code minus carrier" does not appear to show any significant degradation with decreasing physical separation or range. As expected, fewer satellites are tracked as the range decreases. These large oscillations obviously will bias the computation of pseudorange measurement noise when the variance is computed across all epochs and satellites.

The pseudorange measurement noise prior to normalization is plotted in Figure F-5 for all four GPS receivers and the three UWB modes. A separate graph is provided for each receiver – but with each mode overlaid for comparison. The variance has been computed across all epochs and satellites for each range setting; therefore, the x-axis spans these range settings. These graphs depict the obvious nonsensical nature of this MOP in the radiated case -- the trends are not smooth nor do they depict the expected degradation with decreasing range. It is noted that similar oscillations are not observed in the C/N_0 values normalized in the previous section.

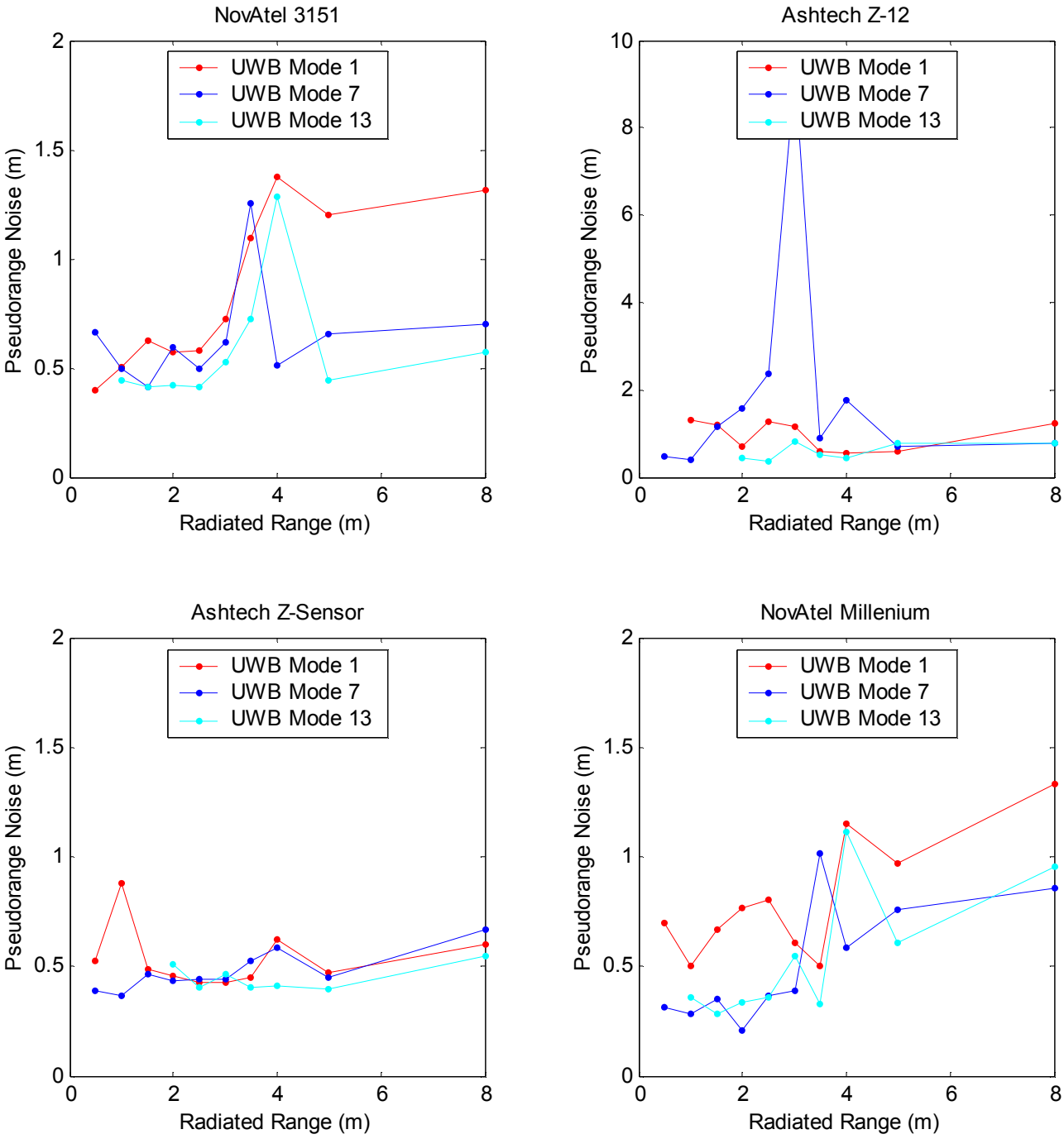

Figure F-5 Pseudorange Noise Statistics Corrupted by Oscillations

APPENDIX G
ANALYSIS OF AGGREGATE RANGING DATA

Besides the conducted ranging, conducted acquisition, and radiated ranging data activities, the Applied Research Laboratories, University of Texas (ARL:UT) test program included one other type of data collection, denoted aggregate ranging. The sole objective of this activity was to gather sufficient data with which to prove or refute the theory that the effect of ultra-wideband (UWB) signals can be added like Guassian noise. If proven correct, this theory can then be used to extend the results of single UWB device testing to other scenarios where multiple UWB devices are operating simultaneously.

Similar to the single device radiated ranging testing, the aggregate ranging test setup was conducted with an actual GPS satellite constellation and used physical separation between the GPS receiver and UWB device, instead of simulated GPS signal and attenuated UWB signals. However, the aggregate testing used a different UWB device than that used in the conducted and radiated testing to allow signals from multiple devices to be injected simultaneously. These devices are not the configurable PulsON Application Developer (PAD) but noise generators that produce two different UWB signals, both with 5-MHz pulse repetition frequencies (PRFs). Noise generator Mode 1 has a continuous duty cycle similar to UWB Mode 7, and noise generator Mode 2 has a 50-percent duty cycle similar to UWB Modes 8 through 10. The primary difference between these noise generators and the PAD is the length of the PRN code used to dither the pulse position. The PAD uses a 1000-length code while the noise generator uses a code length on the order of 10^7, which in theory will reduce any spectral content in the UWB signal and reduce the degradation realized by a GPS receiver. However, even the restricted code length of the PAD produced test results that indicated its signal was sufficiently noise-like. This difference is not relevant given the objective of this testing, but it is mentioned here because in several other venues, direct comparison of the radiated and aggregate results has been discussed. The reader is cautioned against such a comparison.

If UWB signals add like Gaussian noise, then carrier to noise ratio (C/N_0) should decrease as a linear function of 2^N injected signals or devices (when all N devices are at a constant range from the GPS receiver). The slope of the decrease will vary with the range. A similar linear relationship should be observed with the normalized C/N_0 measure of performance. This relationship is fortunate since the normalized C/N_0 is the only measure of performance that does not require a simultaneous baseline with which to remove any degradations that should correctly be attributed to natural variations in GPS performance. In addition, this normalization is independent of when the actual test was performed and whether the different segments of the test were performed sequentially or over several days.

The aggregate testing was performed separately with the Ashtech Z-Sensor and NovAtel Millenium GPS receivers. For each receiver under evaluation, multiple noise generators were

evenly spaced along the circumference of a circle whose center coincided with the GPS antenna connected to that receiver. Six different circle radii were utilized with the number of noise generators starting at 1, and every 20 minutes the number was increased by a power of 2 until 16 noise generators were contained in that circle. The circle radius started at 8.0 meters and decreased to 1.0 meters. These test configurations were repeated for both noise generator modes. No specific relationship is to be analyzed between degradation in the normalized C/N_0 and each circle radius or noise generator mode. Only the linearity of the function is to be analyzed; therefore, to minimize the number of graphs, the two modes are presented in separate graphs, and the five ranges are overlaid on a single graph.

Figure G-1 contains two graphs for the Ashtech Z-Sensor GPS receiver with the noise generator configured in Mode 1. In the left-hand graph, the degradation in normalized C/N_0 is plotted versus the number of devices in the circle. As expected the lines are exponential. Furthermore, in the right-hand graph when the x-axis is changed to 2^N devices rather than N devices, the relationships are nearly linear to within statistical variability. A similar set of graphs is presented in Figure G-2 with the same GPS receiver but with the noise generator configured in Mode 2.

The results from aggregate testing with the NovAtel Millenium are depicted in the two graphs accompanying Figures G-3 and G-4. These graphs are also for noise generator Modes 1 and 2, respectively. Again the relationships are nearly linear when plotted as function of 2N devices. The graphs in Figure G-3 are noted to be missing data for the 1.0 meter range setting. Although the NovAtel Millenium receiver appeared was operating during this configuration, the per satellite elevation angles contained in the measurement data were nonsensical. Elevation angles were negative or both negative and positive even with an elevation mask set. The receiver correctly tagged the corresponding pseudorange measurement data as invalid due to these values. The data for the 1.0-meter case were then obviously deleted from the analysis.

From all four figures, the degradation in normalized C/N_0, and therefore also C/N_0 is a linear function of 2^N devices. Therefore, the theory that UWB signals add like Gaussian noise is demonstrated by the test result.

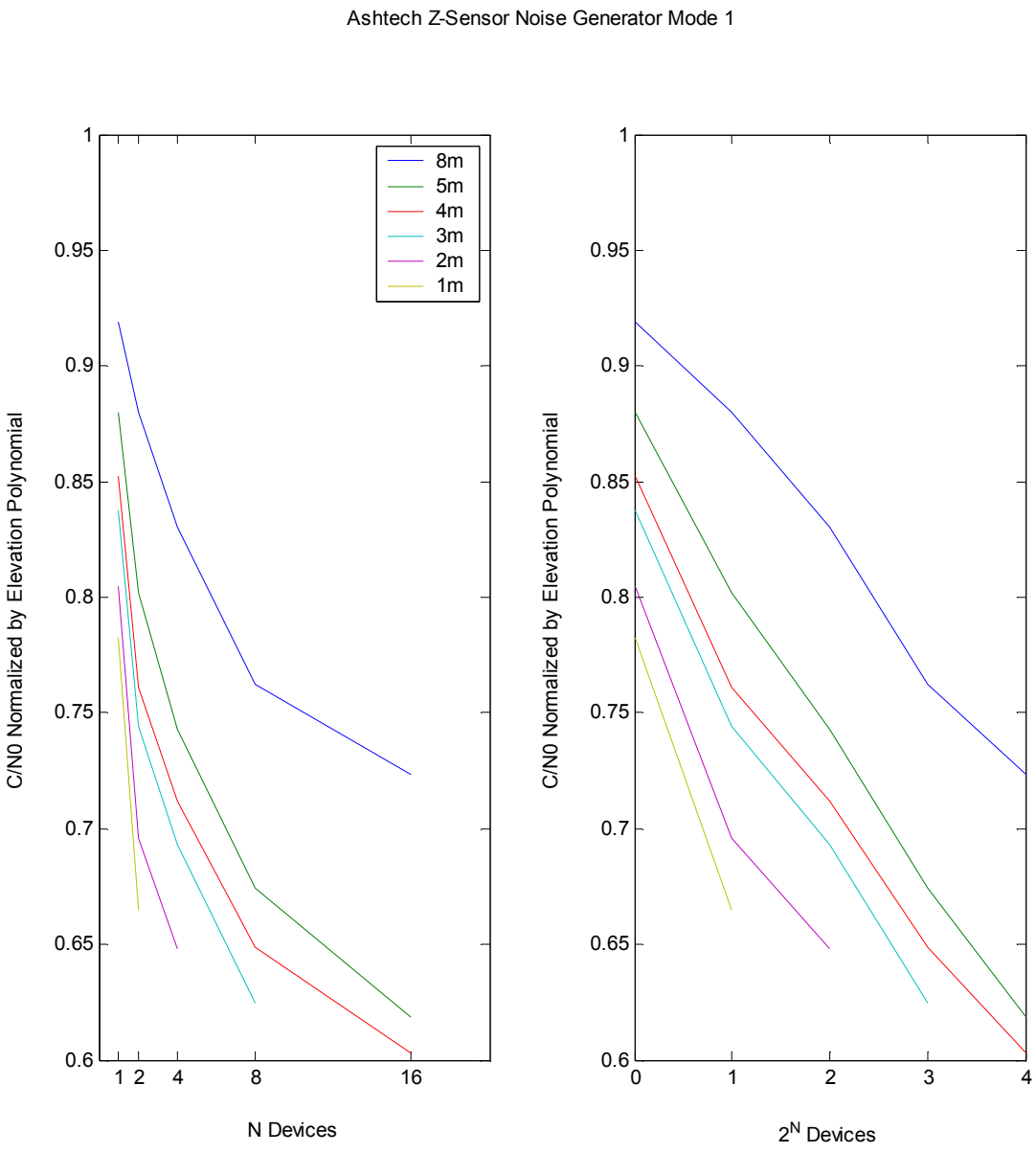

Figure G-1 Ashtech Z-Sensor Noise Generator Mode 1

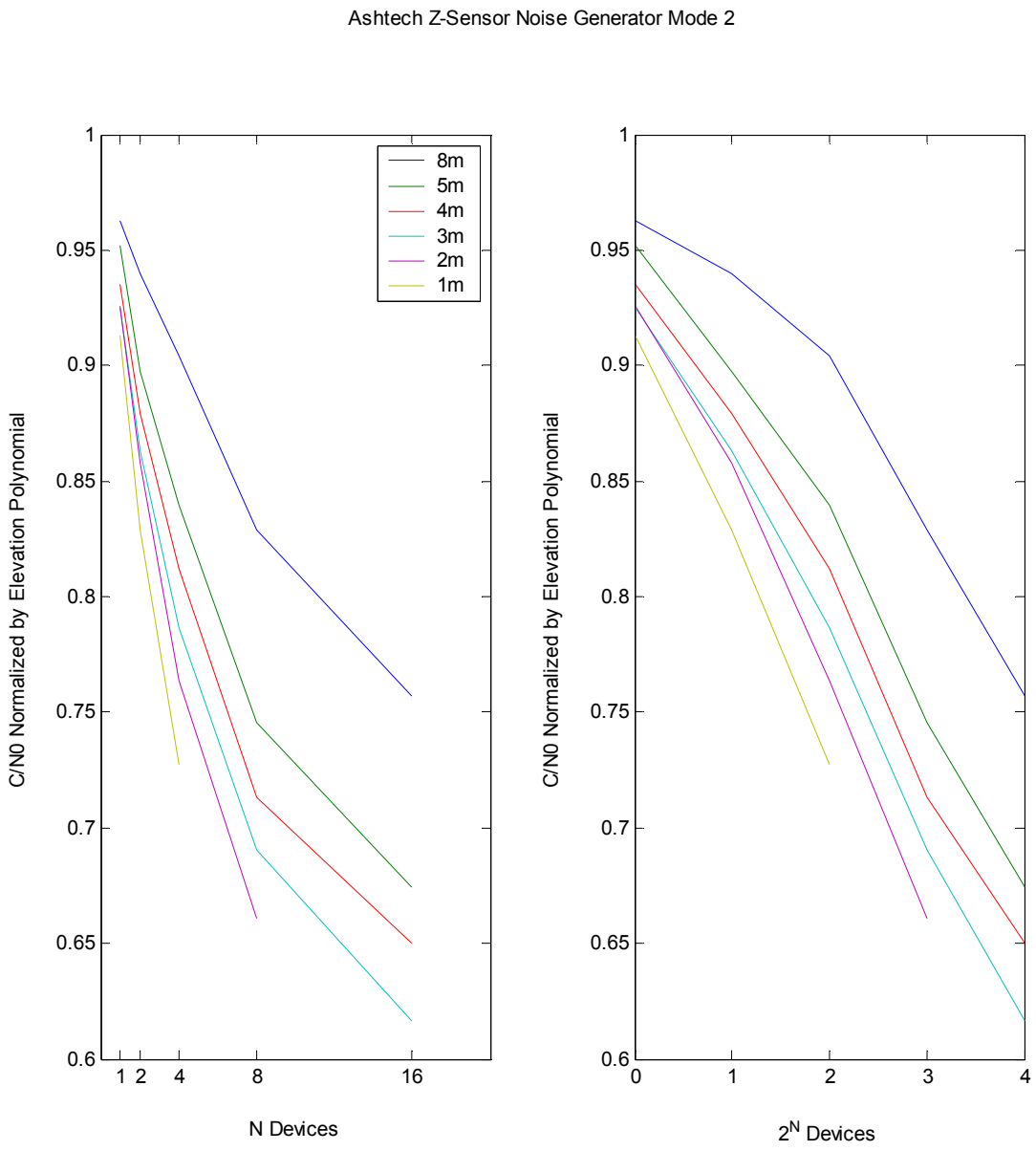

Figure G-2 Ashtech Z-Sensor Noise Generator Mode 2

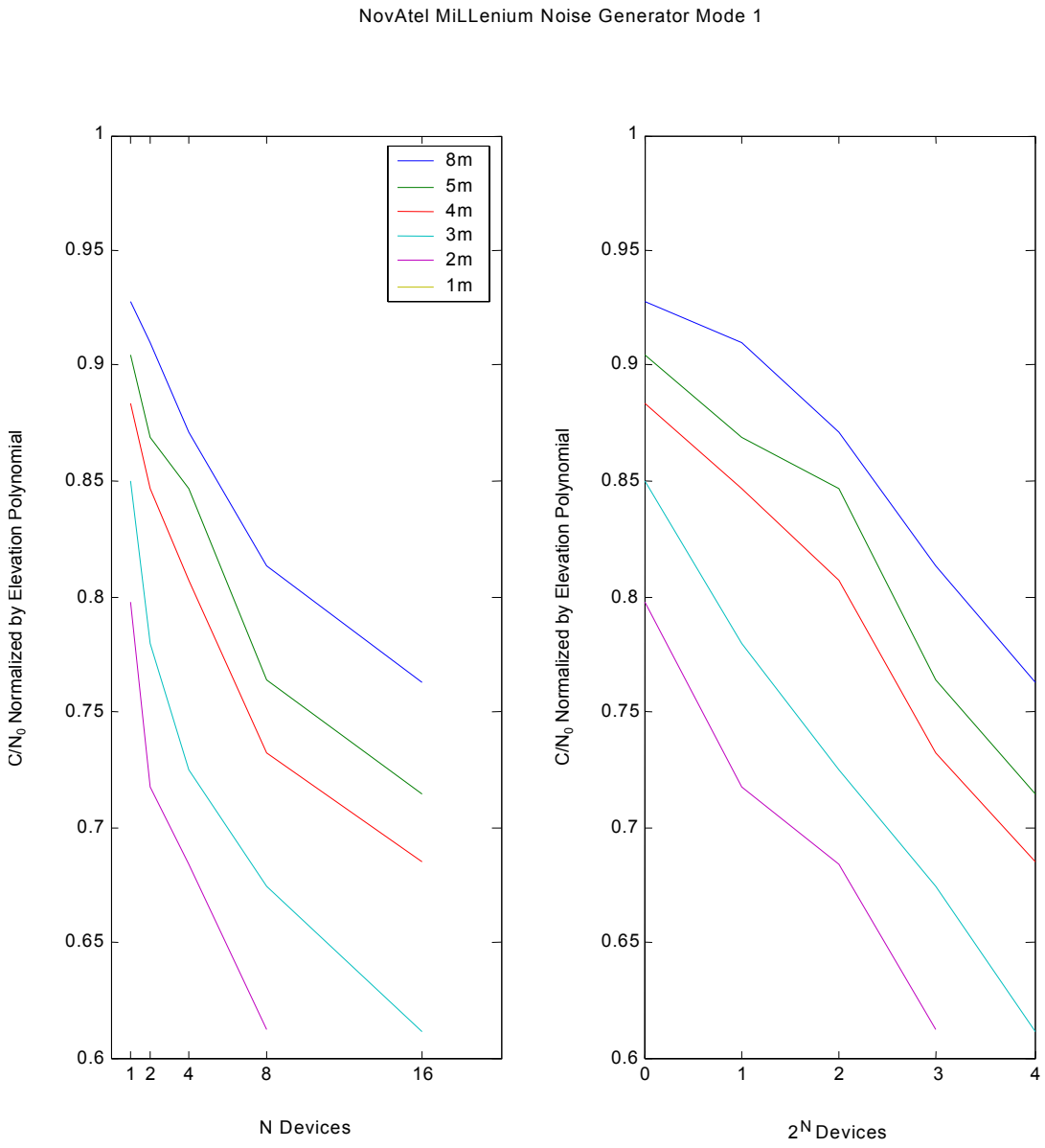

Figure G-3 NovAtel MiLLenium Noise Generator Mode 1

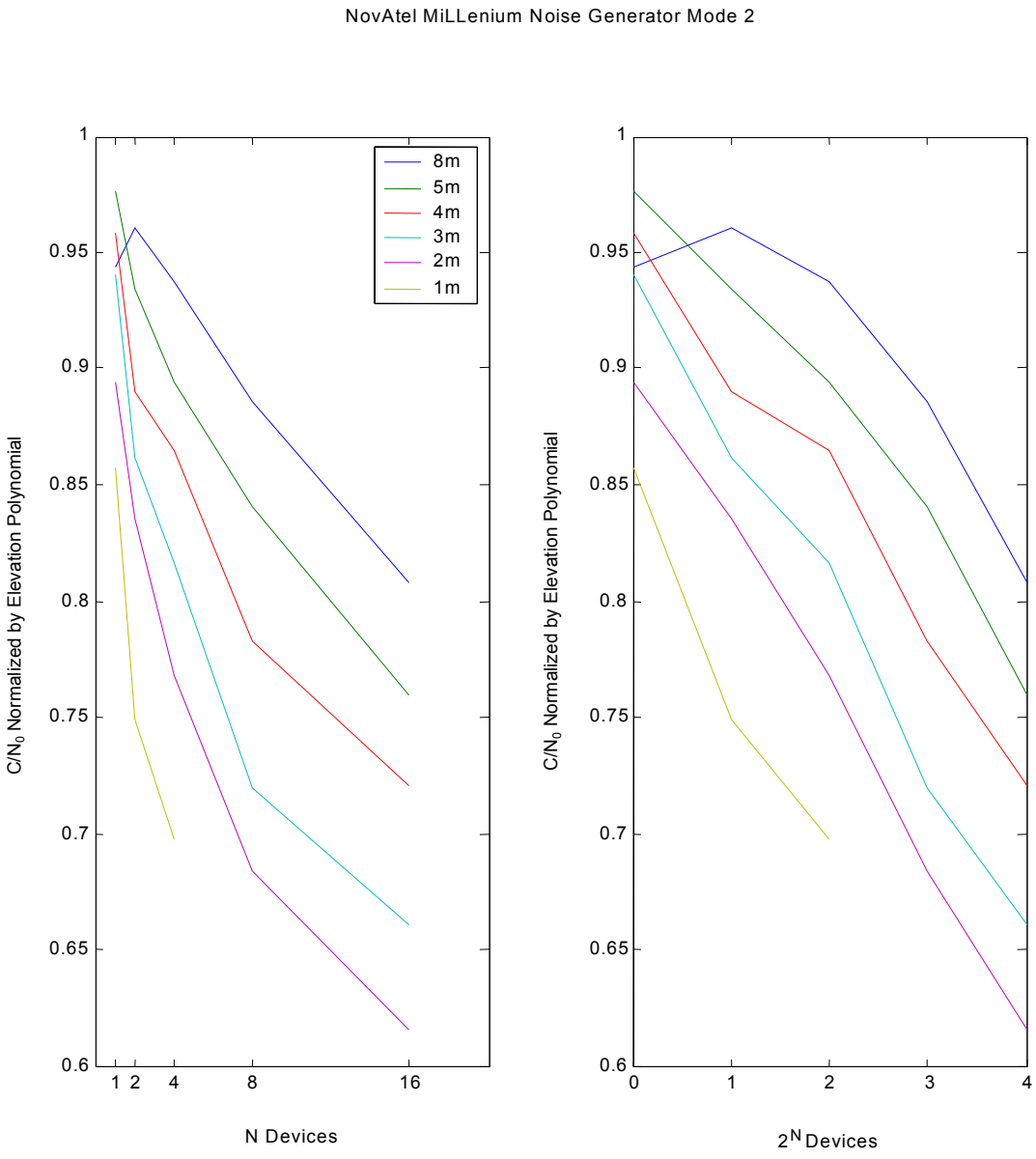

Figure G-4 NovAtel MiLLenium Noise Generator Mode 2

APPENDIX H
ANALYSIS OF FEDERAL COMMUNICATIONS COMMISSION (FCC) PART 15 DEVICES

In addition to testing the ultra-wideband (UWB) devices provided by Time Domain, Applied Research Laboratories, University of Texas (ARL:UT) repeated the radiated ranging portion of their test program with two devices that are considered compliant under the current FCC Part 15 regulations and two devices that have been granted an FCC Part 15 waiver. The generally compliant devices were a Gateway personal computer and a Motorola walkie-talkie; and the waivered items were two US Radar ground-penetrating radars. The former two items were provided to ARL:UT by Time Domain. In previous informal testing, Time Domain found this particular Motorola walkie-talkie when in the unkeyed mode appeared to cause degradation in the performance of a Garmin hand-held Global Positioning System (GPS) receiver. In independent testing at an FCC compliance laboratory, this walkie-talkie was determined to be compliant with the current FCC Part 15 regulations. For this reason alone, JHU/APL decided to evaluate the walkie-talkie. As previously noted in Appendix F, for the radiated ranging testing, most of the measures of performance (MOPs) are difficult to rigorously analyze because no simultaneous baseline data exist with which to remove any degradations that should correctly be attributed to natural variations in GPS performance. One exception to this is carrier to noise ratio (C/N_0) when normalized by the elevation polynomial as described in Appendix F. This normalization is independent of when the actual test was performed and whether the different segments of the test were performed sequentially or over several days.

The ARL:UT testing of the walkie-talkie included both NovAtel, both Ashtech, and the Garmin 155XL GPS receivers. Similar to the previous radiated ranging testing with the UWB devices, these receivers were not run simultaneously. Finally, the walkie-talkie was only tested in the unkeyed mode. Figure H-1 depicts the normalized C/N_0 as a function of range. Separate dotted lines are overloaded on the plot for each receiver. Again, the dotted lines are used to show both the individual points and allow for an easy visualization of the general trend. Similar to the preceding conducted and more noticeably the radiated analyses results, large variations are observed in this MOP across the different GPS receivers.

In addition to separate lines for the five GPS receivers, a green curve is overlaid on the graph. This curve is the hyperbola derived and presented in Appendix A that represents a least-squares fit to the radiated ranging data acquired with the UWB device. Recall that the least-squares fit used data collected with the UWB device operating in Modes 1, 7, and 13 and at ranges between 0.5 and 8.0 meters. These ranges have not been adjusted or shifted to account for differences in the average power between these modes due to pulse repetition frequency. In addition, the least squares fit includes data from the exact same set of five GPS receivers.

Generally, the degradation observed in the normalized C/N_0 for the walkie-talkie follows that experienced with the UWB devices. The one exception is the Ashtech Z-Sensor, which appears to follow in inverse relationship. This observation contradicts that experienced in all of the other conducted and radiated testing with the Ashtech Z-Sensor. Although The Johns Hopkins University Applied Physics Laboratory (JHU/APL) cannot confirm it, JHU/APL hypothesizes that the data for this receiver were collected with the ranges accidentally in the reversed order.

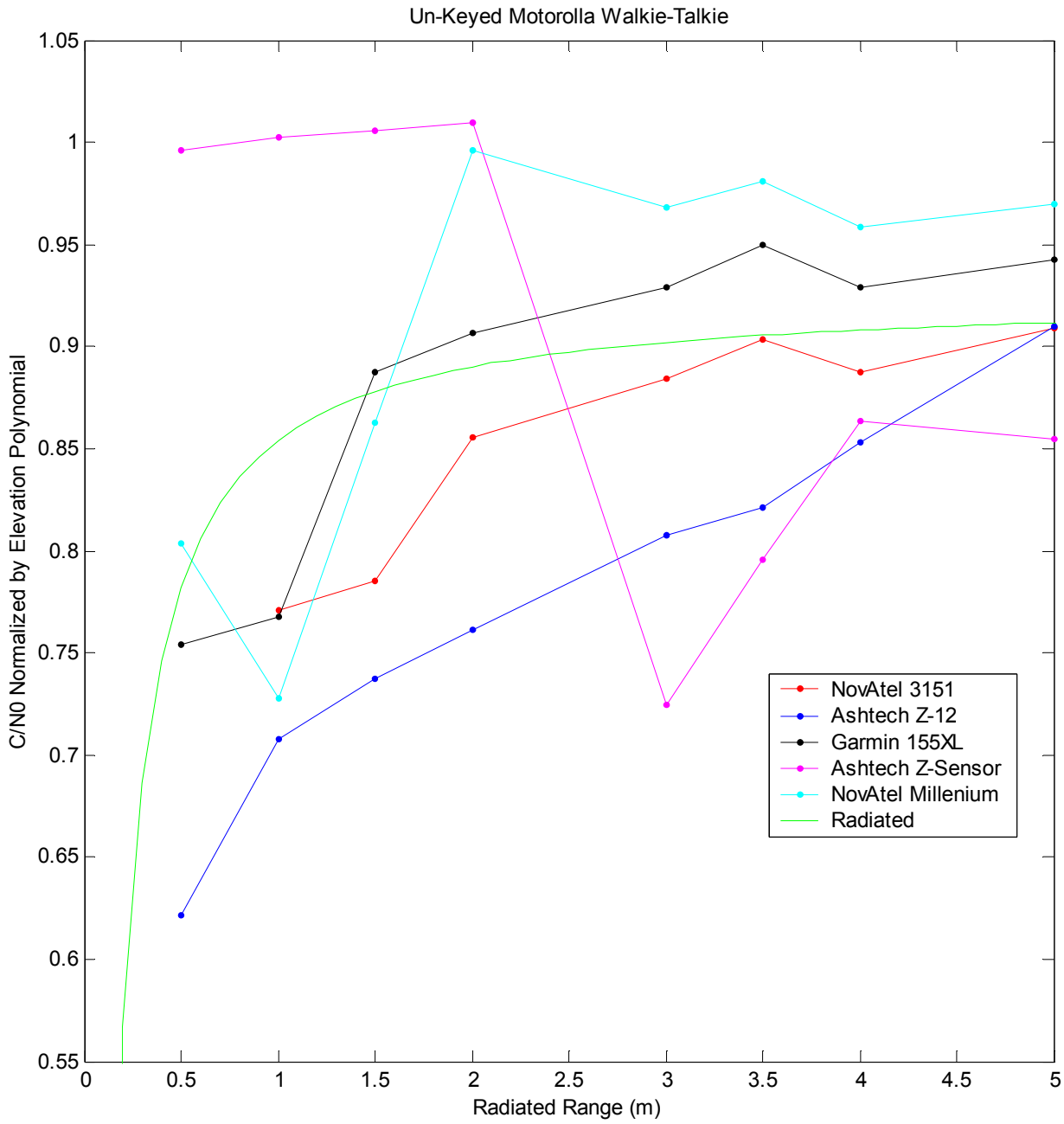

Figure H-1 Normalized C/N_0 for FCC Part 15 Device

APPENDIX I
OTHER PULSON APPLICATION DEVELOPER (PAD) ULTRA-WIDEBAND (UWB) MODES

The UWB device, a Time Domain PAD, used by Applied Research Laboratories, University of Texas (ARL:UT) during their data collection is capable of 18 different modes covering 3 pulse repetition frequencies (PRFs) and various duty cycles. During those portions of the testing that simulated the live-sky Global Positioning System (GPS) signal power, three modes were exercised – continuous duty cycles for the 1-, 5-, and 10-MHz PRFs. For the minimum level testing, between 9 and 18 different modes were exercised depending on the specific test. Although JHU/APL analyzed the data from multiple modes for the minimum level case, only the continuous duty cycles for the 1-, 5-, and 10-MHz PRFs (denoted Modes 1, 7, and 13, respectively) are carried through the entire process. This appendix provides the justification for not carrying all modes.

First, in the mapping to "compliant attenuation" that is described in Appendix A, all UWB modes are considered to be compliant under the current average or quasi-peak radiated power criteria above 960 MHz as stated in Section 15.209 of the Federal Communications Commission (FCC) Part 15 regulations. By the design of the PAD, all modes already have equivalent peak powers. After this mapping, the results in Chapter 6 show that the measures of performance vary more across the different GPS receivers than they do across the three modes. The higher pulse repetition frequencies are noted to produce slightly more degraded GPS performance.

Second, the figures in Appendix A are based on the analysis results prior to the mapping to compliant attenuation. For a single receiver and any measure of performance, the higher pulse repetition frequencies produce greater degradation in the GPS performance due to the higher average power. The intuitive dependency is confirmed by the theoretical modeling in Chapter 5. In addition, Chapter 5 and the Stanford/Department of Transportation testing demonstrate that poorly chosen pulse repetition frequencies, without pulse position dithering (i.e., those with significant spectral lines in the L1 or L2 frequency band) can have devastating effects on the GPS performance.

Finally, Figures I-1 through I-4 depict four simpler measures of performance for three different GPS receivers, the 10 MHz pulse repetition frequency and various duty cycles. Each figure has three separate graphs -- for the NovAtel 3151, Ashtech Z-12, and Ashtech Z-Sensor receivers. Each graph overlays six duty cycles – Mode 13 is the continuous duty cycle, Modes 14 through 16 are 50 percent duty cycles, Mode 17 is a 25-percent duty cycle, and Mode 18 is a 66-percent duty cycle. Figure I-1 depicts the number of satellites tracked, Figure I-2 depicts the number of satellites used in the navigation solution, and finally, Figure I-3 depicts the

normalized C/N_0. Each measure of performance (MOP) is plotted versus "equivalent range" and thus has included the mapping to a "compliant attenuation" as described in Appendix A.

In all figures, regardless of the MOP, the results vary more across the different GPS receivers than they do across the different duty cycles. In Chapter 6, the lower PRFs consistently have a slightly lesser effect even after the mapping to "compliant attenuation" or equivalent average power. However, these figures show that the lower duty cycles (e.g., Mode 17 with the 25-percent duty cycle) do not consistently have the lesser effect. For example, Mode 17 causes the most severe degradation in the normalized C/N_0 for the NovAtel 3151, but the least severe degradation in the same measure of performance for the Ashtech Z-12 and Ashtech Z-Sensor. Numerous other examples of this inconsistency can be found for each measure of performance.

Given these three reasons, The Johns Hopkins University Applied Physics Laboratory (JHU/APL) believes that including modes without continuous duty cycles through the entire report does not convey any additional or necessary information to the reader. In addition, by considering only modes with continuous duty cycles, a consistency is maintained between the live sky and minimum level GPS signal power presentations.

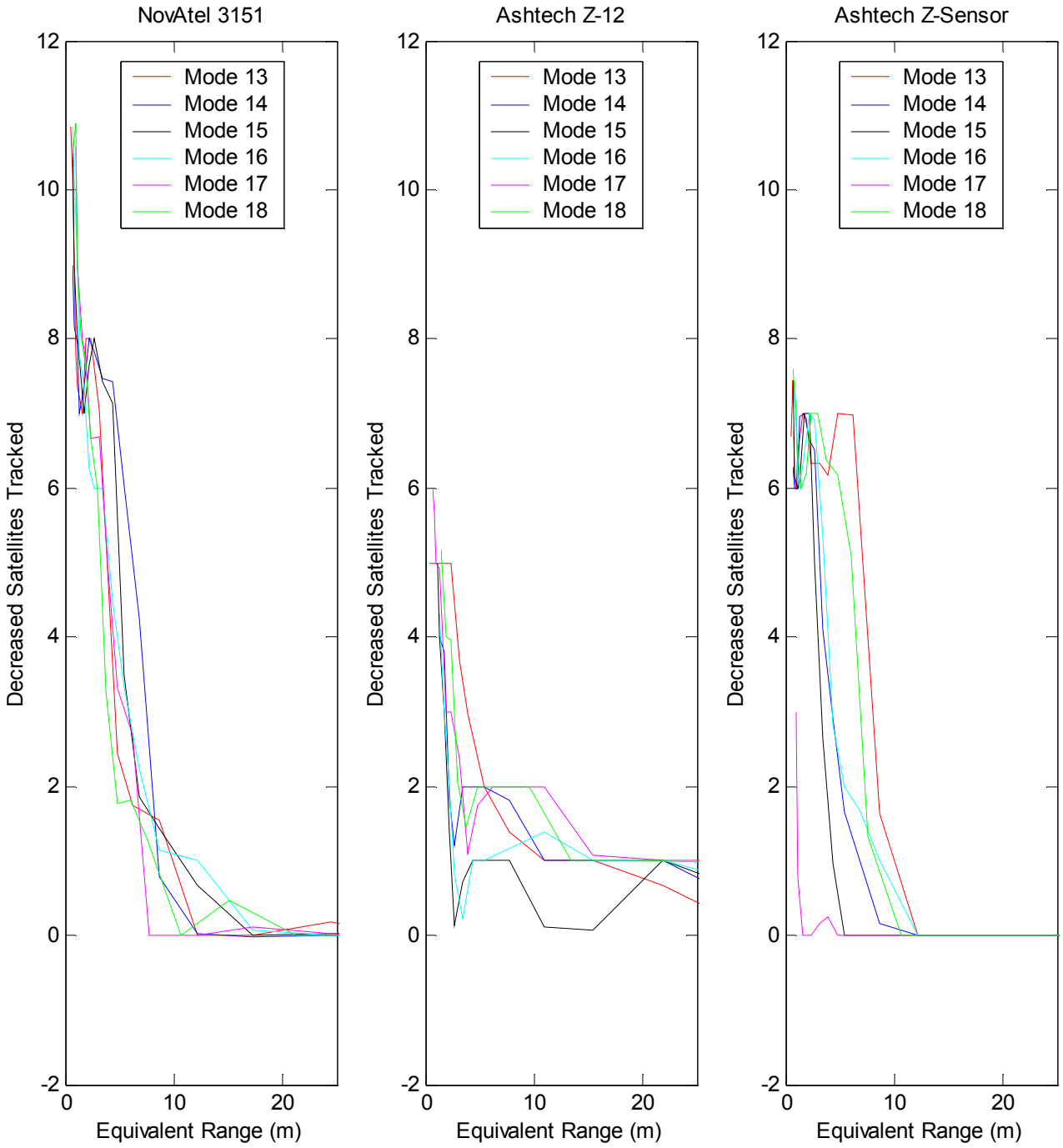

Figure I-1 Number of Satellites Tracked with Various Duty Cycles

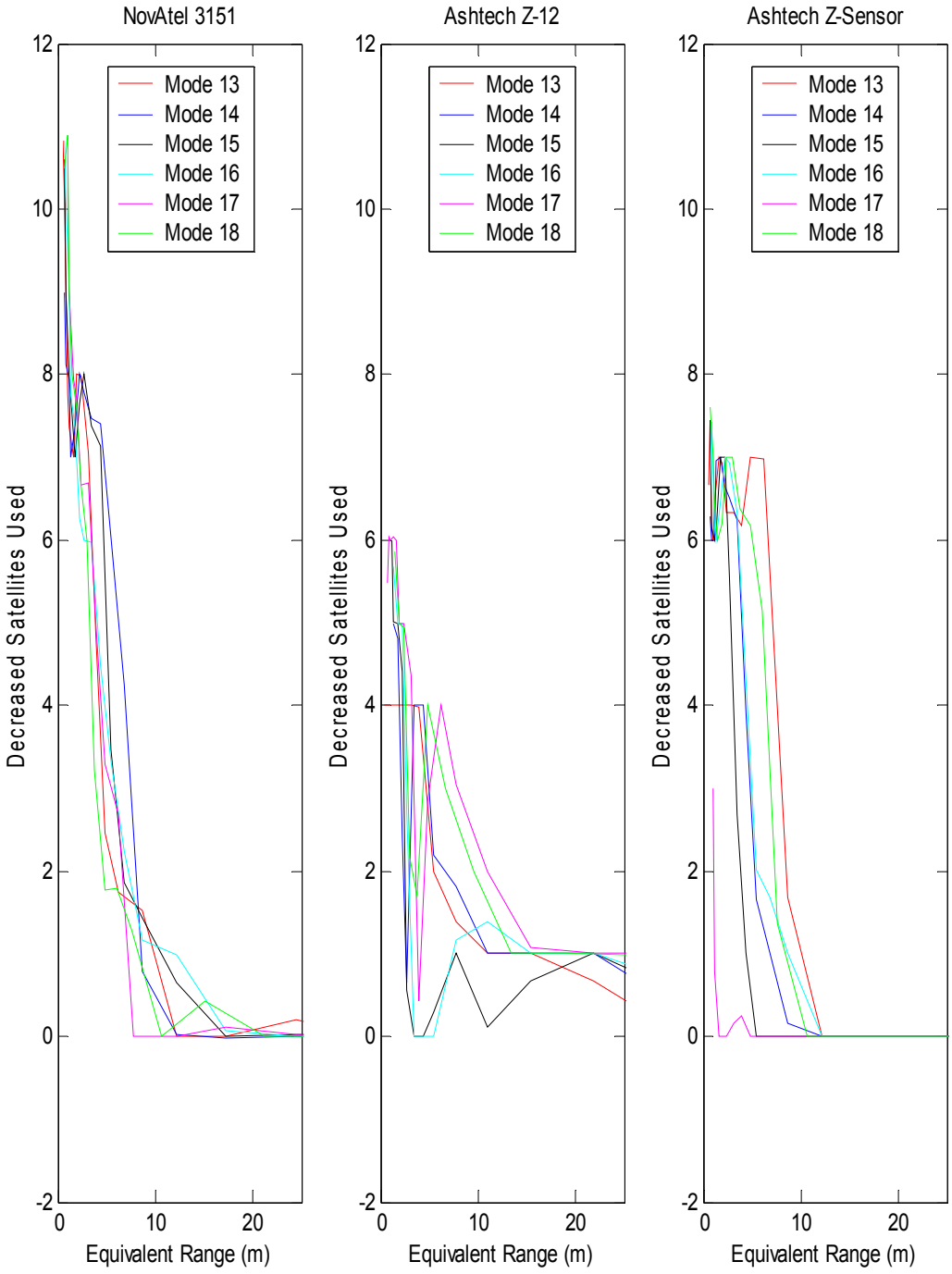

Figure I-2 Number of Satellites Used in the Navigation Solution for Various Duty Cycles

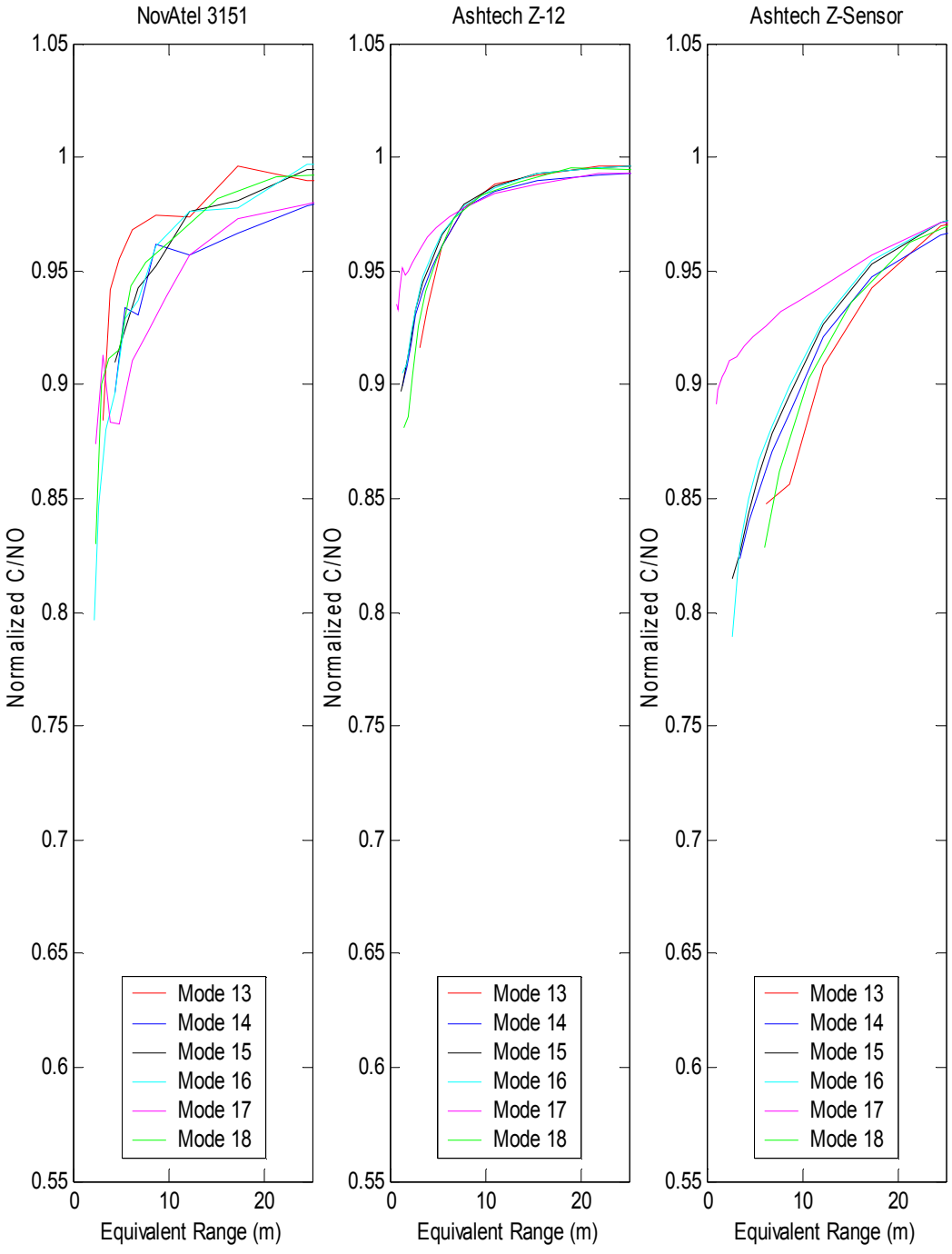

Figure I-3 Normalized C/N_0 for Various Duty Cycles